

การเพิ่มอัตราขยายของสายอากาศปากแตรโดยใช้
โพรงช่องว่างแถบแม่เหล็กไฟฟ้า



นายศรันย์ คัมภีร์ภัทร

วิทยานิพนธ์นี้เป็นส่วนหนึ่งของการศึกษาตามหลักสูตรปริญญาวิศวกรรมศาสตรดุษฎีบัณฑิต
สาขาวิชาวิศวกรรมโทรคมนาคม
มหาวิทยาลัยเทคโนโลยีสุรนารี
ปีการศึกษา 2557

**GAIN ENHANCEMENT OF HORN ANTENNA
USING EBG**

Saran Kampeephat



**A Thesis Submitted in Partial Fulfillment of the Requirements for the
Degree of Doctor of Philosophy in Telecommunication Engineering**

Suranaree University of Technology

Academic Year 2014

**GAIN ENHANCEMENT OF HORN ANTENNA
USING EBG**

Suranaree University of Technology has approved this thesis submitted in partial fulfillment of the requirements for the Degree of Doctor of Philosophy.

Thesis Examining Committee

(Prof. Dr. Prayoot Akkaraekthalin)

Chairperson

(Assoc. Prof. Dr. Rangsan Wongsan)

Member (Thesis Advisor)

(Assoc. Prof. Dr. Chuwong Phongcharoenpanich)

Member

(Asst. Prof. Dr. Chutima Prommak)

Member

(Asst. Prof. Dr. Piyaporn Mesawad)

Member

(Prof. Dr. Sukit Limpijumngong)

Vice Rector for Academic Affairs
and Innovation

(Assoc. Prof. Flt. Dr. Kontorn Chamniprasart)

Dean of Institute of Engineering

ศรันย์ คัมภีร์ภัทร : การเพิ่มอัตรายายของสายอากาศปากแตรโดยใช้โพรงช่องว่าง
แถบแม่เหล็กไฟฟ้า (GAIN ENHANCEMENT OF HORN ANTENNA USING EBG)
อาจารย์ที่ปรึกษา : รองศาสตราจารย์ ดร.รังสรรค์ วงศ์สรรค์, 165 หน้า.

สายอากาศปากแตร (horn antenna) เป็นสายอากาศอะเพอร์เจอร์ (aperture antenna) ชนิดหนึ่งที่มีอัตรายายสูงเมื่อเทียบกับสายอากาศชนิดอื่น ๆ จากข้อดีดังกล่าว จึงมีการนำสายอากาศปากแตรมาประยุกต์ใช้งานอย่างแพร่หลาย นอกจากนี้ยังมีการนำตัวสะท้อนพาราโบลิกมาใช้งานร่วมกับสายอากาศปากแตรเพื่อให้สายอากาศมีอัตรายายที่สูงมากขึ้น เพื่อเป็นการเพิ่มอัตรายายของสายอากาศปากแตรให้มากยิ่งขึ้น ดังนั้นงานวิจัยนี้จึงได้นำเสนอเทคนิคการเพิ่มอัตรายายของสายอากาศปากแตร โดยใช้ช่องว่างแถบแม่เหล็กไฟฟ้า (Electromagnetic Band Gap หรือ EBG) มาประกอบร่วม ซึ่งสามารถพัฒนาและปรับปรุงประสิทธิภาพของสายอากาศ ในส่วนของการเพิ่มอัตรายาย โดยใช้เทคนิคการถ่ายโอนกำลังงาน (power transfer) ผ่าน โครงสร้างของ EBG ดังกล่าวนอกจากนี้ จะทำการวิเคราะห์จุดศูนย์กลางเฟส (phase center) ของสายอากาศปากแตรสำหรับการนำสายอากาศที่พัฒนาแล้วไปใช้งานร่วมกับตัวสะท้อนพาราโบลิกเพื่อเพิ่มอัตรายายให้สูงยิ่งขึ้นไปอีก โดยงานวิจัยนี้ได้ทำการวิเคราะห์การเพิ่มอัตรายายของอะเพอร์เจอร์รูปทรงสี่เหลี่ยมมุมฉากและวงกลมซึ่งเป็นรูปทรงพื้นฐานของสายอากาศปากแตร ที่ความถี่ขึ้นย่านไมโครเวฟ (uplink microwave band) โดยใช้โปรแกรมสำเร็จรูป CST (Computer Simulation Technology) ในการออกแบบและวิเคราะห์ผล สุดท้ายได้สร้างต้นแบบของโครงสร้าง EBG ซึ่งได้จากการคำนวณ เพื่อนำไปใช้งานร่วมกับสายอากาศปากแตรทั้งสองรูปแบบตามที่กำหนด เพื่อนำมาวัดทดสอบเปรียบเทียบผลที่ได้จากการวัดทดสอบและจากโปรแกรมสำเร็จรูป CST

SARAN KAMPEEPHAT : GAIN ENHANCEMENT OF HORN ANTENNA
USING EBG. THESIS ADVISOR : ASSOC. PROF. RANGSAN
WONGSAN, D.Eng., 165 PP.

GAIN ENHANCEMENT/HORN ANTENNA/ELECTROMAGNETIC BAND GAP

A horn antenna is a type of aperture antenna, which provides the moderately high gain as compared to the other antennas. Consequently, the horn antenna is widely applied for various tasks. Applications requiring high gain antenna such as the parabolic reflector can be applied with the horn antenna to enhance the higher gain. Therefore, this research proposes a technique to enhance the gain of horn antenna by using Electromagnetic Band Gap (EBG) transfer the power from its aperture through EBG structure. Moreover, the phase center of a horn antenna was analyzed again for applying with a parabolic reflector to obtain the total gain. This study has analyzed the EBG utilization for gain enhancement both of rectangular and circular apertures, which are the basic shapes of horn antenna at the uplink frequency of microwave band. The CST (Computer Simulation Technology) software is used to design and analyze. Finally, the prototype of EBG structure, which is installed at the front of horn antennas, is fabricated. Then the measured results were compared to the simulated results from the CST software for validation.

School of Telecommunication Engineering Student's Signature _____

Academic Year 2014

Advisor's Signature _____

ACKNOWLEDGEMENTS

I would like to thank the office of the National Research Council of Thailand (NRCT) for supporting by grant under the program strategic scholarships for the joint Ph.D. program Thai doctoral degree.

I am so grateful to my advisor, Assoc. Prof. Dr. Rangsak Wongsak for consistent thesis supervision and thoughtfully comment on several drafts and advice towards the completion of this study.

I would like to express my gratitude to the thesis examination committees, Prof. Dr. Prayoot Akkaraekthalin, Assoc. Prof. Dr. Rangsak Wongsak, Assoc. Prof. Dr. Chuwong Phongcharoenpanich, Asst. Prof. Dr. Chutima Prommak, and Asst. Prof. Dr. Piyaporn Mesawad, for their invaluable advices and kind supports.

I would like to thank for the fellow members of the Wireless Communication Research and Laboratory, Suranaree University of Technology, for providing a pleasant and inspiring environment to work in.

Finally, I am greatly indebted to all of my teachers in the past and my family, who loves me and gives encouragement.

Saran Kampeephat

TABLE OF CONTENTS

	Page
ABSTRACT (THAI).....	I
ABSTRACT (ENGLISH)	II
ACKNOWLEDGMENTS.....	IV
TABLE OF CONTENTS	V
LIST OF TABLES.....	X
LIST OF FIGURES	XI
CHAPTER	
I INTRODUCTION.....	1
1.1 Background of Problems and Significance of the Study	1
1.2 Research Objectives	2
1.3 Scope of the Study.....	3
1.4 Expected Benefits.....	3
1.5 Thesis Organization.....	3
II LITERATURE REVIEW	5
2.1 Introduction.....	5
2.2 Development of A Horn Antenna	5
2.3 Electromagnetic Band Gap	10

TABLE OF CONTENTS (Continued)

	Page
2.3.1 Antenna Substrates for Surface Wave suppressions	11
2.3.2 Antenna Substrates for Efficient Low Profile Antenna Design.....	13
2.3.3 Reflection/Transmission Surface for High Gain Antenna.....	16
2.4 Chapter Summary.....	18
III BACKGROUND THEORY.....	19
3.1 Introduction.....	19
3.2 Horn Antenna.....	19
3.2.1 Types of Horn Antenna	21
3.2.2 Waveguide Feeding	23
3.3 Electromagnetic Band Gap Structures.....	25
3.3.1 EBG Definition.....	25
3.3.2 EBG and Metamaterials	28
3.3.3 Analysis Methods for EBG Structures.....	30
3.3.4 Woodpile EBG Structures.....	36
3.4 Chapter Summary.....	40

TABLE OF CONTENTS (Continued)

	Page
IV ANTENNA ANALYSIS AND DESIGN	41
4.1 Introduction.....	41
4.2 The Woodpile EBG Configuration.....	41
4.3 A Rectangular Horn Antenna Configuration	50
4.3.1 A Conventional Rectangular Horn Antenna (Type-A rectangular horn).....	50
4.3.2 A Conventional Rectangular Horn Antenna and the Designed Woodpile EBG (Type-B rectangular horn).....	54
4.3.3 A Rectangular Horn Antenna with Two Side-Wing Slabs (Type-C rectangular horn).....	58
4.3.4 A Rectangular Horn Antenna with Two Side-Wing Slabs and the Designed Woodpile EBG (Type-D rectangular horn).....	63
4.4 A Circular Horn Antenna Configuration.....	70
4.4.1 A Conventional Circular Horn Antenna (Type-A circular horn)	70

TABLE OF CONTENTS (Continued)

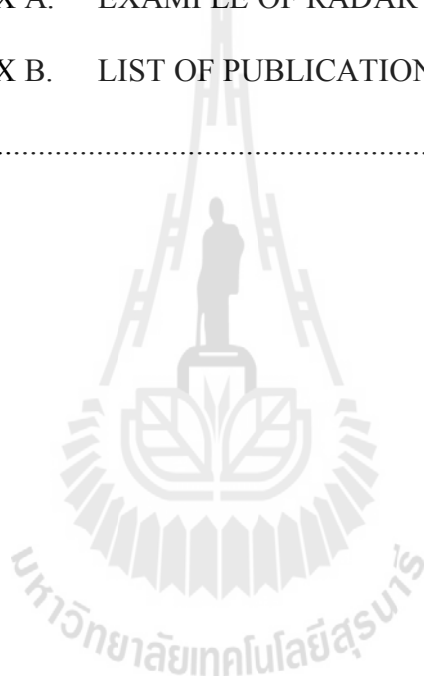
	Page
4.4.2 A Conventional Circular Horn Antenna and the Designed Woodpile EBG (Type-B circular horn)	74
4.4.3 A Circular Horn Antenna with Two Side-Wing Slabs (Type-C circular horn)	78
4.4.4 A Circular Horn Antenna with Two Side-Wing Slabs and the Designed Woodpile EBG (Type-D circular horn)	83
4.5 Chapter Summary.....	90
V MEASUREMENT AND DISCUSSION.....	91
5.1 Introduction.....	91
5.2 The Antenna Prototype.....	91
5.2.1 The Woodpile EBG.....	91
5.2.2 A Rectangular Horn Antenna with Two Side-Wing Slabs.....	94
5.2.3 A Circular Horn Antenna with Two Side-Wing Slabs.....	96

TABLE OF CONTENTS (Continued)

	Page
5.3 Antenna Measurement and Experimental Results of a Type-D Rectangular Horn.....	100
5.3.1 The Reflected Power, Voltage Standing Wave Ratio and Input Impedance.....	107
5.3.2 Bandwidth	113
5.3.3 Radiation Pattern	115
5.3.4 Gain.....	119
5.4 Antenna Measurement and Experimental Results of a Type-D Circular Horn.....	123
5.4.1 The Reflected Power, Voltage Standing Wave Ratio and Input Impedance.....	130
5.4.2 Bandwidth	136
5.4.3 Radiation Pattern	137
5.4.4 Gain.....	141
5.5 Simulated and Measured Results Summary	143
5.6 Chapter Summary.....	144
VI CONCLUSIONS	145
6.1 Thesis Concluding Remarks	145
6.2 Remark for Future Studies.....	146

TABLE OF CONTENTS (Continued)

	Page
REFERENCES	147
APPENDICES	
APPENDIX A. EXAMPLE OF RADAR ANTENNAS	152
APPENDIX B. LIST OF PUBLICATIONS.....	156
BIOGRAPHY	165



LIST OF TABLES

Table	Page
2.1 The comparison of the EBG and the PEC ground planes	14
3.1 Formulations of elementary geometrical function.....	39
4.1 The simulated results of various dimension of two side-wing slabs installed at the aperture of a rectangular horn antenna	59
4.2 The simulated results of four types of the rectangular horn antennas	67
4.3 The simulated results of various dimension of two side-wing slabs installed at the aperture of a circular horn antenna.....	79
4.4 The simulated results of four types of the circular horn antennas.....	87
5.1 The dimension of the designed quadratic shaped woodpile EBG structure	92
5.2 Dimension of a rectangular horn antenna with two side-wing slabs	94
5.3 Dimension of a circular horn antenna with two side-wing slabs	98
5.4 The simulated results of the various heights of a PEC arm for Type-D rectangular horn.....	101
5.5 The simulated results of the various heights of a PEC arm for Type-D circular horn	124
5.6 Comparison of simulated and measured results for antenna characteristics	143
A.1 Comparison of radar antennas.....	153

LIST OF FIGURES

Figure	Page
2.1 The first horn antenna as the microwave apparatus at the Bose Institute, Kolkata, India (http://en.wikipedia.org)	8
2.2 Feed horns for radar antennas in World War II (http://prezi.com/w2ximutsy5c9/horn-antenna/)	8
2.3 Holmdel Horn Antenna (http://en.wikipedia.org).....	9
2.4 A large 177 ft. horn antenna (http://en.wikipedia.org).....	9
2.5 The corrugated horn (Kay, 1962) (http://prezi.com/w2ximutsy5c9/horn-antenna/)	10
2.6 A patch antenna on the PBG substrate formed by four holes in a square lattice (Gonzalo, Maagt, and Sorolla, 1999).....	12
2.7 EBG substrate for reducing the mutual coupling levels on patch antennas (Yang and Rahmat-Samii, 2003).....	13
2.8 A curl antenna on an EBG structures (Yang and Rahmat-Samii, 2001).	15
2.9 A dipole antenna that radiates circularly polarized patterns (Yang and Rahmat-Samii, 2005).	16
2.10 A high gain antenna design using the woodpile EBG structures (Weily <i>et al.</i> , 2005)	17

LIST OF FIGURES (Continued)

Figure	Page
3.1 Typical horn antenna configurations (http://en.wikipedia.org).....	22
3.2 The geometry of the waveguides	24
3.3 A rectangular waveguide fed with a short monopole.....	24
3.4 The 1D EBG transmission lines.....	26
3.5 The 2D EBG planar surfaces	27
3.6 The 3D EBG volumetric structures.....	28
3.7 The geometry of a mushroom-like EBG structures (Sievenpiper <i>et al.</i> , 1999)	32
3.8 The lumped element model for the mushroom-like EBG structures.....	33
3.9 The transmission line model of EBG structures (Rahman and Stuchly, 2001).....	35
3.10 The full wave FDTD model for the EBG analysis (Kim, Yang, and Elsherbeni, 2007)	36
3.11 A unit cell of four layers planar woodpile EBG structures (Weily <i>et al.</i> , 2005)	37
3.12 A unit cell of one layers planar woodpile EBG structures	38
4.1 Simulated gain against the various shaped woodpile EBG	43
4.2 Simulated gain against the distance d	44
4.3 Simulated gain against the radius of shape r	44

LIST OF FIGURES (Continued)

Figure	Page
4.4 The configuration of quadratic shaped woodpile EBG structures.....	45
4.5 The lumped <i>LC</i> model of one unit cell.....	46
4.6 The cavity model of woodpile EBG.....	47
4.7 The bandgap characteristics of woodpile EBG.....	49
4.8 A conventional rectangular horn antenna (Type-A rectangular horn).....	51
4.9 Simulated result of reflected power (S_{11}) of a Type-A rectangular horn	52
4.10 Photograph of the realized 70 cm diameter ADE antenna	52
4.11 Simulated radiation patterns of a Type-A rectangular horn	53
4.12 A conventional rectangular horn antenna and the designed woodpile EBG (Type-B rectangular horn).....	55
4.13 Simulated result of reflected power (S_{11}) of a Type-B rectangular horn.....	56
4.14 Simulated VSWR of a Type-B rectangular horn	56
4.15 Simulated radiation patterns of a Type-B rectangular horn	57
4.16 A rectangular horn antenna with two side-wing slabs (Type-C rectangular horn)	60
4.17 Simulated result of reflected power (S_{11}) of a Type-C rectangular horn.....	61

LIST OF FIGURES (Continued)

Figure	Page
4.18 Simulated VSWR of a Type-C rectangular horn	61
4.19 Simulated radiation patterns of a Type-C rectangular horn	62
4.20 A rectangular horn antenna with two side-wing slabs and the designed woodpile EBG (Type-D rectangular horn)	64
4.21 Simulated result of reflected power (S_{11}) of a Type-D rectangular horn	65
4.22 Simulated VSWR of a Type-D rectangular horn	65
4.23 Simulated radiation patterns of a Type-D rectangular horn	66
4.24 Simulated result of reflected power (S_{11}) four types of the rectangular horn antennas	68
4.25 Simulated VSWR of four types of the rectangular horn antennas	68
4.26 Simulated radiation patterns of four types of the rectangular horn antennas	69
4.27 A conventional circular horn antenna and waveguide adapter (Type-A circular horn)	71
4.28 Simulated result of reflected power (S_{11}) of a Type-A circular horn	72
4.29 Simulated VSWR of a Type-A circular horn	72
4.30 Simulated radiation patterns of a Type-A circular horn	73

LIST OF FIGURES (Continued)

Figure	Page
4.31 A conventional circular horn antenna and the designed woodpile EBG (Type-B circular horn).....	75
4.32 Simulated result of reflected power (S_{11}) of a Type-B circular horn	76
4.33 Simulated VSWR of a Type-B circular horn.....	76
4.34 Simulated radiation patterns of a Type-B circular horn.....	77
4.35 A circular horn antenna with two side-wing slabs (Type-C circular horn).....	80
4.36 Simulated result of reflected power (S_{11}) of a Type-C circular horn	81
4.37 Simulated VSWR of a Type-C circular horn.....	81
4.38 Simulated radiation patterns of a Type-C circular horn.....	82
4.39 A circular horn antenna with two side-wing slabs and the designed woodpile EBG (Type-D circular horn).....	84
4.40 Simulated result of reflected power (S_{11}) of a Type-D circular horn	85
4.41 Simulated VSWR of a Type-D circular horn	85
4.42 Simulated radiation patterns of a Type-D circular horn.....	86
4.43 Simulated result of reflected power (S_{11}) of four types of the circular horn antennas.....	88

LIST OF FIGURES (Continued)

Figure	Page
4.44 Simulated VSWR of four types of the circular horn antennas	88
4.45 Simulated radiation patterns of four types of the circular horn antennas.....	89
5.1 The designed quadratic shaped woodpile EBG model and structure.....	93
5.2 Configuration and prototype of rectangular horn antenna with two side-wing slabs	95
5.3 Directivity of a circular horn as a function of aperture diameter and for different axial horn lengths (Balanis, 2005)	97
5.4 Configuration and prototype of circular horn antenna with two side-wing slabs	99
5.5 The structure and prototype of a Type-D rectangular horn.....	102
5.6 Simulated result of reflected power (S_{11}) of a Type-D rectangular horn with PEC arm.....	104
5.7 Simulated VSWR of a Type-D rectangular horn with PEC arm	104
5.8 Simulated radiation patterns of a Type-D rectangular horn with PEC arm.....	105
5.9 Comparison of radiation patterns of a Type-D rectangular horn with and without PEC arm.....	106

LIST OF FIGURES (Continued)

Figure	Page
5.10 Measured reflected power (S_{11}) of the prototype of a Type-D rectangular horn	108
5.11 Measured VSWR of the prototype of a Type-D rectangular horn.....	109
5.12 Measured input impedance of the prototype of Type-D rectangular horn	110
5.13 Comparison between simulated and measured results of reflected power (S_{11}) for the prototype of a Type-D rectangular horn.....	111
5.14 Comparison between simulated and measured results of VSWR for the prototype of a Type-D rectangular horn	112
5.15 Measured bandwidth of the prototype of Type-D rectangular horn	114
5.16 Measurement set up for the radiation pattern of the prototype of Type-D rectangular horn	116
5.17 The radiation pattern of the prototype of Type-D rectangular horn	118
5.18 Gain measurement of a conventional rectangular horn antenna.....	121
5.19 Gain measurement of the prototype of Type-D rectangular horn.....	122
5.20 The structure and prototype of a Type-D circular horn	125
5.21 Simulated result of reflected power (S_{11}) of a Type-D circular horn with PEC arm.....	127
5.22 Simulated VSWR of a Type-D circular horn with PEC arm.....	127

LIST OF FIGURES (Continued)

Figure	Page
5.23 Simulated radiation patterns of a Type-D circular horn with PEC arm.....	128
5.24 Comparison of radiation patterns of a Type-D circular horn with and without PEC arm.....	129
5.25 Measured reflected power (S_{11}) of the prototype of a Type-D circular horn.....	131
5.26 Measured VSWR of the prototype of a Type-D circular horn	132
5.27 Measured input impedance of the prototype of Type-D circular horn.....	133
5.28 Comparison between simulated and measured results of reflected power (S_{11}) for the prototype of a Type-D circular horn	134
5.29 Comparison between simulated and measured results of VSWR for the prototype of a Type-D circular horn.....	135
5.30 Measured bandwidth of the prototype of Type-D circular horn.....	136
5.31 Measurement set up for the radiation pattern of the prototype of Type-D circular horn.....	138
5.32 The radiation pattern of the prototype of Type-D circular horn.....	140
5.33 Gain measurement of the prototype of Type-D circular horn	142
A.1 The AN/TPQ-36 firefinder weapon locating radar	154

CHAPTER I

INTRODUCTION

1.1 Background of Problems and Significance of the Study

A horn antenna is widely used as antenna at Ultra-High Frequency (UHF) and microwave frequency, above 300 MHz (Maagt *et al.*, 2003; Bevilaqua, 2011), a type of aperture antenna, which provides the moderately high gain as compared to the other antennas. It consists of a flaring metal waveguide shaped like a horn to direct electromagnetic waves in a beam which often have a directional radiation pattern with a high antenna gain, range up to 25 dB in some cases and with 10-20 dB being typical. Consequently, the horn antenna is widely applied for various tasks. A horn antenna has been used in many applications, such as satellite communications, radio astronomy, radar or remote sensing (Love, 1974; Olver *et al.*, 1994). They are used as feeders for larger antenna structures, as standard calibration antennas to measure the gain of other antennas, and as directive antennas (Bakshi *et al.*, 2009; Poole, 2010). Their widespread applicability stems from their simplicity in construction, ease of excitation, versatility, large gain, and preferred overall performance (Constantine, 2005). Applications requiring high gain antenna such as the parabolic reflector can be applied with the horn antenna to enhance the higher gain. Therefore, this research presents a study of new technique, Electromagnetic Band Gap (EBG), to improve their gain for the conventional rectangular and circular horn antennas instead of construction enlargement. The gain enhancement synthesis method for EBG structures when the electromagnetic fields are transferred from aperture of a horn

antenna through EBG structures is presented. By employing, EBG structures are able to eliminate the drawbacks of conducting ground-planes, to prevent the propagation of surface waves, to lower the device profiles, and to improve the performances of antennas, enhancing their directivity and the radiation efficiency (Gonzalo, Maagt, and Sorolla, 1999; Thevenot *et al.*, 1999; Yang and Rahmat-Samii, 2003). Moreover, they can be formed from dielectric structures that are periodic in one or more dimensions (Yang and Rahmat-Samii, 2009). They are creating new possibilities for controlling and manipulating the flow of electromagnetic waves. Also, this research designs to simulate and fabricate a horn antenna with EBG structures based on low loss alumina materials at dominant frequency of 10 GHz, and specify the scope of its utilization for short range radar (SRR) of X-band radar and I-band beyond following the Institute of Electrical and Electronics Engineers (IEEE) and the International Telecommunication Union (ITU), respectively.

1.2 Research Objectives

The objectives of this research are as follows:

1.2.1 To study the method to design and develop the rectangular and circular horn antennas and the EBG structures for applying to improve a horn antenna gain.

1.2.2 To study the proposed concept, the rectangular and circular horn antennas associated with the EBG structures will be designed and simulated by using the Computer Simulation Technology (CST) software.

1.2.3 To implement and experiment the antenna models to validate the developing analysis tool at 10 GHz.

1.3 Scope of the Study

The study of the technique to enhance the gain of the conventional rectangular and circular horn antennas by using woodpile EBG structures are presented. The gain enhancement synthesis method for shaped woodpile EBG that transfers the electromagnetic fields from aperture of a horn antenna through woodpile EBG is presented by using the variety of shaped woodpile EBGs such as planar, triangular, quadratic, circular, gaussian, cosine, and squared cosine structures. The licensed CST software is utilized to investigate and design all of them. To verify the performance of the antennas, the prototypes have been fabricated at dominant frequency of 10 GHz. These proposed antennas are tested experimentally to validate the developing analysis tool.

1.4 Expected Benefits

1.4.1 To obtain the conventional high gain horn antennas for applying to the X-band radar and I-band beyond following the IEEE and the ITU, respectively.

1.4.2 To obtain the antenna prototypes at 10 GHz.

1.5 Thesis Organization

The remainder of this thesis is organized as follows. Chapter 2 presents a development of horn antennas to improve the gain and performance. Then, this section investigates the EBG study of type, design, and application of each type is presented.

Chapter 3 describes the concept and configuration of conventional horn antennas for applying to the X-band radar and I-band and then, presents theory and principle of analysis and design of the EBG structures.

Chapter 4 provides the investigation and design of the conventional rectangular and circular horn antennas associated with woodpile EBG structures to improve the gain and radiation pattern characteristics, controlling the half-power beamwidth (HPBW) symmetrically in the E-plane and H-plane, and demonstrates the simulated results by using the licensed CST software to confirm the proposed concept.

In Chapter 5, experimental setup and the obtained results are presented. The prototype antennas have been designed and developed, and the manufacturing process is described. Then, the prototype antennas are tested in an outdoor and the obtained results are compared with simulated results.

In last chapter, Chapter 6 provides conclusion of the research work and suggestion for further study.

CHAPTER II

LITERATURE REVIEW

2.1 Introduction

This chapter presents the literature review for the proposed research. The basic concept and development of horn antennas are presented. In addition, a generalized study of the EBG structures is also presented. While the conclusion will be presented in the last section of this chapter.

2.2 Development of A Horn Antenna

The first horn antenna was constructed in 1897 by Indian radio researcher Jagadish Chandra Bose in his beginning experiments with microwaves (Emerson, 1997; Rodriguez, 2010). Figure 2.1 shows the microwave apparatus at the Bose Institute, Kolkata, India. The receiver used a galena crystal detector inside a horn antenna and galvanometer to detect microwaves (<http://en.wikipedia.org>). In the 1930s the first experimental research (Southworth and Barrow, 1936) and theoretical analysis (Barrow and Chu, 1939) of horns as be antennas were done. From the development of radar in World War II, the horn researches have been encouraged to design the feed horns for radar antennas as shown in Figure 2.2. A type of antenna that combines a horn with a parabolic reflector is the Hogg or horn reflector antenna, invented by Alfred C. Beck and Harald T. Friis in 1941 and further developed by David C. Hogg at Bell labs in 1961. It consists of a horn antenna with a reflector mounted in the mouth of the horn at a 45 degree angle so the radiated beam is at right

angles to the horn axis. The advantage of this design is that the horn shields the antenna from radiation coming from angles outside the main beam axis, so its radiation pattern has very small side lobes. Nevertheless, it is far larger and heavier for a given aperture area than a parabolic dish and must be mounted on a cumbersome turntable to be fully steerable. This design was used for a few radio telescopes and communication satellite ground antennas during the 1960s. Its largest use, however, was as fixed antennas for microwave relay links in the AT&T Long Lines microwave network. Probably the most photographed and well-known example is the 15 m long Holmdel Horn Antenna at Bell Labs in Holmdel, New Jersey, with which Arno Penzias and Robert Wilson discovered cosmic microwave background radiation in 1965, for which they won the 1978 Nobel Prize in Physics as shown in Figure 2.3. From Figure 2.4 shows large about 54 m (177 ft.) horn antenna at AT&T facility in Andover, Maine, USA, used in 1960s to communicate with the first direct relay satellite communications (http://en.wikipedia.org/wiki/Horn_antenna).

In addition, horn antennas widespread applicability stems from their simplicity in construction, ease of excitation, versatility, large gain, and preferred overall performance. The insertion of a thin metallic strip into a horn is briefly discussed (Silver, 1949). The metallic strip is reported to improve the plane directivity of a horn, but it is suggested that mismatch problems make the technique impractical. There are a wide variety of horn antenna applications such as the corrugated horn, which invented by Kay in 1962, is used as a feed horn for microwave antennas such as satellite dishes and radio telescopes as shown in Figure 2.5. Moreover, techniques for improving the performance of a wide-flare pyramidal horn antenna, metallic baffles are placed inside the horn near its throat the antenna's performance is

improved significantly (Koerner and Rogers, 2000). The metal baffles are simple planar structures that reduce phase curvature at the aperture like as a lens. However, the disadvantages of metallic are heavy, bulky and not easy to integrate with monolithic microwave integrated circuits (MMICs) components. The smooth-walled conical horn (SWCH), by virtue of its desirable qualities such as high gain, construction simplicity and ease of excitation, is used as a standard gain antenna, as a feed for reflectors and in polarization diversity systems (Rodriguez, 2010). On the other hand, its poor pattern symmetry and high cross-polar radiation level make it unsuitable for high performance applications. Much research has been devoted to high performance conical horns such as corrugated horn, lens corrected horn and multimode horn (Clenet and Shafai, 2000). These horns, however, in general impose construction difficulties, and are often heavy, bulky and costly.

Wongsan *et al.* (2012) presented an additional Electromagnetic Band Gap (EBG) to improve the gain of a rectangular horn antenna by using woodpile EBG structures, transfer the power from its aperture through EBG structures. The EBG structures are able to eliminate the drawbacks of conducting ground-planes, to prevent the propagation of surface waves, to lower the device profiles, and to improve the performances of antennas such as enhancing their directivity and the radiation efficiency. Therefore, this research presents a study of the technique to enhance the gain of a conventional rectangular and circular horn antennas by using an EBG structure.

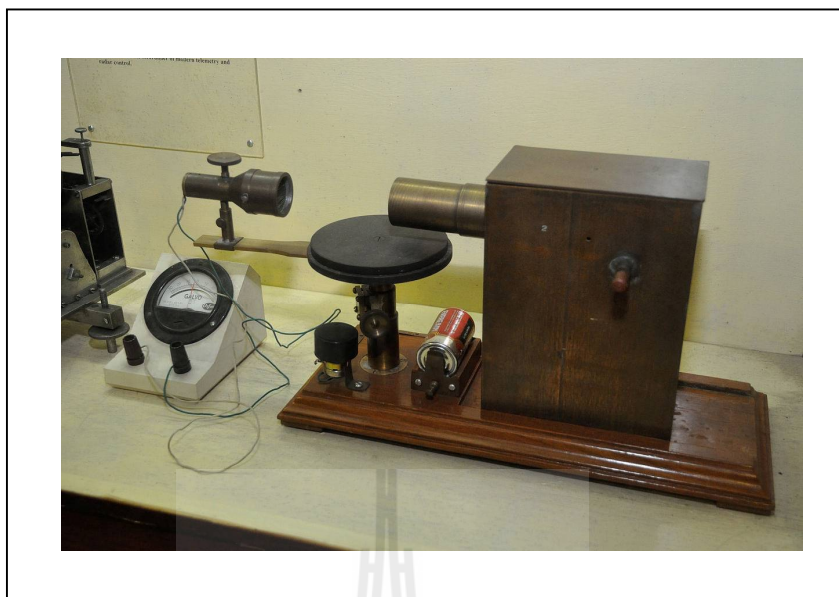


Figure 2.1 The first horn antenna as the microwave apparatus at the Bose Institute, Kolkata, India (<http://en.wikipedia.org>).

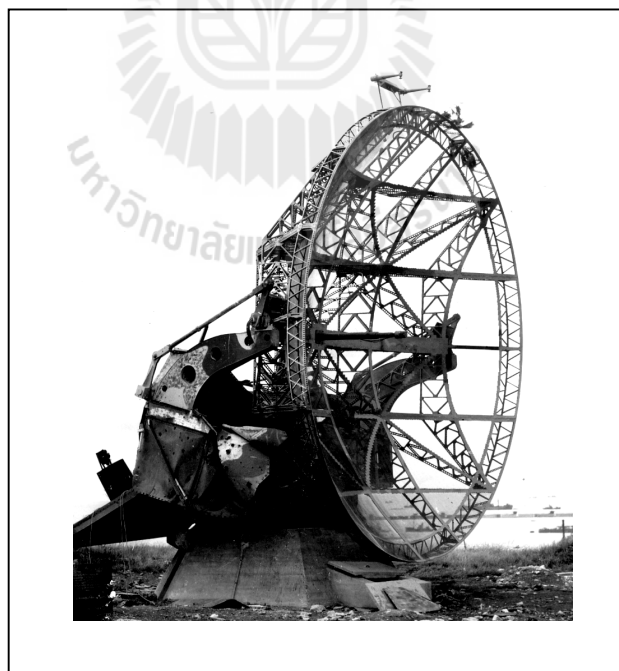


Figure 2.2 Feed horns for radar antennas in World War II
(<http://prezi.com/w2ximutsy5c9/horn-antenna/>).

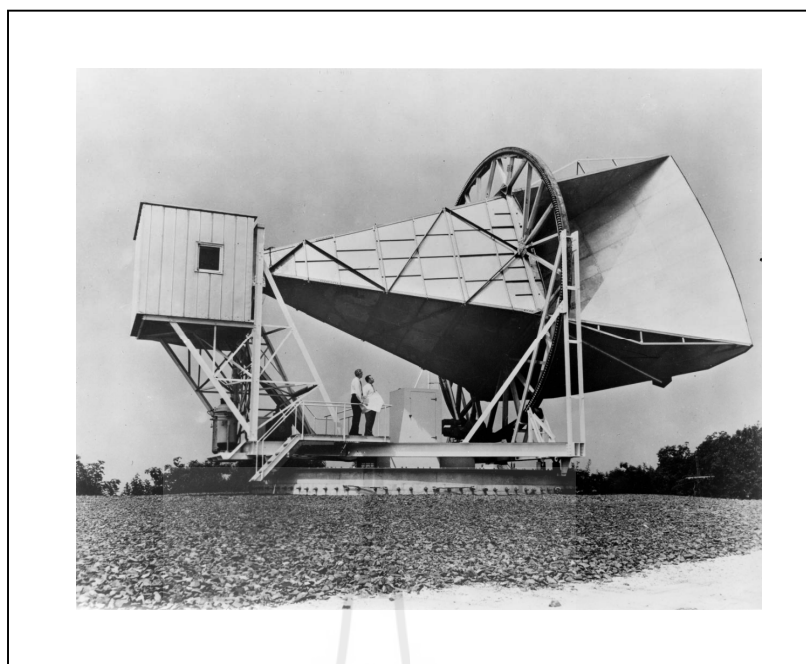


Figure 2.3 Holmdel Horn Antenna (<http://en.wikipedia.org>).



Figure 2.4 A large 177 ft. horn antenna (<http://en.wikipedia.org>).



Figure 2.5 The corrugated horn (Kay, 1962)

(<http://prezi.com/w2ximutsy5c9/horn-antenna/>).

2.3 Electromagnetic Band Gap

EBG technology, one of the most rapidly advancing materials in the electromagnetic arena, has become a significant breakthrough in the radio frequency (RF) and microwave applications due to their unique band gap characteristics at certain frequency ranges that is not possible earlier (Yang *et al.*, 2005; Alam *et al.*, 2013). The unique electromagnetic properties of EBG structures have led to a wide range in antenna engineering applications. In this section, we summarize several typical EBG applications in antenna designs (Yang and Rahmat-Samii, 2009).

2.3.1 Antenna Substrates for Surface WaveSuppressions

In free space, the electromagnetic waves propagation along the ground plane instead of radiation, the antenna gain and efficiency, were reduced by the surface waves. The diffraction of surface waves increases the back lobe radiations, which may deteriorate the signal to noise ratio in wireless communication systems. The EBG structures have found beneficial applications in suppressing the surface waves in various antenna design. By employing, EBG structures as substrates (Coccioli *et al.*, 1999; Colburn and Rahmat-Samii, 1999; McKinzie III *et al.*, 2002), they are able to eliminate the drawbacks of conducting ground-planes, to prevent the propagation of surface waves, to reduce the back lobes, and to improve the performances of antennas, enhancing their directivity and the radiation efficiency. Figure 2.6 shows a patch antenna on the Photonic Band Gap (PBG) substrate where four columns of holes have been added in order to suppress the surface mode (Gonzalo, Maagt, and Sorolla, 1999). The results show that the levels of surface plots of a patch antenna on the PBG substrate have been reduced when compare to a conventional patch antenna. Moreover, the surface waves not only increase the back lobe radiations but also raise the mutual coupling levels in array antenna design. Yang and Rahmat-Samii (2003) presented a comparison of patch antennas with and without EBG structures as shown in Figure 2.7. They found that it can reduce the mutual coupling around 8 dB.

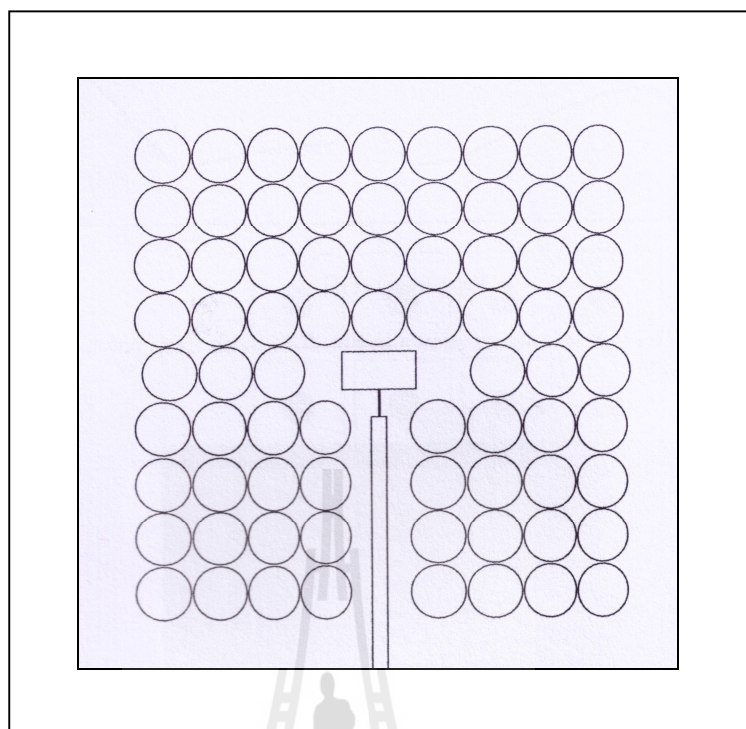


Figure 2.6 A patch antenna on the PBG substrate formed by four holes in a square lattice (Gonzalo, Maagt, and Sorolla, 1999).

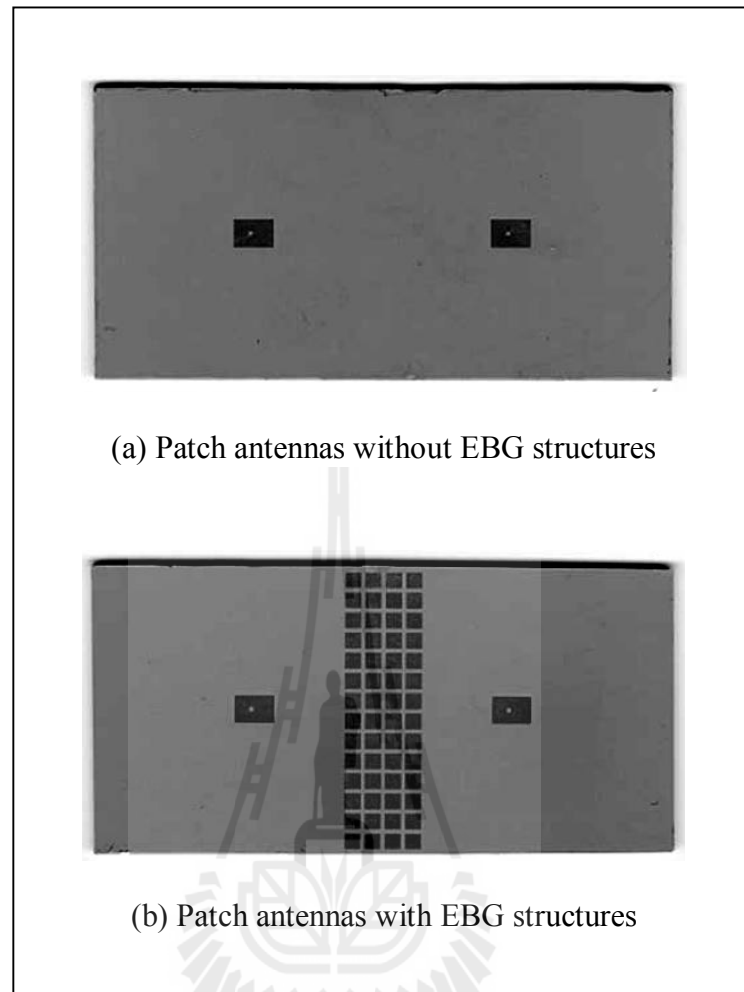


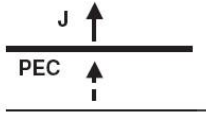
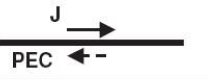
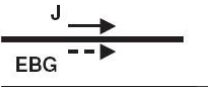
Figure 2.7 EBG substrate for reducing the mutual coupling levels on patch antennas (Yang and Rahmat-Samii, 2003).

2.3.2 Antenna Substrates for Efficient Low Profile Antenna Design

To demonstrate the fundamental principle of antenna designs, Table 2.1 shows the comparison of the EBG structures and the perfect electric conductor (PEC) ground plane in wire antenna designs. When an electric current is vertical to a PEC ground plane, the image current (J) has the same direction and support the radiation from the original current so that this antenna has good radiation efficiency. However, it complains of the relative large antenna height due to the vertical

placement of the current. To achieve a low profile configuration, we can position a wire antenna horizontally close to the ground plane, but the radiation efficiency is poor because of the opposite of image current and original current. In contrast, the EBG surface is capable of providing a constructive image current within a certain frequency band, resulting in good radiation efficiency. Therefore, the EBG structures exhibit a great potential for low profile efficient wire antenna applications (Yang and Rahmat-Samii, 2009).

Table 2.1 The comparison of the EBG and the PEC ground planes.

Direction of current	Efficiency	Low profile
	✓	✗
	✗	✓
	✓	✓

From this fundamental principle concept, there are many various antennas that have been constructed on the EBG ground plane (Li and Rahmat-Samii, 2000; Yang and Rahmat-Samii, 2003). Figure 2.8 shows a curl antenna on an EBG structures, which radiates circularly polarized radiation patterns (Yang and Rahmat-Samii, 2001). A curl antenna with only 0.06λ height has been simulated, and it provides a good axial ratio of less than 3 dB. Moreover, Yang and Rahmat-Samii (2005) presented a single dipole antenna with the aid of a rectangular patch loaded

grounded slab that can generate circularly polarized radiation patterns as shown in Figure 2.9. This complex artificial ground plane exhibits an in-phase reflection coefficient that helps the dipole to obtain a good return loss with a low profile configuration, while the polarization dependent feature of the reflection phase is used to convert the linear polarization of the single dipole to the circular polarization.

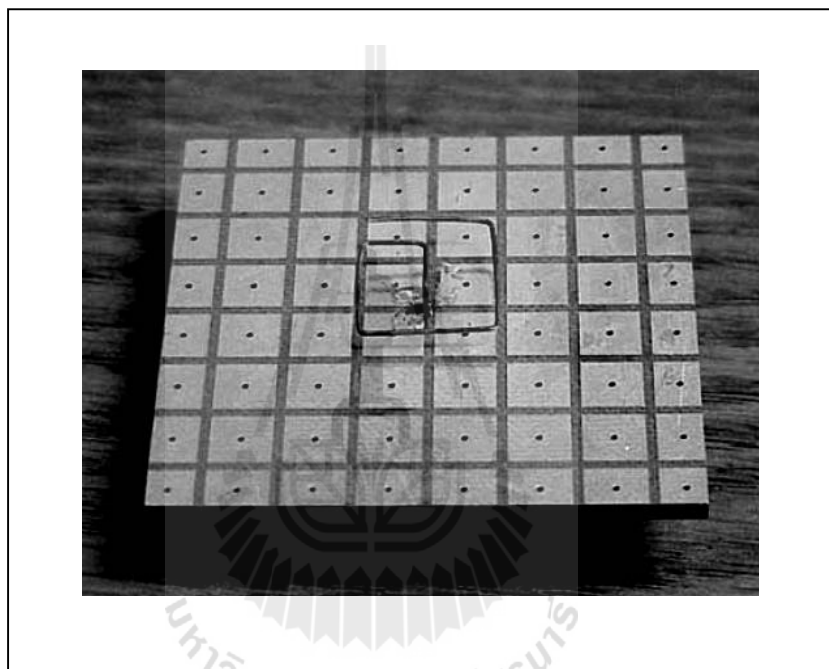


Figure 2.8 A curl antenna on an EBG structures (Yang and Rahmat-Samii, 2001).

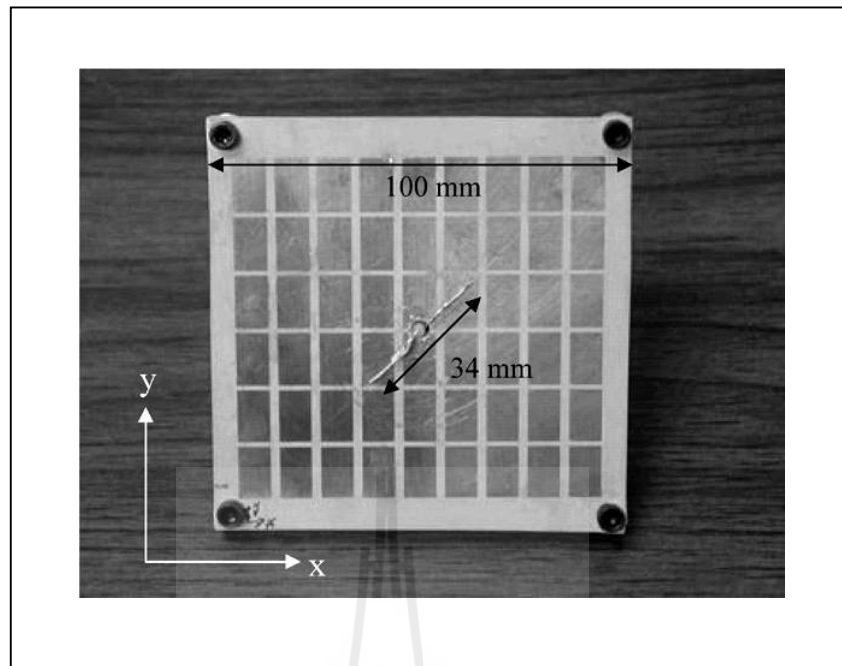


Figure 2.9 A dipole antenna that radiates circularly polarized patterns (Yang and Rahmat-Samii, 2005).

2.3.3 Reflection/Transmission Surface for High Gain Antenna

In the past, the conventional high gain antennas are realized using either parabolic antennas or large antenna arrays. Nevertheless, the curved surface of parabolic antennas makes that it is difficult for them to be conformal, while a lot of elements in the antenna arrays which causes the dimension of antenna is too long and its weight is too heavy. Furthermore, the great number of electromagnetic energy will be lost inside the feeding network. Weily *et al.* (2005) presented a high gain resonator antenna design using a woodpile EBG structures, they found that a 19 dBi antenna gain is obtained in this design as shown in Figure 2.10.

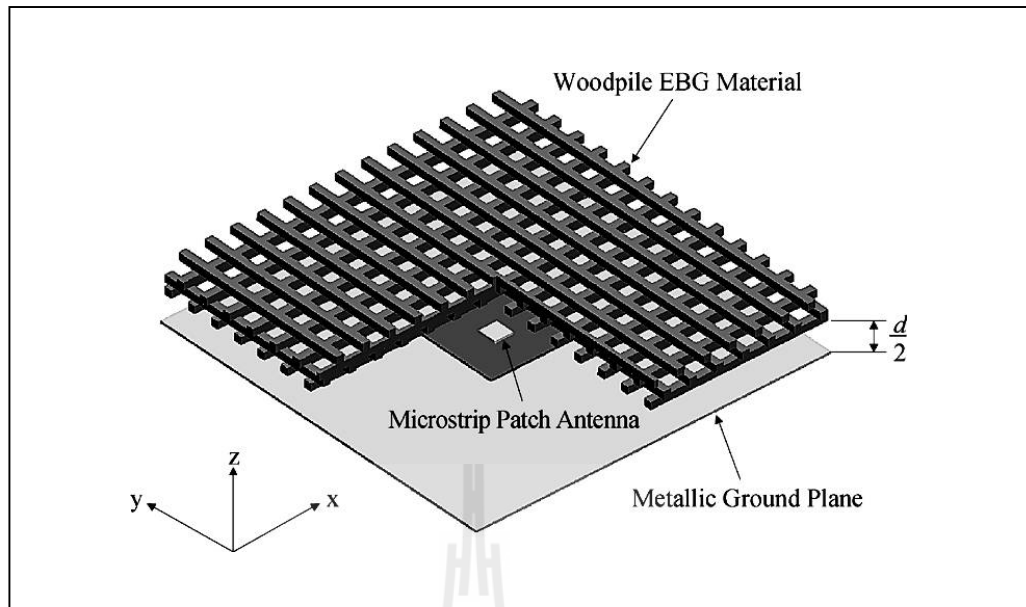


Figure 2.10 A high gain antenna design using the woodpile EBG structures
(Weily *et al.*, 2005).

From this concept, this research presents a study of technique for enhancement the gain of a conventional rectangular and circular horn antennas by using the proper shaped of woodpile EBG structures, as the additional resonant circuit which installed in front of the horn antennas, such as planar, triangular, quadratic, circular, gaussian, cosine, and squared cosine structures. They are creating new possibilities for controlling and manipulating the flow of electromagnetic waves.

2.4 Chapter Summary

This chapter mentioned a detail and literature surveys of development of a horn antenna. Basically, description of the first horn antenna at the Bose Institute, Kolkata, India, is used as the microwave apparatus. After the development of radar was started in World War II, the horn researches have been encouraged to design feed horns for radar antennas. Moreover, horn antennas widespread applicability stems from their simplicity in construction, ease of excitation, versatility, large gain, and preferred overall performance. Then, Wongsan *et al.* (2012) presented an additional the woodpile EBG structures, as the resonant circuit, which installed in front of horn antenna, to improve the gain. The EBG structures have been investigated for improving performances of numerous RF and microwave devices utilizing the surface wave suppression and the AMC properties of these special types of metamaterials.

CHAPTER III

BACKGROUND THEORY

3.1 Introduction

In this chapter, we describe the theory and principle of horn antenna, one type of aperture antennas, that is the most common at microwave frequencies. There are many different geometrical configurations of horn antenna with rectangular and circular of the most popular will be discussed in more details in section 3.2. Additionally, the EBG structures are examined in section 3.3. This section addresses definition of EBG structures, relation between EBG and metamaterials, analysis methods for EBG structures, and woodpile EBG structures. In the last section of this chapter, the conclusion will be presented.

3.2 Horn Antenna

A horn antenna is one of the simplest and probably the most widely used for microwave antenna, especially as a feed element for large radio astronomy, satellite tracking, and communication dishes. Furthermore, its utility as a feed for reflectors and lenses, it is a common element of phased arrays and serves as universal standard for calibration and gain measurements for other high-gain antenna (Constantine, 2005).

A horn antenna consists of a flaring metal waveguide shaped like a horn to direct the radio waves in a beam. It can have different flare angles in the E-field and H-field directions, making possible a wide variety of different beam profiles.

The important dimensions of the horn antenna are horn length, aperture area, and flare angle. The length of a typical horn is usually 2λ to 15λ at the operating frequency, while the longer horns more difficult to mount and work with provide higher gain and better directivity. In addition, the aperture area is the area of the rectangle formed by the opening of the horn and simply the product of the height and width of the horn. The greater this area can offer the higher gain and directivity. The flare angle also affects gain and directivity. The typical flare angle is varied from about 20° to 50° . To increase the flare angle of horn antenna, can increase the aperture area. Each of these dimensions is adjusted to achieve the desired design objective.

An important aspect of a microwave antenna is its bandwidth. The most antennas have a narrow bandwidth because they are resonant at only a single operating frequency. Therefore, the dimension of their antennas will be use to determine their operating frequency. Bandwidth is an important consideration at microwave frequencies because the spectrum transmitted on the microwave carrier is usually wide, so that a considerable amount of information can be carried (<http://www.intechopen.com/books/data-acquisition-applications/microwave-antenna-performance-metrics>). A horn antenna has relatively large bandwidth since it is essentially non-resonant or periodic which means that it will operate over a wide frequency range (Frenzel, 1996).

3.2.1 Types of Horn Antenna

These are the common types of horn antenna. The horns can take many different forms, which are classified into two major types such as rectangular and circular horns. Figure 3.1 shows types of horn antenna such as pyramidal horn, sectoral E-plane horn, sectoral H-plane horn, conical horn, and exponential horn. The pyramidal horn is a rectangular horn antenna with in the shape of a four-sided pyramid, with a rectangular cross section. They are a common type, used with rectangular waveguides, and radiate linearly polarized radio waves (Bakshi *et al.*, 2009). The sectoral horn is a pyramidal horn with only one pair of sides flared and the other pair parallel. It produces a fan-shaped beam, which is narrow in the plane of the flared sides, but wide in the plane of the narrow sides. These types are often used as feed horns for wide search radar antennas. There are two types of sectoral horn such as (1) E-plane horn, a sectoral horn flared in the direction of the electric or E-field in the waveguide and (2) H-plane horn, a sectoral horn flared in the direction of the magnetic or H-field in the waveguide. The conical horn is a circular horn in the shape of a cone and has a circular cross section. They are used with cylindrical waveguides. The exponential horn is a circular horn with curved sides, in which the separation of the sides increases as an exponential function of length. Also called a scalar horn, they can have pyramidal or conical cross sections. The exponential horns have minimum internal reflections, and almost constant impedance and other characteristics over a wide frequency range. They are used in applications requiring high performance, such as feed horns for communication satellite antennas and radio telescopes (http://en.wikipedia.org/wiki/Horn_antenna).

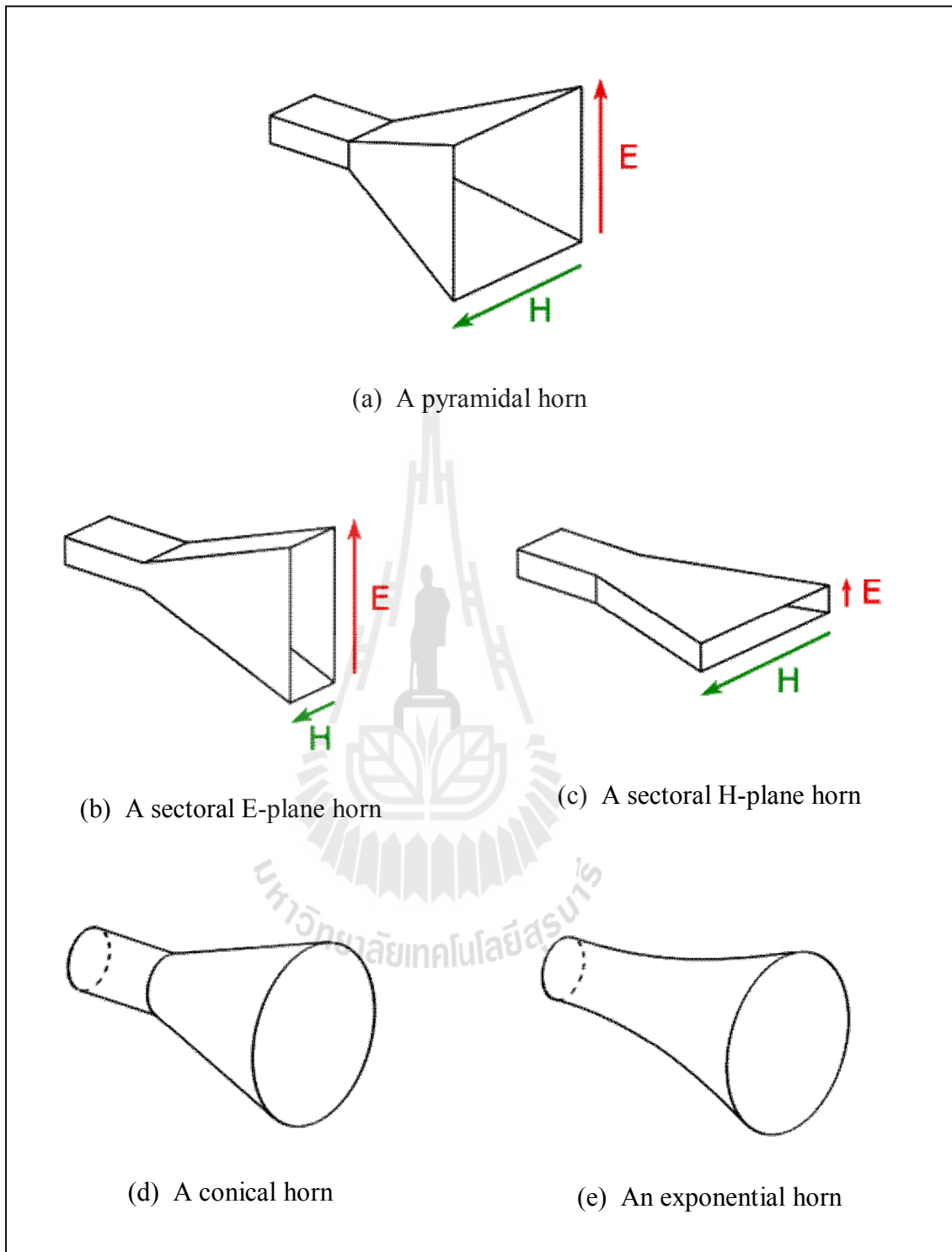


Figure 3.1 Typical horn antenna configurations (<http://en.wikipedia.org>).

3.2.2 Waveguide Feeding

The horn antennas are typically fed by a section of waveguide, which is a hollow conductive metal pipe used to carry electromagnetic waves, high frequency radio waves and particularly microwaves. The geometry of a waveguide reflects its function, such as rectangle and cylinder, that depends on its application, as shown in Figure 3.2. The rectangular horns are ideally suited for rectangular waveguide feeders. The horn acts as a gradual transition the electromagnetic wave from a waveguide mode to a free-space mode. If the feeder is a cylindrical waveguide, the antenna is usually a circular horn. It is necessary to consider the horns separately instead of applying the waveguide aperture antennas directly because of the phase error occurs due to the difference between the lengths from the center of the feeder to the center of the horn aperture and the horn edge. This makes the uniform-phase aperture results invalid for the horn apertures (Nikolova, 2010). A waveguide can be made from copper or alumina, which inside surfaces are enameled with silver to be a perfect conductor. In addition, a waveguide itself is often fed with a short monopole. In the case of the rectangular waveguide as shown in Figure 3.3, the length of a rectangular waveguide is $3\lambda_g/4$, the length of a short monopole is $\lambda_0/4$, and the backshort wall about $\lambda_g/4$ behind the short monopole ensures that the dipole sees only radiation coming from the direction of the horn opening, where λ_g is a wavelength of the signal in the guide and λ_0 is a wavelength in free space.

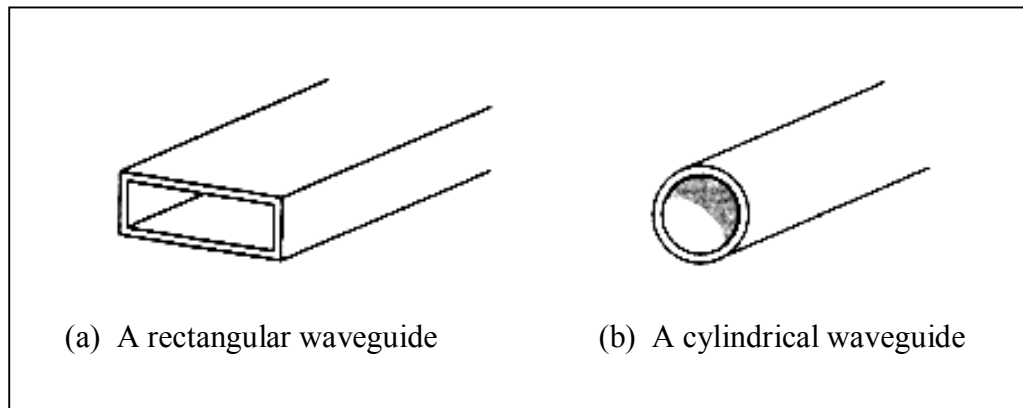


Figure 3.2 The geometry of the waveguides.

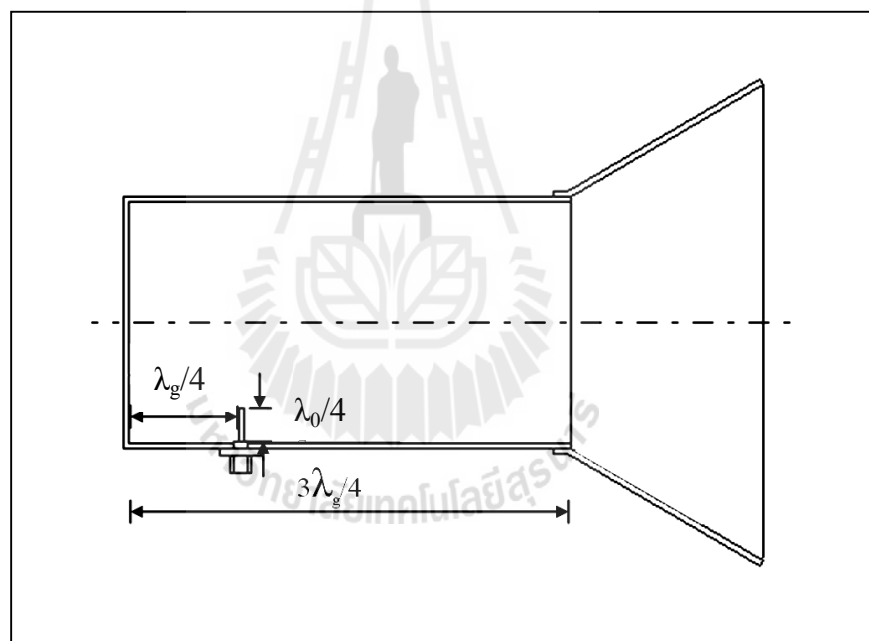


Figure 3.3 A rectangular waveguide fed with a short monopole.

3.3 Electromagnetic Band Gap Structures

This section will mention the definition of EBG structures, the relation between EBG and metamaterials, and the analysis methods for EBG structures. Moreover, the woodpile EBG structures are investigated in this section.

3.3.1 EBG Definition

The EBG structures, also known as Photonic Crystals (Joannopoulos, Meade, and Finn, 1995) or Photonic Band Gap (PBG) Materials (Yablonovitch, 1987) are periodic structures, which do not allow the propagation of electromagnetic waves with in certain frequency ranges. Generally speaking, the EBG structures are defined as “*artificial periodic (or sometimes non-periodic) objects that prevent/assist the propagation of electromagnetic waves in a specified band of frequency for all incident angles and all polarization states*” (Yang and Rahmat-Samii, 2009). The EBG structures are usually realized by periodic arrangement of dielectric material and metallic conductors. In general, they can be categorized into three groups according to their geometric configuration such as (1) one-dimensional (1D) transmission lines, (2) two-dimensional (2D) planar surfaces, and (3) three-dimensional (3D) volumetric structures.

Figure 3.4 shows the 1D EBG transmission lines design, a microstrip line with periodic holes on the ground plane (Radisic *et al.*, 1998) and a composite right-handed and left-handed transmission line (Caloz and Itoh, 2005). The 2D planar surfaces, a mushroom-like surface (Sievenpiper *et al.*, 1999) and a uni-planar design without vertical vias (Yang *et al.*, 1999), are shown in Figure 3.5. In Figure 3.6, the 3D volumetric structures are shown in two representative structures such as a

woodpile structure consisting of square dielectric bars (Ozbay *et al.*, 1994) and a multi-layer metallic tripod array (Barlevy and Rahmat-Samii, 2001).

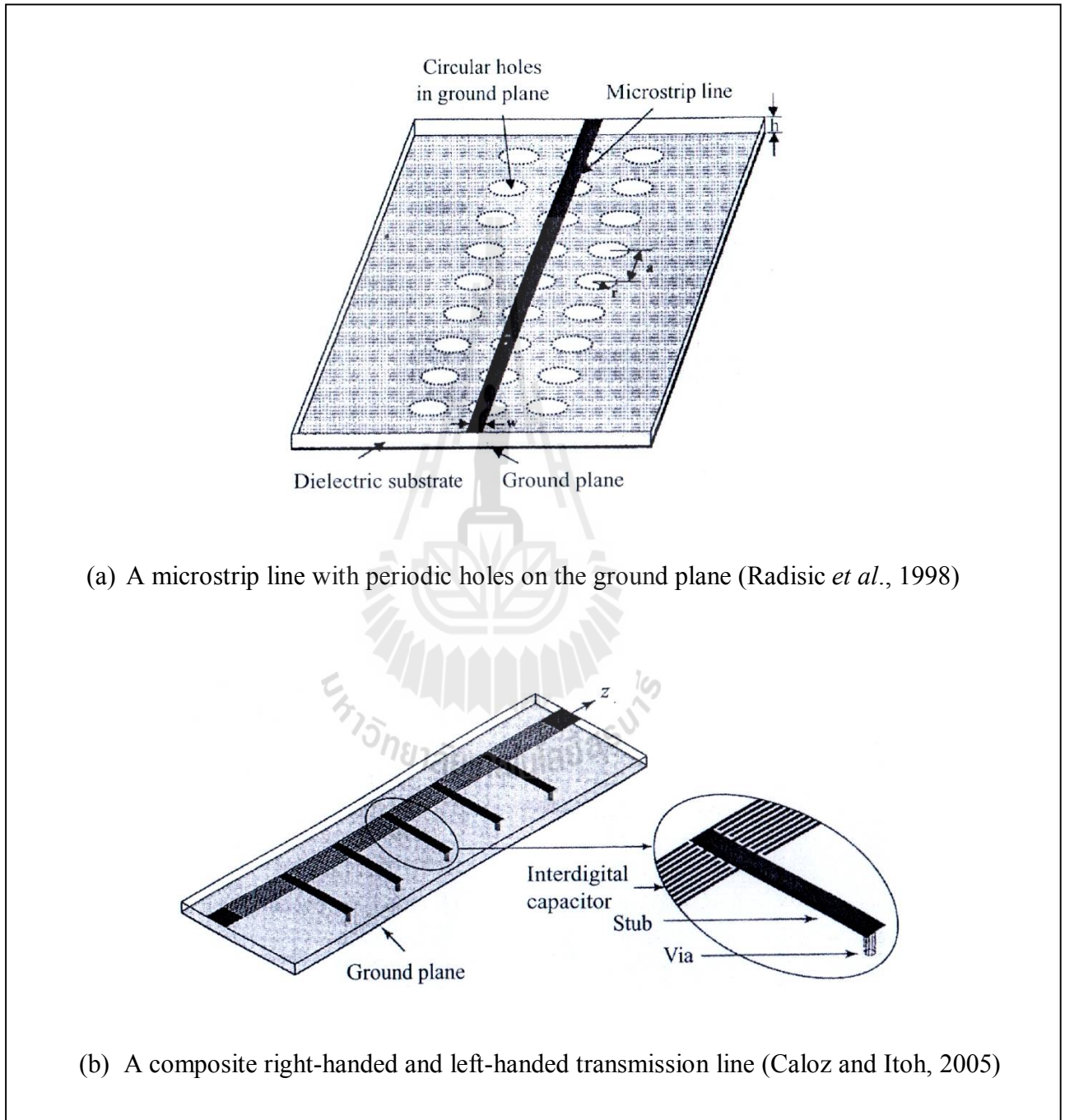


Figure 3.4 The 1D EBG transmission lines.

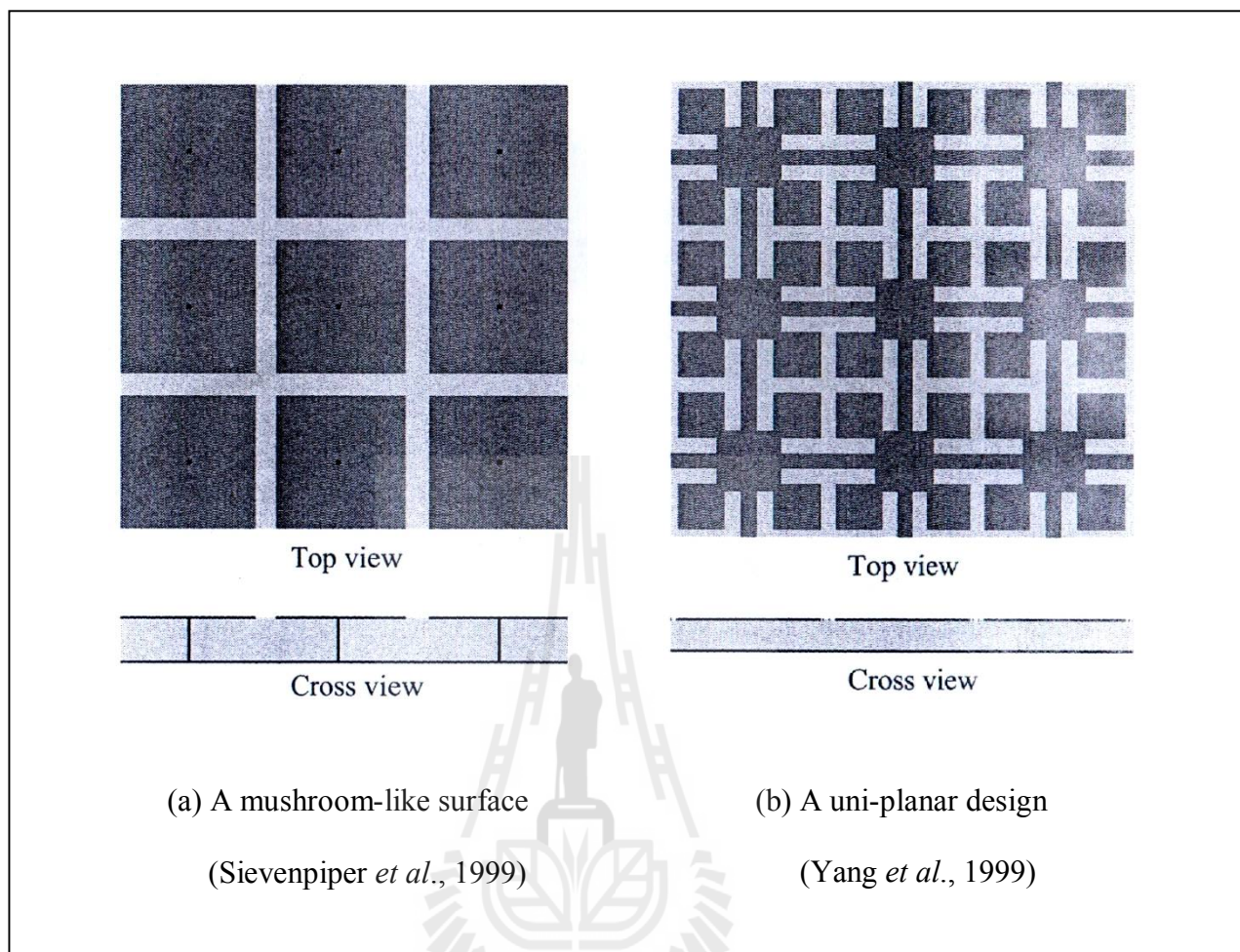


Figure 3.5 The 2D EBG planar surfaces.

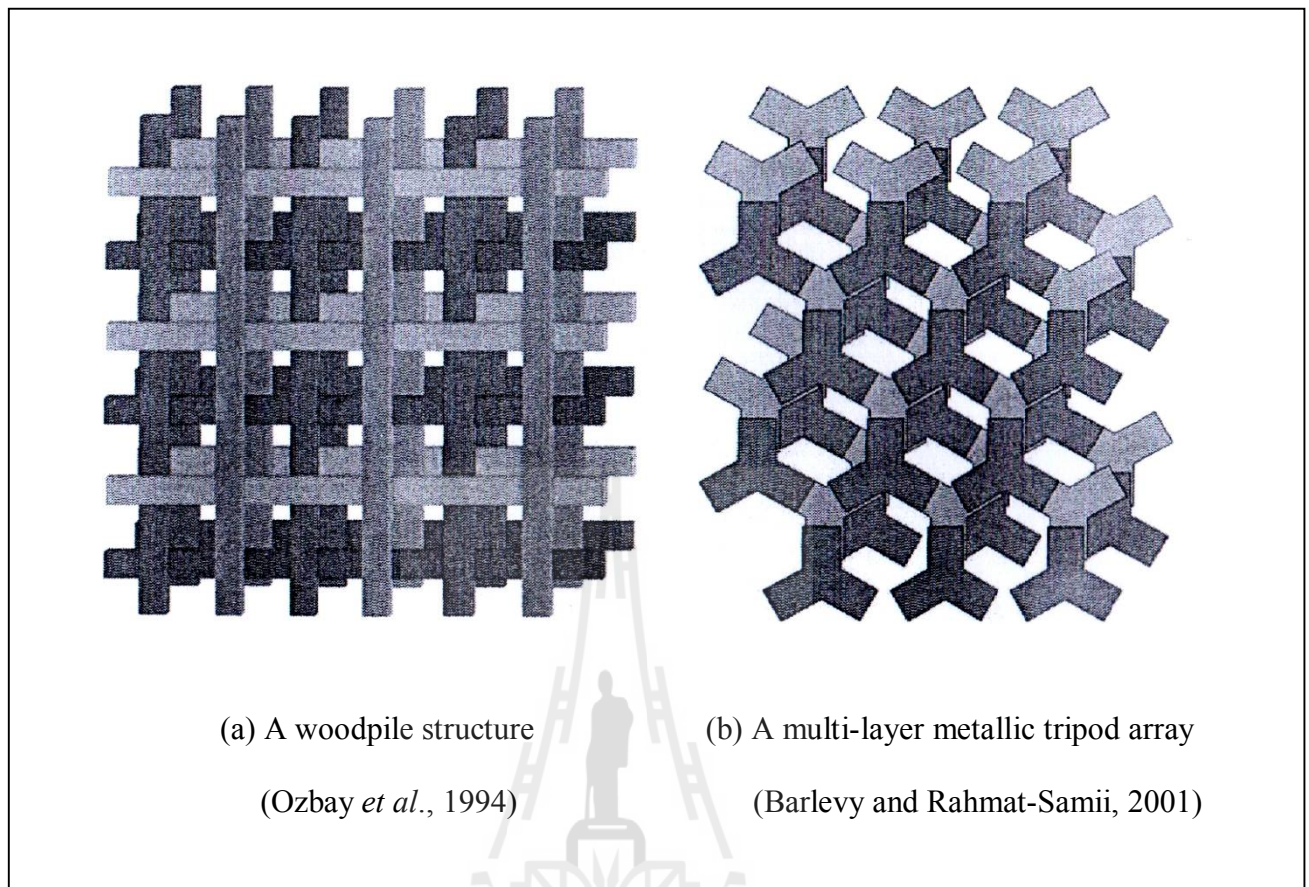


Figure 3.6 The 3D EBG volumetric structures.

3.3.2 EBG and Metamaterials

Metamaterials, materials of interest exhibit properties not found in nature such as negative index of refraction, are artificial media structure on a size scale smaller than the wavelength of external stimuli. Its research is interdisciplinary and involves fields including electrical engineering, electromagnetic, solid state physics, microwave and antenna engineering, optoelectronics, classic optics, material sciences, semiconductor engineering, and nanoscience (Zouhdi *et al.*, 2008). The electromagnetic metamaterials affect electromagnetic waves by having structural features smaller than the wavelength of the respective electromagnetic waves. To

behave as a homogeneous material accurately described by an effective refractive index, its features must be much smaller than the wavelength. Depending on the exhibited electromagnetic properties, various names have been introduced in the literature, including (Yang and Rahmat-Samii, 2009):

- Double negative (DNG) materials with both negative permittivity and permeability;
- Left-handed (LH) materials inside which the electric field (E-field) direction, magnetic field (H-field) direction, and propagation direction satisfy a left-hand relation;
- Negative refractive index (NRI) materials that have a negative refractive index;
- Magneto materials with artificially controlled high permeability;
- Soft and hard surfaces that stop or support the propagation of waves;
- High impedance surfaces with relatively large surface impedances for both TE and TM waves;
- Artificial magnetic conductors (AMC) that exhibit the same properties as a perfect magnetic conductor.

Due to their unique band gap features, EBG structures can be regarded as a special type of metamaterials. The EBG structures have the goal of creating high quality, low loss, periodic, and dielectric structures. An EBG affects photons in the same way semiconductor materials affect electrons. The EBG structures are designed to prevent the propagation of an allocated bandwidth of frequencies, for certain arrival

angles and polarizations. The various geometries and structures have been proposed to fabricate EBG special properties (Engheta *et al.*, 2006; Zouhdi *et al.*, 2008). The EBG structures have been manufactured for frequencies ranging from a few gigahertz (GHz) up to a few terahertz (THz), radio, microwave and mid-infrared frequency regions. Besides the band gap feature, EBG also possesses some other exciting properties such as high impedance and AMC. For example, a mushroom-like EBG surface exhibits high surface impedances for both TE and TM polarizations. In addition, soft and hard operations of an EBG surface have also been identified in the frequency-wave number plane. These interesting features have led to a wide range of applications in antenna engineering, from wire antennas to microstrip antennas, from linearly polarized antennas to circularly polarized antennas, and from the conventional antenna structures to novel surface wave antenna concepts and reconfigurable antenna designs (Yang and Rahmat-Samii, 2009).

3.3.3 Analysis Methods for EBG Structures

To analyze unique features of EBG structures, three categories have been implemented: (1) lumped element model, (2) periodic transmission line method, and (3) full wave numerical methods.

The lumped element model is the simplest one that describes the EBG structures as an LC resonant circuit (Sievenpiper, 1999). The values of the inductance L and capacitance C are determined by the EBG geometry and its resonance behavior is used to explain the band gap feature of EBG structures. This model is simple to understand, but the results are not very accurate because of the simplified approximation of L and C . A simple 2D planar EBG structures, the geometry is

similar to the shape of a mushroom, consists of four parts: a metal ground plane, a dielectric substrate, periodic metal patches on top of the substrate, and vertical vias connecting the patches to the ground plane (Sievenpiper *et al.*, 1999) as shown in Figure 3.7. The parameters of the EBG structure are the patch width (W), the gap width (g), the substrate thickness (h), the dielectric constant (ϵ_r), and the vias radius (r). When the periodicity ($W + g$) is small compared to the operating wavelength, the operation mechanism of this EBG structure can be explained using an effective medium model with equivalent lumped LC elements, as shown in Figure 3.8. The capacitor results from the gap between the patches and the inductor results from the current a long adjacent patches. The impedance of parallel resonant LC circuit is given by:

$$Z = \frac{j\omega L}{1 - \omega^2 LC} \quad (3.1)$$

The resonance frequency of the circuit is calculated as following:

$$\omega_0 = \frac{1}{\sqrt{LC}} \quad (3.2)$$

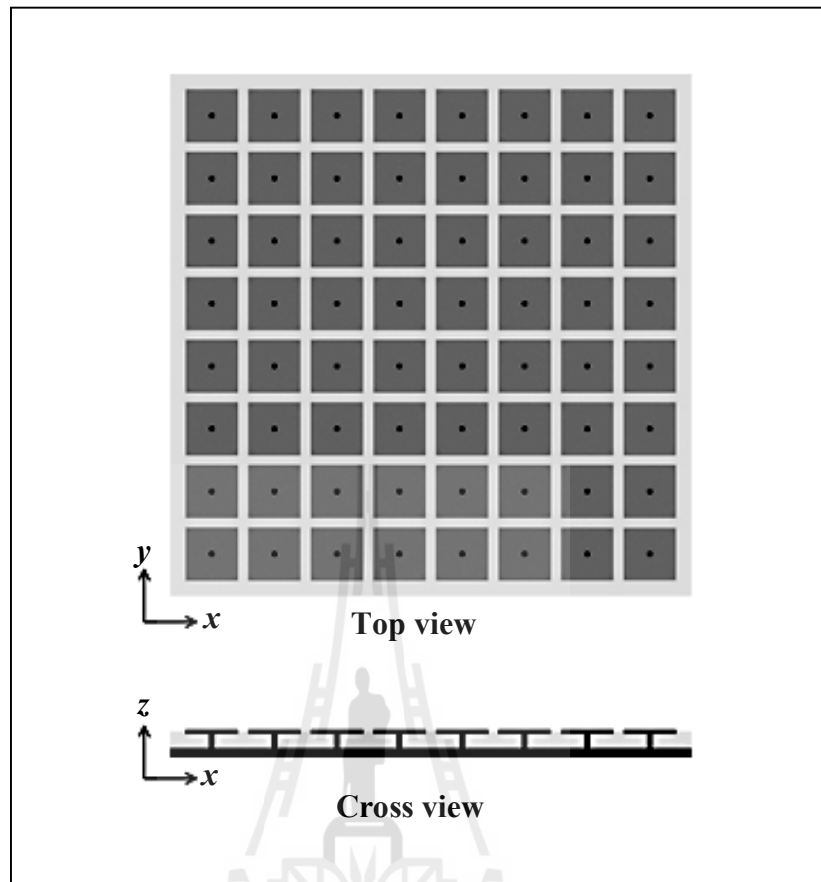


Figure 3.7 The geometry of a mushroom-like EBG structures
(Sievenpiper *et al.*, 1999).

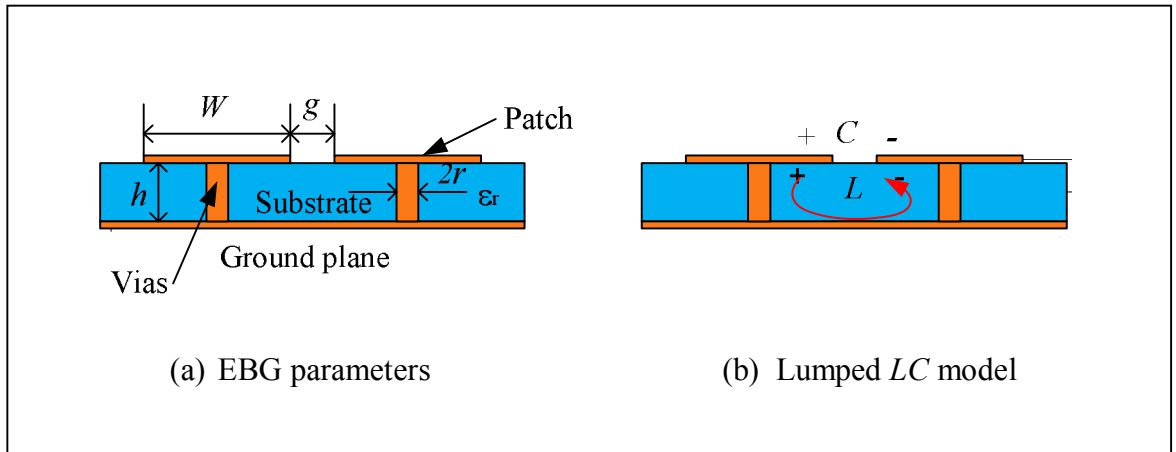


Figure 3.8 The lumped element model for the mushroom-like EBG structures.

At low frequencies, the impedance is inductive and will supports TM surface waves. Inversely, it becomes capacitive at high frequencies and TE surface waves are supported. At near the resonance frequency ω_0 , high impedance is obtained and the EBG does not support any surface waves, resulting in frequency band gap. The high surface impedance also ensures that a plane wave will be reflected without the phase reversal that occurs on a perfect electric conductor (PEC).

The value of the capacitor is given by the fringing capacitance between neighboring co-planar metal sheets. This can be derived using conformal mapping, a common technique for determining 2D electrostatic field distributions. The edge capacitance for narrow gap situation is given by the following equation (Sievenpiper, 1999):

$$C = \frac{W\epsilon_0(1+\epsilon_r)}{\pi} \cosh^{-1}\left(\frac{W+g}{g}\right). \quad (3.3)$$

The value of the inductor is derived from the current loop in Figure 3.8(b), consisting of the vias and metal sheets. The equivalent inductor is then computed from the stored H-field energy and the excitation current. The inductance is expressed as below (Sievenpiper, 1999), which depends only on the thickness of the structure and the permeability:

$$L = \mu h . \quad (3.4)$$

The periodic transmission line method is another analytical model proposed to characterize EBG structures (Rahman and Stuchly, 2001). A mushroom-like EBG structure as shown in Figure 3.7, the impedance of each section is calculated using transmission line theory, and the whole structure is then cascaded together using the theory of periodic circuit. Figure 3.9 depicts a transmission line model of EBG structures. Between two nodes of the periodic structure, there are two contributions (Z_P and X_C) to the total impedance, which Z_P is the impedance for each periodic element and X_C is the coupling capacitor. After analyzing the cascaded transmission line, the dispersion curve can be readily obtained, which provides more information than the lumped element method. A challenge in this method is how to accurately obtain the equivalent Z_P and X_C values for general EBG structures with arbitrary geometries. In addition, the surface wave modes, the leaky wave modes, the left- and right-hand regions, and the band gaps can be easily identified from the dispersion curve. However, it is not applicable for plane wave incidences.

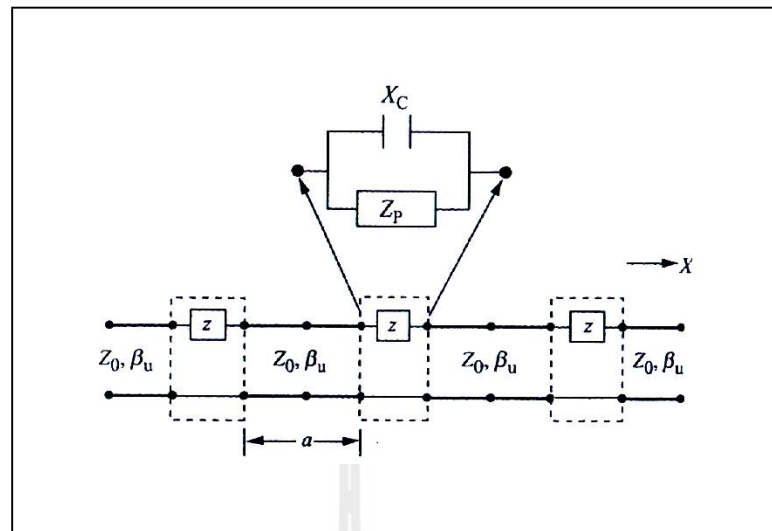


Figure 3.9 The transmission line model of EBG structures
(Rahman and Stuchly, 2001).

The full wave numerical methods, both the frequency domain methods such as the Method of Moments (MoM) and the Finite Element Method (FEM) and the time domain method like the FDTD method have been utilized by different research groups to characterize EBG structures. For instance, Figure 3.10 shows an FDTD model for the mushroom-like EBG analysis (Kim, Yang, and Elsherbeni, 2007). The computational code is based on a Cartesian grid cell with the absorbing boundary conditions (Jensen, 1994). The important advantages of the full wave numerical methods are the versatility and accuracy in analyzing different EBG geometries and the capability to the various EBG characteristics, such as the surface impedance, reflection phase, dispersion curve, and band gap.

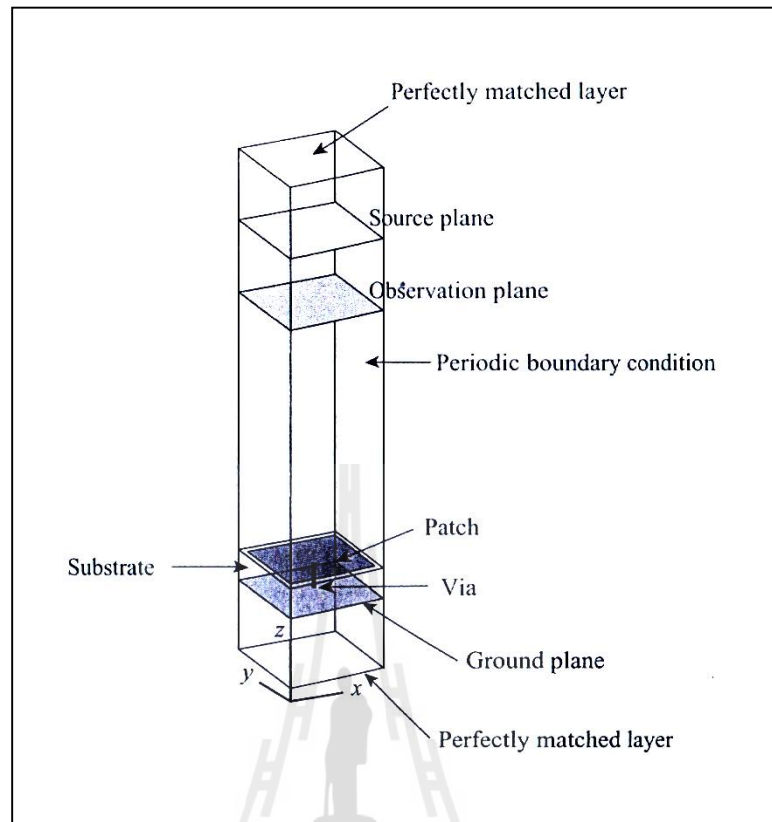


Figure 3.10 The full wave FDTD model for the EBG analysis
(Kim, Yang, and Elsherbeni, 2007).

3.3.4 Woodpile EBG Structures

In this section provides some background information of the planar woodpile EBG structures which are also referred to as a layer-by-layer photonic crystal in the physics literature. A unit cell of the planar woodpile EBG structures is defined by the lattice constant or repeat distance in the horizontal plane (a), the rod width (w), the rod height (h), and the total height of the unit cell (b) as shown in Figure 3.11. These consecutive layers are orthogonal to each other, and the parallel rods are offset from the rods two layers below by half of a lattice constant, to obtain a four layer stacking sequence. The lattice symmetry of this material is face-centered

tetragonal (FCT) from solid state physics theory. The cross section of the rods may be circular or square shape, and the inverse structure made of air rods in dielectric background also has a completed bandgap (Weily *et al.*, 2005).

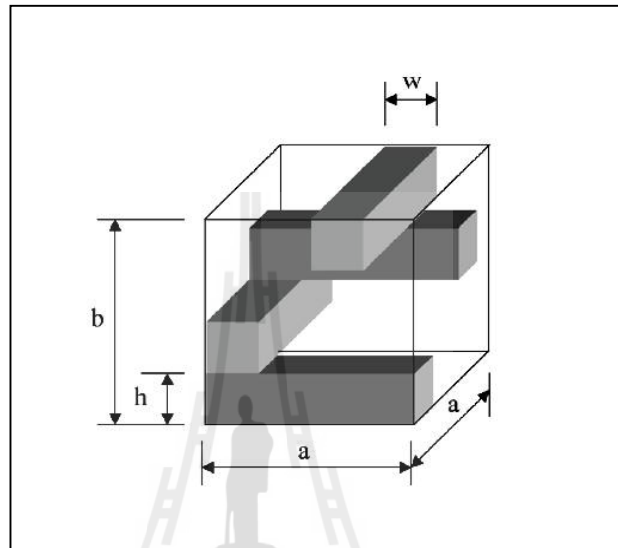


Figure 3.11 A unit cell of four layers planar woodpile EBG structures (Weily *et al.*, 2005).

From a unit cell of four layers of planar woodpile EBG structures, this research modify from four layers to one layer as shown in Figure 3.12. Besides applying one layer of planar woodpile EBG structures, we design the format of variety shaped woodpile EBG structures as follow the function of geometry (Thaiviro, Krachodnok, and Wongsan, 2008) as shown in Table 3.1, such as planar, triangular, quadratic, circular, gaussian, cosine, and squared cosine structures to enhance the gain of the conventional rectangular and circular horn antennas. They are creating new possibilities for controlling and manipulating the flow of electromagnetic waves. Also, this research designs to simulate and fabricate the horn

antennas with EBG structures based on low loss alumina materials at dominant frequency of 10 GHz, and demonstrate its utilization in a horn antenna for X-band radar and I-band beyond following the IEEE and the ITU, respectively.

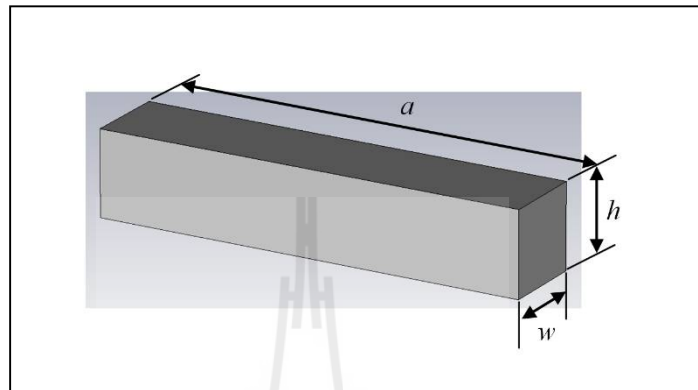


Figure 3.12 A unit cell of one layers planar woodpile EBG structures.

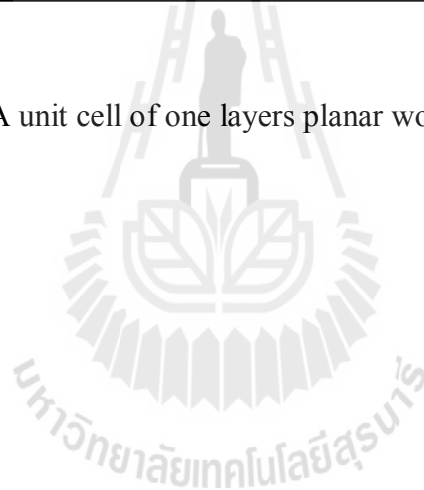
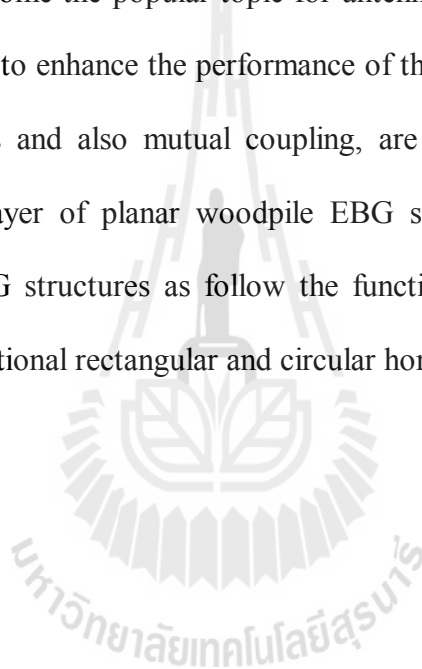


Table 3.1 Formulations of elementary geometrical function.

Distributed Function	Formulations	Shapes of EBG Structure
Planar	$f(x, y) = A$	
Triangular,	$f(x, y) = A \left(1 - \frac{2}{D} \sqrt{x^2 + y^2} \right)$	
Quadratic	$f(x, y) = A \left[1 - \left(\frac{2}{D} \sqrt{x^2 + y^2} \right)^2 \right]$	
Circular	$f(x, y) = A \sqrt{1 - \left(\frac{2}{D} \sqrt{x^2 + y^2} \right)^2}$	
Gaussian	$f(x, y) = A e^{-\left(\frac{2}{D} \sqrt{x^2 + y^2} \right)^2}$	
Cosine	$f(x, y) = A \cos \left(\frac{\pi}{D} \sqrt{x^2 + y^2} \right)$	
Squared cosine	$f(x, y) = A \cos^2 \left(\frac{\pi}{D} \sqrt{x^2 + y^2} \right)$	

3.4 Chapter Summary

This chapter has presented the theory and principle of a horn antenna and EBG structures. From the theory is shown that a horn antenna consists of a flaring metal to transmit electromagnetic waves in a beam from a waveguide out into space. This research exemplify the rectangular and circular horn antennas which are classified two major types. Then, the applications of EBG structures in antenna designs, that have become the popular topic for antenna engineering since these EBG structures are capable to enhance the performance of the antenna in terms of gain, side and back lobes levels and also mutual coupling, are presented. Furthermore, this research apply one layer of planar woodpile EBG structures to format of variety shaped woodpile EBG structures as follow the function of geometry for increasing the gain of the conventional rectangular and circular horn antennas.



CHAPTER III

BACKGROUND THEORY

3.1 Introduction

In this chapter, we describe the theory and principle of horn antenna, one type of aperture antennas, that is the most common at microwave frequencies. There are many different geometrical configurations of horn antenna with rectangular and circular of the most popular will be discussed in more details in section 3.2. Additionally, the EBG structures are examined in section 3.3. This section addresses definition of EBG structures, relation between EBG and metamaterials, analysis methods for EBG structures, and woodpile EBG structures. In the last section of this chapter, the conclusion will be presented.

3.2 Horn Antenna

A horn antenna is one of the simplest and probably the most widely used for microwave antenna, especially as a feed element for large radio astronomy, satellite tracking, and communication dishes. Furthermore, its utility as a feed for reflectors and lenses, it is a common element of phased arrays and serves as universal standard for calibration and gain measurements for other high-gain antenna (Constantine, 2005).

A horn antenna consists of a flaring metal waveguide shaped like a horn to direct the radio waves in a beam. It can have different flare angles in the E-field and H-field directions, making possible a wide variety of different beam profiles.

The important dimensions of the horn antenna are horn length, aperture area, and flare angle. The length of a typical horn is usually 2λ to 15λ at the operating frequency, while the longer horns more difficult to mount and work with provide higher gain and better directivity. In addition, the aperture area is the area of the rectangle formed by the opening of the horn and simply the product of the height and width of the horn. The greater this area can offer the higher gain and directivity. The flare angle also affects gain and directivity. The typical flare angle is varied from about 20° to 50° . To increase the flare angle of horn antenna, can increase the aperture area. Each of these dimensions is adjusted to achieve the desired design objective.

An important aspect of a microwave antenna is its bandwidth. The most antennas have a narrow bandwidth because they are resonant at only a single operating frequency. Therefore, the dimension of their antennas will be use to determine their operating frequency. Bandwidth is an important consideration at microwave frequencies because the spectrum transmitted on the microwave carrier is usually wide, so that a considerable amount of information can be carried (<http://www.intechopen.com/books/data-acquisition-applications/microwave-antenna-performance-metrics>). A horn antenna has relatively large bandwidth since it is essentially non-resonant or periodic which means that it will operate over a wide frequency range (Frenzel, 1996).

3.2.1 Types of Horn Antenna

These are the common types of horn antenna. The horns can take many different forms, which are classified into two major types such as rectangular and circular horns. Figure 3.1 shows types of horn antenna such as pyramidal horn, sectoral E-plane horn, sectoral H-plane horn, conical horn, and exponential horn. The pyramidal horn is a rectangular horn antenna with in the shape of a four-sided pyramid, with a rectangular cross section. They are a common type, used with rectangular waveguides, and radiate linearly polarized radio waves (Bakshi *et al.*, 2009). The sectoral horn is a pyramidal horn with only one pair of sides flared and the other pair parallel. It produces a fan-shaped beam, which is narrow in the plane of the flared sides, but wide in the plane of the narrow sides. These types are often used as feed horns for wide search radar antennas. There are two types of sectoral horn such as (1) E-plane horn, a sectoral horn flared in the direction of the electric or E-field in the waveguide and (2) H-plane horn, a sectoral horn flared in the direction of the magnetic or H-field in the waveguide. The conical horn is a circular horn in the shape of a cone and has a circular cross section. They are used with cylindrical waveguides. The exponential horn is a circular horn with curved sides, in which the separation of the sides increases as an exponential function of length. Also called a scalar horn, they can have pyramidal or conical cross sections. The exponential horns have minimum internal reflections, and almost constant impedance and other characteristics over a wide frequency range. They are used in applications requiring high performance, such as feed horns for communication satellite antennas and radio telescopes (http://en.wikipedia.org/wiki/Horn_antenna).

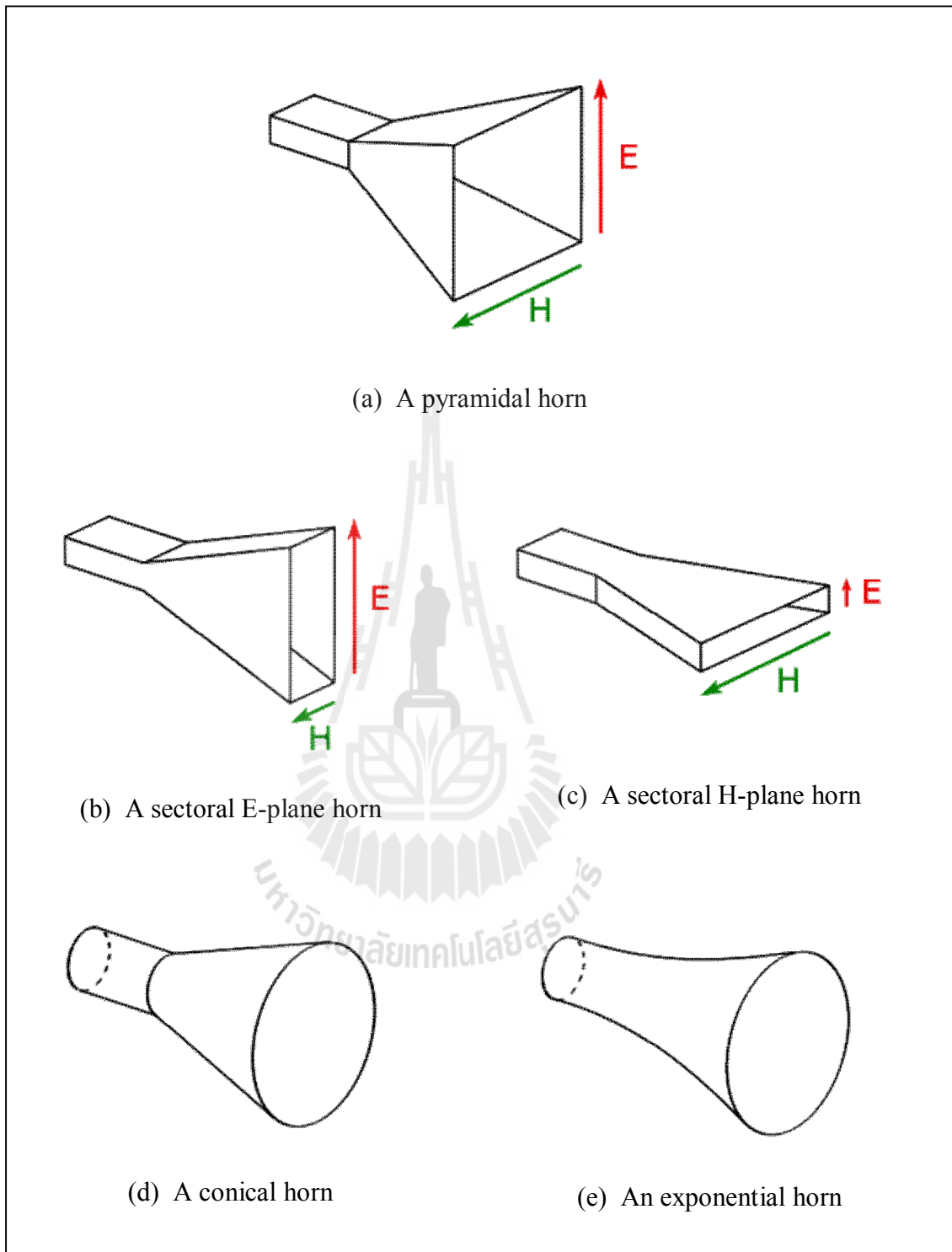


Figure 3.1 Typical horn antenna configurations (<http://en.wikipedia.org>).

3.2.2 Waveguide Feeding

The horn antennas are typically fed by a section of waveguide, which is a hollow conductive metal pipe used to carry electromagnetic waves, high frequency radio waves and particularly microwaves. The geometry of a waveguide reflects its function, such as rectangle and cylinder, that depends on its application, as shown in Figure 3.2. The rectangular horns are ideally suited for rectangular waveguide feeders. The horn acts as a gradual transition the electromagnetic wave from a waveguide mode to a free-space mode. If the feeder is a cylindrical waveguide, the antenna is usually a circular horn. It is necessary to consider the horns separately instead of applying the waveguide aperture antennas directly because of the phase error occurs due to the difference between the lengths from the center of the feeder to the center of the horn aperture and the horn edge. This makes the uniform-phase aperture results invalid for the horn apertures (Nikolova, 2010). A waveguide can be made from copper or alumina, which inside surfaces are enameled with silver to be a perfect conductor. In addition, a waveguide itself is often fed with a short monopole. In the case of the rectangular waveguide as shown in Figure 3.3, the length of a rectangular waveguide is $3\lambda_g/4$, the length of a short monopole is $\lambda_0/4$, and the backshort wall about $\lambda_g/4$ behind the short monopole ensures that the dipole sees only radiation coming from the direction of the horn opening, where λ_g is a wavelength of the signal in the guide and λ_0 is a wavelength in free space.

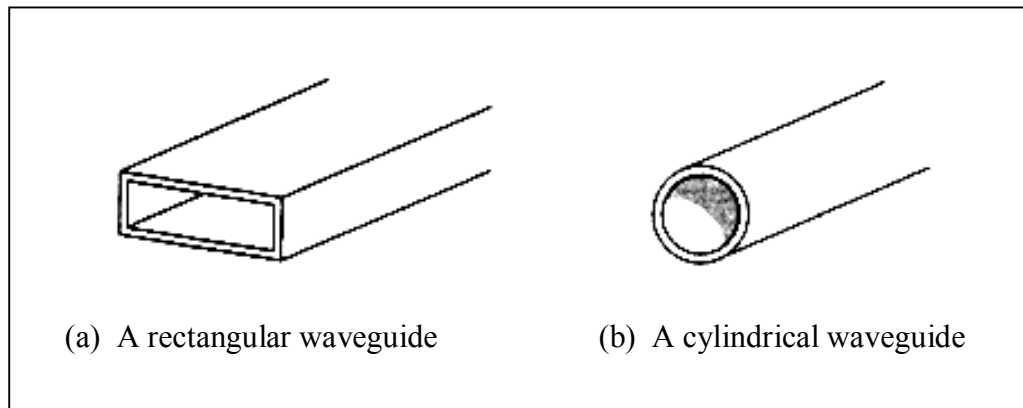


Figure 3.2 The geometry of the waveguides.

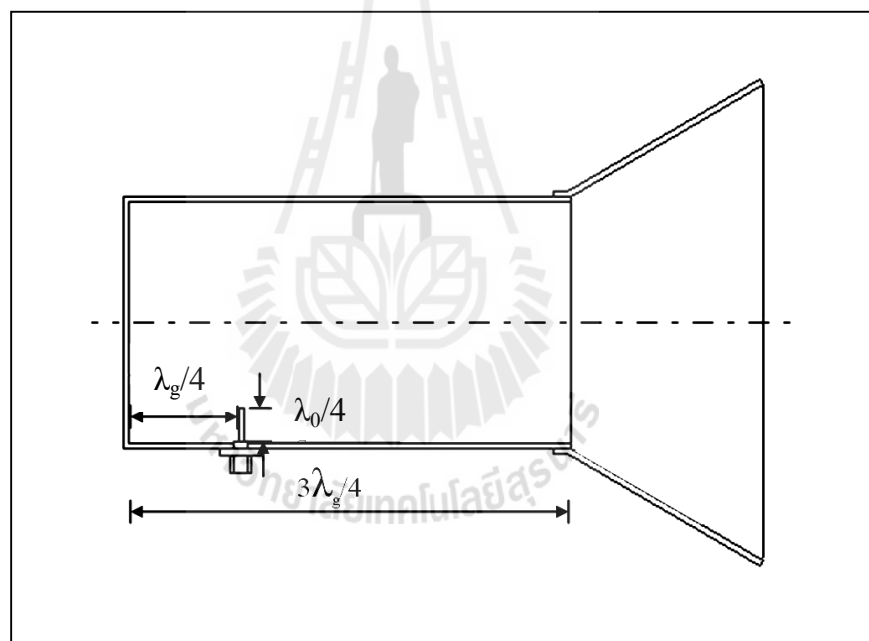


Figure 3.3 A rectangular waveguide fed with a short monopole.

3.3 Electromagnetic Band Gap Structures

This section will mention the definition of EBG structures, the relation between EBG and metamaterials, and the analysis methods for EBG structures. Moreover, the woodpile EBG structures are investigated in this section.

3.3.1 EBG Definition

The EBG structures, also known as Photonic Crystals (Joannopoulos, Meade, and Finn, 1995) or Photonic Band Gap (PBG) Materials (Yablonovitch, 1987) are periodic structures, which do not allow the propagation of electromagnetic waves with in certain frequency ranges. Generally speaking, the EBG structures are defined as “*artificial periodic (or sometimes non-periodic) objects that prevent/assist the propagation of electromagnetic waves in a specified band of frequency for all incident angles and all polarization states*” (Yang and Rahmat-Samii, 2009). The EBG structures are usually realized by periodic arrangement of dielectric material and metallic conductors. In general, they can be categorized into three groups according to their geometric configuration such as (1) one-dimensional (1D) transmission lines, (2) two-dimensional (2D) planar surfaces, and (3) three-dimensional (3D) volumetric structures.

Figure 3.4 shows the 1D EBG transmission lines design, a microstrip line with periodic holes on the ground plane (Radisic *et al.*, 1998) and a composite right-handed and left-handed transmission line (Caloz and Itoh, 2005). The 2D planar surfaces, a mushroom-like surface (Sievenpiper *et al.*, 1999) and a uni-planar design without vertical vias (Yang *et al.*, 1999), are shown in Figure 3.5. In Figure 3.6, the 3D volumetric structures are shown in two representative structures such as a

woodpile structure consisting of square dielectric bars (Ozbay *et al.*, 1994) and a multi-layer metallic tripod array (Barlevy and Rahmat-Samii, 2001).

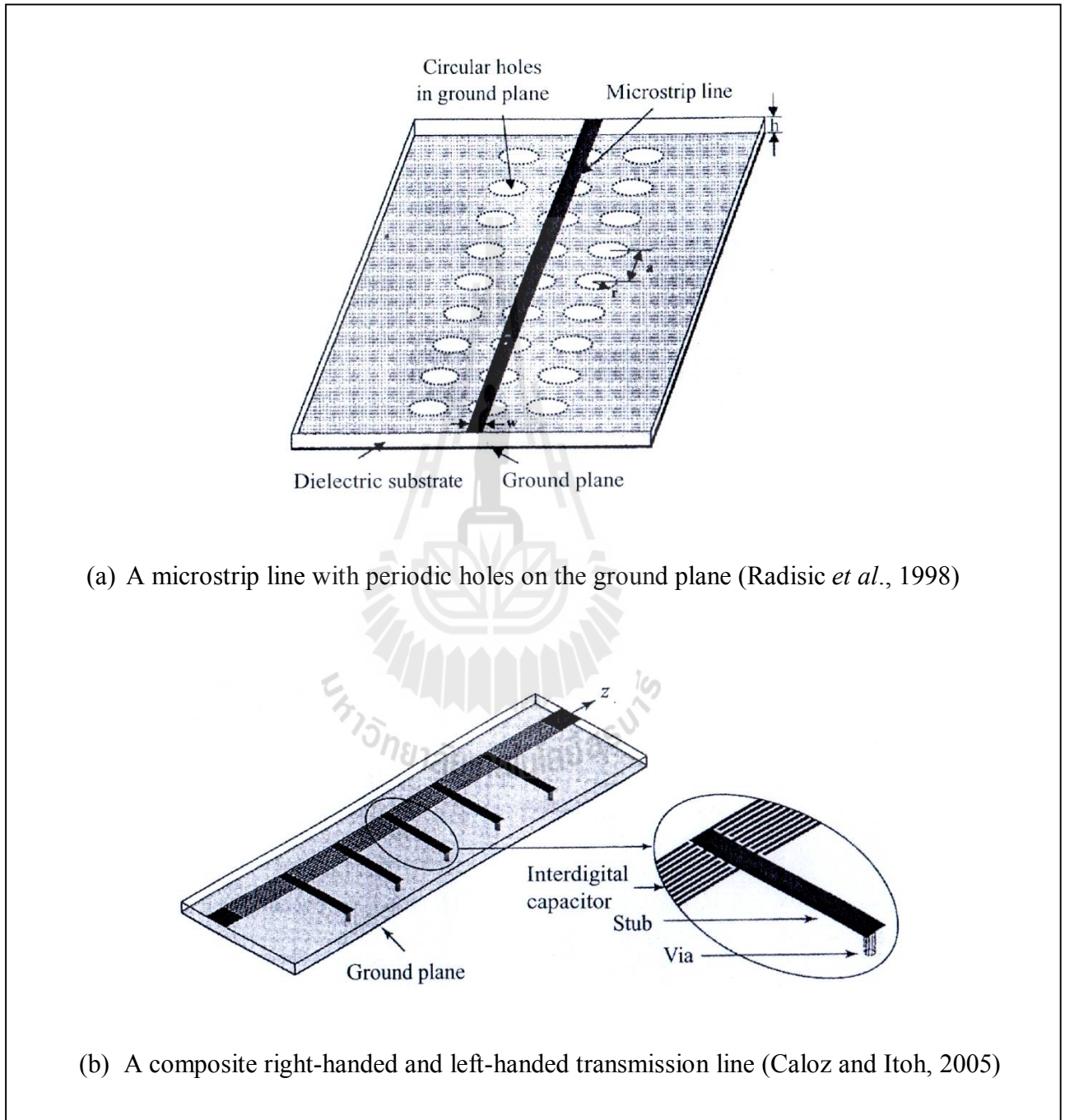


Figure 3.4 The 1D EBG transmission lines.

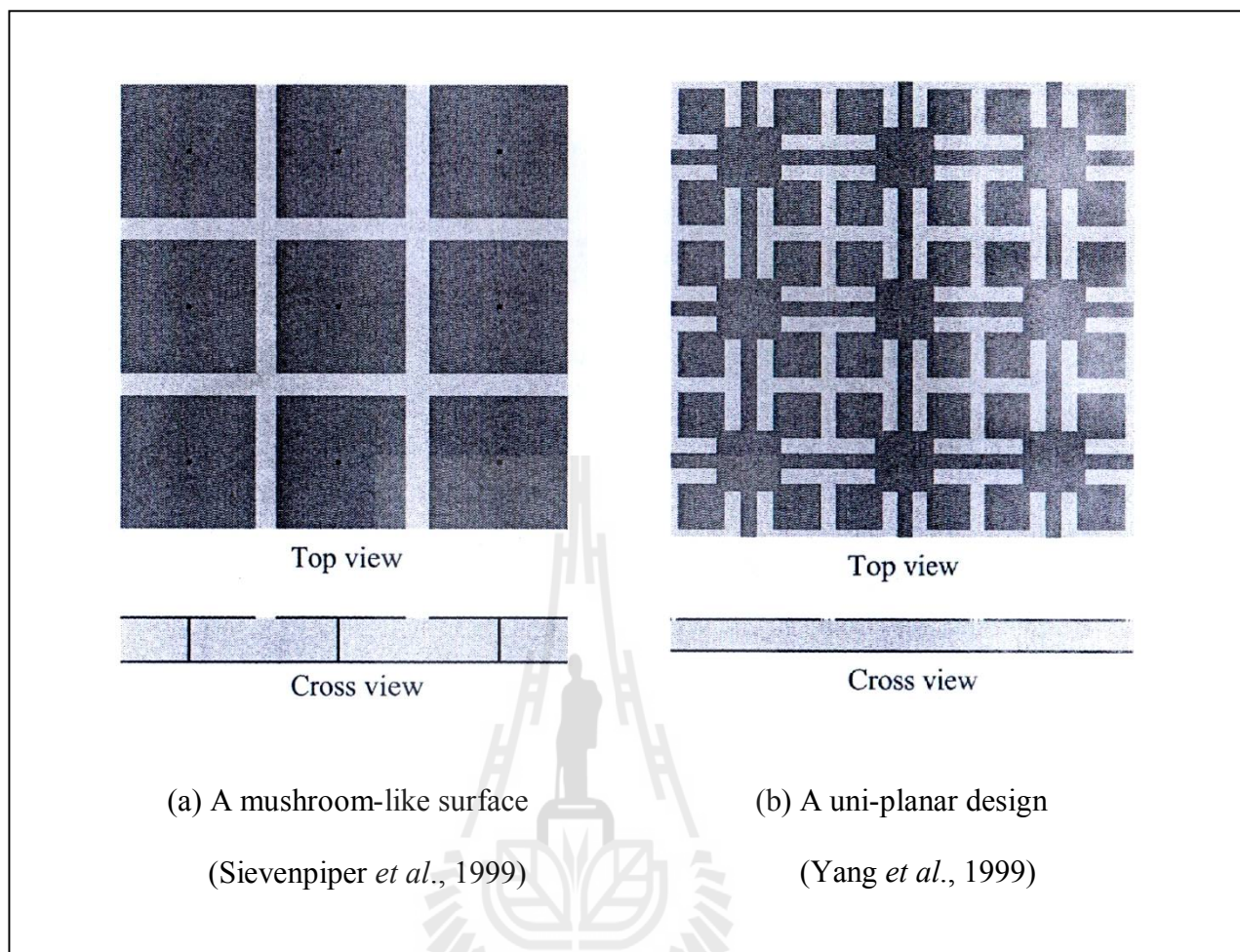


Figure 3.5 The 2D EBG planar surfaces.

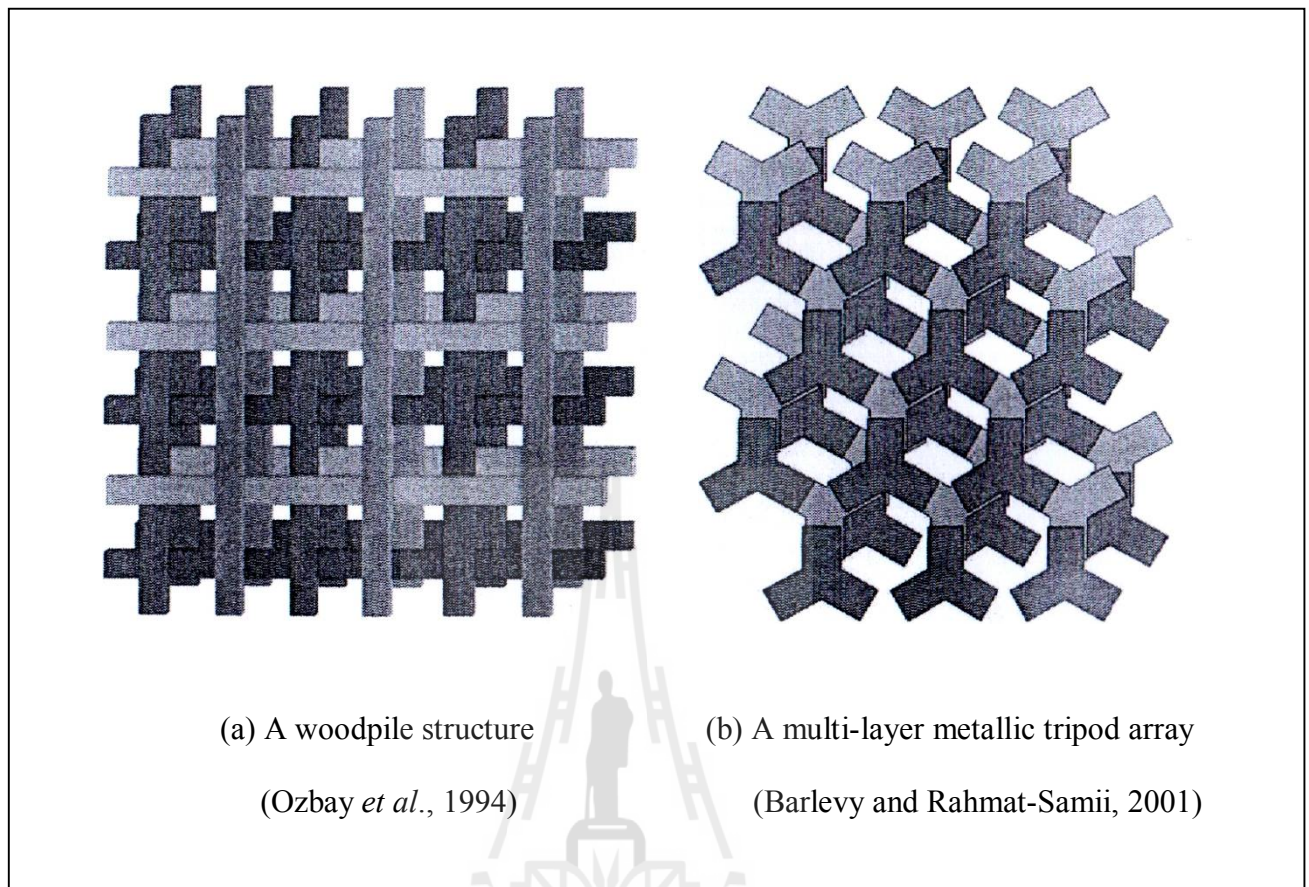


Figure 3.6 The 3D EBG volumetric structures.

3.3.2 EBG and Metamaterials

Metamaterials, materials of interest exhibit properties not found in nature such as negative index of refraction, are artificial media structure on a size scale smaller than the wavelength of external stimuli. Its research is interdisciplinary and involves fields including electrical engineering, electromagnetic, solid state physics, microwave and antenna engineering, optoelectronics, classic optics, material sciences, semiconductor engineering, and nanoscience (Zouhdi *et al.*, 2008). The electromagnetic metamaterials affect electromagnetic waves by having structural features smaller than the wavelength of the respective electromagnetic waves. To

behave as a homogeneous material accurately described by an effective refractive index, its features must be much smaller than the wavelength. Depending on the exhibited electromagnetic properties, various names have been introduced in the literature, including (Yang and Rahmat-Samii, 2009):

- Double negative (DNG) materials with both negative permittivity and permeability;
- Left-handed (LH) materials inside which the electric field (E-field) direction, magnetic field (H-field) direction, and propagation direction satisfy a left-hand relation;
- Negative refractive index (NRI) materials that have a negative refractive index;
- Magneto materials with artificially controlled high permeability;
- Soft and hard surfaces that stop or support the propagation of waves;
- High impedance surfaces with relatively large surface impedances for both TE and TM waves;
- Artificial magnetic conductors (AMC) that exhibit the same properties as a perfect magnetic conductor.

Due to their unique band gap features, EBG structures can be regarded as a special type of metamaterials. The EBG structures have the goal of creating high quality, low loss, periodic, and dielectric structures. An EBG affects photons in the same way semiconductor materials affect electrons. The EBG structures are designed to prevent the propagation of an allocated bandwidth of frequencies, for certain arrival

angles and polarizations. The various geometries and structures have been proposed to fabricate EBG special properties (Engheta *et al.*, 2006; Zouhdi *et al.*, 2008). The EBG structures have been manufactured for frequencies ranging from a few gigahertz (GHz) up to a few terahertz (THz), radio, microwave and mid-infrared frequency regions. Besides the band gap feature, EBG also possesses some other exciting properties such as high impedance and AMC. For example, a mushroom-like EBG surface exhibits high surface impedances for both TE and TM polarizations. In addition, soft and hard operations of an EBG surface have also been identified in the frequency-wave number plane. These interesting features have led to a wide range of applications in antenna engineering, from wire antennas to microstrip antennas, from linearly polarized antennas to circularly polarized antennas, and from the conventional antenna structures to novel surface wave antenna concepts and reconfigurable antenna designs (Yang and Rahmat-Samii, 2009).

3.3.3 Analysis Methods for EBG Structures

To analyze unique features of EBG structures, three categories have been implemented: (1) lumped element model, (2) periodic transmission line method, and (3) full wave numerical methods.

The lumped element model is the simplest one that describes the EBG structures as an LC resonant circuit (Sievenpiper, 1999). The values of the inductance L and capacitance C are determined by the EBG geometry and its resonance behavior is used to explain the band gap feature of EBG structures. This model is simple to understand, but the results are not very accurate because of the simplified approximation of L and C . A simple 2D planar EBG structures, the geometry is

similar to the shape of a mushroom, consists of four parts: a metal ground plane, a dielectric substrate, periodic metal patches on top of the substrate, and vertical vias connecting the patches to the ground plane (Sievenpiper *et al.*, 1999) as shown in Figure 3.7. The parameters of the EBG structure are the patch width (W), the gap width (g), the substrate thickness (h), the dielectric constant (ϵ_r), and the vias radius (r). When the periodicity ($W + g$) is small compared to the operating wavelength, the operation mechanism of this EBG structure can be explained using an effective medium model with equivalent lumped LC elements, as shown in Figure 3.8. The capacitor results from the gap between the patches and the inductor results from the current a long adjacent patches. The impedance of parallel resonant LC circuit is given by:

$$Z = \frac{j\omega L}{1 - \omega^2 LC} \quad (3.1)$$

The resonance frequency of the circuit is calculated as following:

$$\omega_0 = \frac{1}{\sqrt{LC}} \quad (3.2)$$

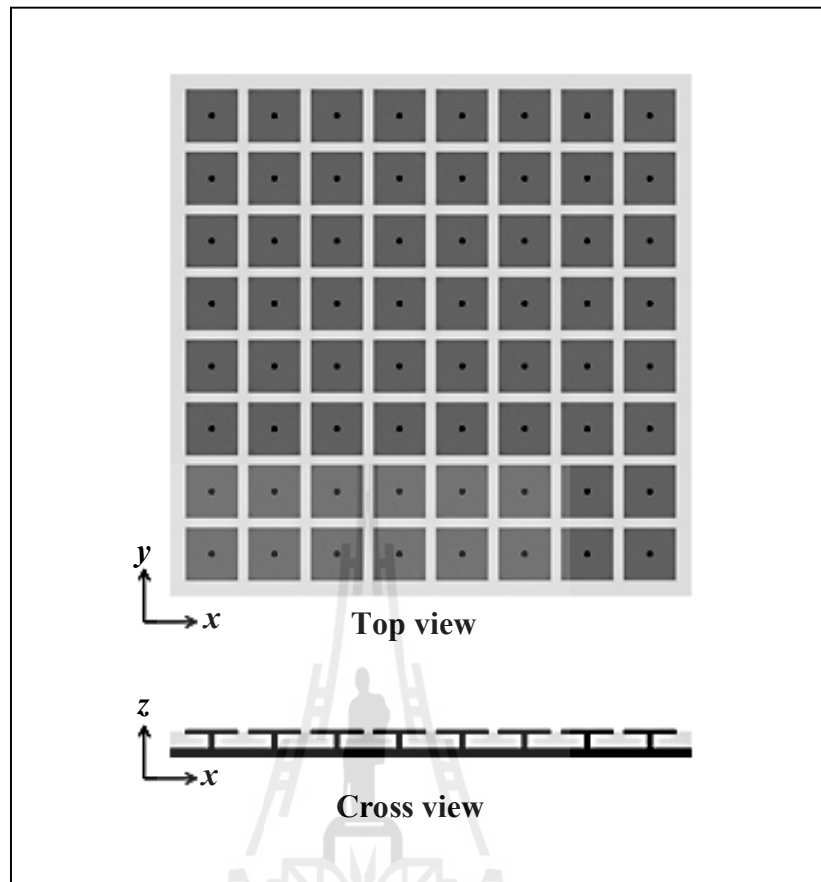


Figure 3.7 The geometry of a mushroom-like EBG structures
(Sievenpiper *et al.*, 1999).

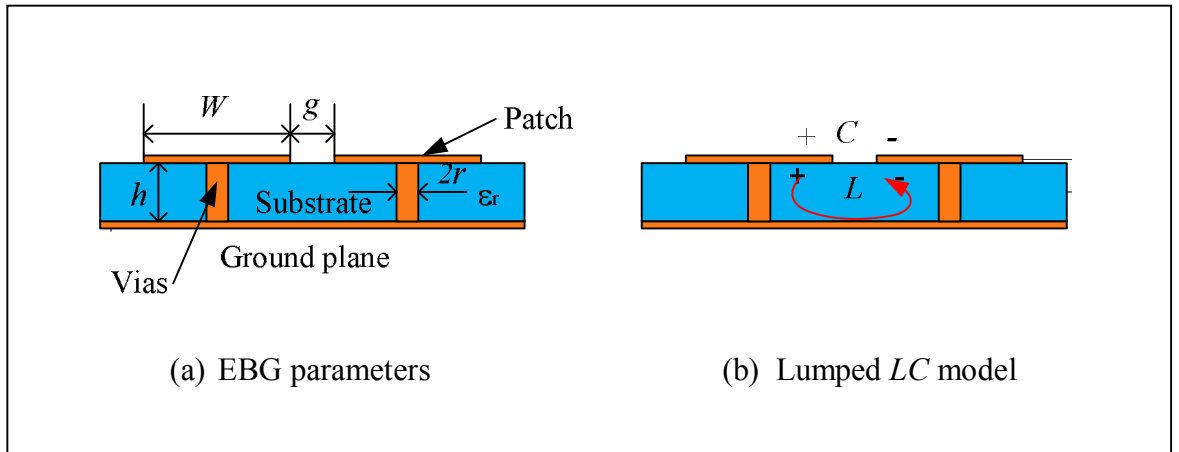


Figure 3.8 The lumped element model for the mushroom-like EBG structures.

At low frequencies, the impedance is inductive and will support TM surface waves. Inversely, it becomes capacitive at high frequencies and TE surface waves are supported. At near the resonance frequency ω_0 , high impedance is obtained and the EBG does not support any surface waves, resulting in frequency band gap. The high surface impedance also ensures that a plane wave will be reflected without the phase reversal that occurs on a perfect electric conductor (PEC).

The value of the capacitor is given by the fringing capacitance between neighboring co-planar metal sheets. This can be derived using conformal mapping, a common technique for determining 2D electrostatic field distributions. The edge capacitance for narrow gap situation is given by the following equation (Sievenpiper, 1999):

$$C = \frac{W\epsilon_0(1+\epsilon_r)}{\pi} \cosh^{-1}\left(\frac{W+g}{g}\right). \quad (3.3)$$

The value of the inductor is derived from the current loop in Figure 3.8(b), consisting of the vias and metal sheets. The equivalent inductor is then computed from the stored H-field energy and the excitation current. The inductance is expressed as below (Sievenpiper, 1999), which depends only on the thickness of the structure and the permeability:

$$L = \mu h . \quad (3.4)$$

The periodic transmission line method is another analytical model proposed to characterize EBG structures (Rahman and Stuchly, 2001). A mushroom-like EBG structure as shown in Figure 3.7, the impedance of each section is calculated using transmission line theory, and the whole structure is then cascaded together using the theory of periodic circuit. Figure 3.9 depicts a transmission line model of EBG structures. Between two nodes of the periodic structure, there are two contributions (Z_P and X_C) to the total impedance, which Z_P is the impedance for each periodic element and X_C is the coupling capacitor. After analyzing the cascaded transmission line, the dispersion curve can be readily obtained, which provides more information than the lumped element method. A challenge in this method is how to accurately obtain the equivalent Z_P and X_C values for general EBG structures with arbitrary geometries. In addition, the surface wave modes, the leaky wave modes, the left- and right-hand regions, and the band gaps can be easily identified from the dispersion curve. However, it is not applicable for plane wave incidences.

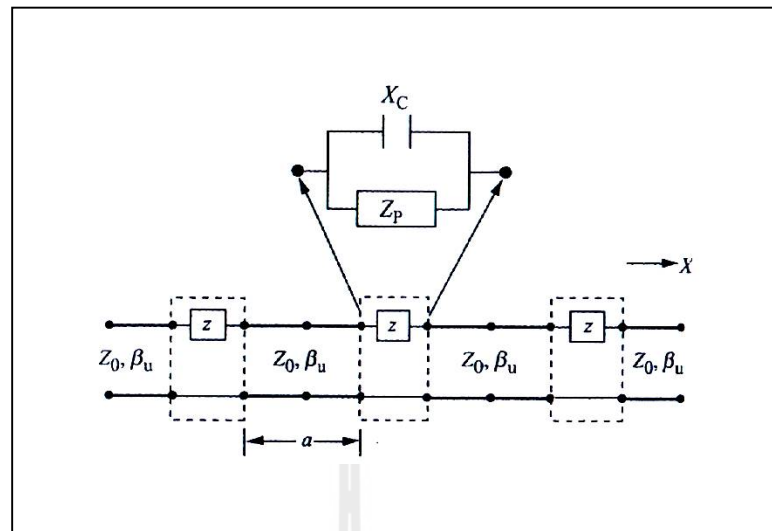


Figure 3.9 The transmission line model of EBG structures
(Rahman and Stuchly, 2001).

The full wave numerical methods, both the frequency domain methods such as the Method of Moments (MoM) and the Finite Element Method (FEM) and the time domain method like the FDTD method have been utilized by different research groups to characterize EBG structures. For instance, Figure 3.10 shows an FDTD model for the mushroom-like EBG analysis (Kim, Yang, and Elsherbeni, 2007). The computational code is based on a Cartesian grid cell with the absorbing boundary conditions (Jensen, 1994). The important advantages of the full wave numerical methods are the versatility and accuracy in analyzing different EBG geometries and the capability to the various EBG characteristics, such as the surface impedance, reflection phase, dispersion curve, and band gap.

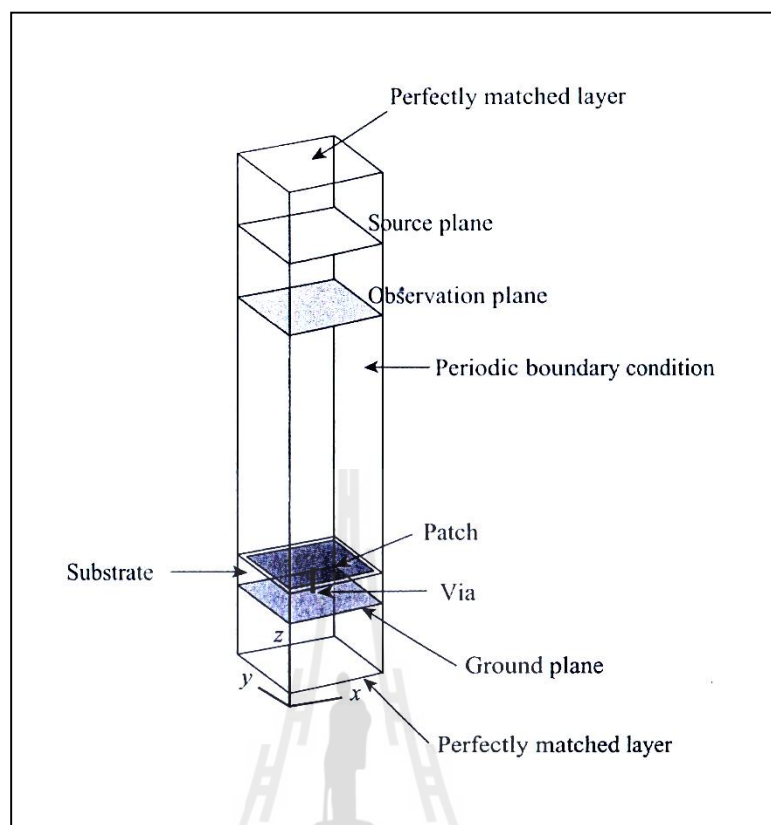


Figure 3.10 The full wave FDTD model for the EBG analysis

(Kim, Yang, and Elsherbeni, 2007).

3.3.4 Woodpile EBG Structures

In this section provides some background information of the planar woodpile EBG structures which are also referred to as a layer-by-layer photonic crystal in the physics literature. A unit cell of the planar woodpile EBG structures is defined by the lattice constant or repeat distance in the horizontal plane (a), the rod width (w), the rod height (h), and the total height of the unit cell (b) as shown in Figure 3.11. These consecutive layers are orthogonal to each other, and the parallel rods are offset from the rods two layers below by half of a lattice constant, to obtain a four layer stacking sequence. The lattice symmetry of this material is face-centered

tetragonal (FCT) from solid state physics theory. The cross section of the rods may be circular or square shape, and the inverse structure made of air rods in dielectric background also has a completed bandgap (Weily *et al.*, 2005).

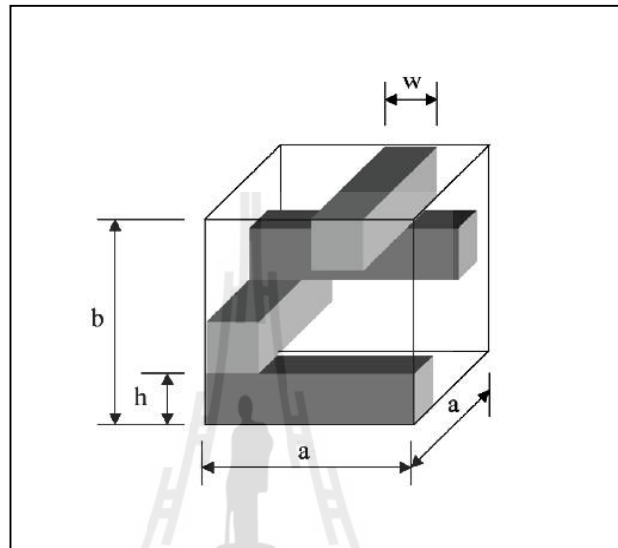


Figure 3.11 A unit cell of four layers planar woodpile EBG structures (Weily *et al.*, 2005).

From a unit cell of four layers of planar woodpile EBG structures, this research modify from four layers to one layer as shown in Figure 3.12. Besides applying one layer of planar woodpile EBG structures, we design the format of variety shaped woodpile EBG structures as follow the function of geometry (Thaivrot, Krachodnok, and Wongsan, 2008) as shown in Table 3.1, such as planar, triangular, quadratic, circular, gaussian, cosine, and squared cosine structures to enhance the gain of the conventional rectangular and circular horn antennas. They are creating new possibilities for controlling and manipulating the flow of electromagnetic waves. Also, this research designs to simulate and fabricate the horn

antennas with EBG structures based on low loss alumina materials at dominant frequency of 10 GHz, and demonstrate its utilization in a horn antenna for X-band radar and I-band beyond following the IEEE and the ITU, respectively.

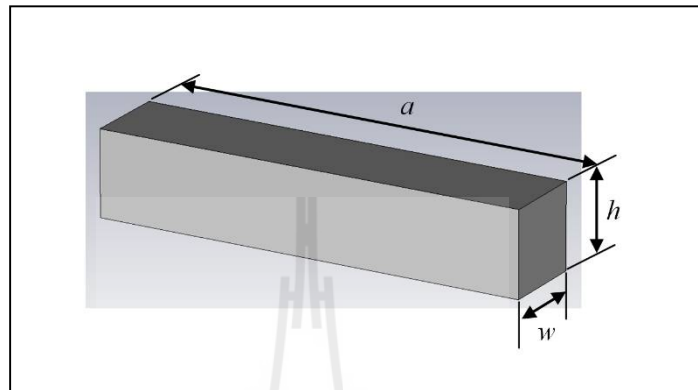


Figure 3.12 A unit cell of one layers planar woodpile EBG structures.

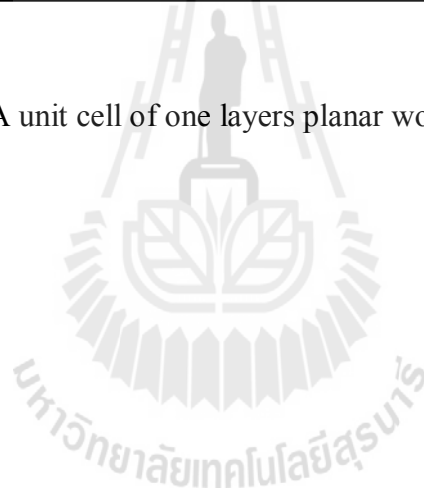
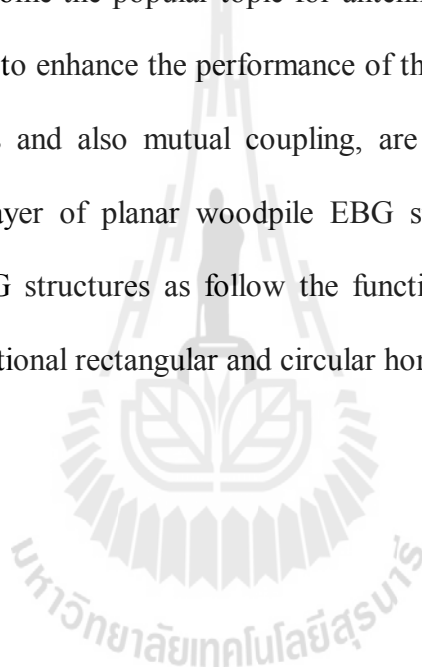


Table 3.1 Formulations of elementary geometrical function.

Distributed Function	Formulations	Shapes of EBG Structure
Planar	$f(x, y) = A$	
Triangular,	$f(x, y) = A \left(1 - \frac{2}{D} \sqrt{x^2 + y^2} \right)$	
Quadratic	$f(x, y) = A \left[1 - \left(\frac{2}{D} \sqrt{x^2 + y^2} \right)^2 \right]$	
Circular	$f(x, y) = A \sqrt{1 - \left(\frac{2}{D} \sqrt{x^2 + y^2} \right)^2}$	
Gaussian	$f(x, y) = A e^{-\left(\frac{2}{D} \sqrt{x^2 + y^2} \right)^2}$	
Cosine	$f(x, y) = A \cos \left(\frac{\pi}{D} \sqrt{x^2 + y^2} \right)$	
Squared cosine	$f(x, y) = A \cos^2 \left(\frac{\pi}{D} \sqrt{x^2 + y^2} \right)$	

3.4 Chapter Summary

This chapter has presented the theory and principle of a horn antenna and EBG structures. From the theory is shown that a horn antenna consists of a flaring metal to transmit electromagnetic waves in a beam from a waveguide out into space. This research exemplify the rectangular and circular horn antennas which are classified two major types. Then, the applications of EBG structures in antenna designs, that have become the popular topic for antenna engineering since these EBG structures are capable to enhance the performance of the antenna in terms of gain, side and back lobes levels and also mutual coupling, are presented. Furthermore, this research apply one layer of planar woodpile EBG structures to format of variety shaped woodpile EBG structures as follow the function of geometry for increasing the gain of the conventional rectangular and circular horn antennas.



CHAPTER IV

ANTENNA ANALYSIS AND DESIGN

4.1 Introduction

This chapter presents analysis and design of horn antennas and EBG structures. In the first section, the woodpile EBG structures are designed to utilize with horn antennas for providing higher gain and symmetrical radiation pattern. Next section will mention the details of increasing gains of rectangular and circular horn antennas with same designed the woodpile EBG structures by controlling the radiation pattern in the E-plane and H-plane symmetrically. The antenna characteristics such as reflected power (S_{11}), voltage standing wave ratio (VSWR), radiation patterns and gain are simulated by using the CST software. Finally, conclusion will be the last section of this chapter.

4.2 The Woodpile EBG Configuration

A woodpile is a 3D EBG structures made of a stack of square cross-section rod. The unit cell of one layers planar woodpile EBG structures is shown in Figure 3.12 (in Chapter 3). The dimension of woodpile EBG structures is specified by the distance in the horizontal plane (a), the rod width (w), and the rod height (h). To implement the woodpile, this research used alumina rods ($\epsilon_r = 8.4$, $\tan\delta = 0.002$) and the cross section of each one is rectangular shape. The lattice parameters are given as follow Kampeephat *et al.* (2014) with $a = 0.225\lambda$ and $w = h = 0.053\lambda$. To design the appropriate shape of woodpile EBG structures, this research used functions

of geometries (Thaiviro, Krachodnok, and Wongsan, 2008) as shown in Table 3.1 (in Chapter 3), such as planar, triangular, quadratic, circular, gaussian, cosine, and squared cosine structures to investigate the desired performance, especially radiation pattern and gain. The design parameters of the gain improvement for a rectangular horn antenna with two side-wing slabs are the most proper shaped woodpile EBG structure, the distance between a horn and woodpile EBG structures (d), and the radius of quadratic shaped (r). Firstly, we look at the effect of the variation of shaped woodpile EBG structures; d and r are fixed at 30λ and 5λ , respectively. Figure 4.1 shows the gain against the various shaped woodpile EBG structures at the operating frequency of 10 GHz. The highest gain of 24.34 dB is provided when the woodpile EBG structure is quadratic shaped. Also, the appropriate HPBW in the E-plane and H-plane are the narrowest. Therefore, the quadratic-shaped woodpile EBG is used to gain some parts of the electromagnetic energy and suppress the surface wave that occurred on the slabs. Secondly, we look at the effect of the variation of distance d , and r is fixed at 5λ . Figure 4.2 shows the gain against the d at the operating frequency of 10 GHz. The highest gain of 25.70 dB is provided at d equal to 16.5λ . Next, we have been studied the effect of the r variation on the gain of a rectangular horn antenna with two side-wing slabs and quadratic shaped woodpile EBG, while d is fixed at 16.5λ , thus the result is improved as shown in Figure 4.3. We found that the gain is increased from 25.70 dB to 25.74 dB at r equal to 5.3λ approximately. Finally, we found that the highest gain of a rectangular horn antenna with two side-wing slabs was obtained by using the quadratic shaped woodpile EBG structures and optimized the distance $d = 16.5\lambda$ and the radius of shape $r = 5.3\lambda$ as shown in Figure 4.4.

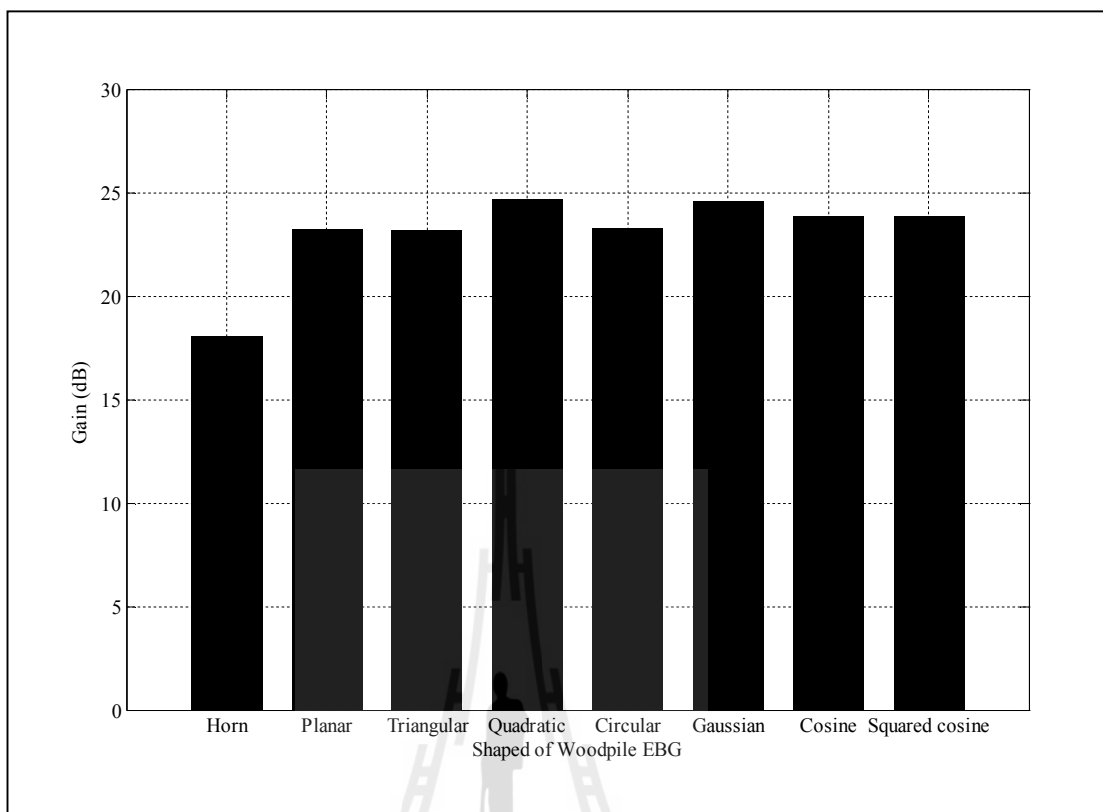


Figure 4.1 Simulated gain against the various shaped woodpile EBG.

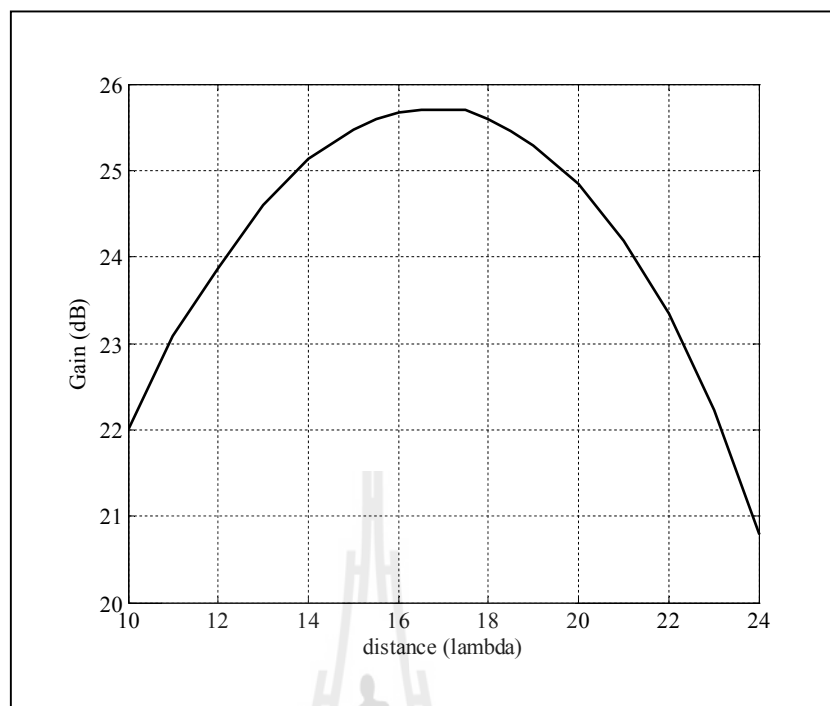


Figure 4.2 Simulated gain against the distance d .

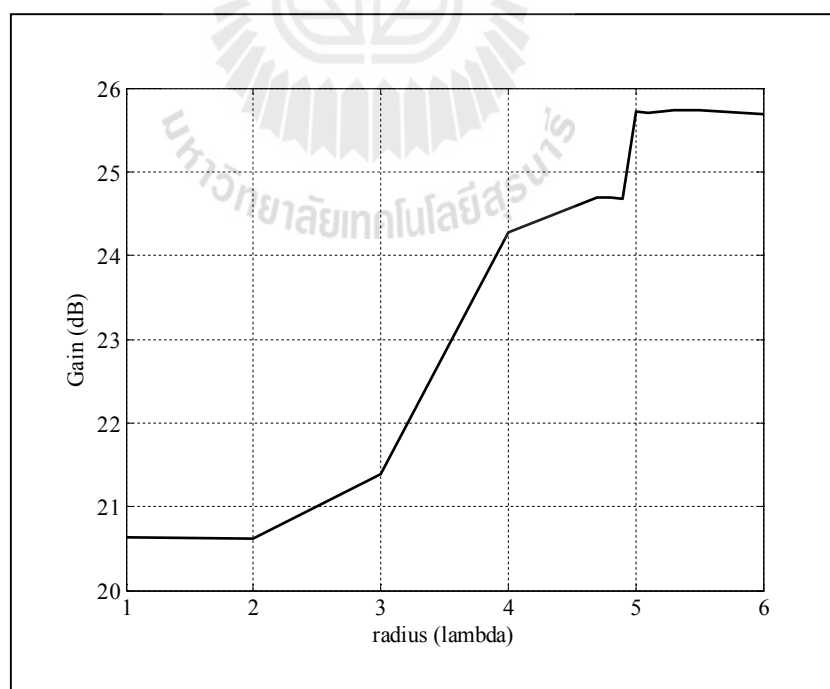


Figure 4.3 Simulated gain against the radius of shape r .

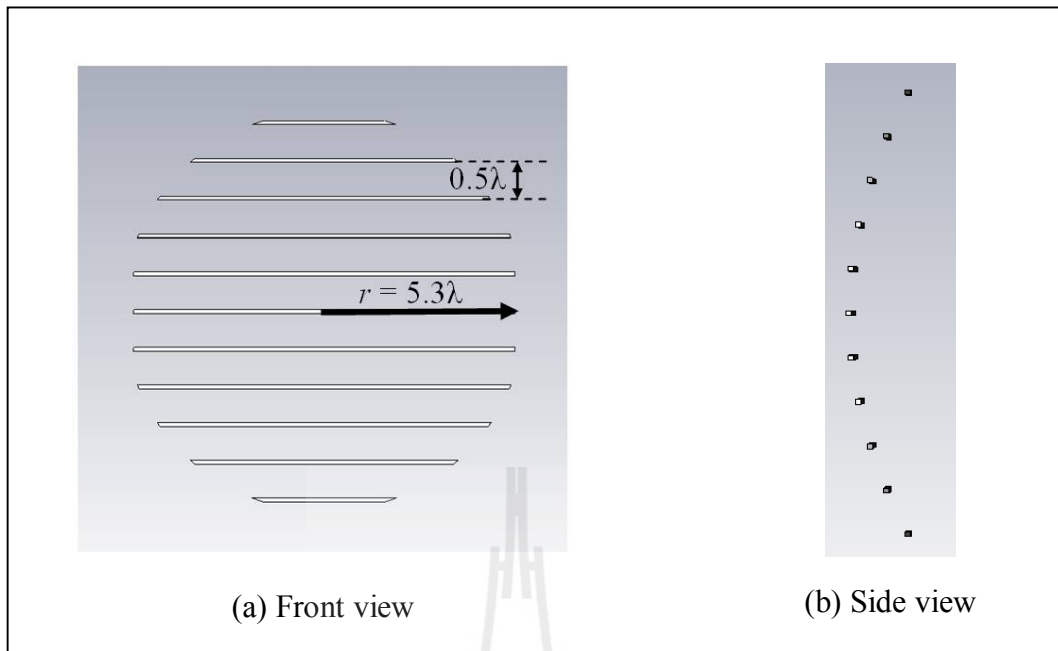


Figure 4.4 The configuration of quadratic shaped woodpile EBG structures.

To analyze the unique features of this quadratic shaped woodpile EBG structures, the lumped element model has been implemented as shown in Figure 4.5. From the results of the design parameters for gain improvement, we found that the capacitance C can be used to adjust HPBW in the E-plane, when C is increased HPBW in the E-plane is also enlarged, and the inductance L can be used to control HPBW in the H-plane, when L is increased, HPBW in the H-plane will be increased. Furthermore, one unit cell and all of the quadratic shaped woodpile EBG structures have been analyzed by using the cavity model with CST software to obtain the exhibition bandgap characteristics as shown in Figure 4.6. Figure 4.7 shows the bandgap characteristics of these woodpile EBG structures, which are designed from 9.22 GHz to 10.72 GHz for one unit cell and from 9.24 GHz to 10.71 GHz for the quadratic shaped. We found that the results of Figure 4.6 and 4.7 are not different.

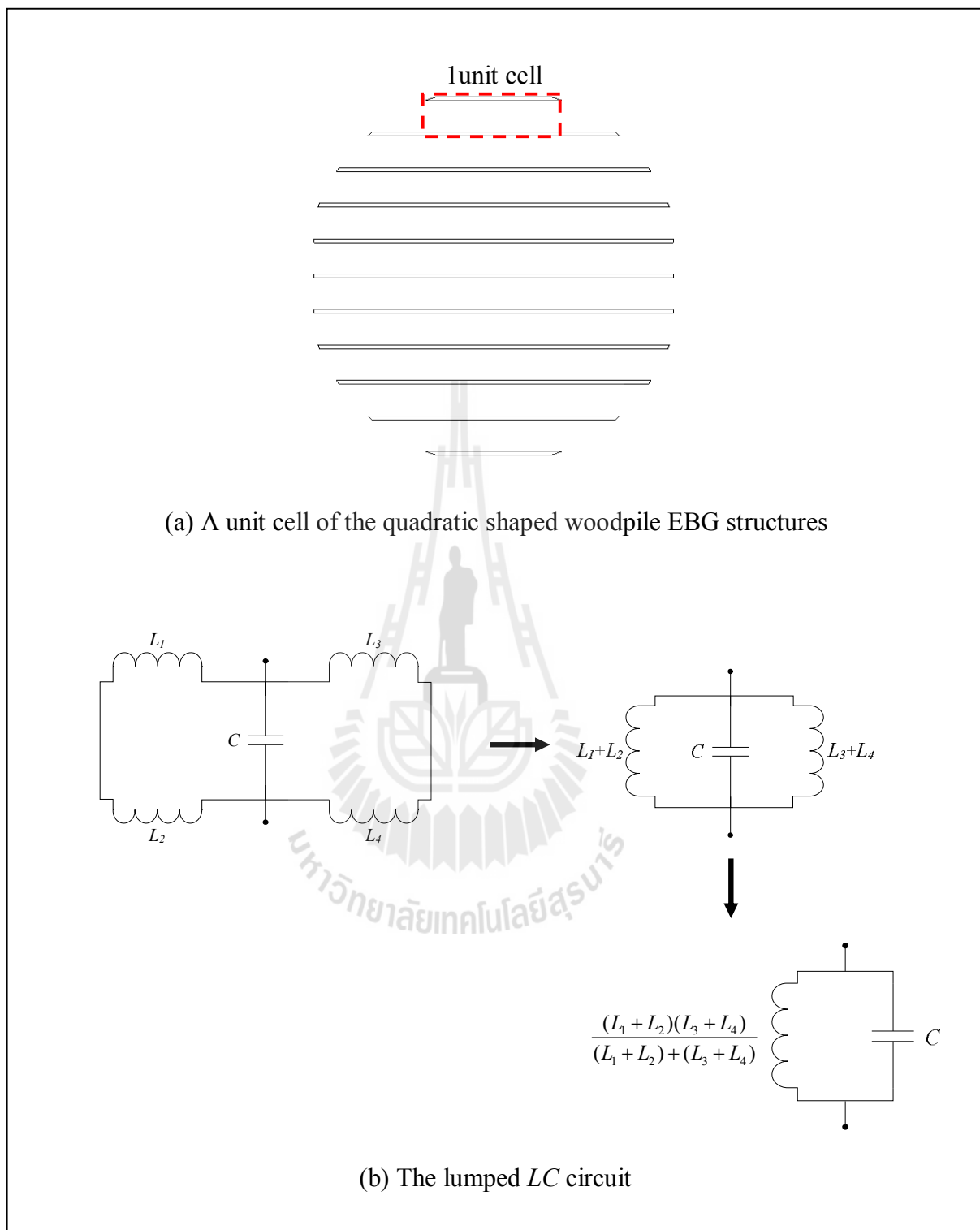
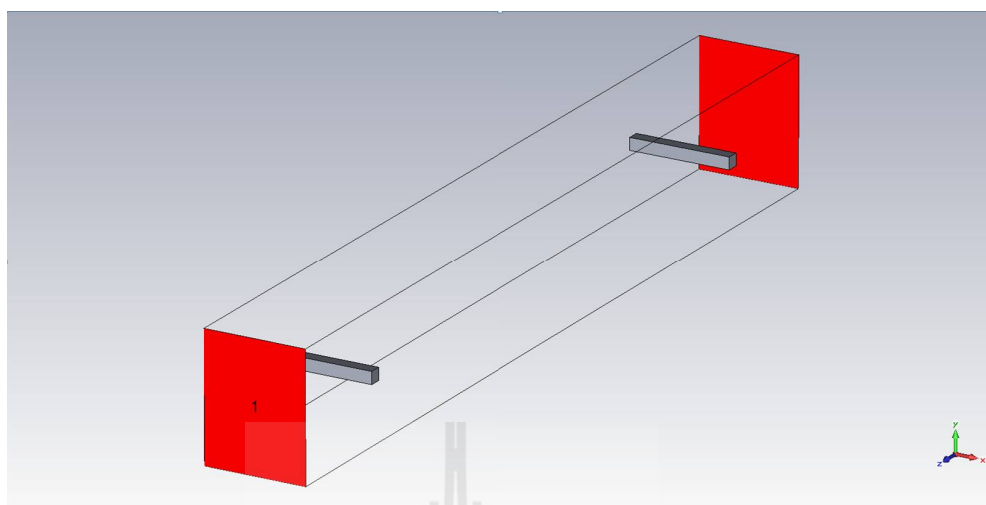
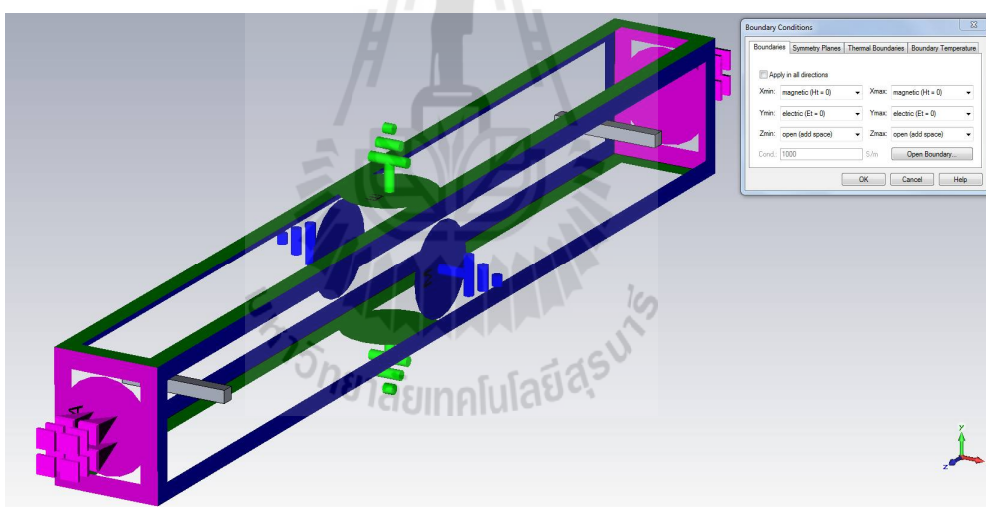


Figure 4.5 The lumped LC model of one unit cell.

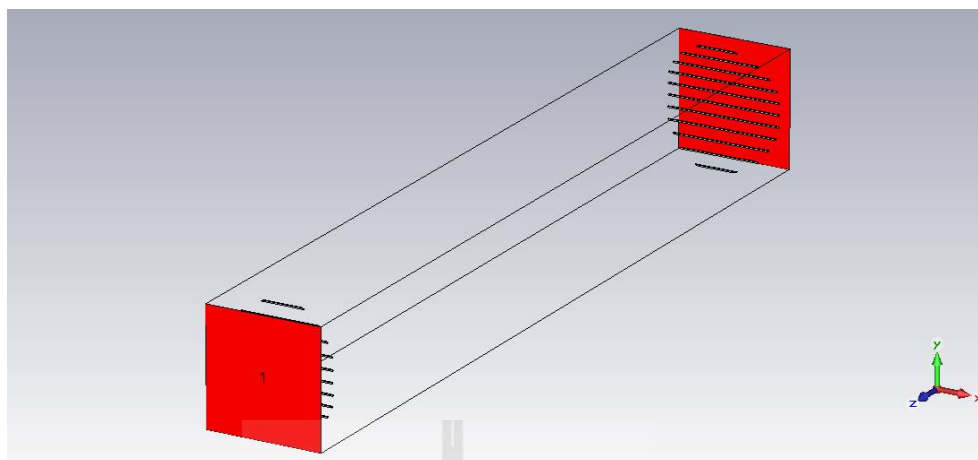


(a) Determining feed ports of one unit cell

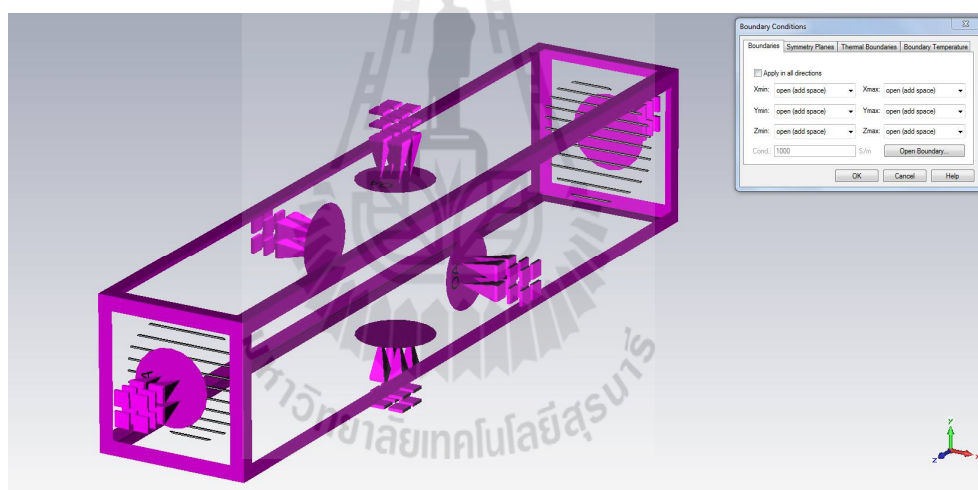


(b) Determining boundary conditions one unit cell

Figure 4.6 The cavity model of woodpile EBG.

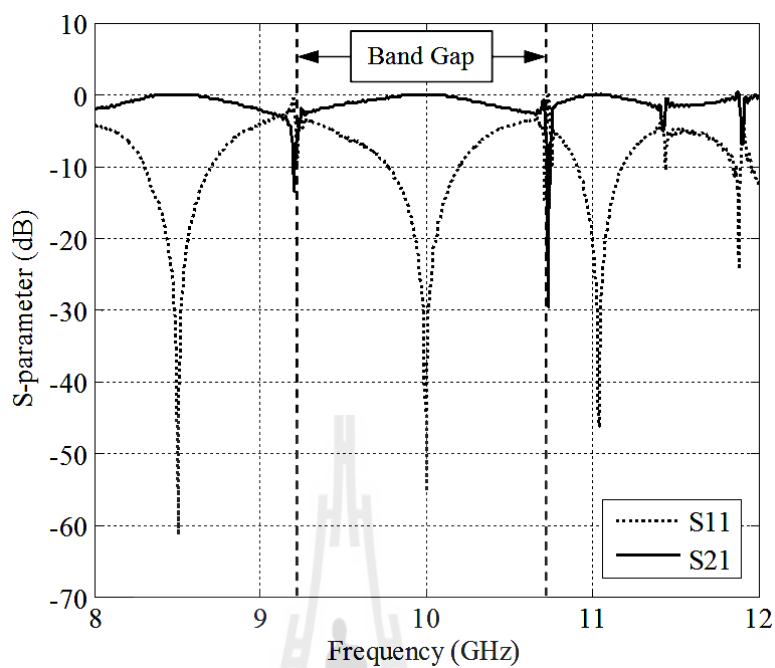


(c) Determining feed ports of the quadratic shaped

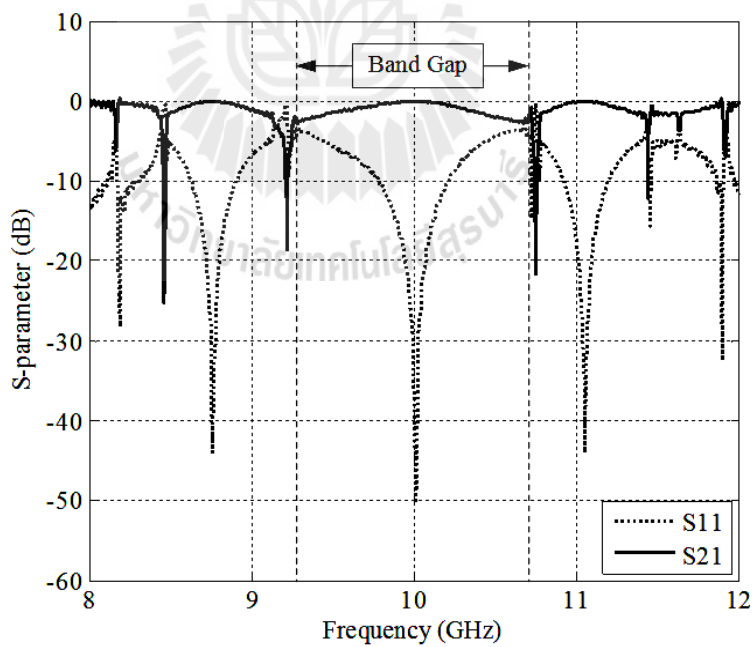


(d) Determining boundary conditions of the quadratic shaped

Figure 4.6 The cavity model of woodpile EBG (Continued).



(a) The bandgap characteristics of one unit cell



(b) The bandgap characteristics of the quadratic shaped

Figure 4.7 The bandgap characteristics of woodpile EBG.

4.3 A Rectangular Horn Antenna Configuration

4.3.1 A Conventional Rectangular Horn Antenna

(Type-A rectangular horn)

A horn antenna may be considered as a transformer from the impedance of a transmission line to the impedance of free space, 377Ω . A common microwave transmission line is waveguide, which is a hollow pipe for carrying an electromagnetic wave. The horn antenna consists of a flaring metal waveguide for guiding the radio waves into free space. The design of a conventional rectangular horn antenna was initiated by determining its aperture dimension as follow Bakshi *et al.* (2009) as shown in Figure 4.8. The simulated results with CST software show that reflected power or S_{11} (at -10 dB), VSWR, and normalized radiation patterns of a conventional rectangular horn antenna at the operating frequency of 10 GHz (next, we will call this horn antenna as Type-A rectangular horn) with the gain of 17.67 dB as shown in Figure 4.9, 4.10, and 4.11, respectively. It is found that the simulated S_{11} of Type-A rectangular horn is -22.28 dB and correspond to VSWR is around 1.17. The HPBW results in the E-plane and H-plane, which shown as the ratio of evaluation pattern to azimuth pattern (EL:AZ), is $21.7^\circ:24^\circ$ (1:1.11).

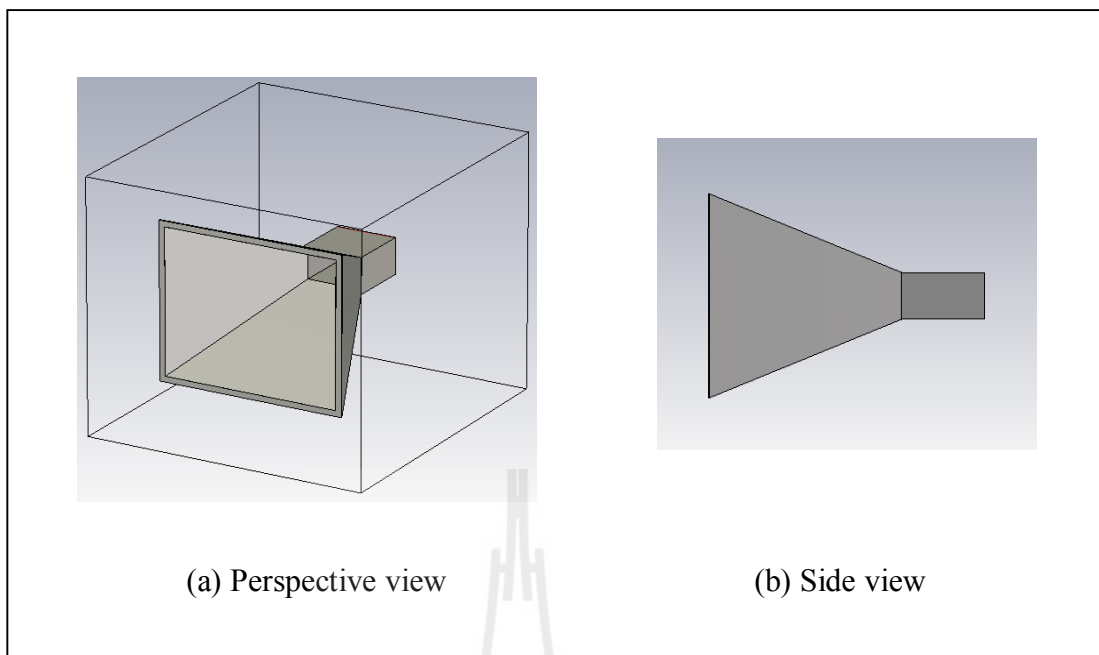


Figure 4.8 A conventional rectangular horn antenna (Type-A rectangular horn).



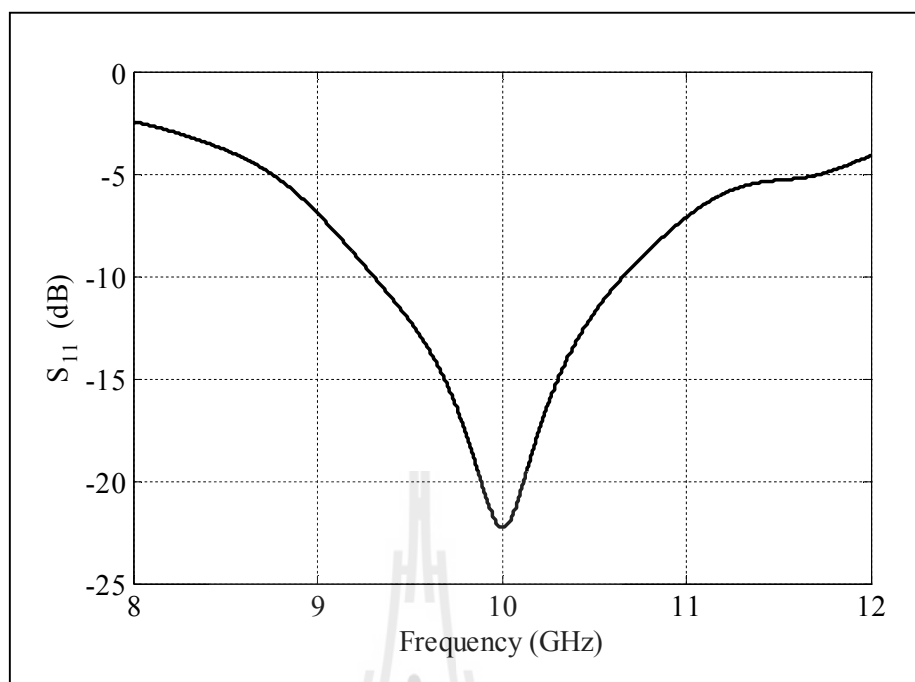


Figure 4.9 Simulated result of reflected power (S_{11}) of a Type-A rectangular horn.

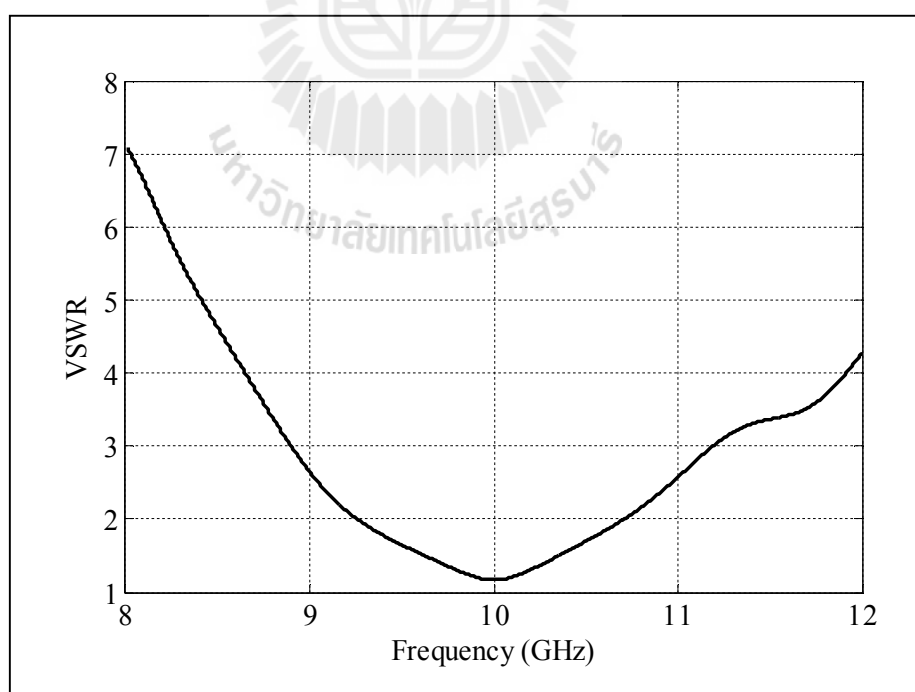


Figure 4.10 Simulated VSWR of a Type-A rectangular horn.

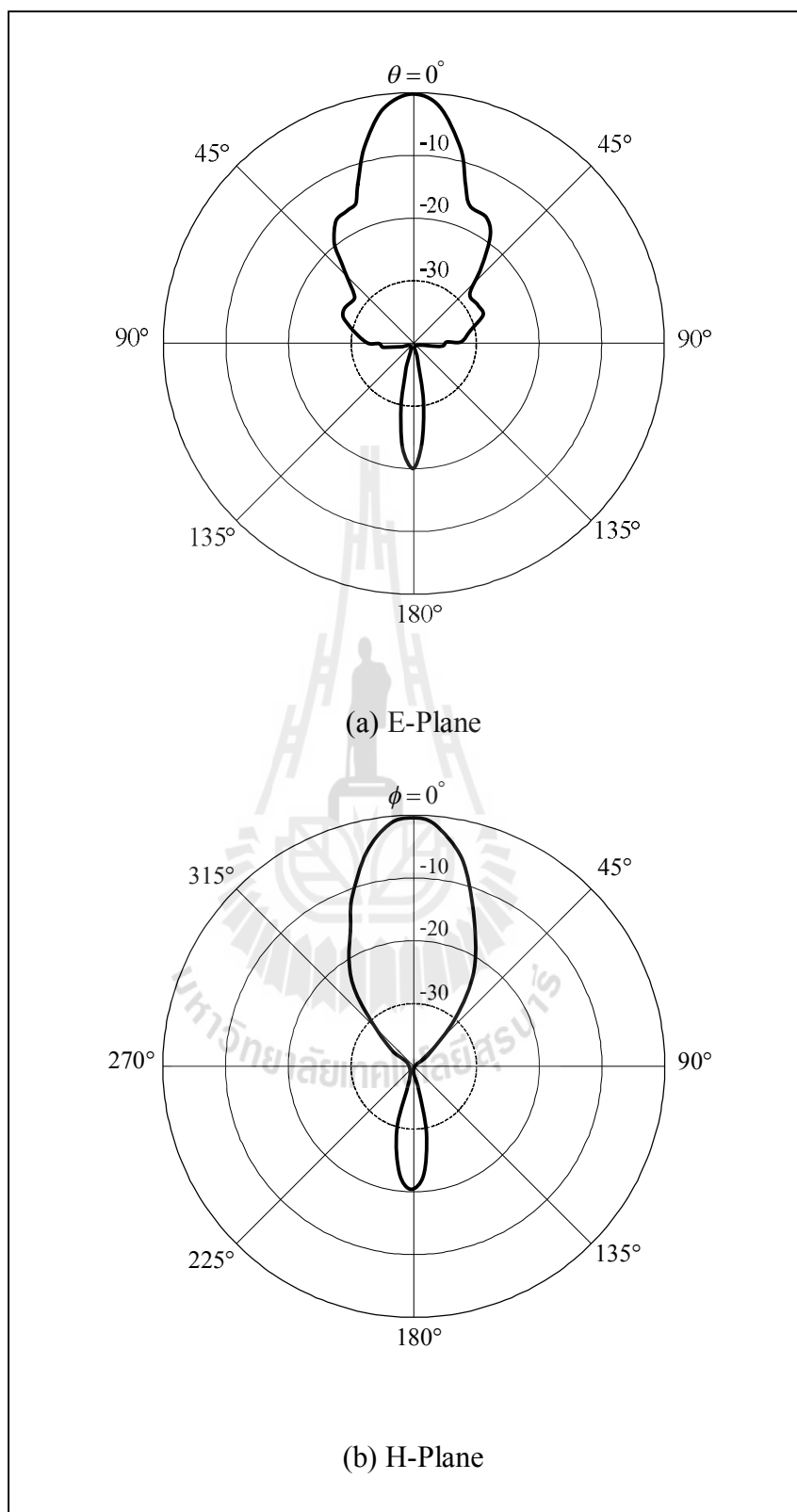


Figure 4.11 Simulated radiation patterns of a Type-A rectangular horn.

4.3.2 A Conventional Rectangular Horn Antenna and the Designed Woodpile EBG (Type-B rectangular horn)

The principle for gain increment of antenna, the HPBW will be narrow and side lobe level (SLL) should be decreased. From our study, we found that the proper structure of woodpile EBG is capable to enhance the gain of antenna as the additional resonant circuit which installed at front of a horn antenna. Furthermore, the woodpile EBG structures can be appropriately shaped for reducing side and back lobes of the directional antenna (Weily *et al.*, 2005; Lee *et al.*, 2009). Therefore, the designed quadratic shaped woodpile EBG is additionally installed in front of a conventional rectangular horn antenna with distance $d = 16.5\lambda$. This case will be called that Type-B rectangular horn, as shown in Figure 4.12. From the simulated results by using CST software, we found that the gain is increased from 17.67 dB to 25.58 dB but SLLs are also increased as shown in Figure 4.15. The HPBW ratio in the E-plane and H-plane, EL:AZ, is $7.1^\circ:6.9^\circ$ (1.03:1). The S_{11} and VSWR at the operating frequency of 10 GHz are shown in Figure 4.13 and 4.14, respectively. It notes that S_{11} and VSWR of Type-B rectangular horn are not varied when compared to the Type-A rectangular horn, therefore, the designed woodpile EBG is not the effect of the operating frequency of a rectangular horn antenna.

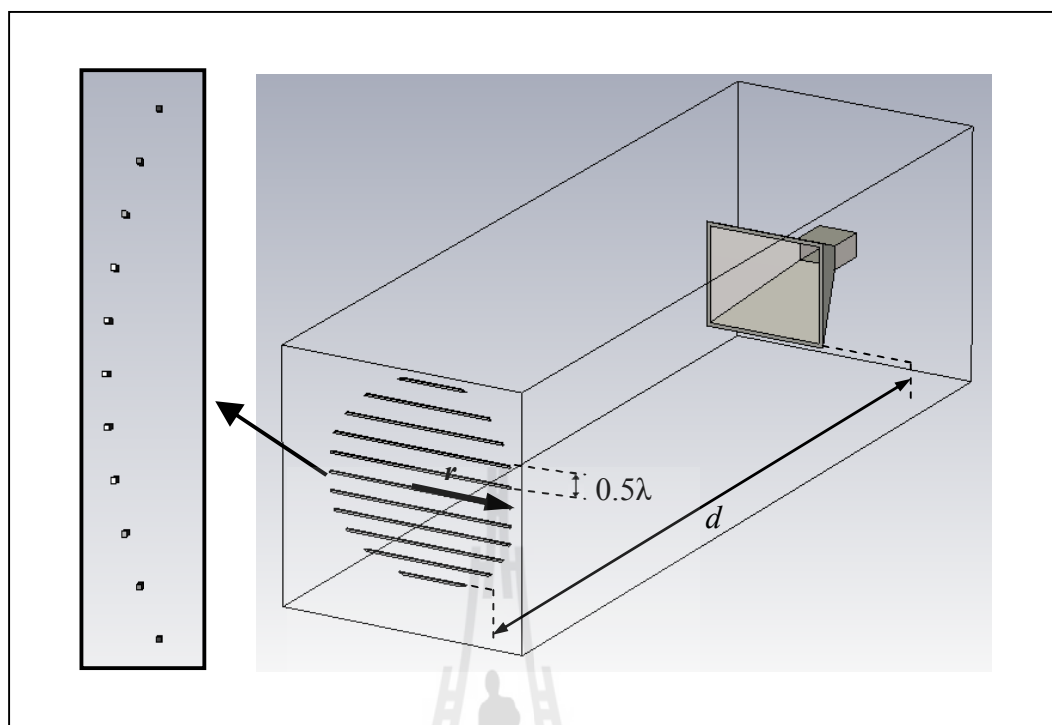


Figure 4.12 A conventional rectangular horn antenna and the designed woodpile EBG (Type-B rectangular horn).

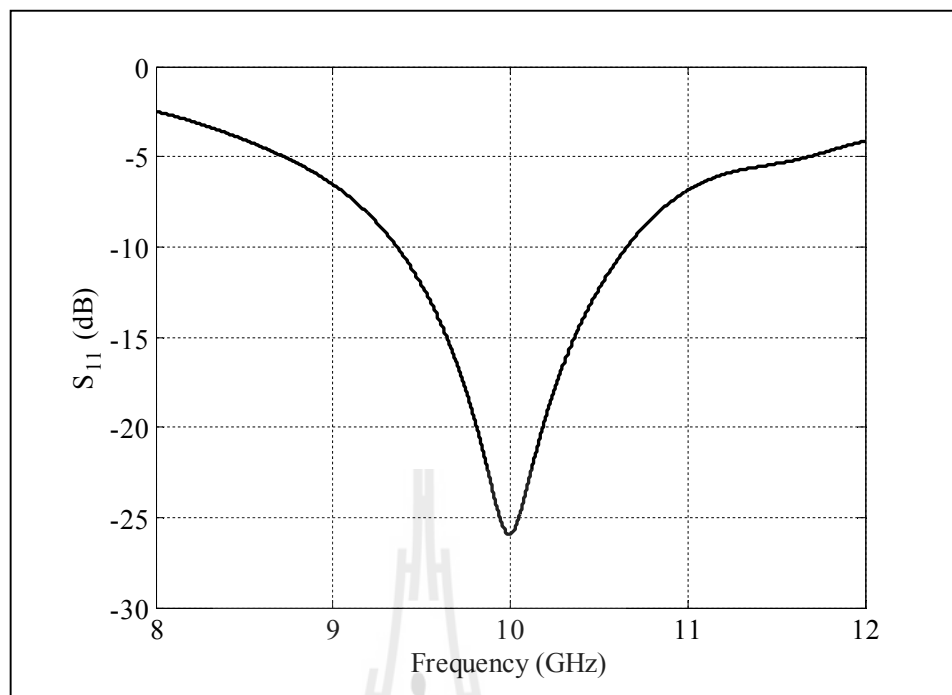


Figure 4.13 Simulated result of reflected power (S_{11}) of a Type-B rectangular horn.

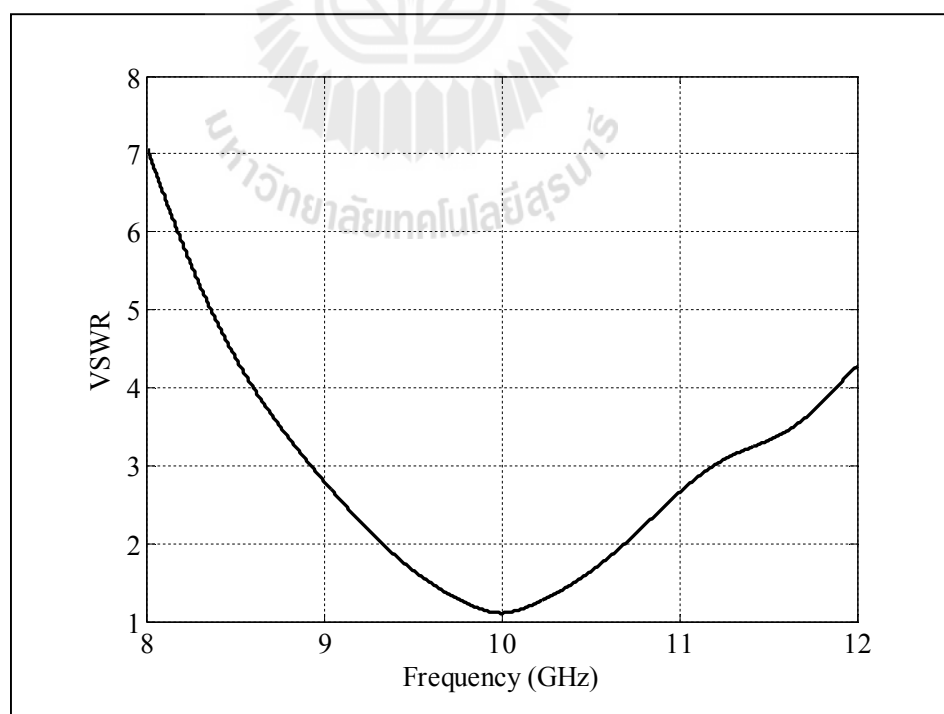


Figure 4.14 Simulated VSWR of a Type-B rectangular horn.

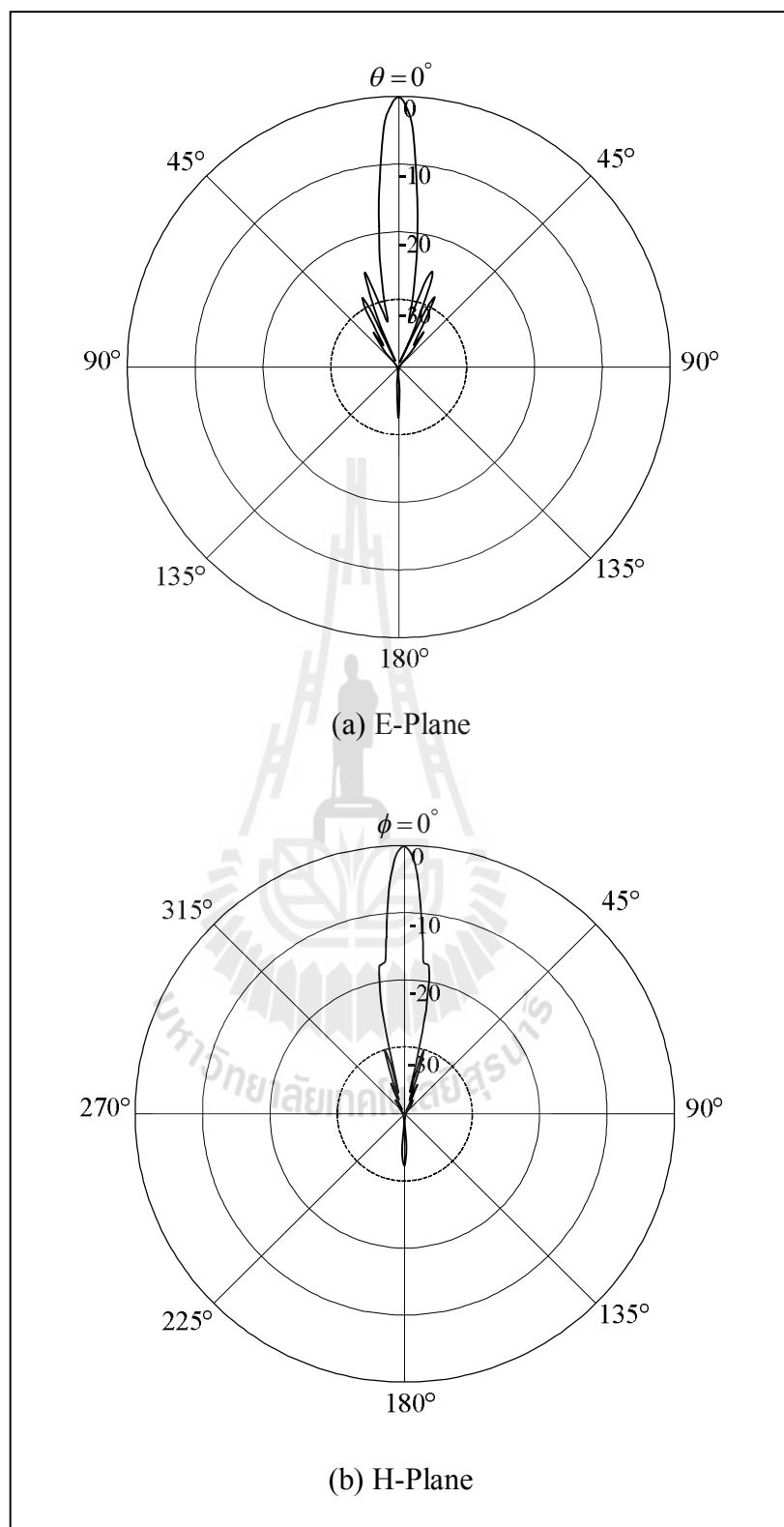


Figure 4.15 Simulated radiation patterns of a Type-B rectangular horn.

4.3.3 A Rectangular Horn Antenna with Two Side-Wing Slabs

(Type-C rectangular horn)

From the results of a Type-B rectangular horn, SLL in H-plane is also high even if its HPBW is narrow and high gain. Then, we suppose that if the designed quadratic shaped woodpile EBG is symmetrical shape, which is placed in front of horn antenna which has the symmetrical radiation pattern. The SLL will be decreased and higher gain is obtained. Therefore, to improve the radiation pattern, a conventional rectangular horn antenna will be added with two side-wing slabs on the left and right sides, to control HPBW symmetrically in the E-plane and H-plane as shown in Figure 4.16 and it is called that Type-C rectangular horn. From the simulated results by using CST software, we found that the dimension for each side-wing slab is 0.625λ as shown in Table 4.1. It yields quite symmetrical HPBW, high gain, and low SLLs when compared to the conventional rectangular horn. The simulated results show that S_{11} of Type-C rectangular horn at the operating frequency of 10 GHz is around -25.08 dB and VSWR is around 1.12 as shown in Figure 4.17 and 4.18, respectively. The normalized radiation patterns of a Type-C rectangular horn with the gain of 18.08 dB is shown in Figure 4.19. The HPBW ratio in the E-plane and H-plane, EL:AZ, is $21.7^\circ:20.6^\circ$ (1.05:1).

Table 4.1 The simulated results of various dimension of two side-wing slabs installed at the aperture of a rectangular horn antenna.

Dimension of wing slab	Gain (dB)	HPBW EL:AZ	SLL (dB) E-plane/H-plane
0λ	17.40	$21.7^{\circ}:24.0^{\circ}$ (1:1.11)	-18.1/-22.2
0.25λ	17.68	$21.5^{\circ}:22.3^{\circ}$ (1:1.04)	-17.8/-25.9
0.375λ	17.74	$21.7^{\circ}:21.7^{\circ}$ (1:1)	-17.6/-21.8
0.5λ	17.90	$21.8^{\circ}:21.1^{\circ}$ (1.03:1)	-17.8/-22.4
0.625λ	18.08	$21.7^{\circ}:20.6^{\circ}$ (1.05:1)	-18.1/-26.4
0.75λ	18.08	$21.6^{\circ}:20.3^{\circ}$ (1.06:1)	-18.0/-25.8
0.875λ	18.14	$21.8^{\circ}:20.0^{\circ}$ (1.09:1)	-18.0/-13.9
1λ	18.22	$22.0^{\circ}:19.8^{\circ}$ (1.11:1)	-18.3/-14.0

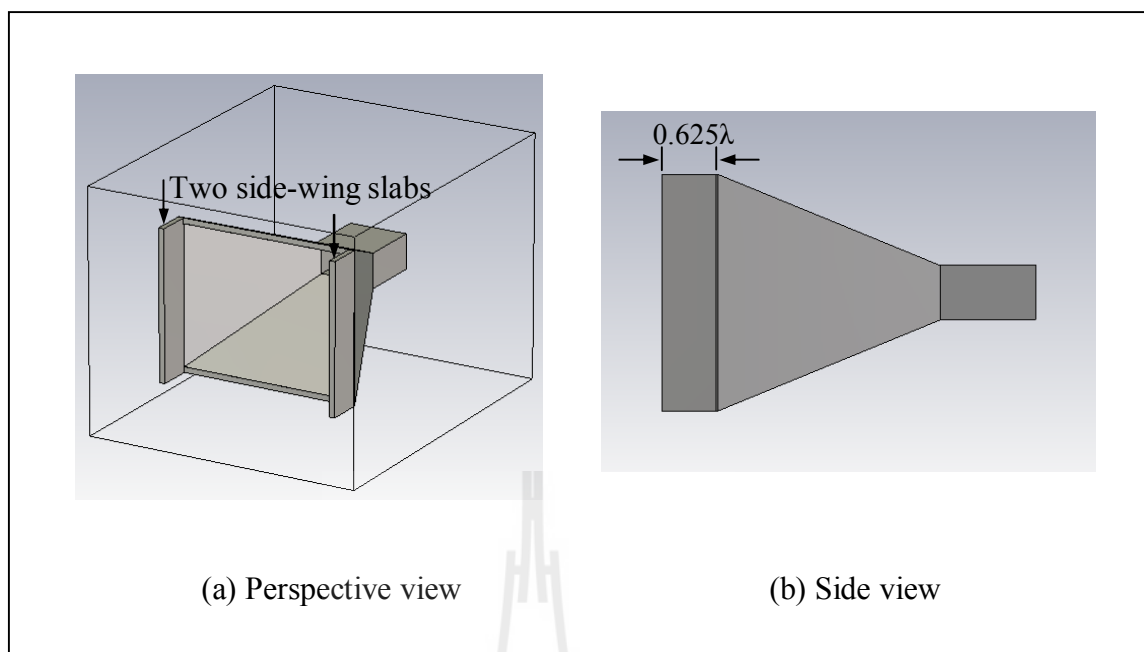


Figure 4.16 A rectangular horn antenna with two side-wing slabs
(Type-C rectangular horn).



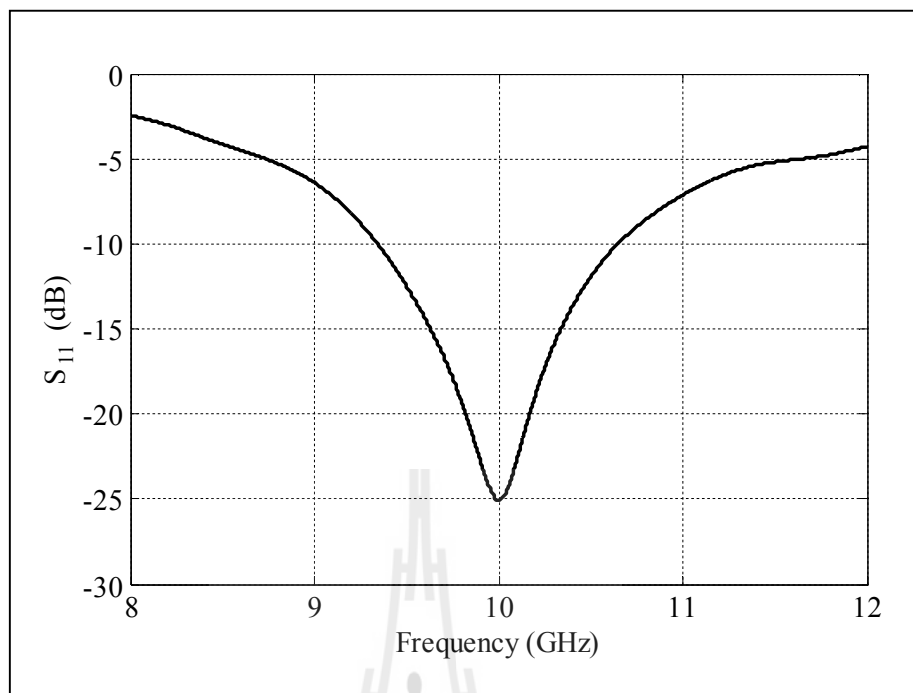


Figure 4.17 Simulated result of reflected power (S_{11}) of a Type-C rectangular horn.

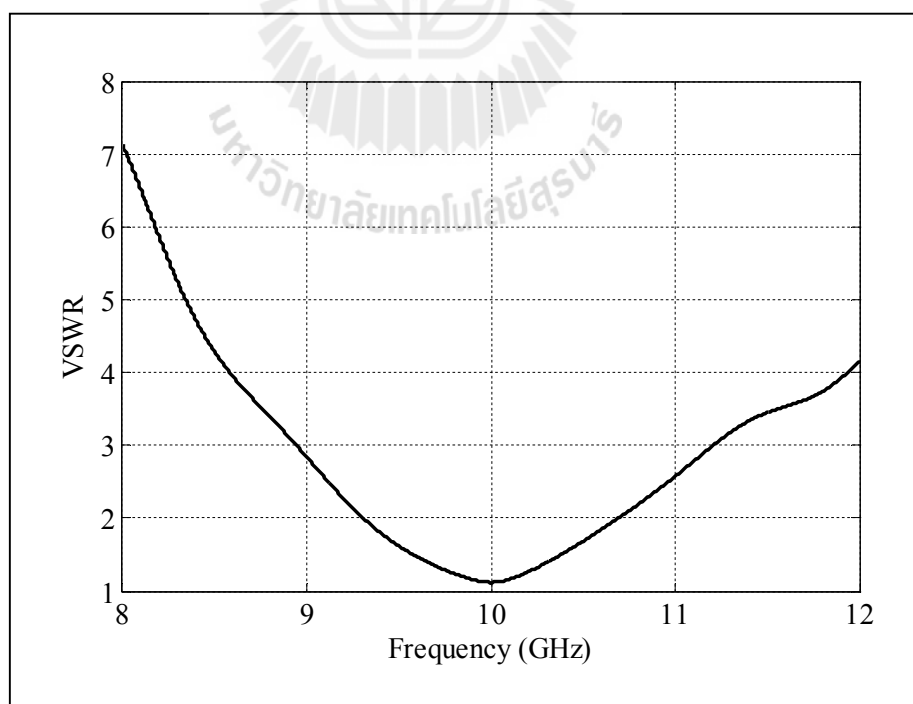


Figure 4.18 Simulated VSWR of a Type-C rectangular horn.

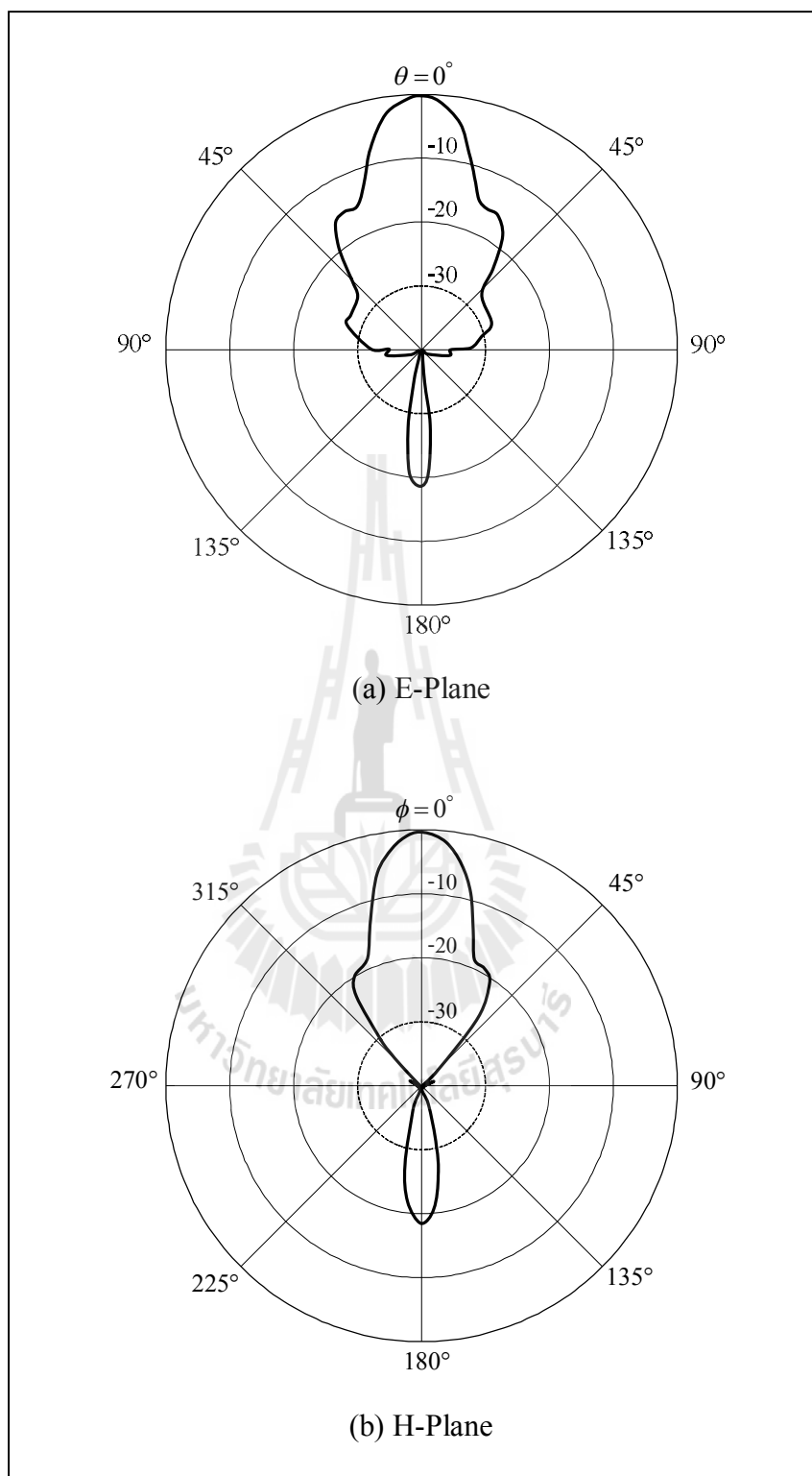


Figure 4.19 Simulated radiation patterns of a Type-C rectangular horn.

4.3.4 A Rectangular Horn Antenna with Two Side-Wing Slabs and the Designed Woodpile EBG (Type-D rectangular horn)

After, the radiation patterns of a rectangular horn antenna are improved to be quite symmetrical by adding two side-wing slabs on the left and right sides. The designed quadratic shaped woodpile EBG is installed in front of this modified rectangular horn antenna with distance $d = 16.5\lambda$, we called this case that Type-D rectangular horn, as shown in Figure 4.20. From the results of CST software, we found that the gain is increased from 18.08 dB to 25.75 dB. Moreover, it evidently provides the symmetrical radiation patterns both in E-plane and H-plane and moderately yields higher gain around 8 dB when compared to a conventional rectangular horn antenna. Its bandwidth is started from 9.36 GHz to 10.64 GHz or about 1.28 GHz (12.8%) at S_{11} is at -10 dB, which are wide enough and can be well utilized for X-band radar and I-band beyond following the IEEE and the ITU, respectively, as shown in Figure 4.21. The VSWR and normalized radiation patterns at the operating frequency of 10 GHz of a Type-D rectangular horn are shown in Figure 4.22 and 4.23, respectively. The HPBW ratio in the E-plane and H-plane, EL:AZ, is $6.8^\circ:6.9^\circ$ or 1:1.01.

Table 4.2 shows the comparison of simulated results of four types of the rectangular horn antennas such as the gains, HPBWs, and SLLs. Besides, the comparison of S_{11} , VSWR, and radiation patterns of four types of the rectangular horn antennas are shown in Figure 4.24, 4.25, and 4.26, respectively. In consequence, the proper designed quadratic shaped woodpile EBG structures can provide the moderately highest gain of 25.75 dB at the operating frequency of 10 GHz and the radiation patterns of a rectangular horn antenna are quite symmetrical.

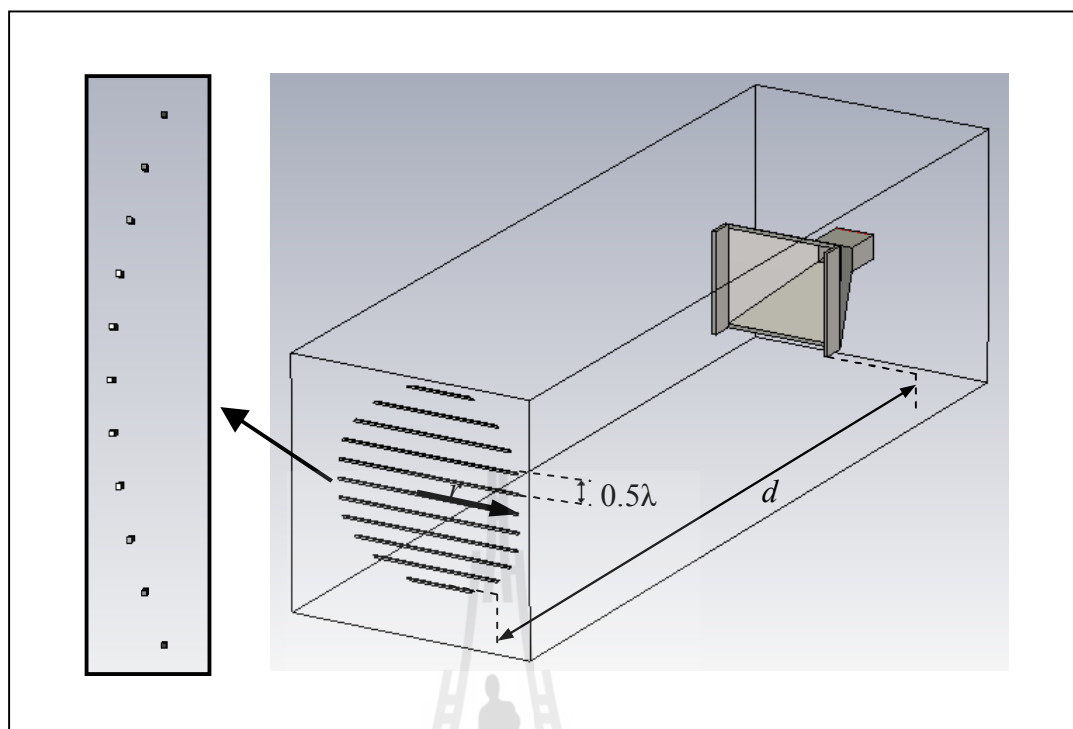


Figure 4.20 A rectangular horn antenna with two side-wing slabs and the designed woodpile EBG (Type-D rectangular horn).

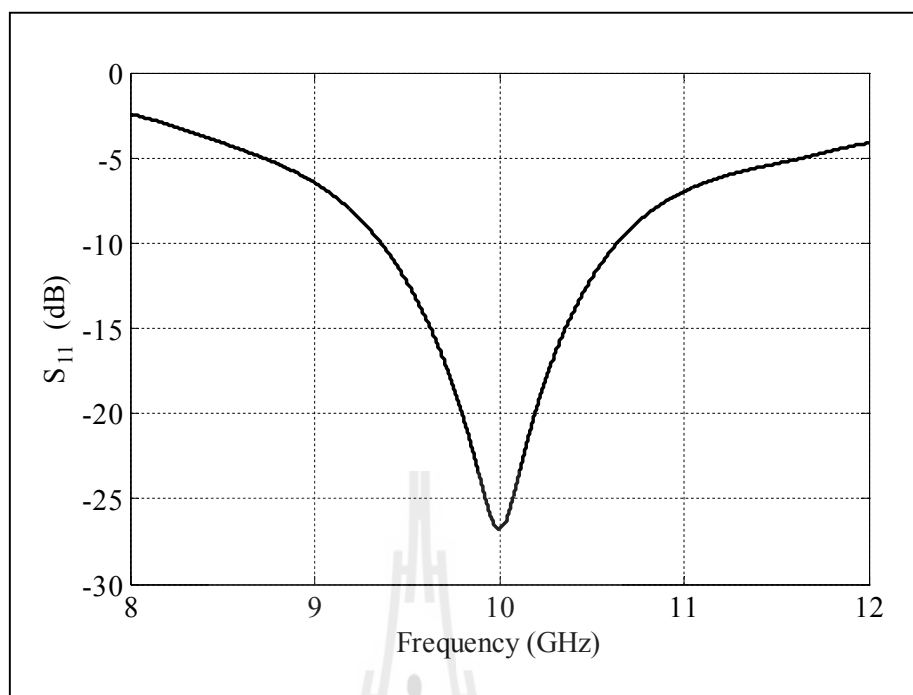


Figure 4.21 Simulated result of reflected power (S_{11}) of a Type-D rectangular horn.

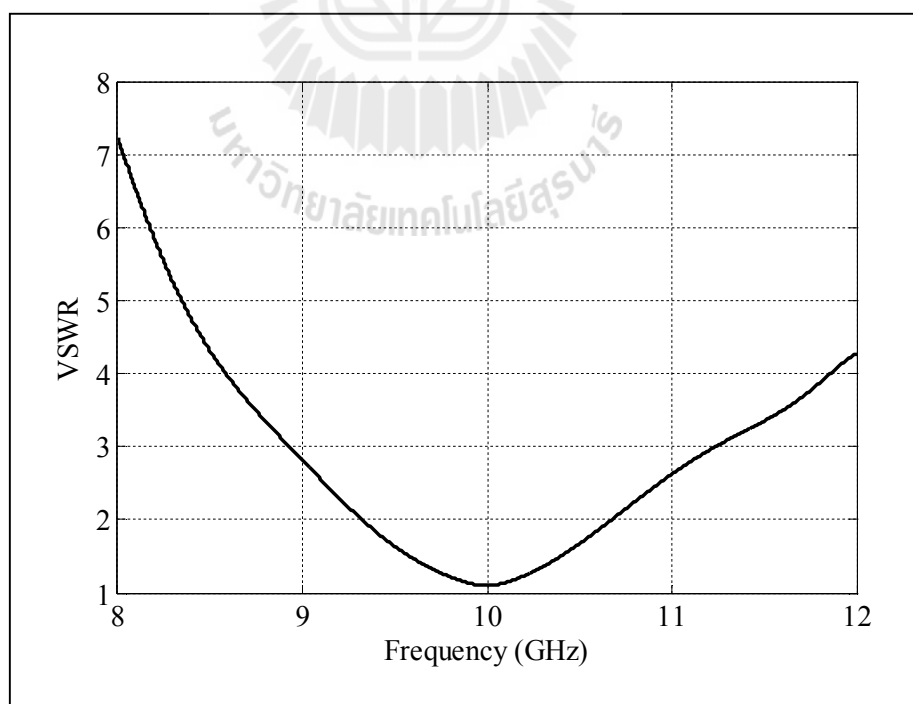


Figure 4.22 Simulated VSWR of a Type-D rectangular horn.

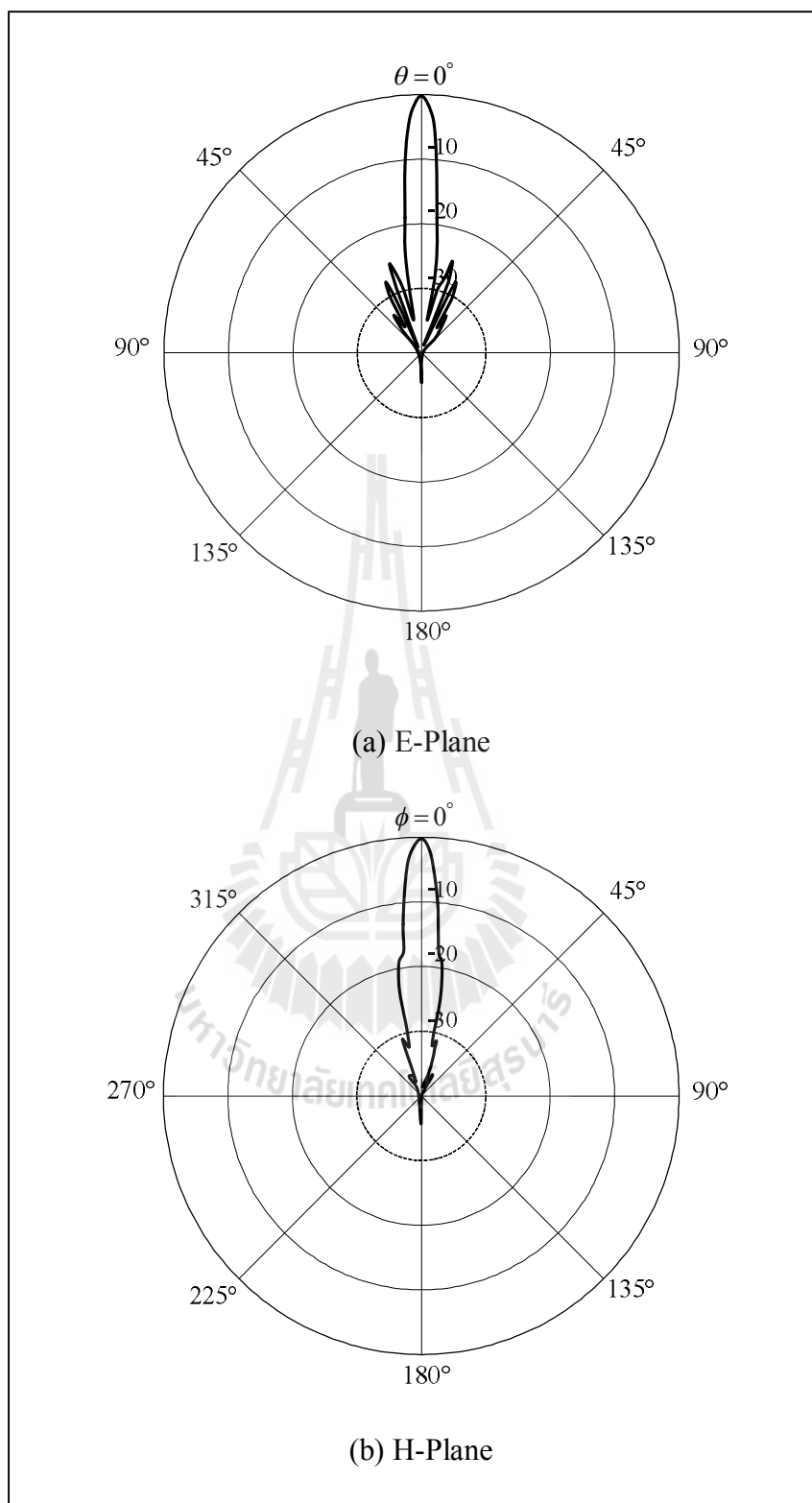
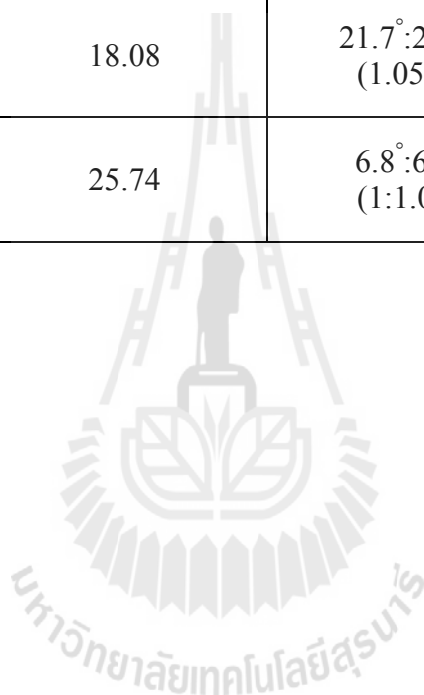


Figure 4.23 Simulated radiation patterns of a Type-D rectangular horn.

Table 4.2 The simulated results of four types of the rectangular horn antennas.

The rectangular horn antennas	Gain (dB)	HPBW EL:AZ	SLL (dB) E-plane/H-plane
Type-A rectangular horn	17.67	21.7°:24° (1:1.11)	-18.1/-22.2
Type-B rectangular horn	25.58	7.1°:6.9° (1.03:1)	-16.3/-11.0
Type-C rectangular horn	18.08	21.7°:20.6° (1.05:1)	-18.1/-26.4
Type-D rectangular horn	25.74	6.8°:6.9° (1:1.01)	-16.5/-20.0



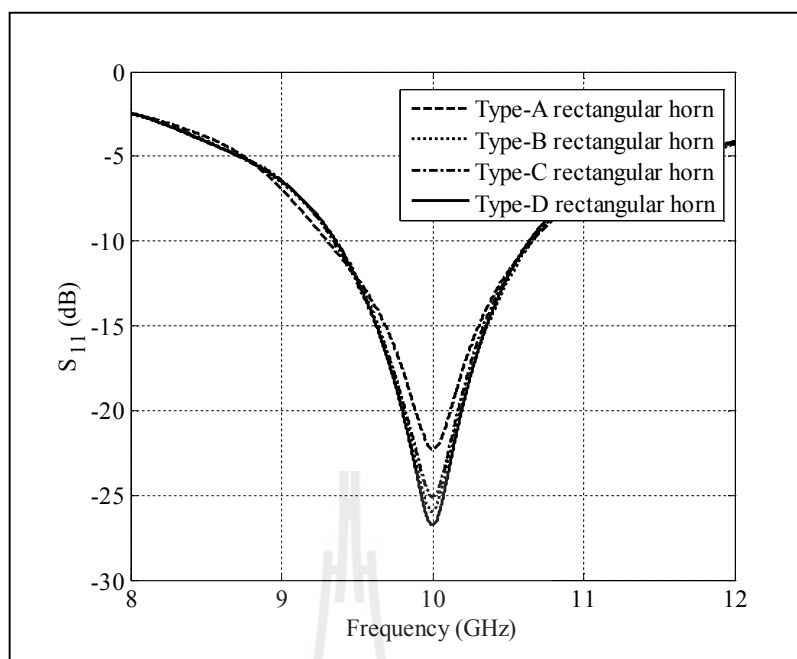


Figure 4.24 Simulated result of reflected power (S_{11}) of four types of the rectangular horn antennas.

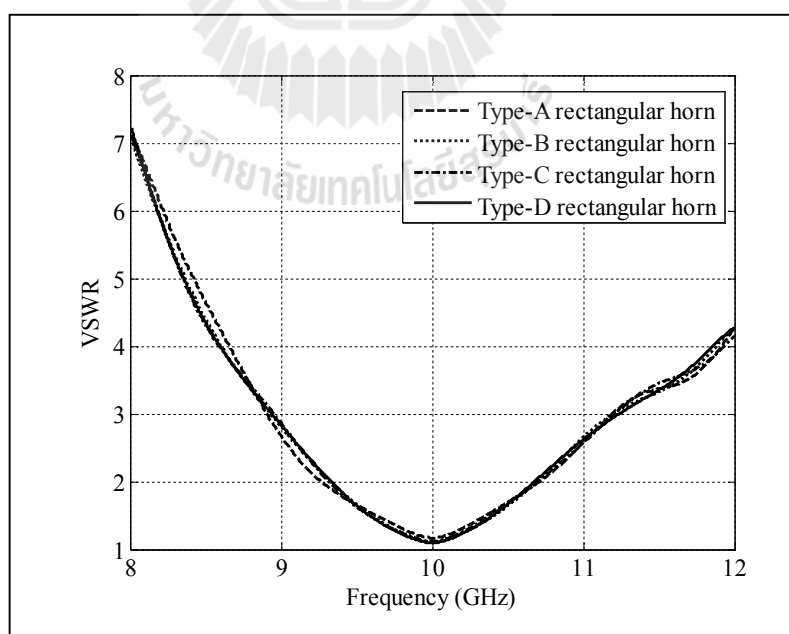


Figure 4.25 Simulated VSWR of four types of the rectangular horn antennas.

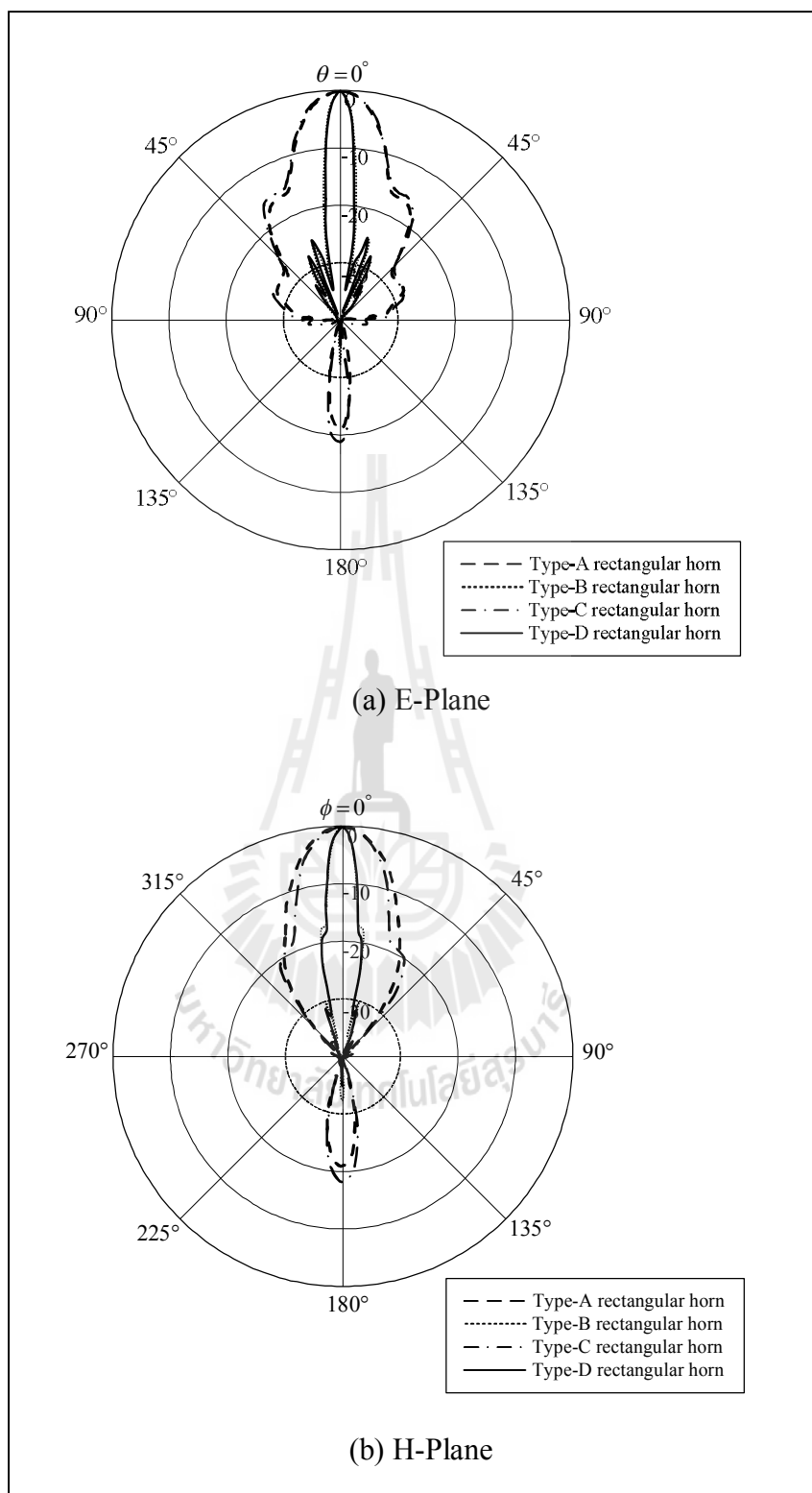


Figure 4.26 Simulated radiation patterns of four types of the rectangular horn antennas.

4.4 A Circular Horn Antenna Configuration

4.4.1 A Conventional Circular Horn Antenna (Type-A circular horn)

The circular or conical horn antenna is the second horn that is popularly utilized applications in microwave band. While the rectangular horn antennas are usually fed by the rectangular waveguide but the feed of the circular horn antenna is the circular waveguide. However, in this research, a rectangular waveguide and a converter circular to rectangular waveguide adapter has been used to feed the signal into the circular horn antenna, because it is simple to design and there is a rectangular waveguide in laboratory. The design of a conventional circular horn antenna (next, we will call this horn antenna as Type-A circular horn) is initiated by determining its aperture dimension as follow Balanis (2005) as shown in Figure 4.27. The simulated results by using CST software, show the reflected power or S_{11} of a Type-A circular horn at the operating frequency of 10 GHz is around -31.72 which answer to VSWR is around 1.05 as shown in Figure 4.28 and 4.29, respectively. The normalized radiation patterns of a Type-A circular horn with the gain of 19.33 dB is shown in Figure 4.30. The ratio of HPBW in the E-plane and H-plane, EL:AZ, is equal $16.7^\circ:19.5^\circ$ or 1:1.17.

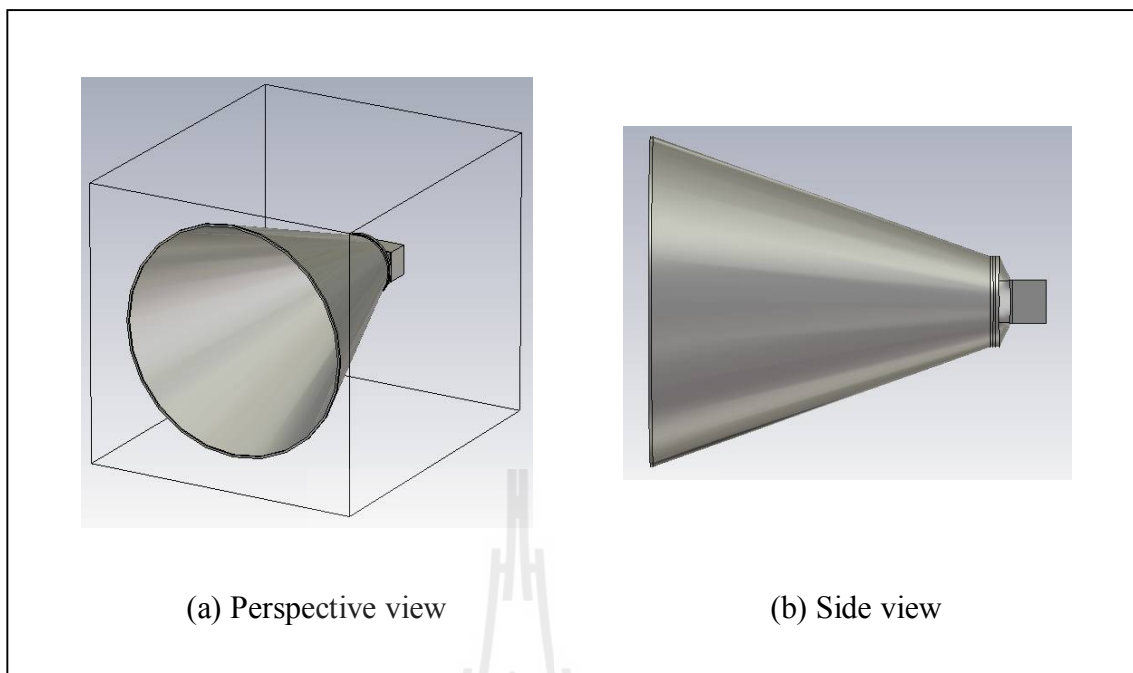


Figure 4.27 A conventional circular horn antenna and waveguide adapter
(Type-A circular horn).



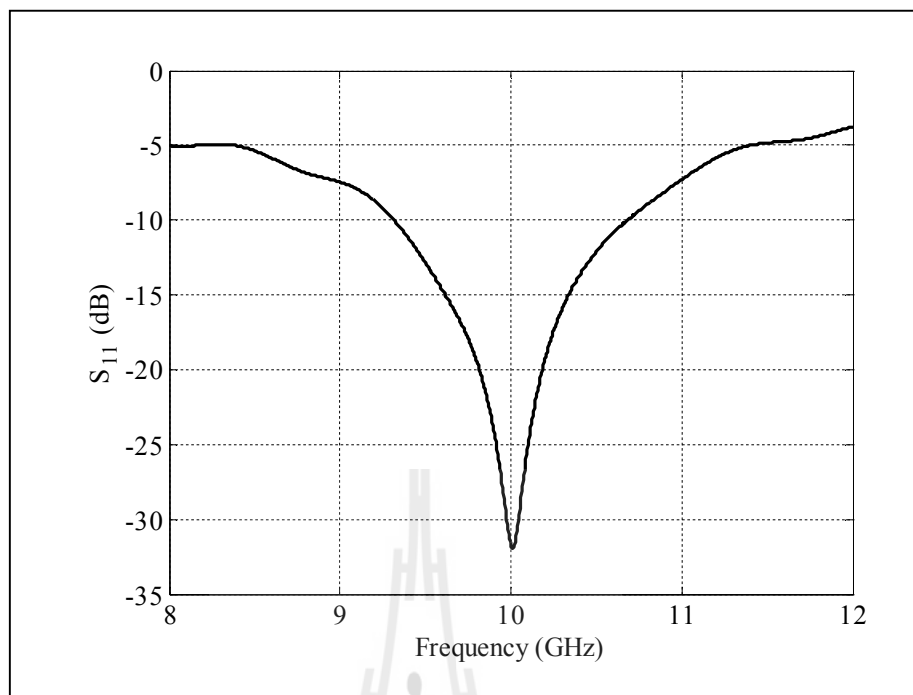


Figure 4.28 Simulated result of reflected power (S_{11}) of a Type-A circular horn.

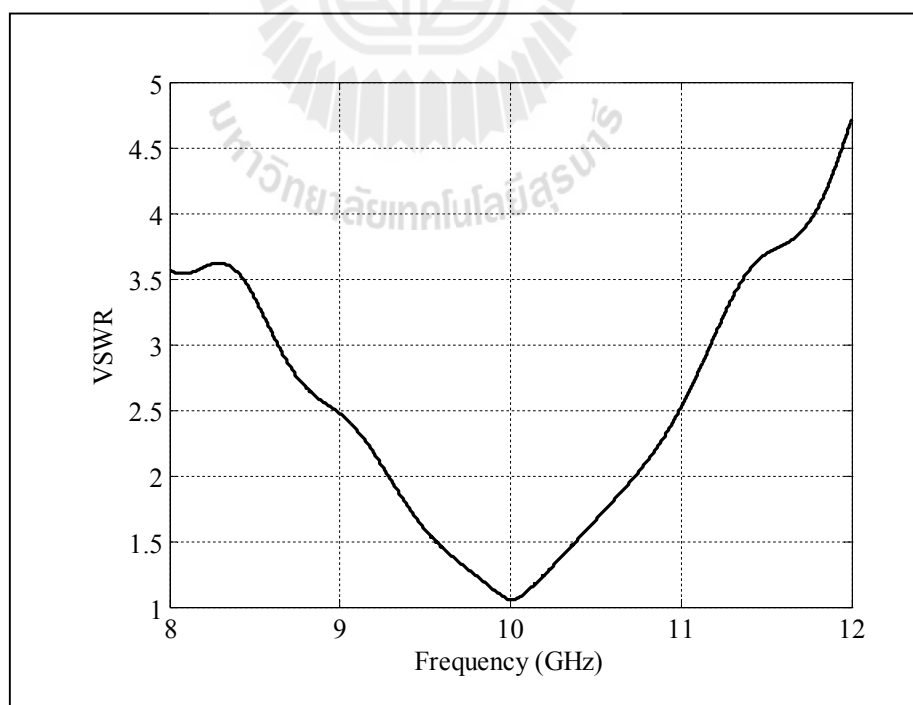


Figure 4.29 Simulated VSWR of a Type-A circular horn.

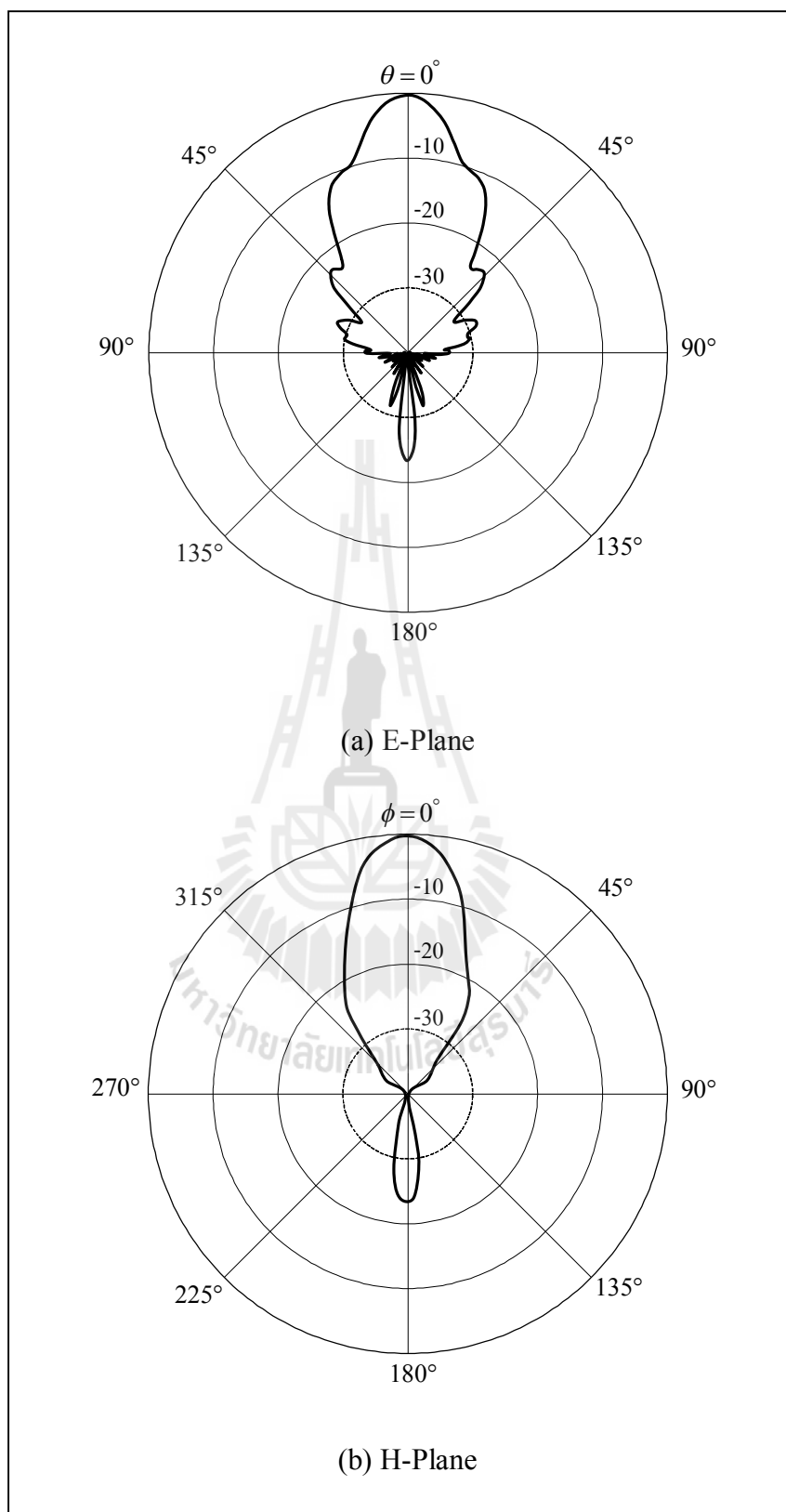


Figure 4.30 Simulated radiation patterns of a Type-A circular horn.

4.4.2 A Conventional Circular Horn Antenna and the Designed Woodpile EBG (Type-B circular horn)

In addition, a similar quadratic shaped woodpile EBG, which was used with the rectangular horn, is used again and installed in front of a conventional circular horn antenna with distance $d = 16.5\lambda$ as shown in Figure 4.31, and it is called that Type-B circular horn. From the simulated results by using CST software, we found that the gain is increased from 19.33 dB to 25.76 dB but SLLs are also increased as shown in Figure 4.34, the same as a Type-B rectangular horn case. The S_{11} of a Type-B circular horn at the operating frequency of 10 GHz is around -35.80 dB and agree with VSWR is around 1.03 as shown in Figure 4.32 and 4.33, respectively. Furthermore, we found that the designed quadratic shaped woodpile EBG is not the effect of the operating frequency of a circular horn antenna. From Figure 4.34, the ratio of HPBW in the E-plane and H-plane, EL:AZ, is equal $6.4^\circ:7.3^\circ$ or 1:1.14.

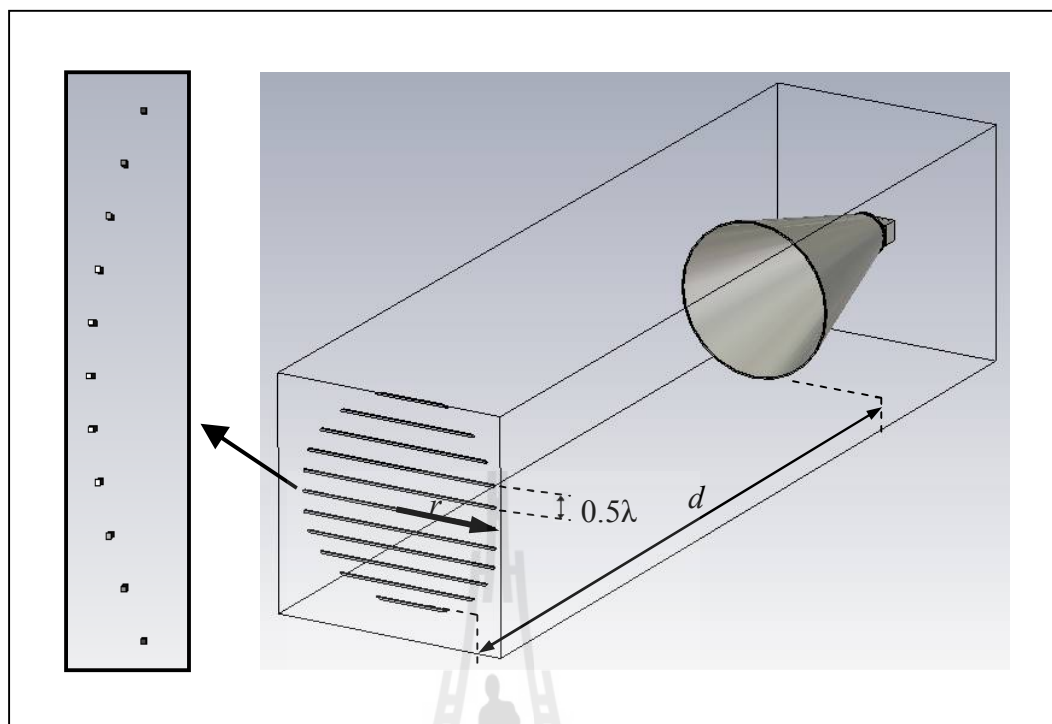


Figure 4.31 A conventional circular horn antenna and the designed woodpile EBG (Type-B circular horn).

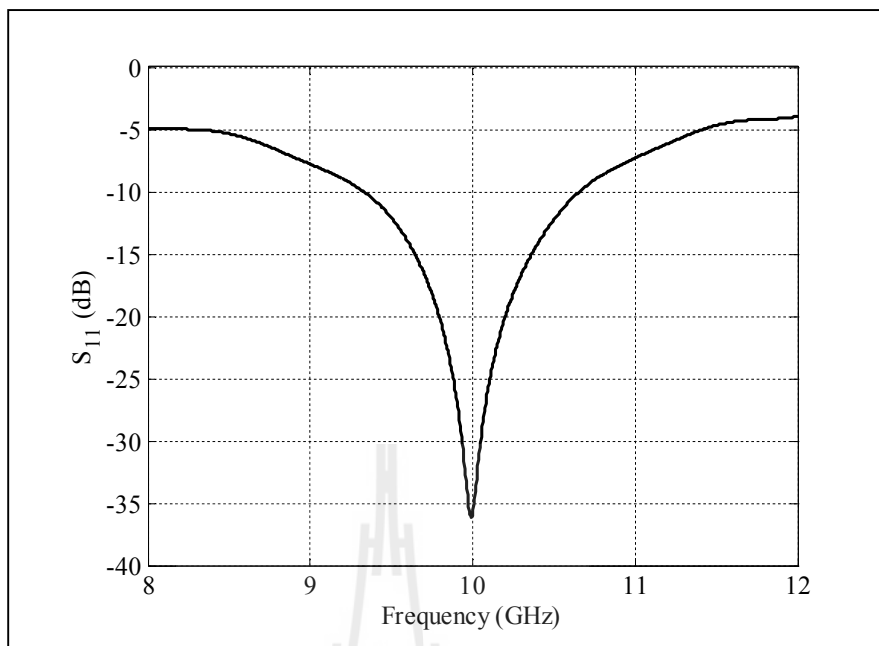


Figure 4.32 Simulated result of reflected power (S_{11}) of a Type-B circular horn.

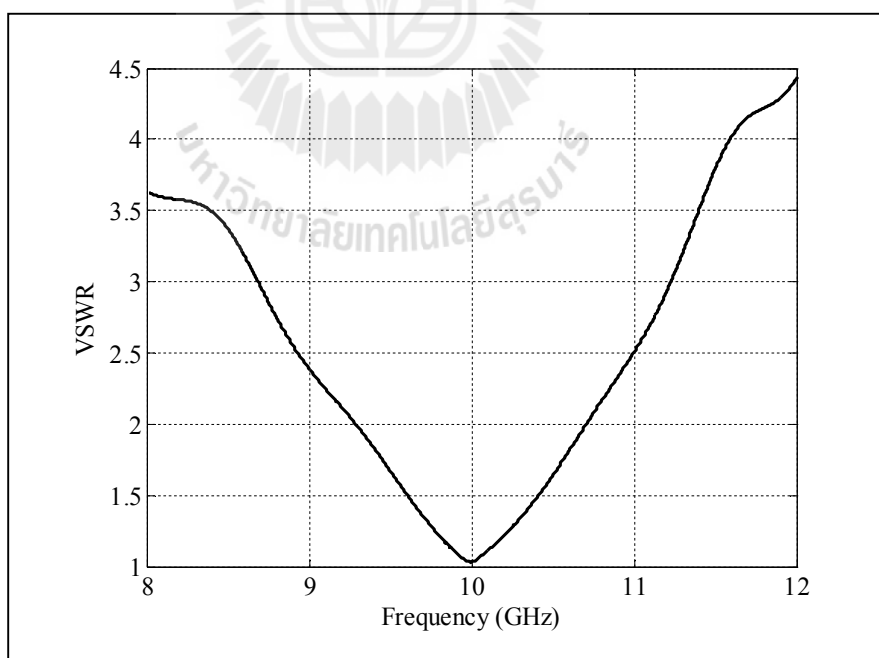


Figure 4.33 Simulated VSWR of a Type-B circular horn.

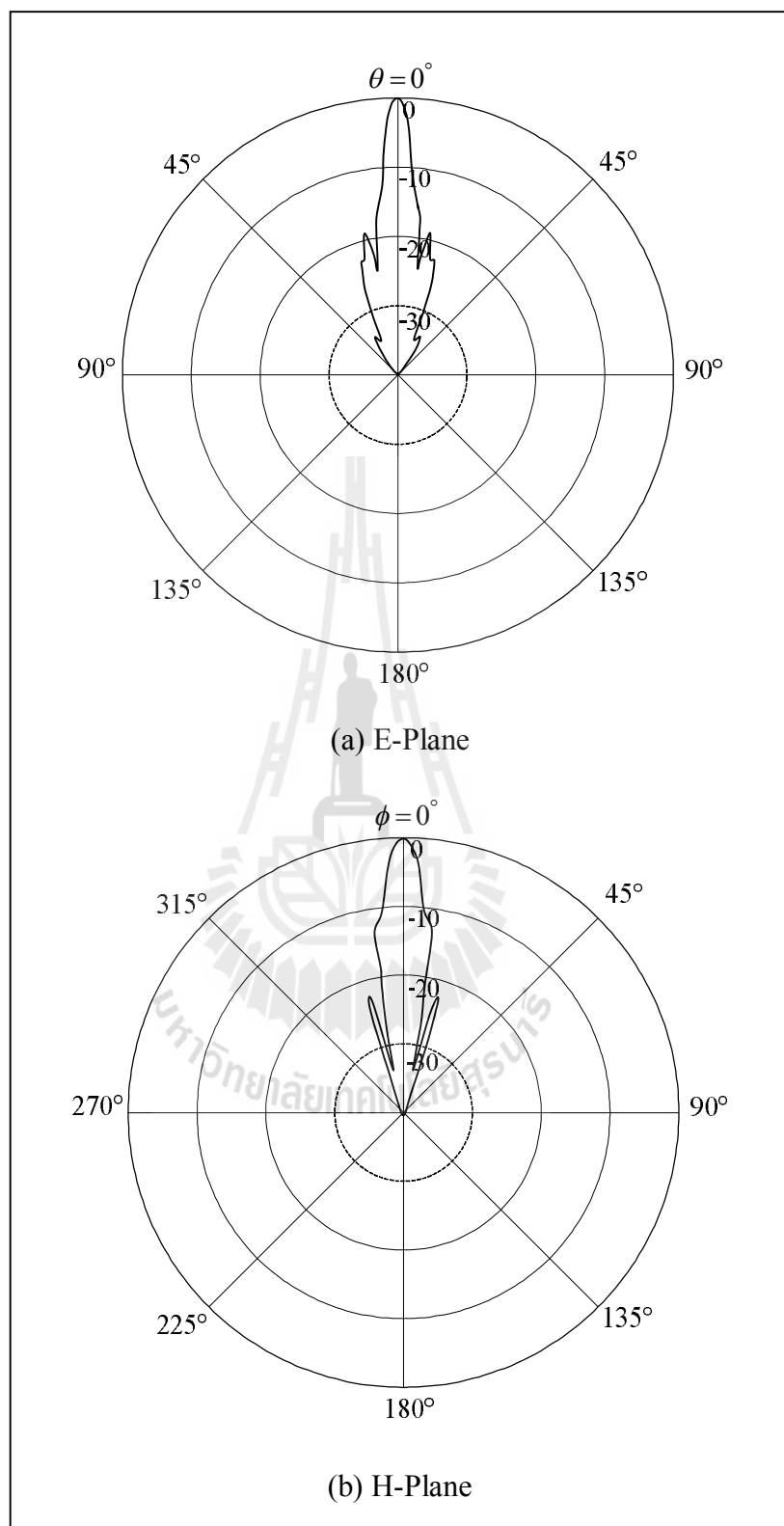


Figure 4.34 Simulated radiation patterns of a Type-B circular horn.

4.4.3 A Circular Horn Antenna with Two Side-Wing Slabs (Type-C circular horn)

In the same way as a Type-C rectangular horn case, we suppose that if the designed quadratic shaped woodpile EBG is symmetrical shape, which is placed in front of circular horn antenna which has the symmetrical radiation pattern. The SLL will be decreased and higher gain is obtained. Therefore, to improve the radiation pattern, a conventional circular horn antenna will be added with two side-wing slabs on the left and right sides, to control HPBW symmetrically in the E-plane and H-plane as shown in Figure 4.35 and it is called that Type-C circular horn. From the simulated results by using CST software, we found that the dimension for each side-wing slab is approximately 0.75λ , it yields quite symmetrical HPBW, high gain, and low SLLs as shown in Table 4.3. The S_{11} of a Type-C circular horn at the operating frequency of 10 GHz is around -33.22 dB and VSWR is around 1.04 as shown in Figure 4.36 and 4.37, respectively. The normalized radiation patterns of a Type-C circular horn with the gain of 19.67 dB is shown in Figure 4.38. The ratio of HPBW in the E-plane and H-plane, EL:AZ, is $16.7^\circ:18.1^\circ$ (1:1.08).

Table 4.3 The simulated results of various dimension of two side-wing slabs installed at the aperture of a circular horn antenna.

Dimension of wing slab	Gain (dB)	HPBW EL:AZ	SLL (dB) E-plane/H-plane
0λ	19.33	$16.7^{\circ}:19.5^{\circ}$ (1:1.17)	-22.5/-22.5
0.25λ	19.46	$16.7^{\circ}:18.8^{\circ}$ (1:1.13)	-20.6/-29.1
0.375λ	19.53	$16.8^{\circ}:18.6^{\circ}$ (1:1.1)	-20.3/-24.3
0.5λ	19.63	$16.6^{\circ}:18.5^{\circ}$ (1:1.11)	-20.9/-23.0
0.625λ	19.66	$16.5^{\circ}:18.3^{\circ}$ (1:1.11)	-21.0/-27.6
0.75λ	19.67	$16.7^{\circ}:18.1^{\circ}$ (1:1.08)	-20.5/-27.4
0.875λ	19.70	$16.8^{\circ}:18.1^{\circ}$ (1:1.08)	-19.9/-17.4
1λ	19.77	$16.7^{\circ}:18.0^{\circ}$ (1:1.08)	-19.3/-17.6

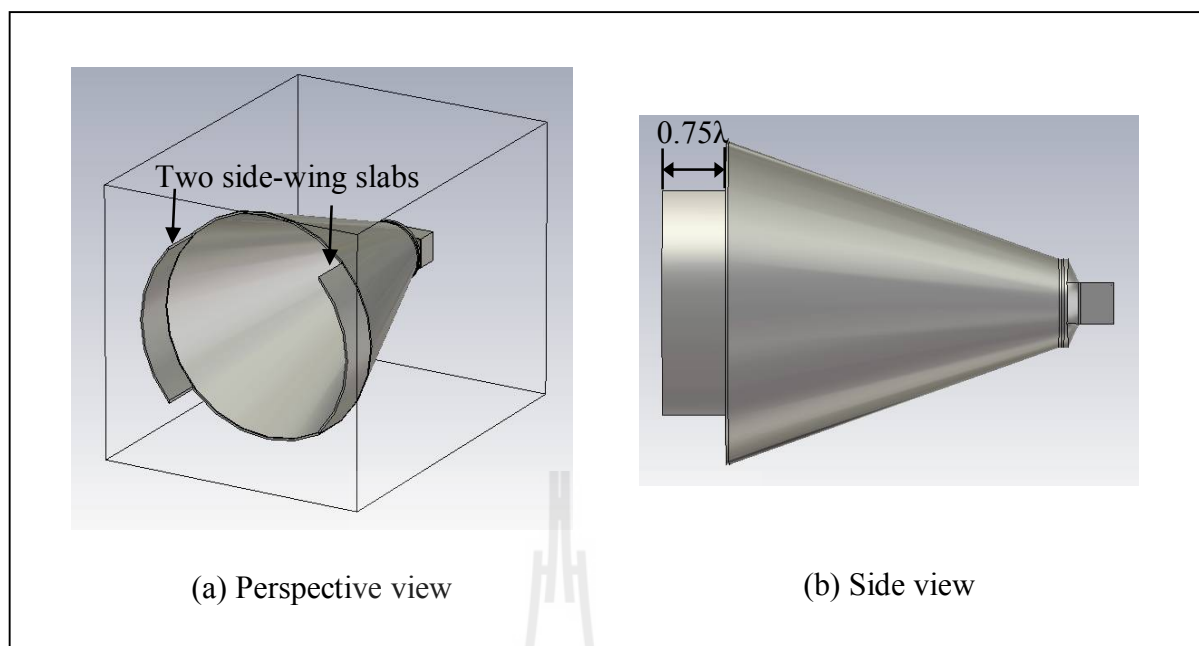
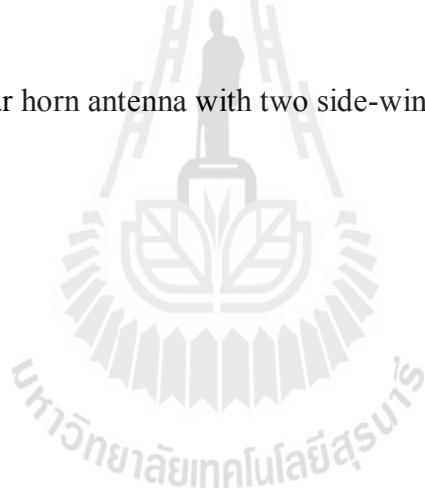


Figure 4.35 A circular horn antenna with two side-wing slabs (Type-C circular horn).



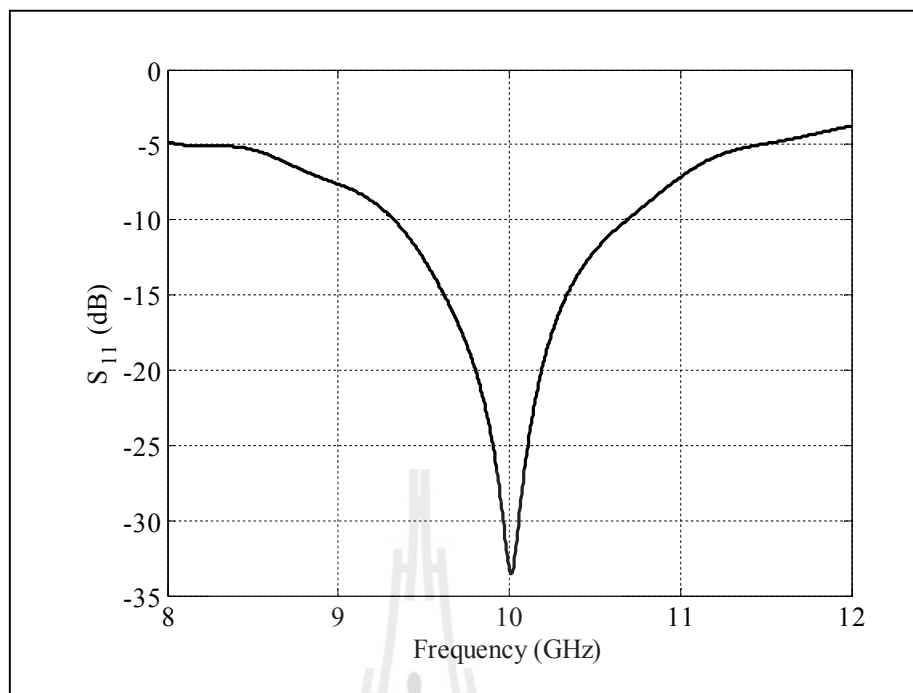


Figure 4.36 Simulated result of reflected power (S_{11}) of a Type-C circular horn.

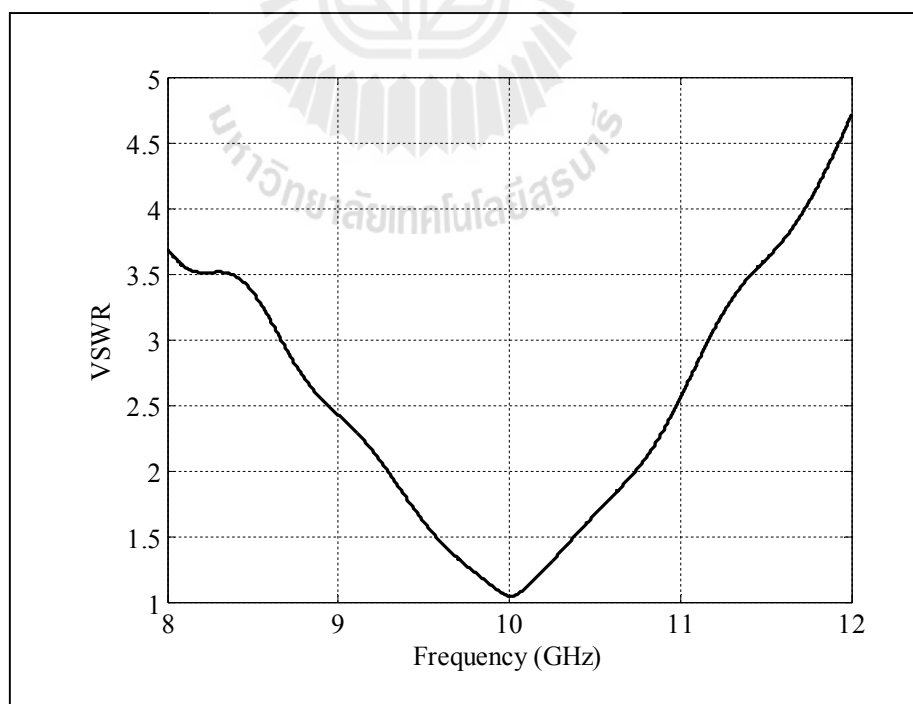


Figure 4.37 Simulated VSWR of a Type-C circular horn.

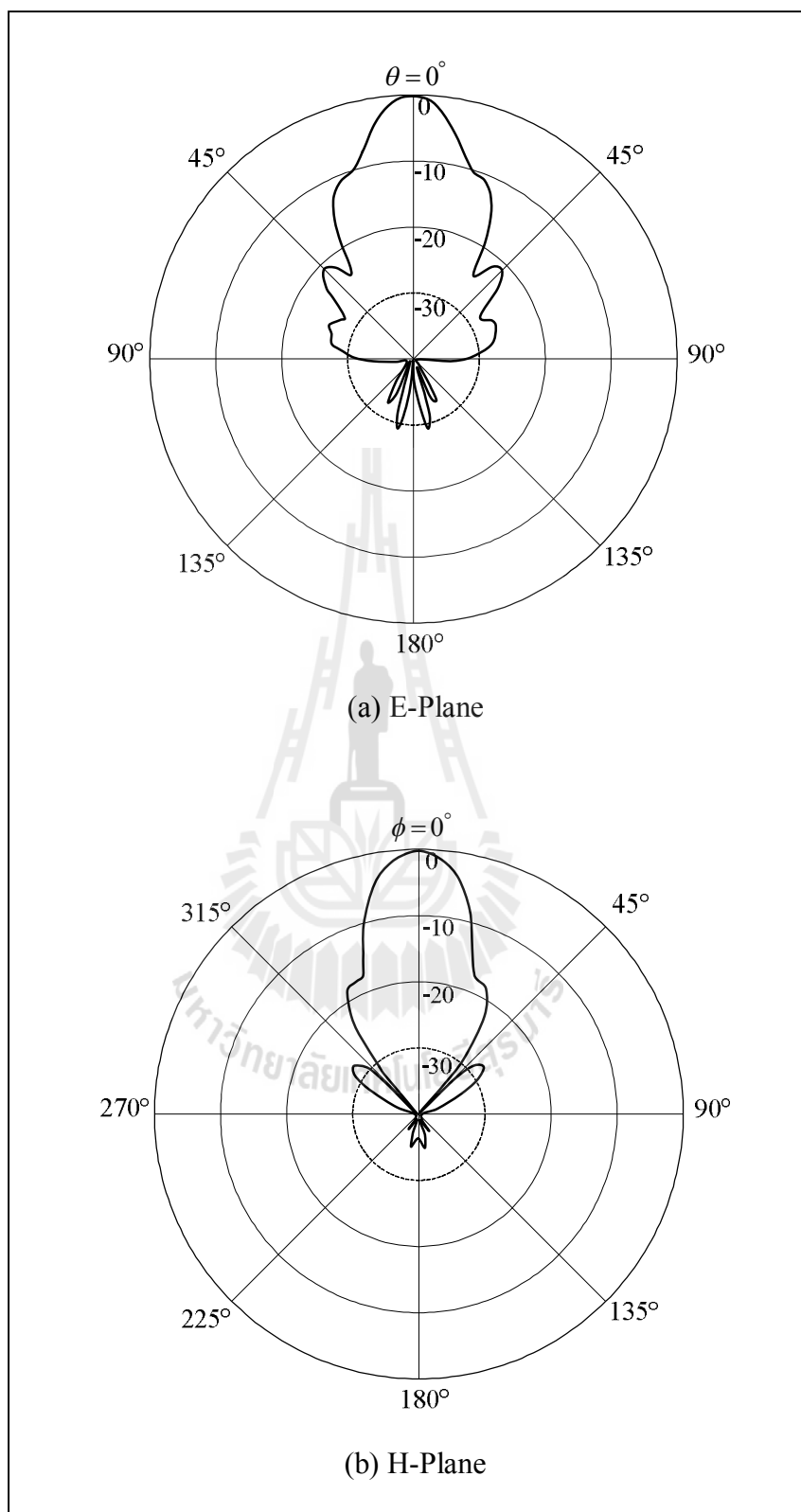


Figure 4.38 Simulated radiation patterns of a Type-C circular horn.

4.4.4 A Circular Horn Antenna with Two Side-Wing Slabs and the Designed Woodpile EBG (Type-D circular horn)

After the radiation patterns of a circular horn antenna are improved to be quite symmetrical by adding two side-wing slabs on the left and right sides. The designed quadratic shaped woodpile EBG is installed in front of this modified circular horn antenna with distance $d = 16.5\lambda$, we called this case that Type-D circular horn, as shown in Figure 4.39. From the simulated results by using CST software, we found that the gain is increased from 19.33 dB to 26.03 dB. Besides, it provides the symmetrical radiation patterns both in E-plane and H-plane and moderately higher gain around 6.7 dB when compared to a conventional circular horn antenna. The S_{11} at -10 dB, started 9.31 GHz to 10.67 GHz and its bandwidth is around 1.36 GHz or 13.6%, which are wide enough and can be well utilized for X-band radar and I-band beyond following the IEEE and the ITU, respectively, as shown in Figure 4.40. The VSWR of a Type-D circular horn at the operating frequency of 10 GHz is 1.03 as shown in Figure 4.41. From Figure 4.42, the HPBW ratio in the E-plane and H-plane, EL:AZ, is equal $6.3^\circ:6.6^\circ$ (1:1.05).

Table 4.4 shows the comparison of simulated results by using the CST software of four types of the circular horn antennas such as the gains, HPBWs, and SLLs. In addition, the comparison of S_{11} , VSWR, and radiation patterns of four types of the circular horn antennas are shown in Figure 4.43, 4.44, and 4.45, respectively. We found that the proper designed quadratic shaped woodpile EBG structures can provide the moderately highest gain of 26.03 dB at the operating frequency of 10 GHz and the radiation patterns of a circular horn antenna are quite symmetrical.

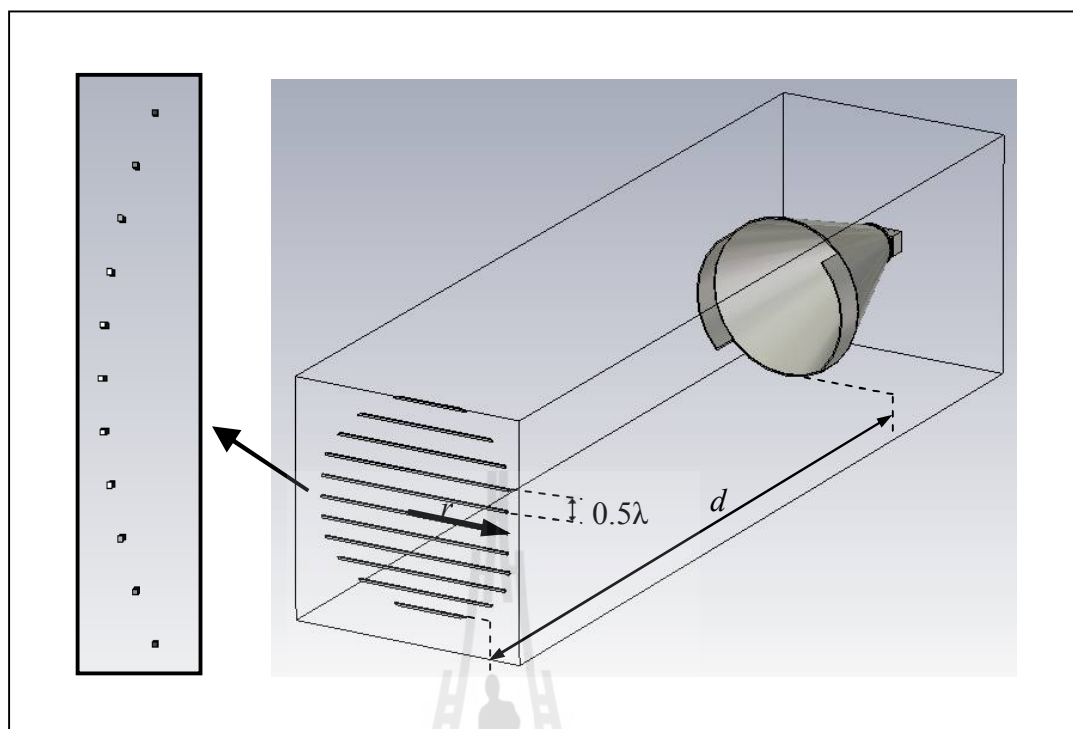


Figure 4.39 A circular horn antenna with two side-wing slabs and the designed woodpile EBG (Type-D circular horn).

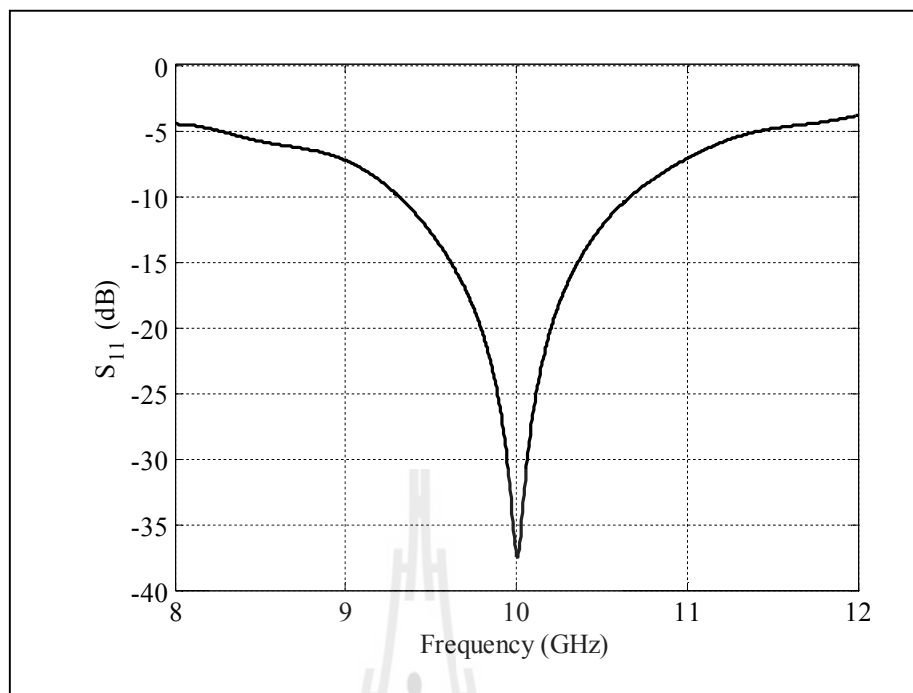


Figure 4.40 Simulated result of reflected power (S_{11}) of a Type-D circular horn.

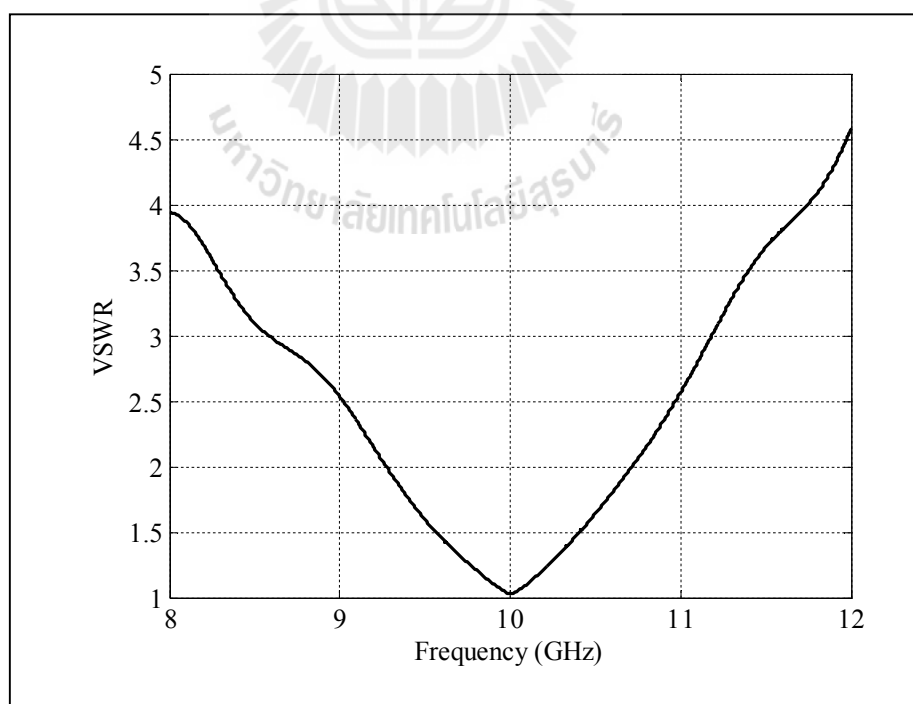


Figure 4.41 Simulated VSWR of a Type-D circular horn.

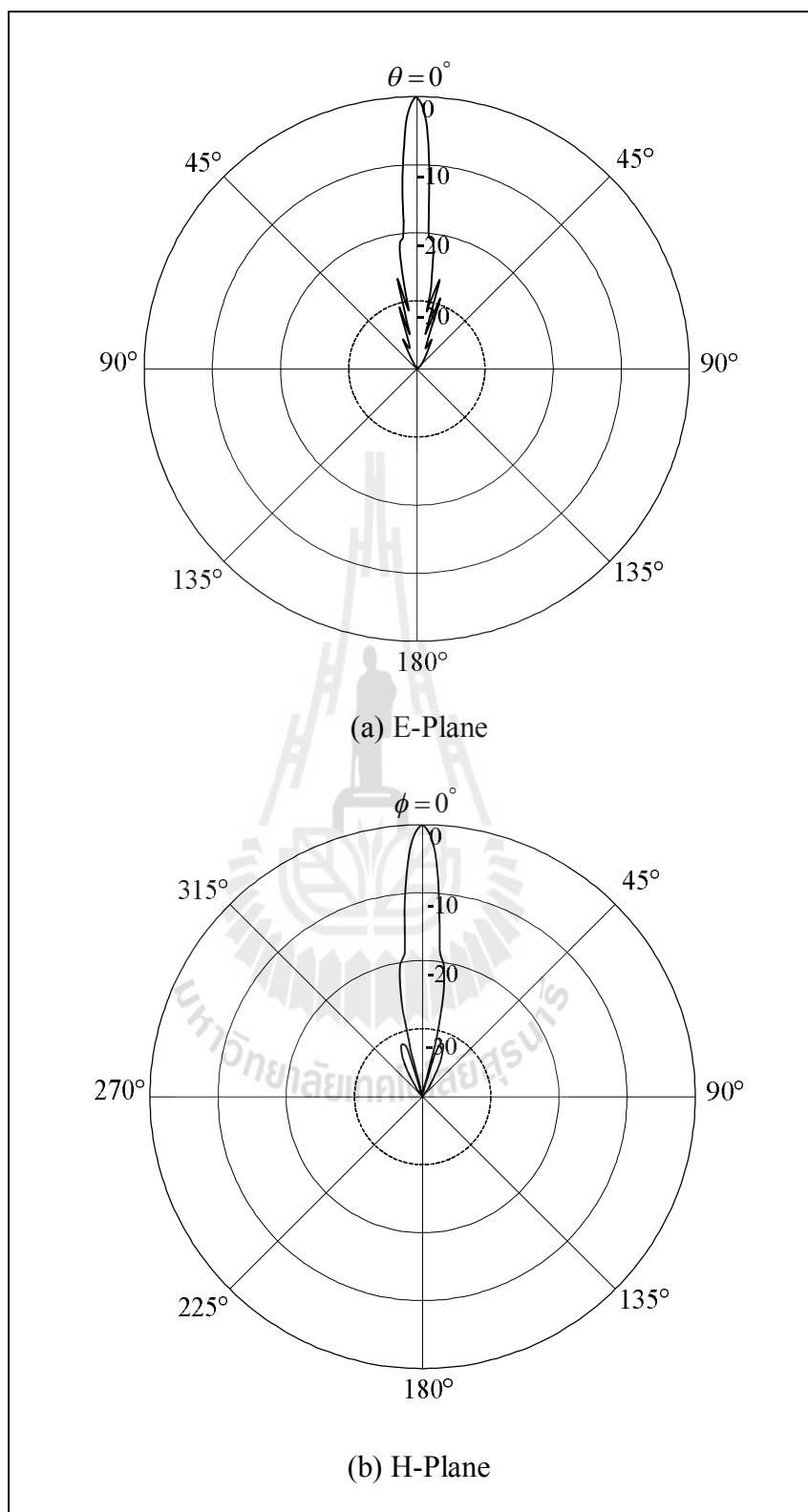
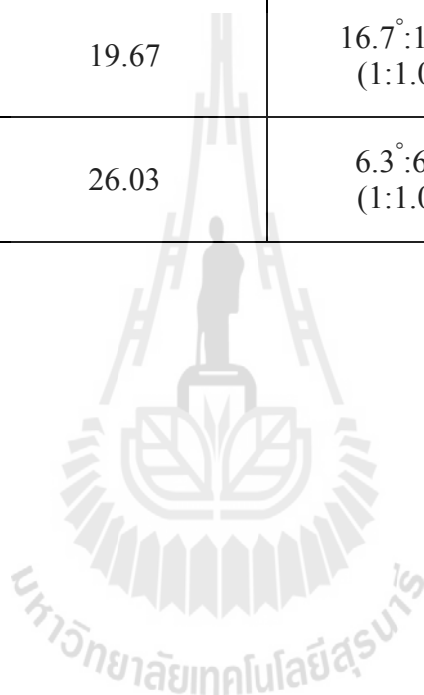


Figure 4.42 Simulated radiation patterns of a Type-D circular horn.

Table 4.4 The simulated results of four types of the circular horn antennas.

The circular horn antennas	Gain (dB)	HPBW EL:AZ	SLL (dB) E-plane/H-plane
Type-A circular horn	19.33	16.7°:19.5° (1:1.17)	-22.5/-22.5
Type-B circular horn	25.76	6.4°:7.3° (1:1.4)	-18.2/-11.5
Type-C circular horn	19.67	16.7°:18.1° (1:1.08)	-20.5/-27.4
Type-D circular horn	26.03	6.3°:6.6° (1:1.05)	-18.8/-21.4



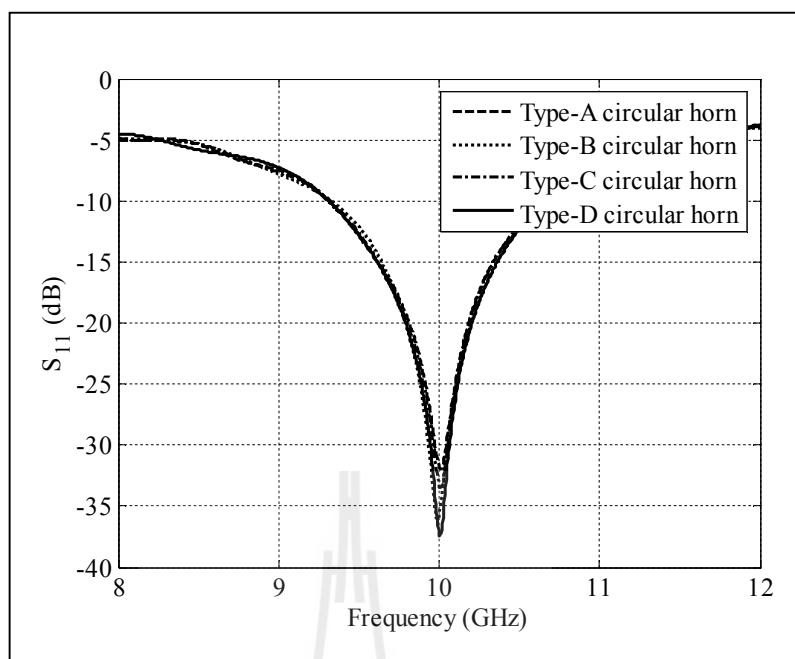


Figure 4.43 Simulated result of reflected power (S_{11}) of four types of the circular horn antennas.

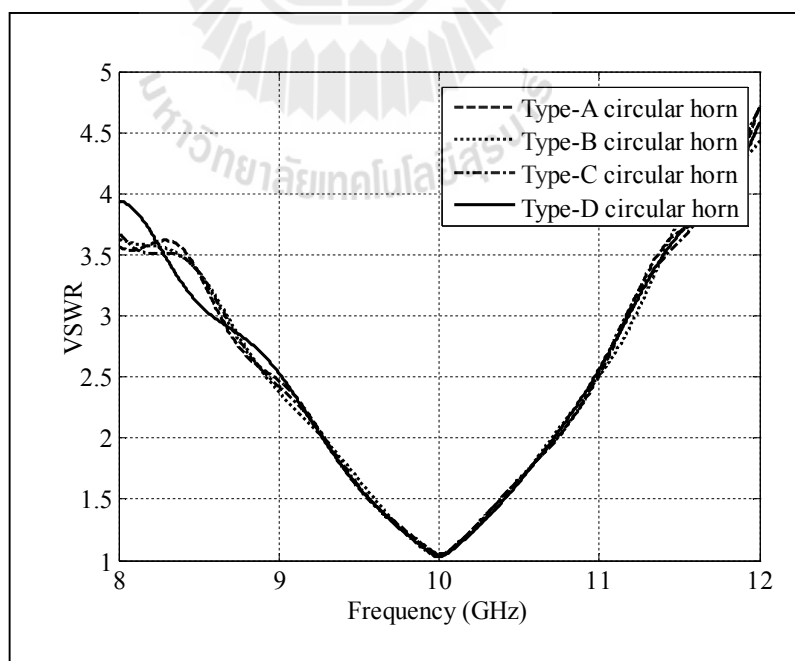


Figure 4.44 Simulated VSWR of four types of the circular horn antennas.

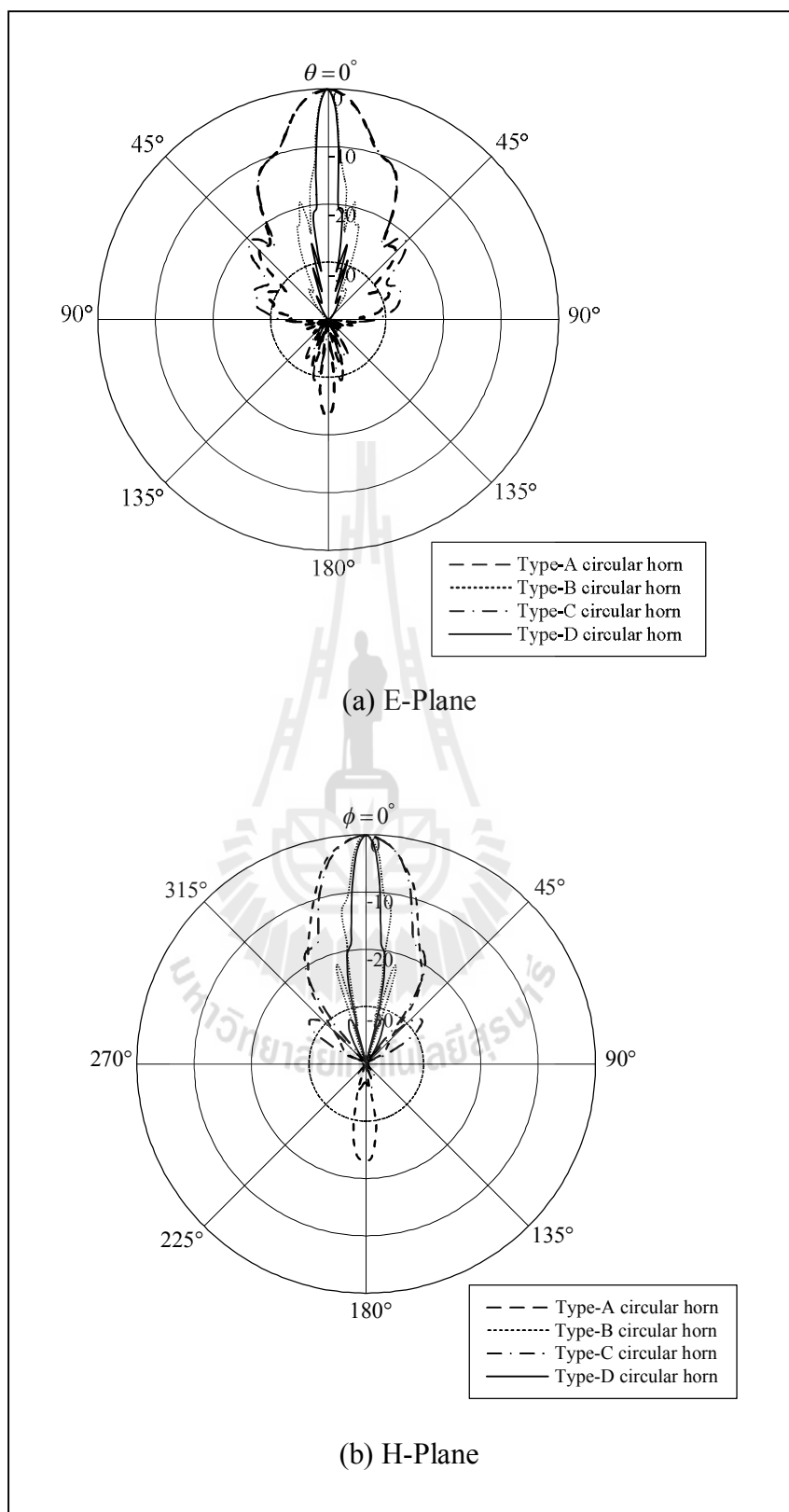


Figure 4.45 Simulated radiation patterns of four types of the circular horn antennas.

4.5 Chapter Summary

In this chapter presented the analysis and design of the rectangular and circular horn antennas with the same quadratic shaped woodpile EBG. Because the structure of the designed quadratic shaped woodpile EBG is symmetrical, which is proper to use with the symmetrical radiation patterns in the E-plane and H-plane of antenna. Therefore, we have designed the conventional rectangular and circular horn antennas to provide the symmetrical radiation patterns in the E-plane and H-plane by adding two side-wing slabs on the left and right sides. Then, same structures of the quadratic shaped woodpile EBG are installed in front of such two horn antennas. We found that the designed quadratic shaped woodpile EBG is able to gain some parts of the electromagnetic energy and suppress the surface wave that occurred on the slabs with the proper distance between horn antennas and woodpile EBG structures equal to 16.5λ while the structure radius of quadratic shaped woodpile EBG equal to 5.3λ . Be aforementioned, we found that the designed quadratic shaped woodpile EBG can use associated with both of rectangular and circular horns, only we modified their radiation patterns to be symmetrical.

CHAPTER V

MEASUREMENT AND DISCUSSION

5.1 Introduction

The previous chapter has focused on the concept of refinement method and also the idea was confirmed through simulation results from CST software. In order to understand the general background and the theory behind the rectangular and circular horn antennas with the designed quadratic shaped woodpile EBG structures, the antenna measurements for the final verification will be presented in this chapter. The prototype of horn antennas are designed and fabricated for operating frequency at 10 GHz. To verify the theoretical calculation, the radiation patterns were measured in the outdoor place by using vector network analyzer HP 8722D and compared with the simulated results from CST software.

5.2 The Antenna Prototype

5.2.1 The Woodpile EBG

The designed quadratic shaped woodpile EBG structure consists of the eleven alumina rods, which each rod has a square-shaped cross sectional area of $1.6 \times 1.6 \text{ mm}^2$ and the lengths as shown in Table 5.1. The prototype of the designed quadratic shaped woodpile EBG structure is shown in Figure 5.1.

Table 5.1 The dimension of the designed quadratic shaped woodpile EBG structure.

Description	Dimension (λ)	Dimension (mm)
The first alumina rod (L_1)	1.90 λ	57.08
The second alumina rod (L_2)	3.54 λ	106.12
The third alumina rod (L_3)	4.41 λ	132.16
The fourth alumina rod (L_4)	4.93 λ	147.89
The fifth alumina rod (L_5)	5.04 λ	151.20
The sixth alumina rod (L_6)	5.04 λ	151.20
The seventh alumina rod (L_7)	5.04 λ	151.20
The eighth alumina rod (L_8)	4.93 λ	147.89
The ninth alumina rod (L_9)	4.41 λ	132.16
The tenth alumina rod (L_{10})	3.54 λ	106.12
The eleventh alumina rod (L_{11})	1.90 λ	57.08

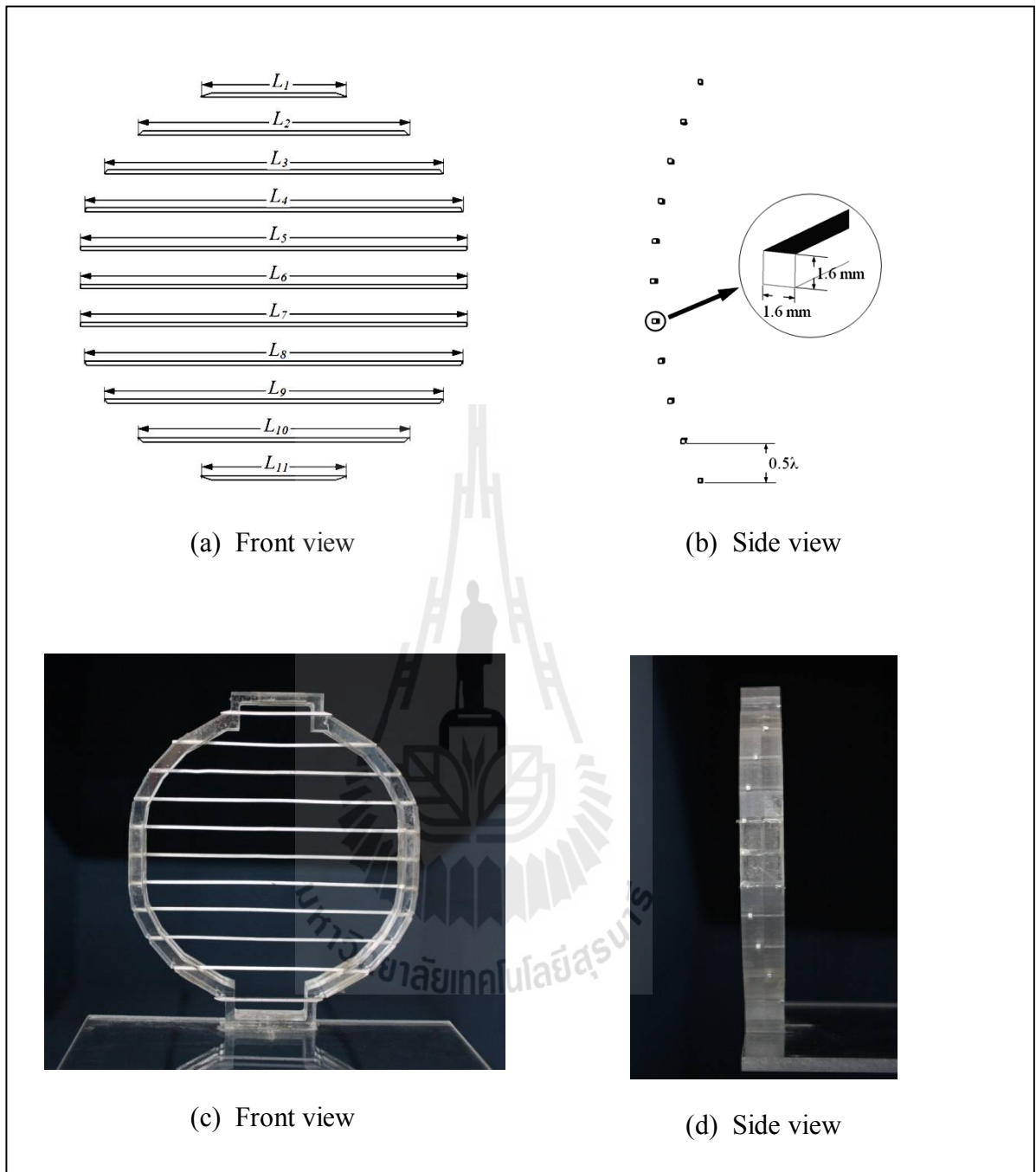


Figure 5.1 The designed quadratic shaped woodpile EBG model and structure.

5.2.2 A Rectangular Horn Antenna with Two Side-Wing Slabs

In this research, we have chosen a pyramidal horn for applying to a prototype of rectangular horn antenna, because it is flared in both directions and its radiation characteristics are essentially a combination of the E-plane and H-plane sectoral horns (Balanis, 2005). As describe in chapter 4, a rectangular horn antenna with two side-wing slabs was designed and analyzed by using the CST software to obtain the proper parameters as summarized in Table 5.2. It is fabricated with PEC, thickness of 3 mm, at the operating frequency of 10 GHz as shown in Figure 5.2.

Table 5.2 Dimension of a rectangular horn antenna with two side-wing slabs.

Description	Dimension (λ)	Dimension (mm)
The height of an aperture (H_a)	2.73λ	81.97
The width of an aperture (W_a)	3.30λ	99.00
The depth of an aperture (D_a)	2.59λ	77.59
The height of a waveguide (H_w)	0.63λ	19.00
The width of a waveguide (W_w)	1.07λ	32.03
The depth of a waveguide (D_w)	1.11λ	33.38
The height of an each wing slab (H_{ws})	2.73λ	81.97
The width of an each wing slab (W_{ws})	0.63λ	18.75

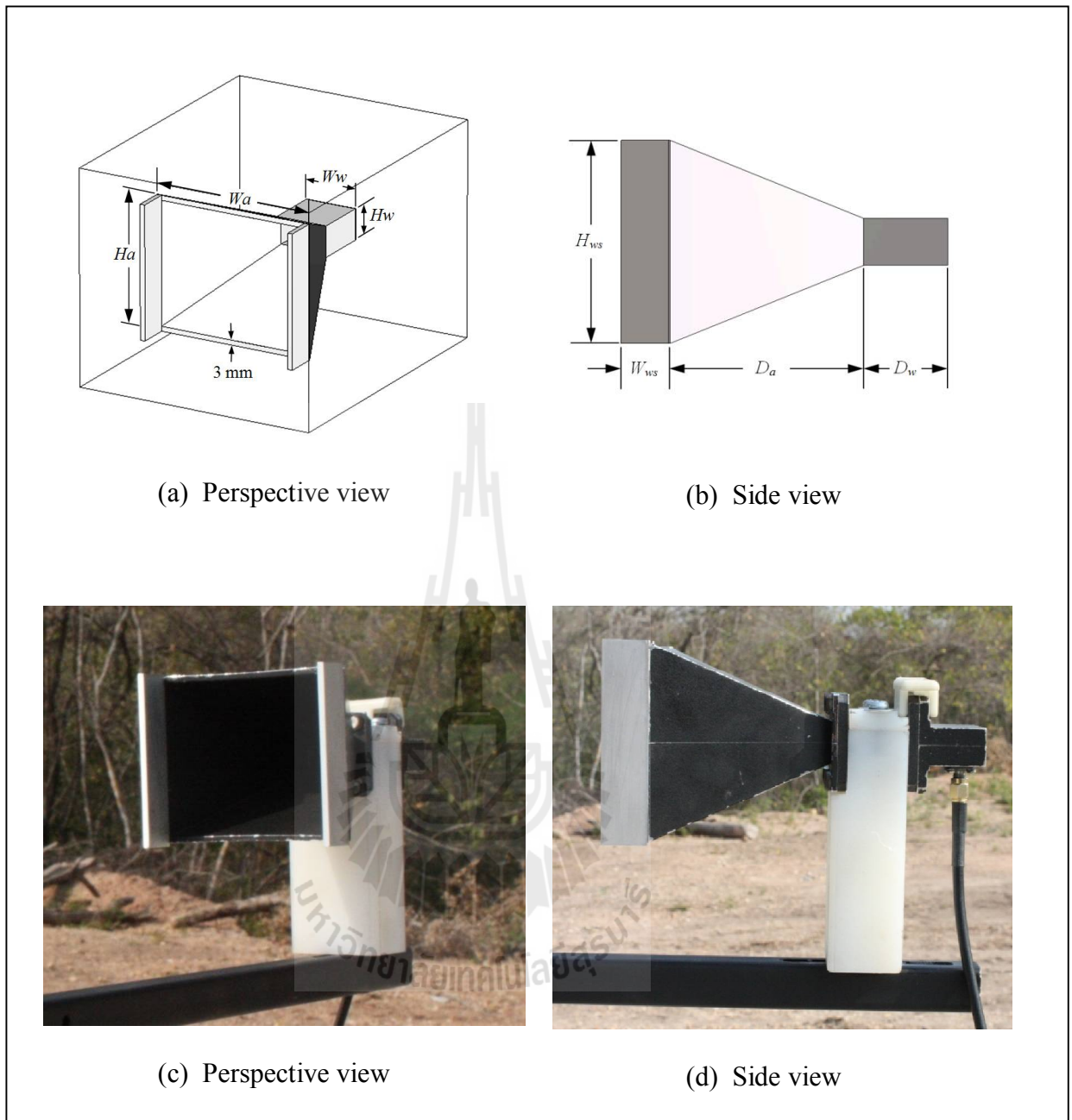


Figure 5.2 Configuration and prototype of rectangular horn antenna with two side-wing slabs.

5.2.3 A Circular Horn Antenna with Two Side-Wing Slabs

Referring to Figure 5.3, it is apparent that the behavior of a circular horn antenna. As the flare angle increase, the directivity for a given length circular horn will be increased until it reaches a maximum beyond which it begins to decrease (Balanis, 2005). When the horn aperture (d_m) is fixed as constant and its length (L) is varied, the maximum directivity is obtained when the flare angle is zero (King, 1950). In this research, we choose a circular horn that has directivity of 19 dB and its aperture diameter of 4λ . From graph in Figure 5.3, the length of a circular horn is 5.5λ , approximately. However, when a circular horn antenna with two side-wing slabs was designed and analyzed by using the CST software to obtain the input parameters, we found that its aperture diameter and length are minor changed as summarized in Table 5.3. Then, a circular horn antenna with two side-wing slabs is fabricated with PEC, thickness of 3 mm, at the operating frequency of 10 GHz as shown in Figure 5.4.

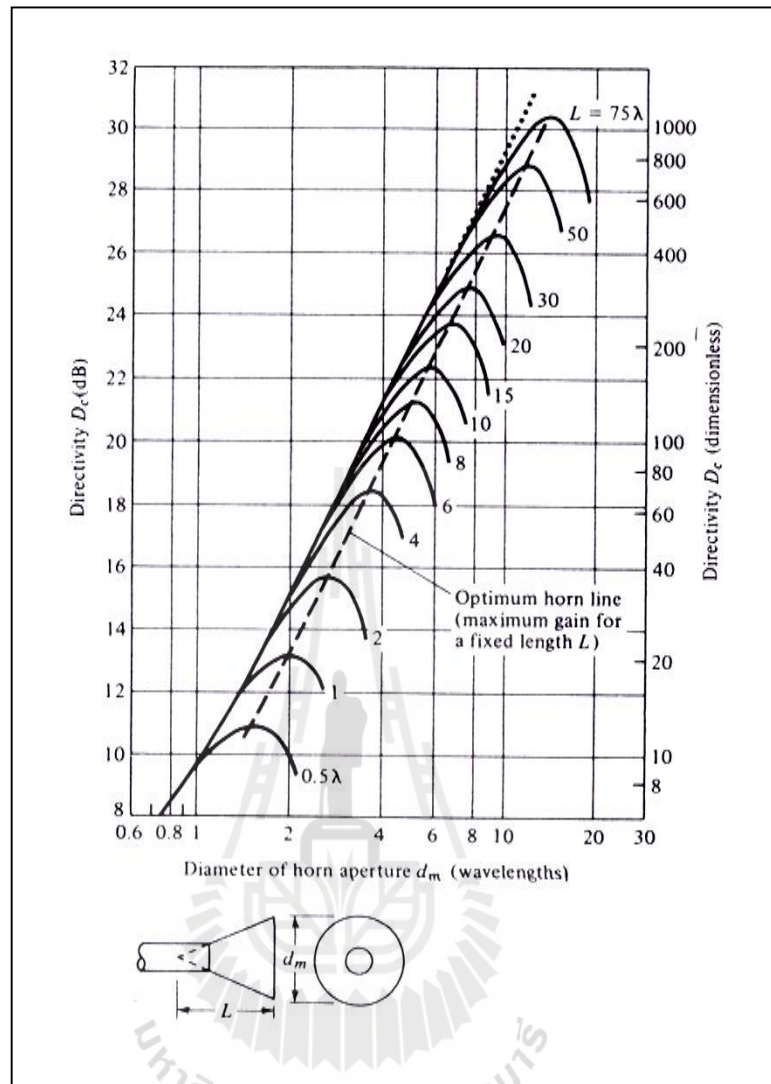


Figure 5.3 Directivity of a circular horn as a function of aperture diameter and for different axial horn lengths (Balanis, 2005).

Table 5.3 Dimension of a circular horn antenna with two side-wing slabs.

Description	Dimension (λ)	Dimension (mm)
The diameter of an aperture (d_m)	3.87	116.06
The length of horn (L)	5.45	163.45
The diameter of a converter (d_{mc})	1.06λ	31.89
The length of a converter (L_c)	0.23λ	6.77
The height of a waveguide (H_w)	0.63λ	19.00
The width of a waveguide (W_w)	1.07λ	32.03
The depth of a waveguide (D_w)	1.11λ	33.38
The length of an each wing slab (L_{ws})	2.95	88.39
The width of an each wing slab (W_{ws})	0.75λ	22.50



Figure 5.4 Configuration and prototype of circular horn antenna with two side-wing slabs.

5.3 Antenna Measurement and Experimental Results of a Type-D Rectangular Horn

Antenna measurements are required for the final verification of the antenna operation. Modern simulation with CST software predicts quite accurately the antenna characteristics, however, in some case of complicated structures the fabricated antenna must be also measured the characteristics comparing to the simulated result from such software. Therefore, a rectangular horn antenna with two side-wing slabs and the designed woodpile EBG or Type-D rectangular horn was constructed for measurement.

To fix and strengthen the structures of a rectangular horn and the woodpile EBG, the PEC arm, which dimension is $20 \times 20 \times 630 \text{ mm}^3$, was added in the Type-D rectangular horn as shown in Figure 5.5. In order that, we have studied the effect of the height of a PEC arm, it is found that the proper gain of 25.30 dB and SLL in E-plane/H-plane of -16.3 dB/-16.4 dB are achieved when the height of arm is equal to 110 mm as shown in Table 5.4. From the simulated results by using CST software of Type-D rectangular horn with PEC arm at the operating frequency of 10 GHz, the S_{11} is -26.71 dB, which is correspond to VSWR of 1.10 as shown in Figure 5.6 and 5.7, respectively. The HPBW ratio in the E-plane and H-plane, (EL:AZ), is $7.4^\circ:6.6^\circ$ (1.12:1) as shown in Figure 5.8. It notices that the PEC arm has an effect for the HPBWs, which are wider in E-plane and narrower in H-plane, and cause to increase the SLL when compare to the radiation patterns of Type-D rectangular horn as shown in Figure 5.9.

Table 5.4 The simulated results of the various heights of a PEC arm
for Type-D rectangular horn.

The height of a PEC arm (mm)	Gain (dB)	HPBW EL:AZ	SLL (dB) E-plane/H-plane
0	25.75	6.9°:7.1° (1:1.03)	-16.1/-19.8
80	24.86	7.3°:6.5° (1:1.12)	-14.2/-14.9
90	24.86	7.9°:6.5° (1.22:1)	-15.2/-15.5
100	25.04	8.1°:6.5° (1.25:1)	-15.8/-16.2
110	25.30	7.4°:6.6° (1.12:1)	-16.3/-16.4
120	25.52	6.4°:6.6° (1:1.03)	-5.2/-15.9
130	25.62	5.9°:6.6° (1:1.12)	-5.3/-16.0
140	25.60	5.5°:6.6° (1:1.20)	-5.4/-16.2
150	25.50	5.6°:6.6° (1:1.18)	-5.5/-16.4
200	25.37	6.4°:6.6° (1:1.03)	-5.8/-16.2

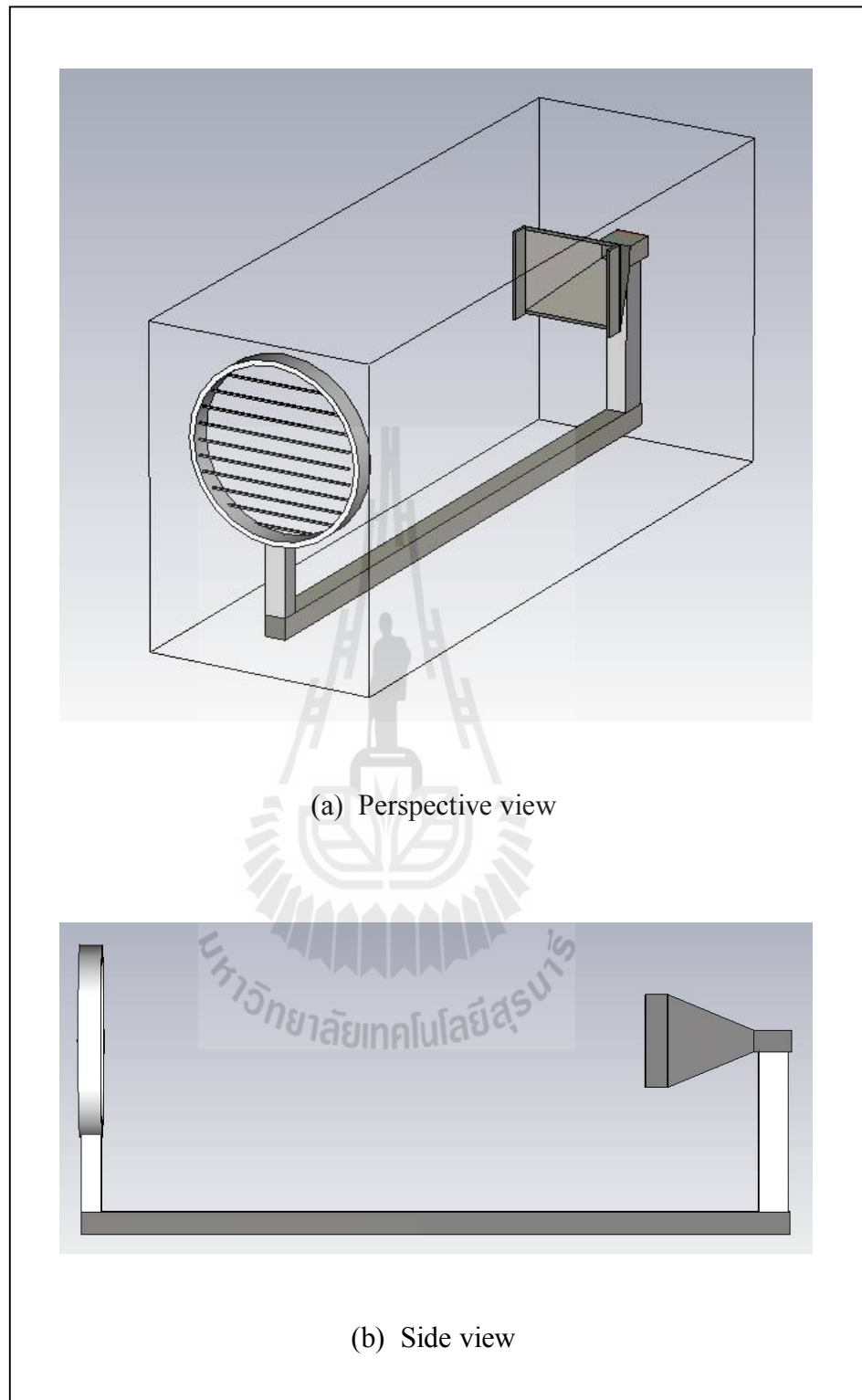


Figure 5.5 The structure and prototype of a Type-D rectangular horn.



(c) Perspective view



(d) Side view

Figure 5.5 The structure and prototype of a Type-D rectangular horn (Continued).

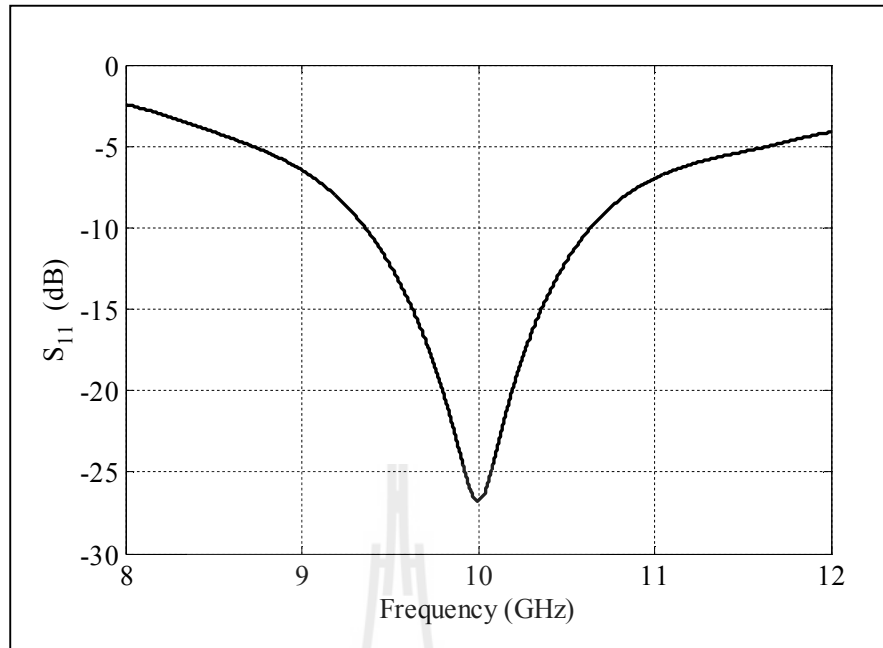


Figure 5.6 Simulated reflected power (S_{11}) of a Type-D rectangular horn with PEC arm.

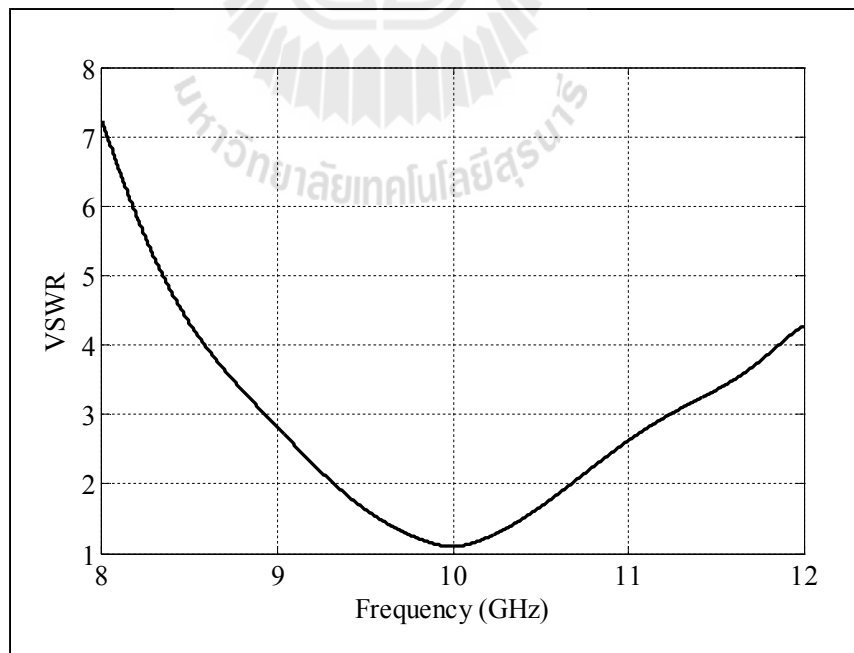


Figure 5.7 Simulated VSWR of a Type-D rectangular horn with PEC arm.

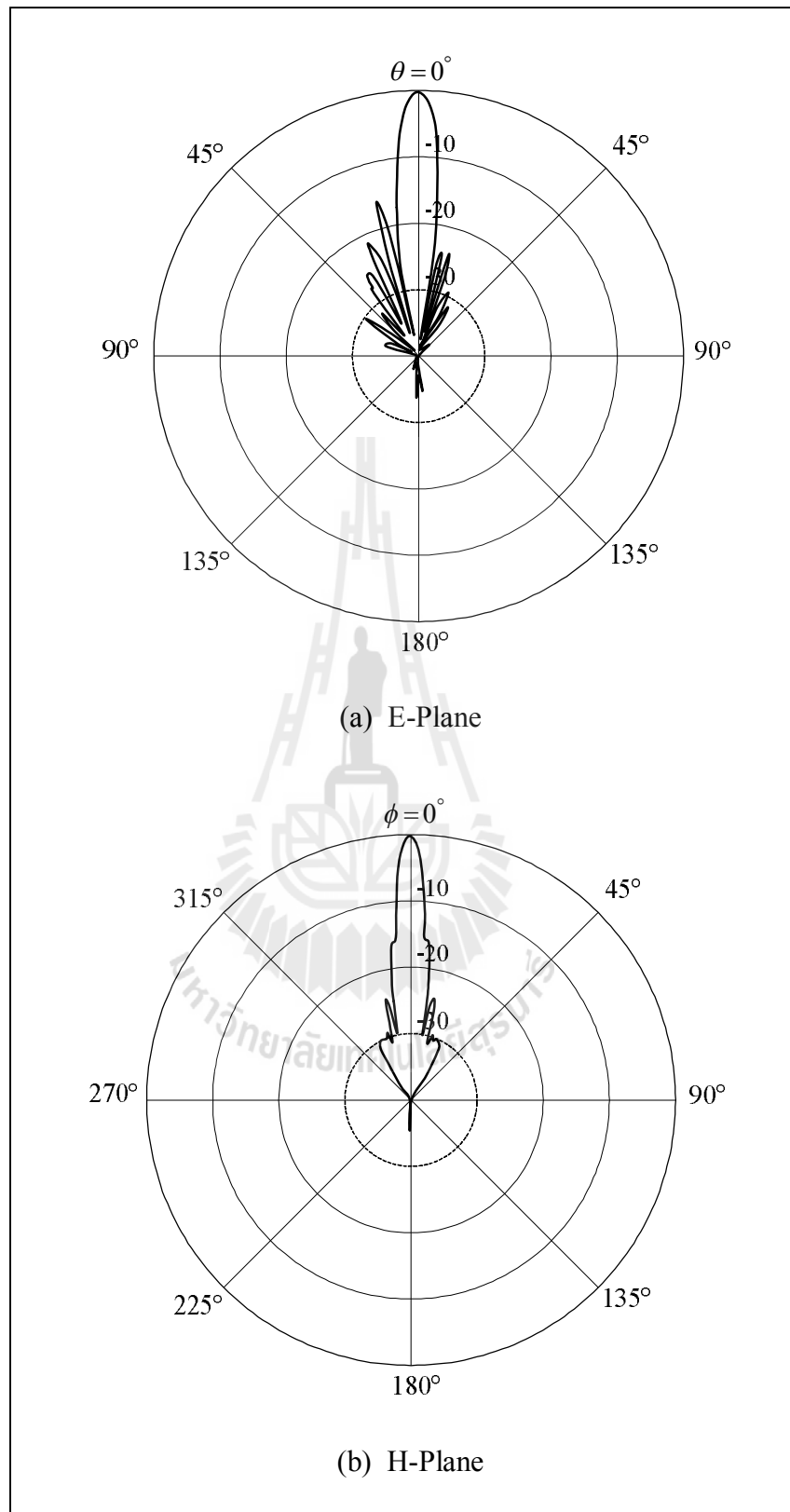


Figure 5.8 Simulated radiation patterns of a Type-D rectangular horn with PEC arm.

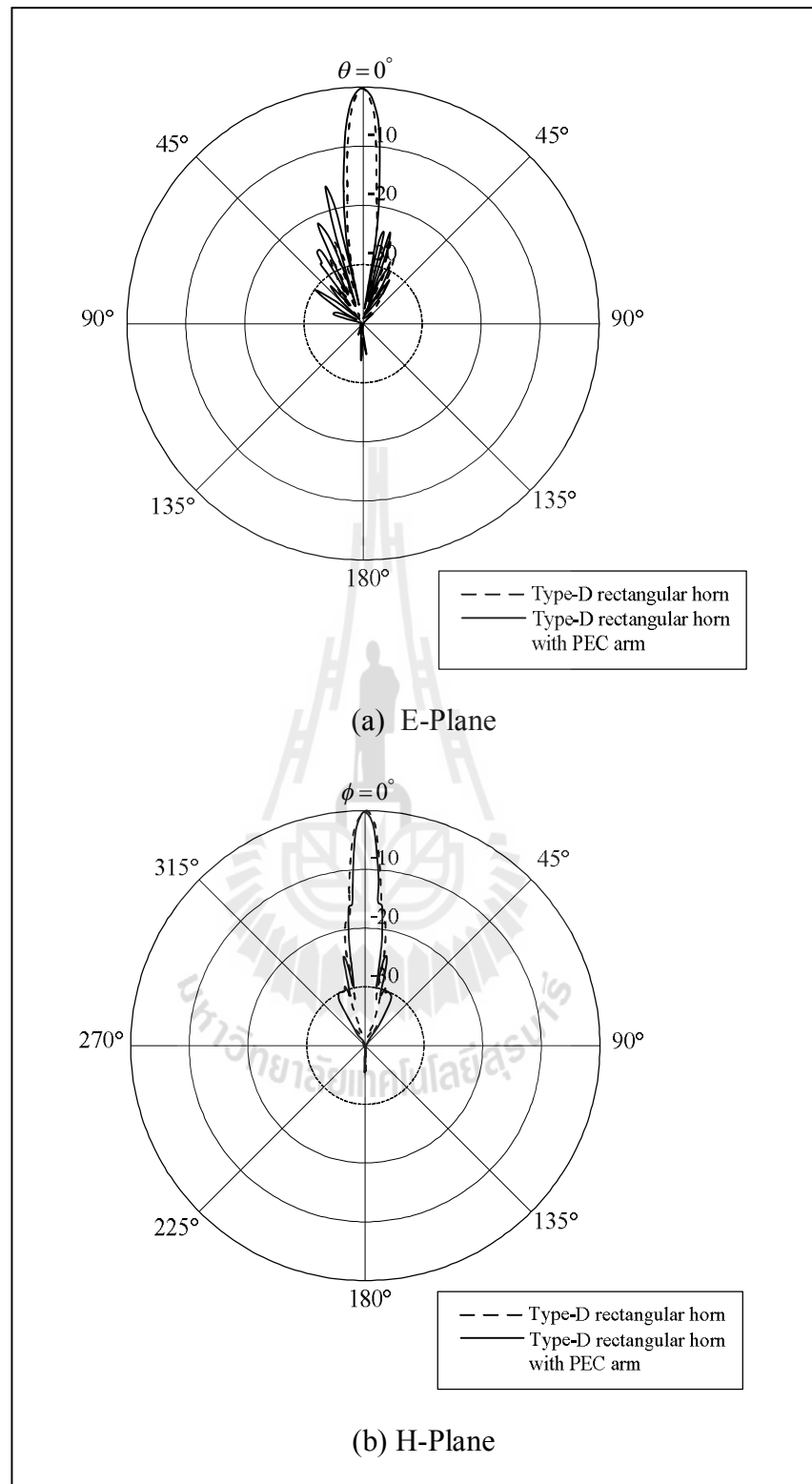


Figure 5.9 Comparison of radiation patterns of a Type-D rectangular horn with and without PEC arm.

5.3.1 The Reflected Power, Voltage Standing Wave Ratio and Input Impedance

The reflected power or S_{11} (at -10 dB), voltage standing wave ratio (VSWR) and input impedance are the parameters which can be used to indicate the degree of mismatch between transmission line and its load (usually a radio antenna), or evaluate the effectiveness of impedance matching efforts. The impedance is in the range of 40Ω to 60Ω and VSWR less than 2.0, that can be accepted for impedance matching between transmission line and the antenna which correspond to S_{11} less than -10 dB.

In this research, the operating frequency of this proposed antenna is 10 GHz. The measured results of S_{11} of the prototype of a Type-D rectangular horn is -26.711 dB, which accord to VSWR of 1.0978 as shown in Figure 5.10 and 5.11, respectively. So its impedance matching that is referred to $S_{11} \leq -10$ dB and $VSWR \leq 2$ is achieved. The measured input impedance of the prototype of a Type-D rectangular horn is $46.016 + j1.9609 \Omega$, which is accepted, because it is in the range of 40Ω to 60Ω as shown in Figure 5.12. Good agreement between simulated and measured results of S_{11} and VSWR are obtained as shown in Figure 5.13 and 5.14, respectively.

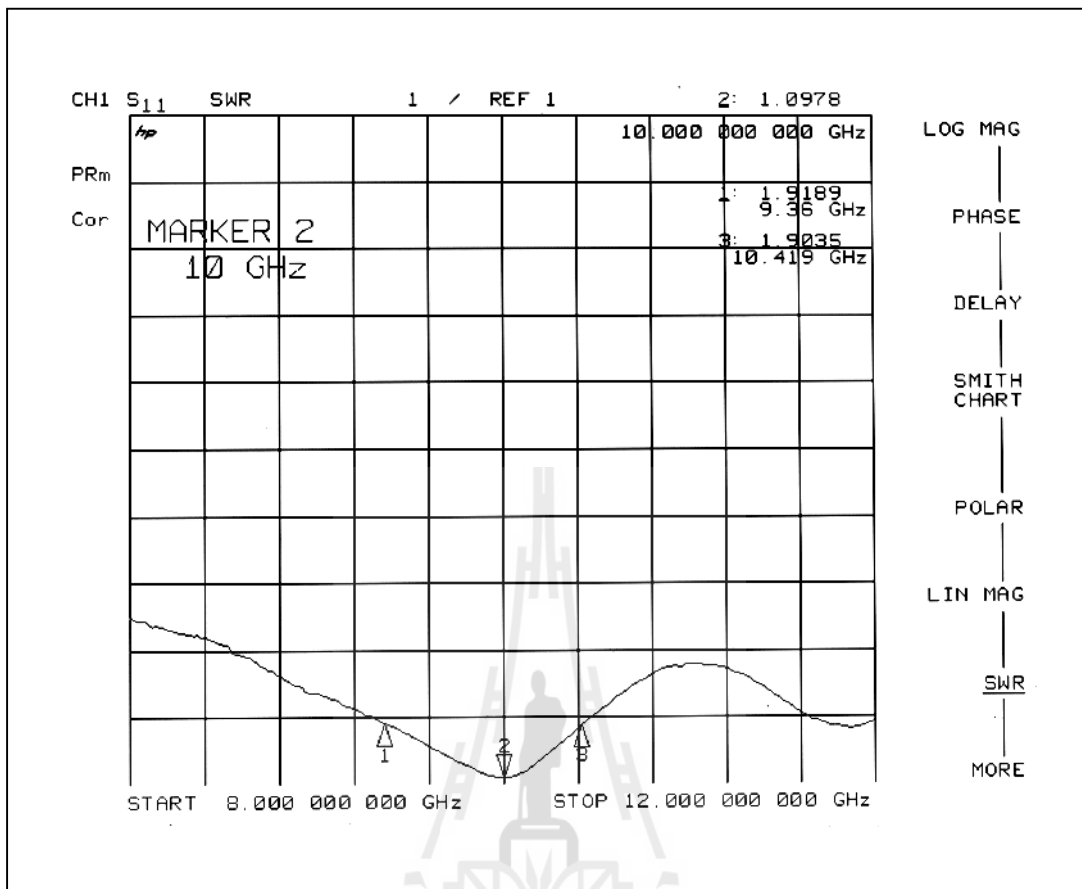


Figure 5.11 Measured VSWR of the prototype of a Type-D rectangular horn.

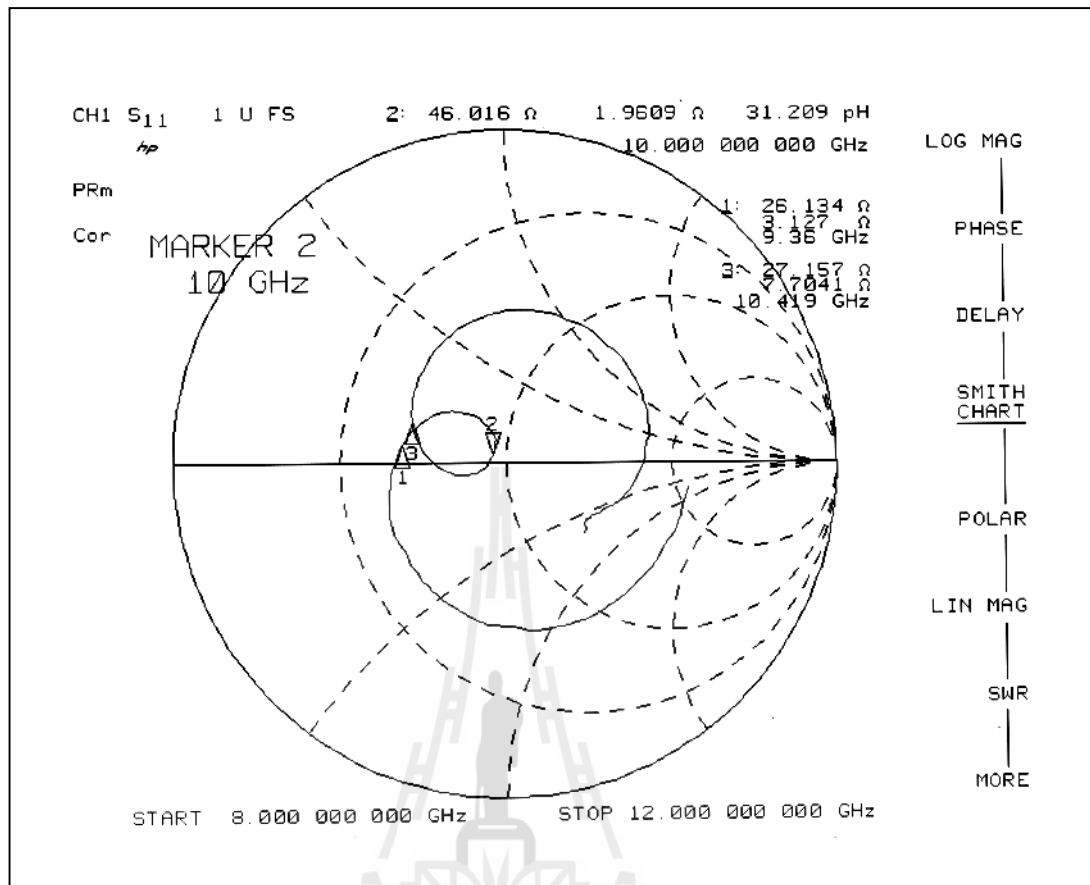


Figure 5.12 Measured input impedance of the prototype of Type-D rectangular horn.

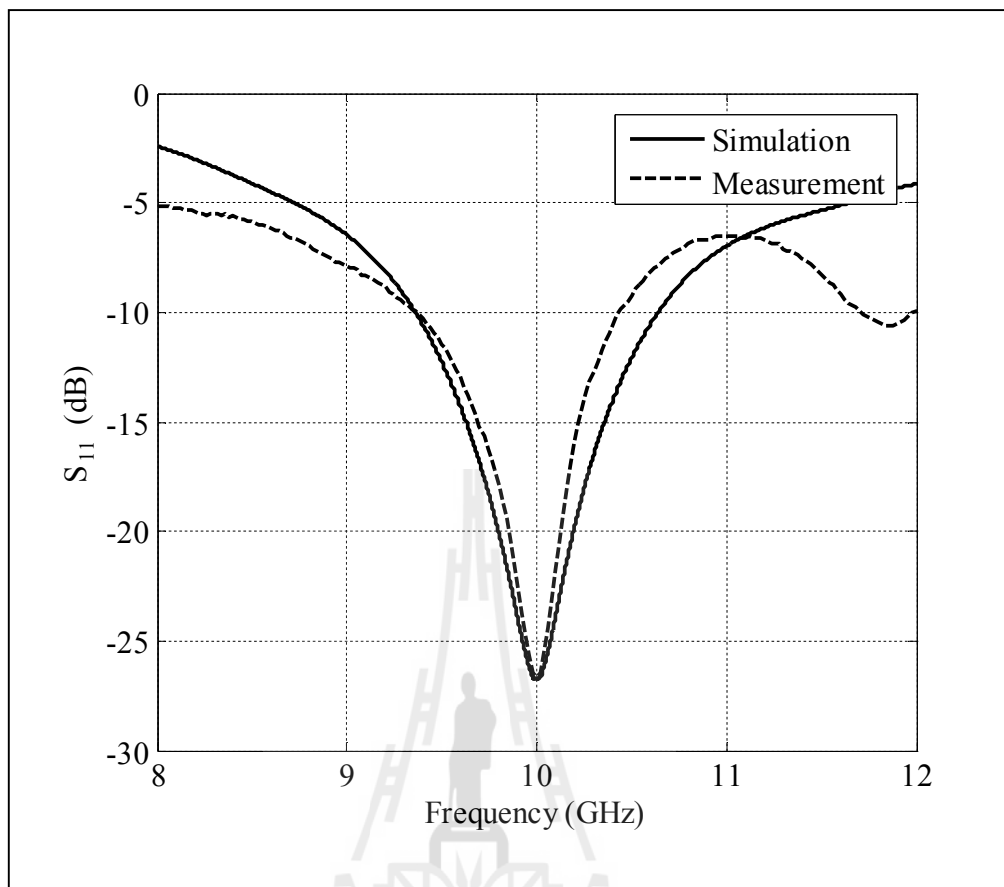


Figure 5.13 Comparison between simulated and measured results of reflected power (S_{11}) for the prototype of a Type-D rectangular horn.

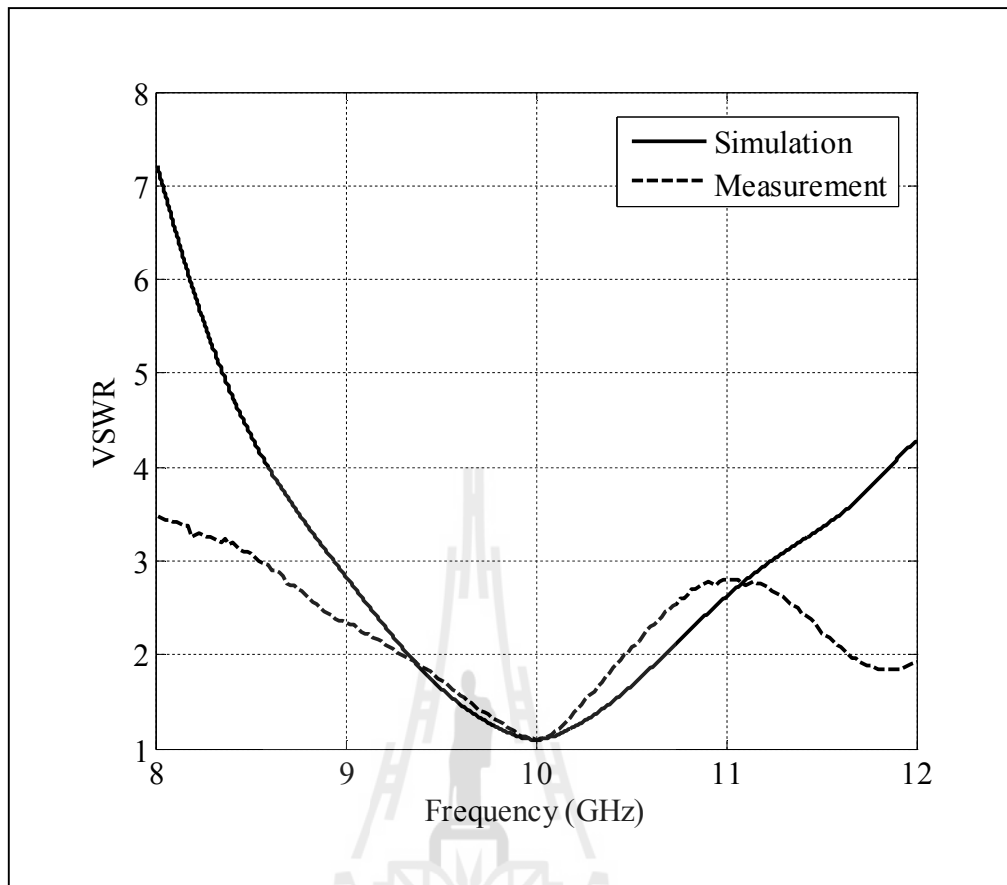


Figure 5.14 Comparison between simulated and measured results of VSWR for the prototype of a Type-D rectangular horn.

5.3.2 Bandwidth

Bandwidth is another fundamental antenna parameter, which describes the range of frequencies over, on either side of a center frequency, that the antenna can properly radiate or receive electromagnetic fields (<http://www.antenna-theory.com/>). For narrowband antennas, the bandwidth is expressed as a percentage of the frequency difference (upper minus lower) over the center frequency of the bandwidth. Equation (5.1) is the fundamental formula to calculate the bandwidth of the antenna from the reflected power versus the frequency plot.

$$\text{Bandwidth (\%)} = \left[\frac{(f_{\text{upper}} - f_{\text{lower}})}{f_0} \right] \times 100\% \quad (5.1)$$

From the measured results, the bandwidth of the prototype of Type-D rectangular horn is 1.059 GHz (9.360 GHz to 10.419 GHz) or 10.71% as shown in Figure 5.15. The percentage bandwidth of the prototype of type-d rectangular horn can demonstrate calculation as

$$\text{Bandwidth (\%)} = \left[\frac{(10.419 - 9.360)}{9.8895} \right] \times 100\% = 10.71\% . \quad (5.2)$$

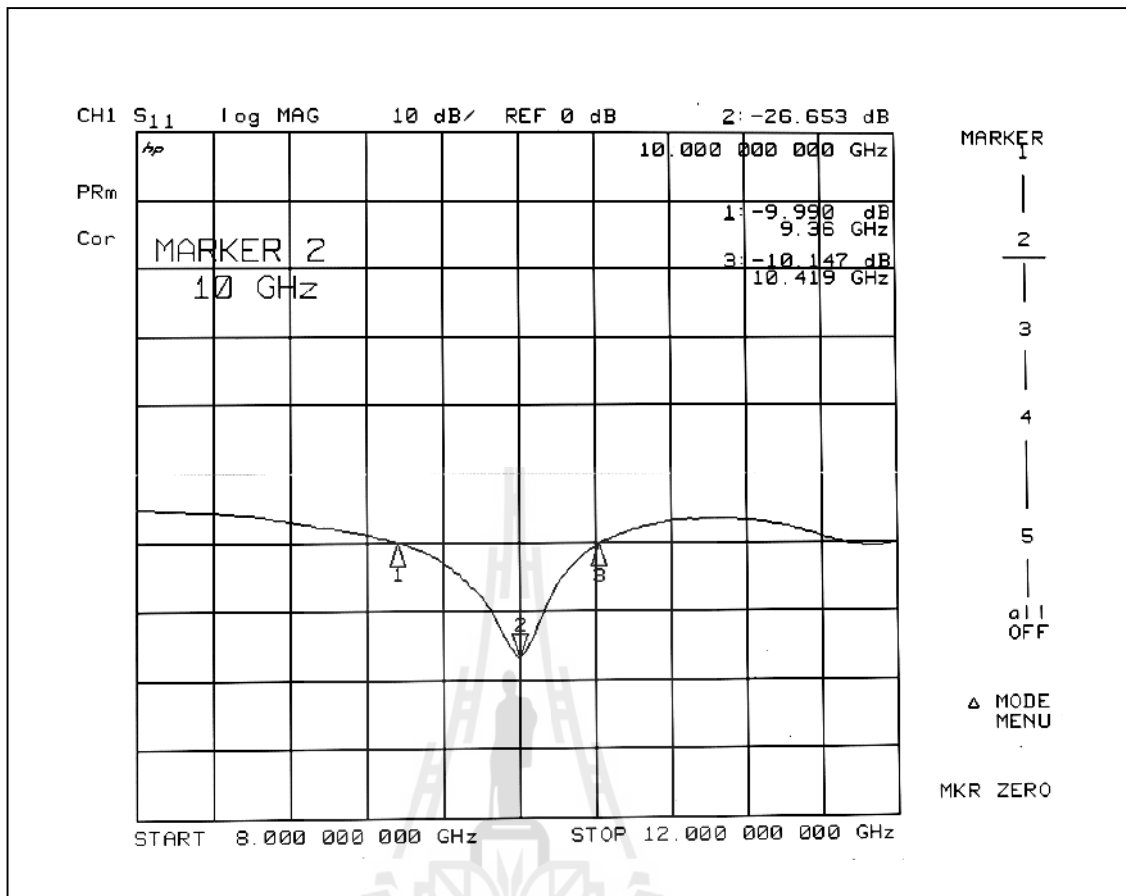


Figure 5.15 Measured bandwidth of the prototype of Type-D rectangular horn.

5.3.3 Radiation Pattern

Radiation pattern or antenna pattern is the variation of the power radiated of an antenna. This power variation as a function of the arrival angle is in spherical coordinates at a constant radial distance and frequency, which is observed in the far field region. A far-field (Fraunhofer) region is the region that farthest away from an antenna where the field distribution is essentially independent of the distance from an antenna. Besides, in this region is dominated by radiated electromagnetic fields with orthogonal to each other and the direction of propagation as with the plane waves. If we determine D is the maximum linear dimension of an antenna, then the following three conditions must all be satisfied to be in a far field region (<http://www.antenna-theory.com/>):

$$R > \frac{2D^2}{\lambda}, \quad (5.3)$$

where $R \gg D$ and $R \gg \lambda$. In the far field antenna test, the prototype of Type-D rectangular horn was measured in outdoor place as shown in Figure 5.16. A conventional rectangular horn antenna is used to be the transmitting antenna, while the prototype of Type-D rectangular horn antenna is in receiving mode. It is installed on a turntable with the distance $R > 18.1$ m that was calculated from (5.3), far from the transmitting antenna. During the measurements, the prototype of Type-D rectangular horn was illuminated with a uniform plane wave and their receiving characteristics were measured. The measured far field patterns in E-plane and H-plane of the prototype of Type-D rectangular horn are plotted together with the simulated results by using CST software as shown in Figure 5.17. The ratio of HPBW in the

E-plane and H-plane, (EL:AZ), is $7.6^\circ:6.9^\circ$ (1.10:1) as summarized in Table 5.6.

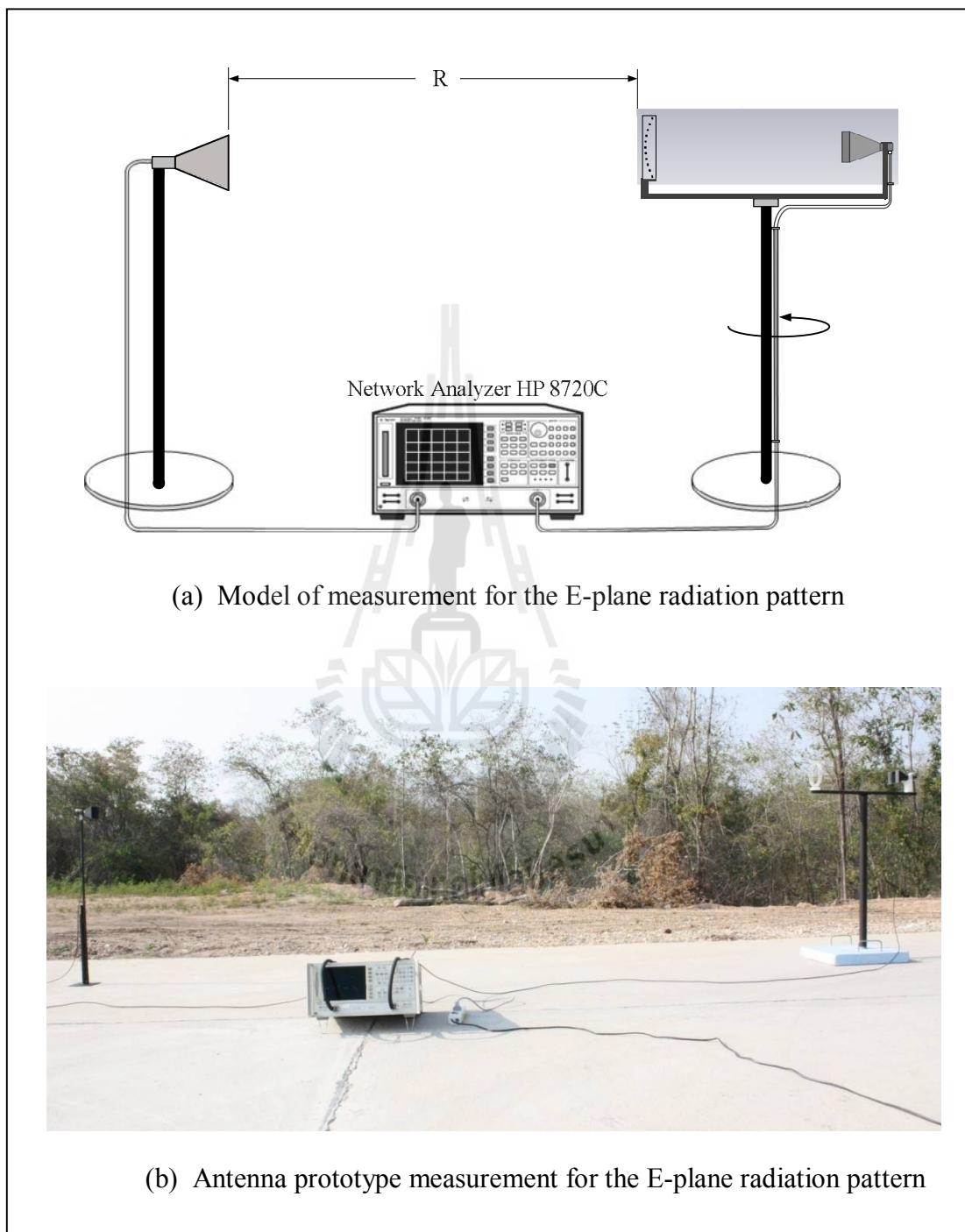


Figure 5.16 Measurement set up for the radiation pattern of the prototype of Type-D rectangular horn.

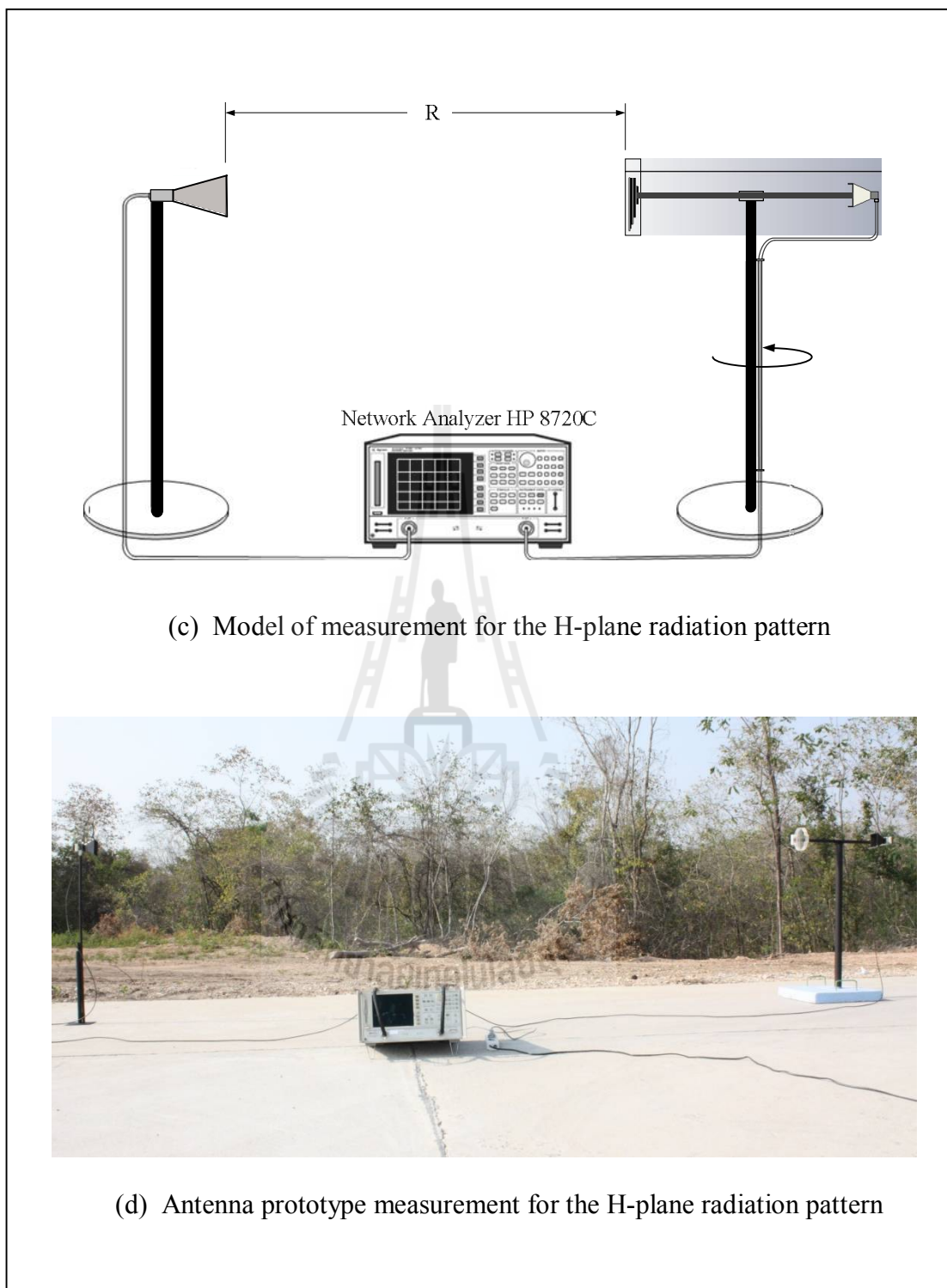


Figure 5.16 Measurement set up for the radiation pattern of the prototype of Type-D rectangular horn (Continued).

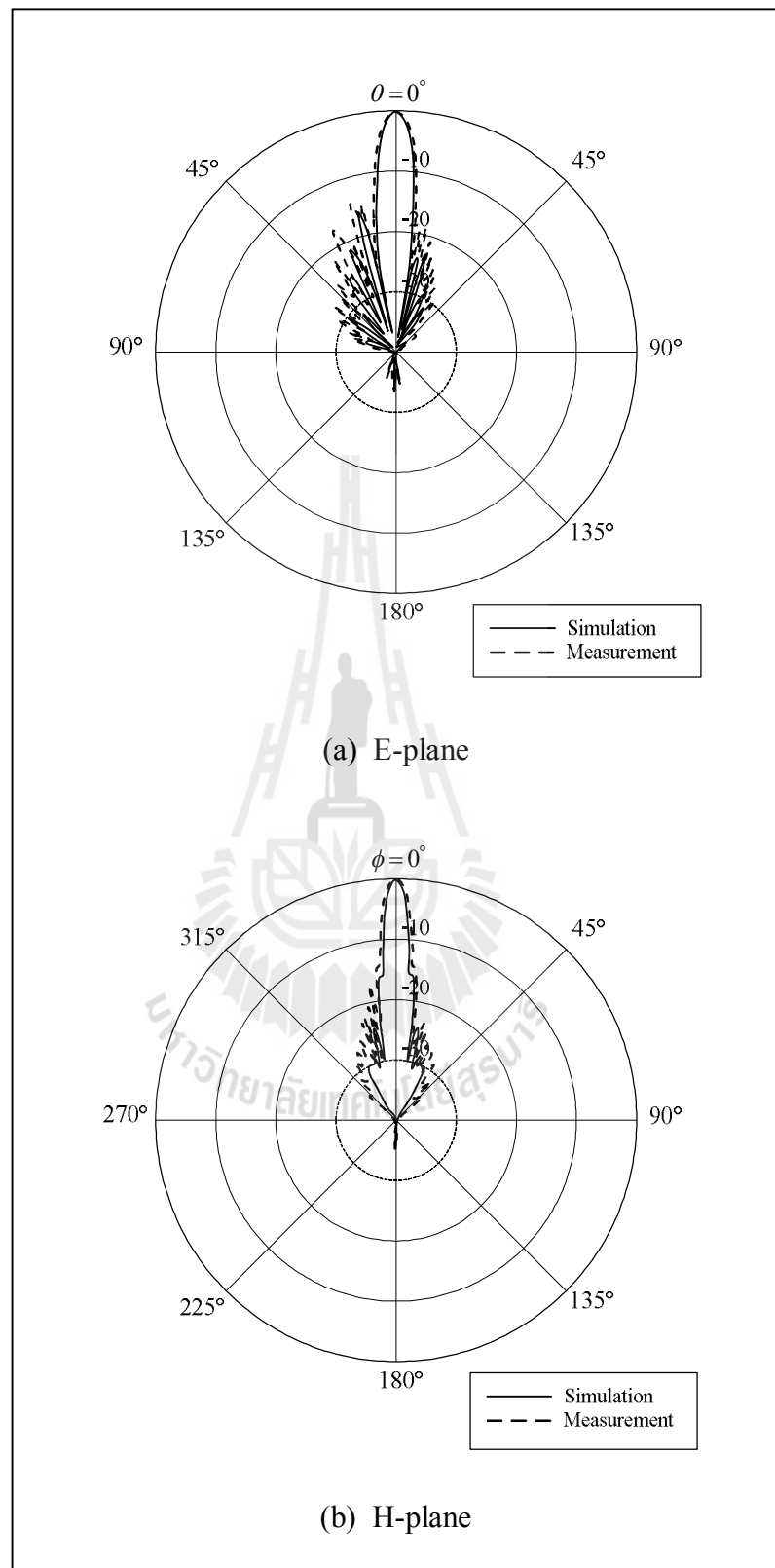


Figure 5.17 The radiation pattern of the prototype of Type-D rectangular horn.

5.3.4 Gain

The gain is an important parameter, which is the useful measure for describing the performance of an antenna. It is defined as the ratio of the radiation intensity, in a given direction, to the radiation intensity that would be obtained if the power accepted by the antenna is radiated isotropically (Balanis, 2005). There are two methods to measure the gain of an antenna such as relative gain and absolute gain. The relative gain is the ratio of the power gain in a given direction to the power gain of a reference antenna in its reference direction, while the absolute gain is the ratio of the power gain in a given direction to the power gain of receiving. The absolute gain method, one of the basic methods to measure the gain of an antenna (Balanis, 1997), is based on the Friis transmission formula as expressed in (5.4), which can be applied when two polarizations matched antennas aligned for the maximum directional radiation, and separated by a distance R that meets the far field criteria, are used for the measurements,

$$G_{r,dB} + G_{t,dB} = P_{r,dB} - P_{t,dB} + 20 \log \left(\frac{4\pi R}{\lambda} \right), \quad (5.4)$$

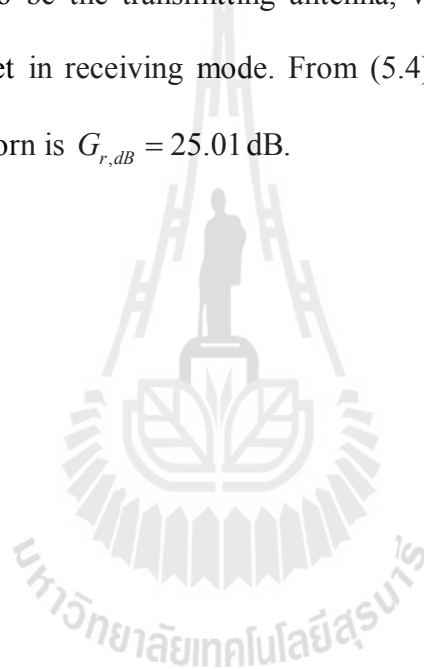
where P_r is the received power,

P_t is the transmitted power,

G_r is the gain of the receiving antenna,

G_t is the gain of the transmitting antenna.

In this research, firstly, a conventional rectangular horn antenna is measured the gain for using to be the transmitting antenna as shown in Figure 5.18. Therefore, if the receiving and transmitting antennas are identical, only one measurement is required and (5.4) can calculate the gain of a conventional rectangular horn antenna such $G_{t,dB} = 16.68$ dB. Secondly, the gain of the prototype of Type-D rectangular horn is measured as shown in Figure 5.19. A conventional rectangular horn antenna is set to be the transmitting antenna, while the prototype of Type-D rectangular horn is set in receiving mode. From (5.4), the gain of the prototype of Type-D rectangular horn is $G_{r,dB} = 25.01$ dB.



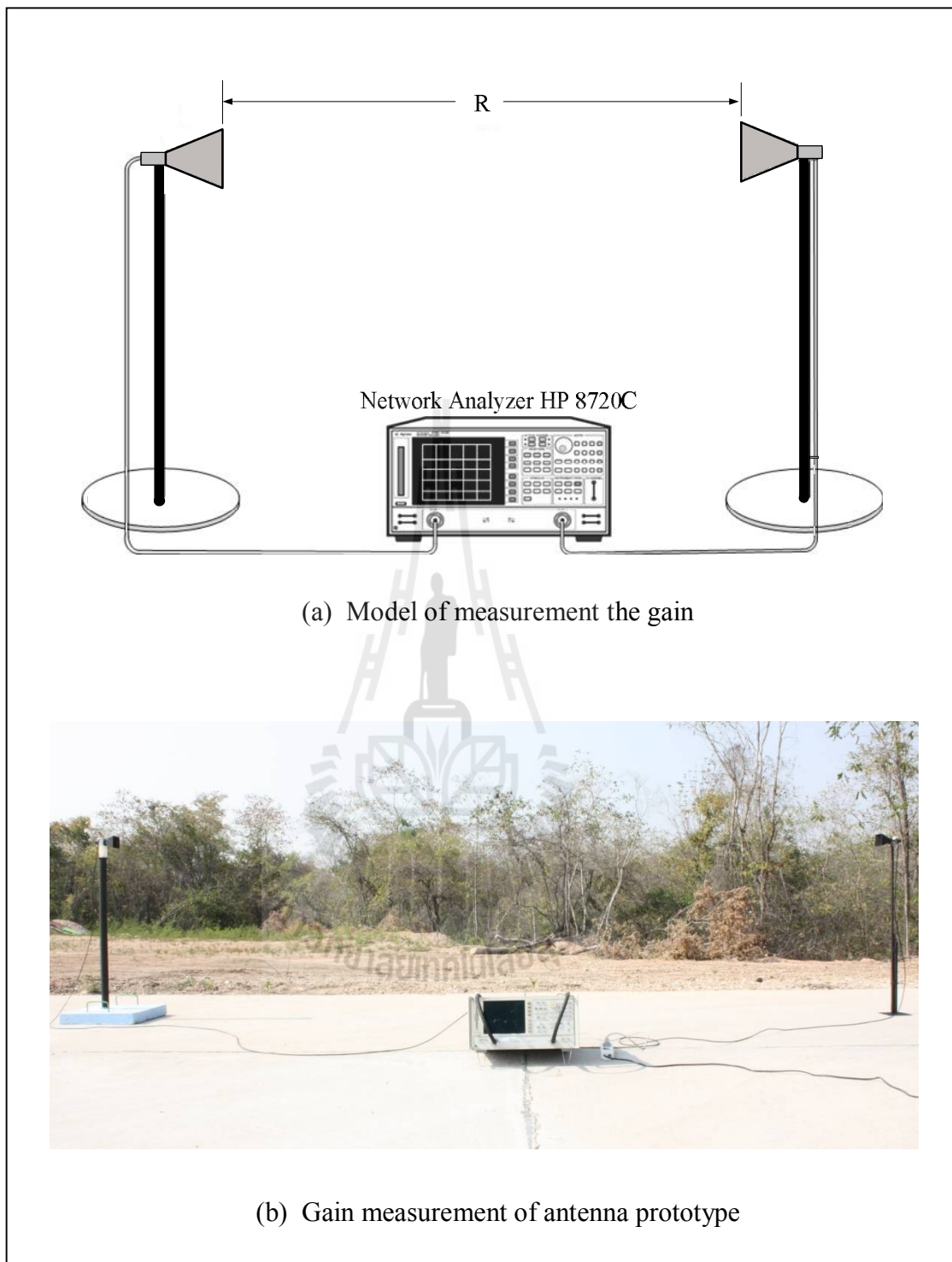


Figure 5.18 Gain measurement of a conventional rectangular horn antenna.

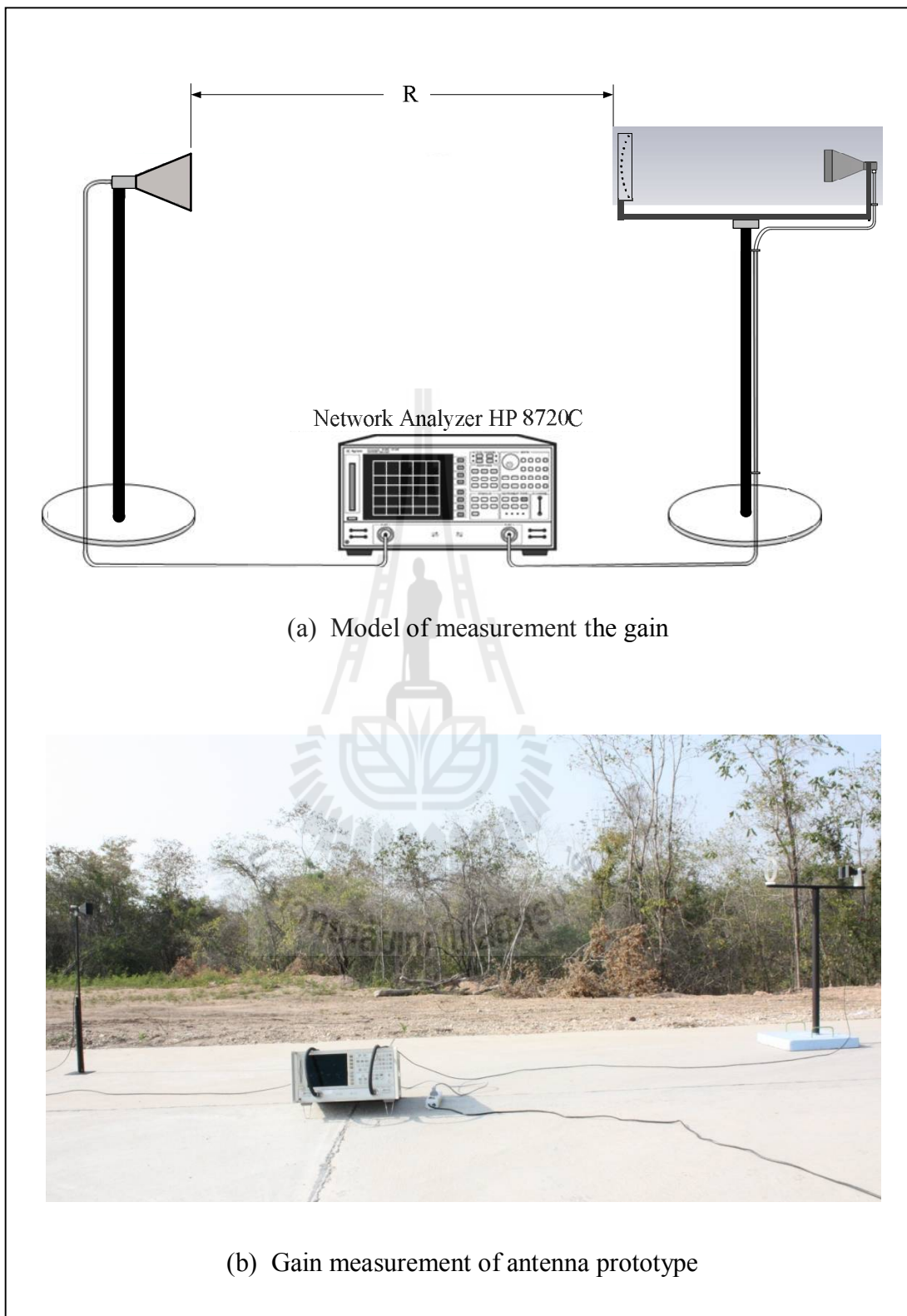


Figure 5.19 Gain measurement of the prototype of Type-D rectangular horn.

5.4 Antenna Measurement and Experimental Results of a Type-D Circular Horn

In this section, we describe the design and construction of a circular horn antenna with two side-wing slabs and the woodpile EBG or Type-D circular horn. The antenna characteristics have been measured for the final verification of the antenna operation. In the similar way as a Type-D rectangular horn, the PEC arm, which dimension is $20 \times 20 \times 650 \text{ mm}^3$, was added in the Type-D circular horn to fix and strengthen the structures of a circular horn and the woodpile EBG as shown in Figure 5.20. Moreover, we look at the effect of the various of the height of a PEC arm, it found that the proper gain of 25.63 dB and SLLs of E-plane/H-plane around -15.7 dB/-18.2 dB are occurred at the height of arm at 100 mm as shown in Table 5.5. The simulated results from CST software show that the S_{11} of Type-D circular horn with PEC arm at the operating frequency of 10 GHz is -36.11 dB, which is correspond to VSWR of 1.03 as shown in Figure 5.21 and 5.22, respectively. The normalized radiation patterns of a Type-D circular horn with PEC arm at 10 GHz is shown in Figure 5.23. The HPBW ratio in the E-plane and H-plane, EL:AZ, is $6.6^\circ:6.4^\circ$ (1.03:1). From Figure 5.24 shows the comparison of radiation patterns of a Type-D circular horn with and without PEC arm, thus its results is that the HPBWs of a Type-D circular horn with PEC arm are wider in E-plane and narrower in H-plane which cause to increase the higher SLL.

Table 5.5 The simulated results of the various heights of a PEC arm
for Type-D circular horn.

The height of a PEC arm (mm)	Gain (dB)	HPBW EL:AZ	SLL (dB) E-plane/H-plane
0	26.03	6.3°:6.6° (1:1.05)	-18.8/-21.4
80	25.32	7.7°:6.3° (1.22:1)	-17.4/-17.3
90	25.52	7.1°:6.4° (1.10:1)	-16.4/-18.0
100	25.63	6.6°:6.4° (1.03:1)	-15.7/-18.2
110	25.78	6.2°:6.4° (1:1.03)	-12.8/-18.5
120	25.86	5.8°:6.5° (1:1.12)	-11.8/-18.8
130	25.81	5.4°:6.6° (1:1.22)	-10.8/-18.8
140	25.82	5.1°:6.6° (1:1.29)	-10.4/-18.9
150	25.81	4.8°:6.5° (1:1.35)	-10.0/-18.9
200	25.83	3.8°:6.5° (1:1.71)	-8.4/-18.8

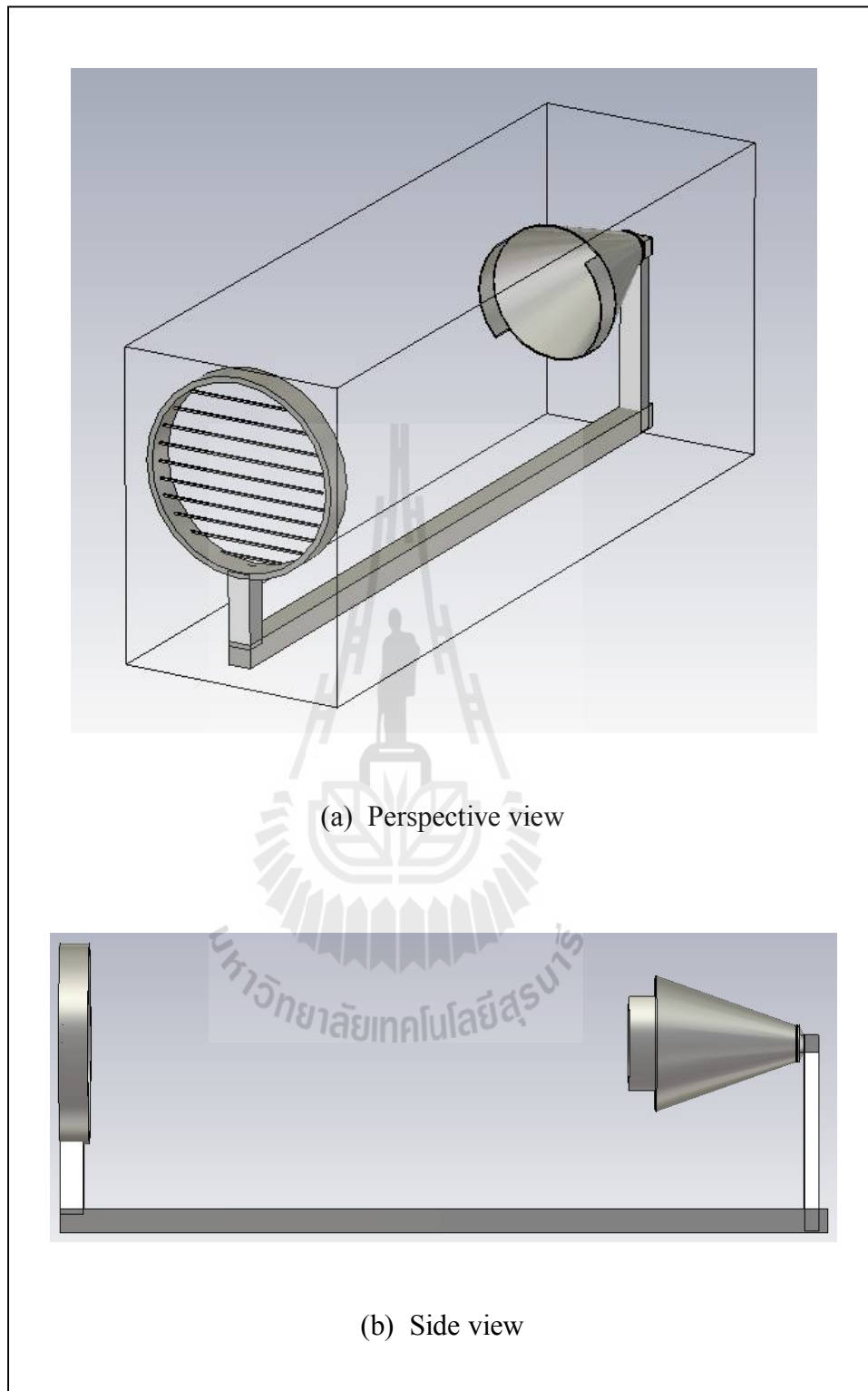


Figure 5.20 The structure and prototype of a Type-D circular horn.



(c) Perspective view



(d) Side view

Figure 5.20 The structure and prototype of a Type-D circular horn (Continued).

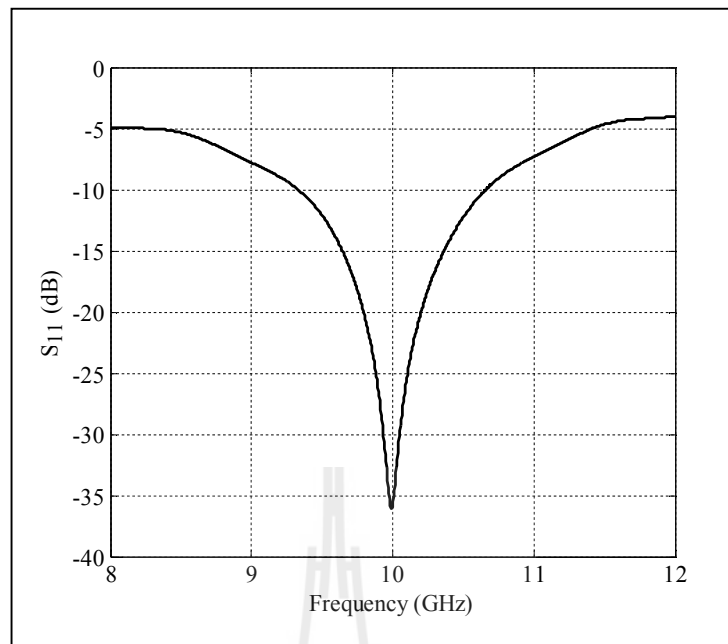


Figure 5.21 Simulated reflected power (S_{11}) of a Type-D circular horn with PEC arm.

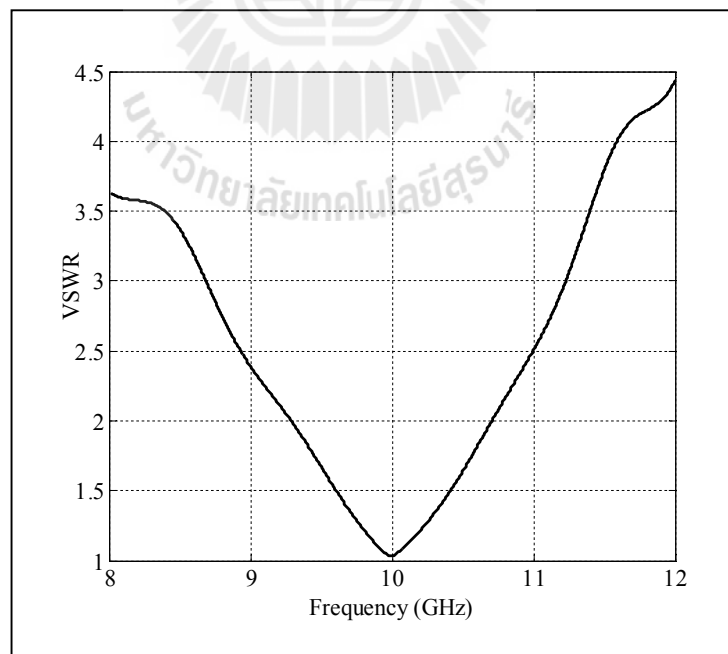


Figure 5.22 Simulated VSWR of a Type-D circular horn with PEC arm.

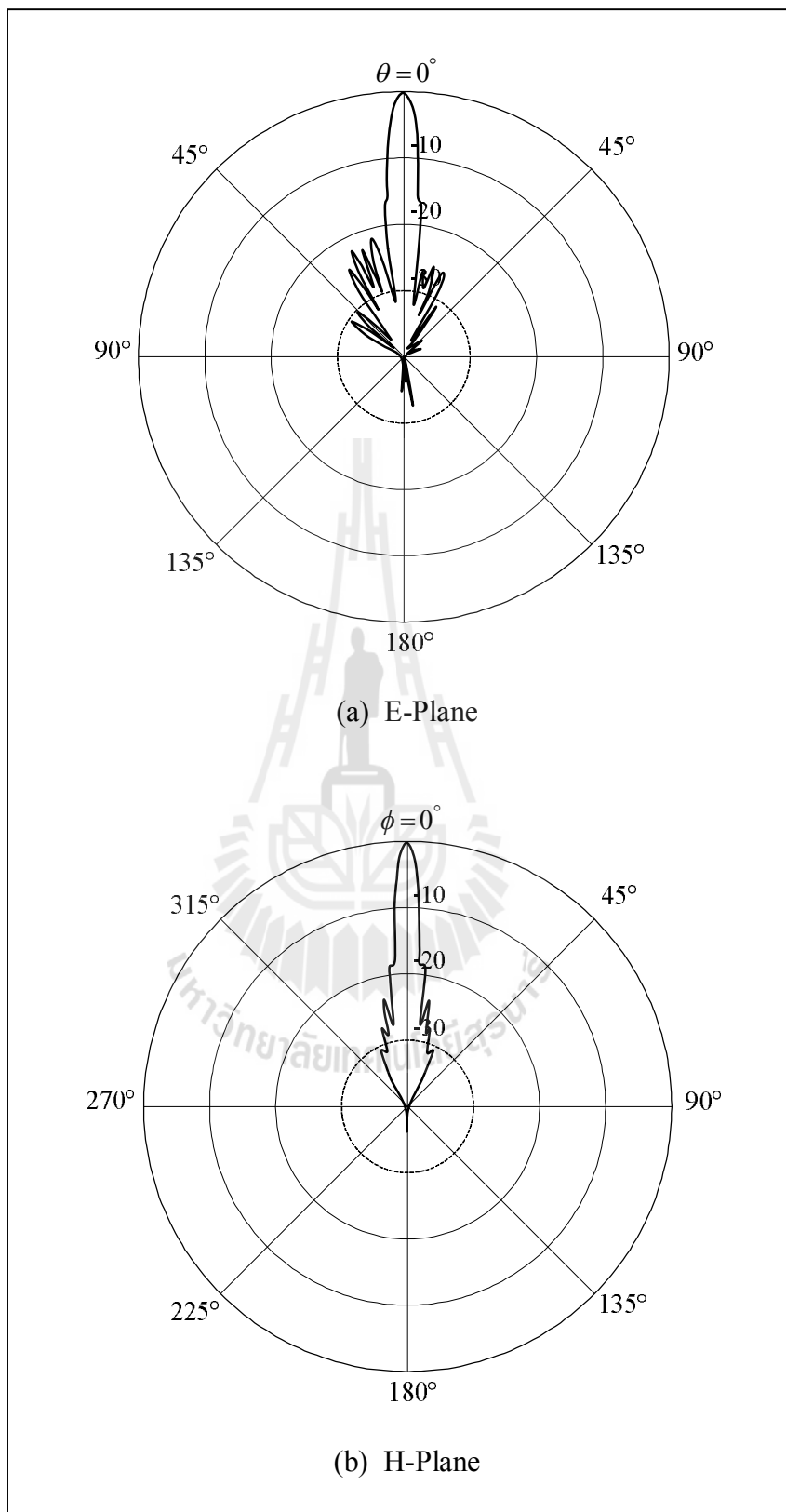


Figure 5.23 Simulated radiation patterns of a Type-D circular horn with PEC arm.

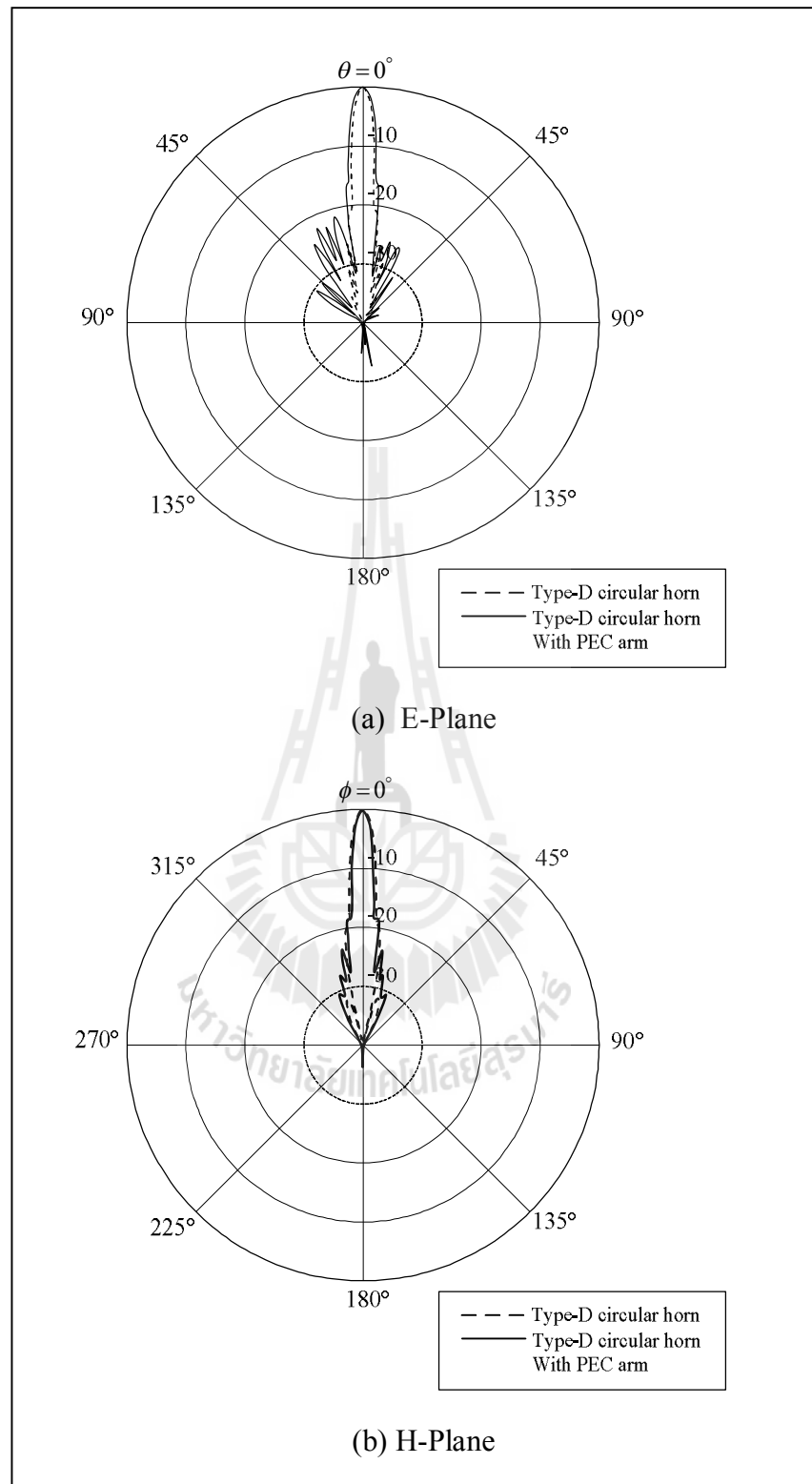


Figure 5.24 Comparison of radiation patterns of a Type-D circular horn with and without PEC arm.

5.4.1 The Reflected Power, Voltage Standing Wave Ratio and Input Impedance

In this section, we have reported the antenna measurements of the prototype of a Type-D circular horn. Similarly, we measured the parameters which evaluate the effectiveness of impedance matching efforts such as the S_{11} , VSWR and input impedance. It is found that the measured S_{11} of the prototype of a Type-D circular horn at the operating frequency of 10 GHz is -33.068 dB that is achieved for impedance matching, which is referred to $S_{11} \leq -10$ dB as shown in Figure 5.25. The VSWR is 1.0454 which agrees with impedance matching at $VSWR \leq 2$ as shown in Figure 5.26. The measured input impedance of the prototype of a Type-D circular horn is $48.064 + j0.9531 \Omega$, which is accepted because it is in the range of 40Ω to 60Ω as shown in Figure 5.27. From Figure 5.28 and 5.29 show the comparison of measured and simulated results of S_{11} and VSWR, respectively. A good qualitative agreement between measured and simulated results was obtained.

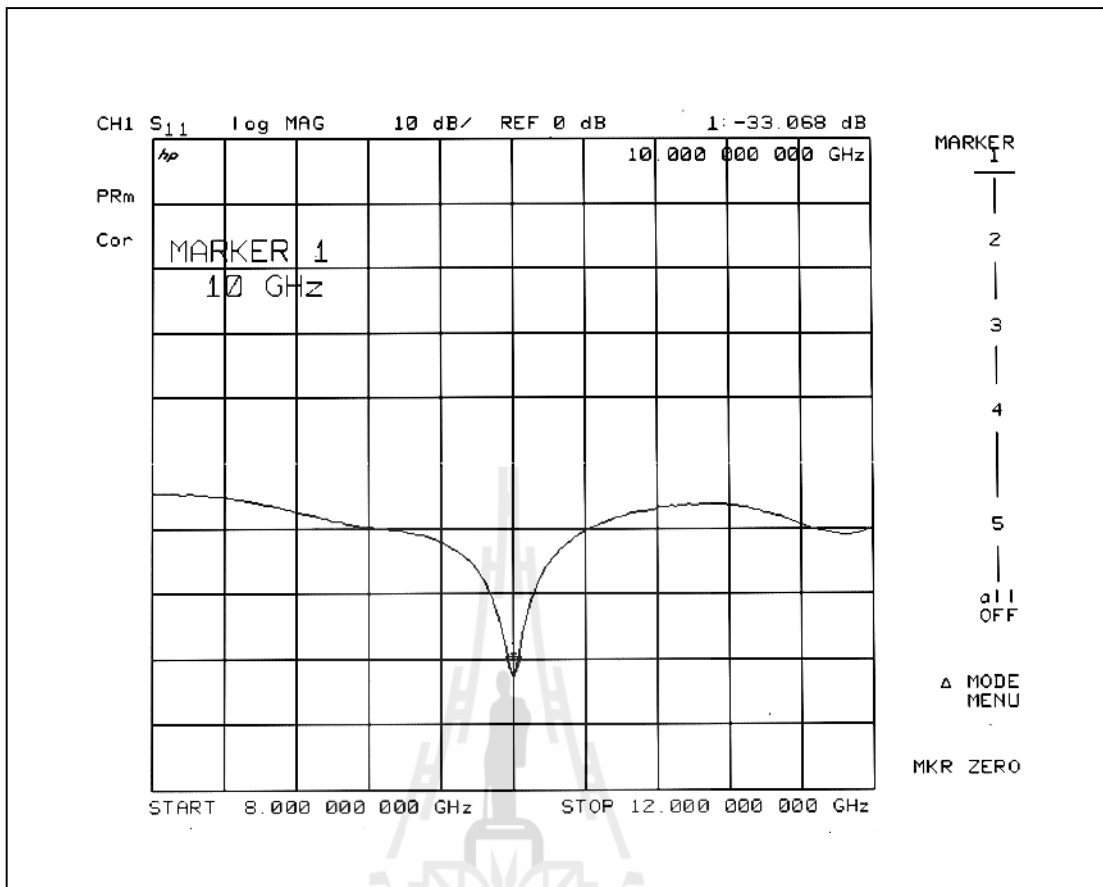


Figure 5.25 Measured reflected power (S_{11}) of the prototype of a Type-D circular horn.

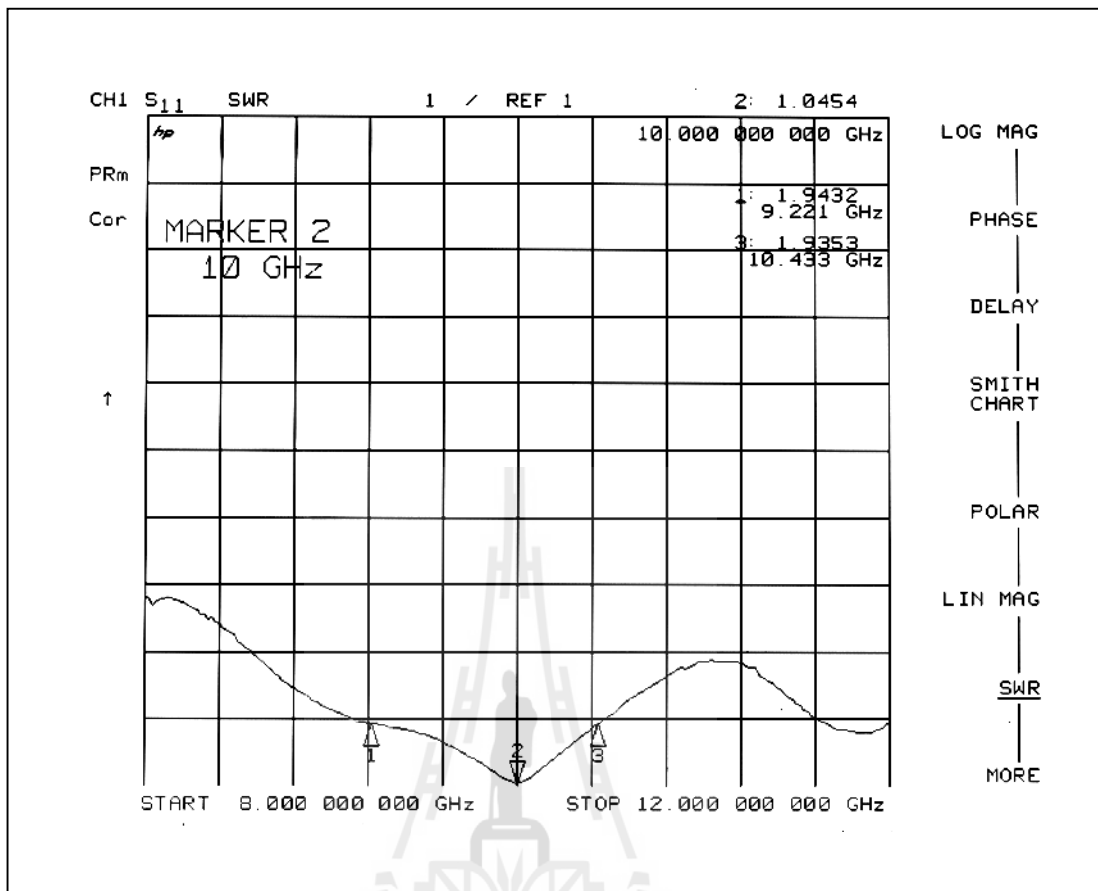


Figure 5.26 Measured VSWR of the prototype of a Type-D circular horn.

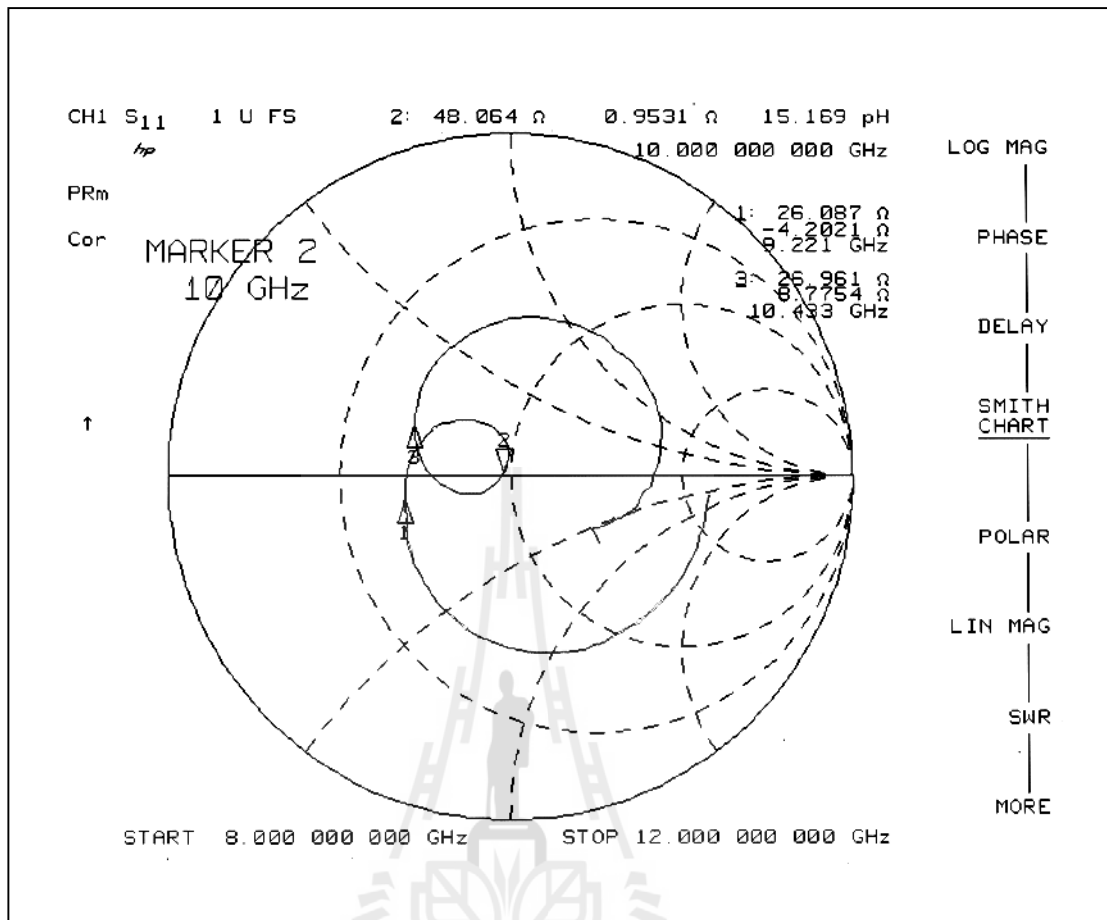


Figure 5.27 Measured input impedance of the prototype of Type-D circular horn.

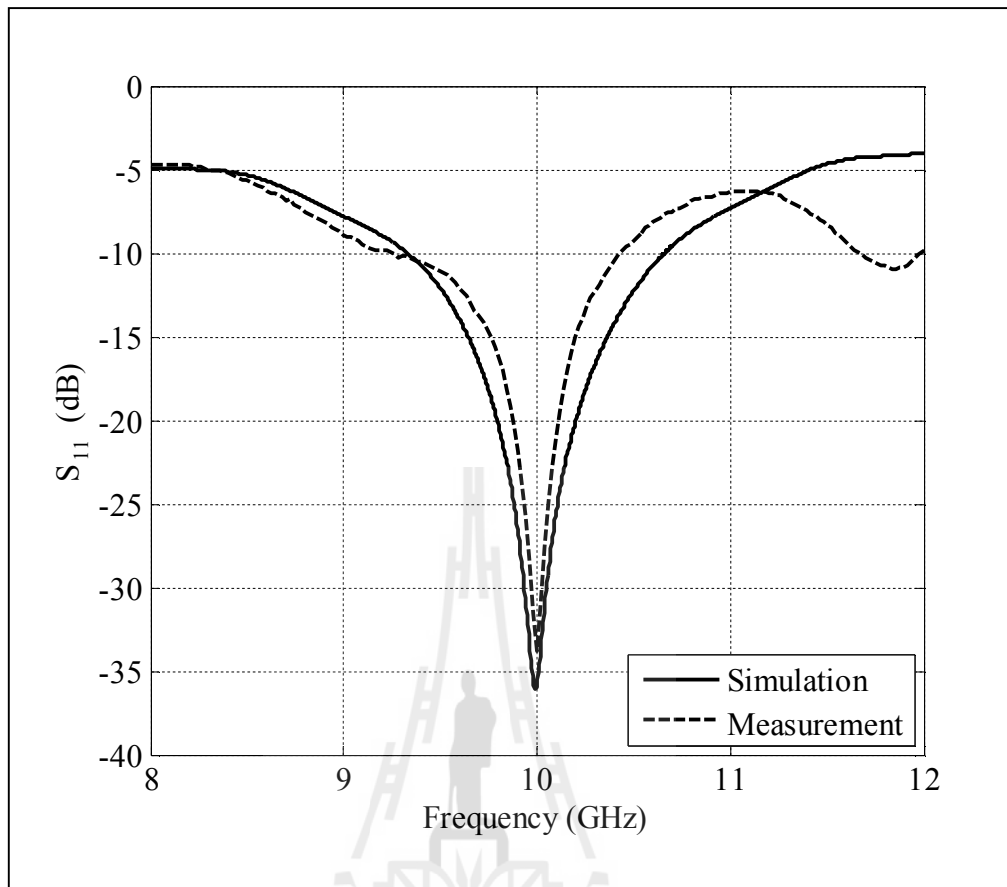


Figure 5.28 Comparison between simulated and measured results of reflected power (S_{11}) for the prototype of a Type-D circular horn.

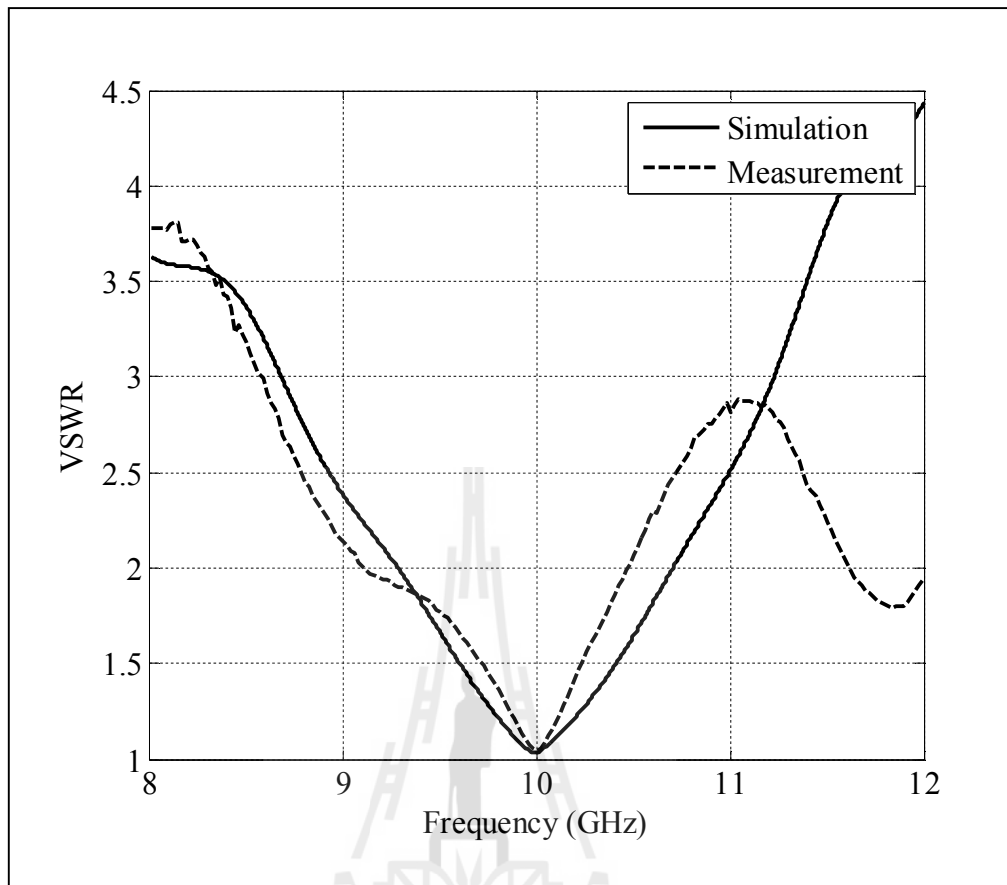


Figure 5.29 Comparison between simulated and measured results of VSWR for the prototype of a Type-D circular horn.

5.4.2 Bandwidth

The bandwidth of a circular horn antenna is expressed as a percentage of the frequency difference (upper minus lower) over the center frequency of the bandwidth. From the measured results, the bandwidth of the prototype of Type-D circular horn is 1.212 GHz (9.221 GHz to 10.433 GHz) or 12.33%, as shown in Figure 5.30. As referred in equation (5.1), the percentage bandwidth of the prototype of Type-D circular horn can demonstrate calculation as

$$\text{Bandwidth(\%)} = \left[\frac{(10.433 - 9.221)}{9.827} \right] \times 100\% = 12.33\% . \quad (5.5)$$

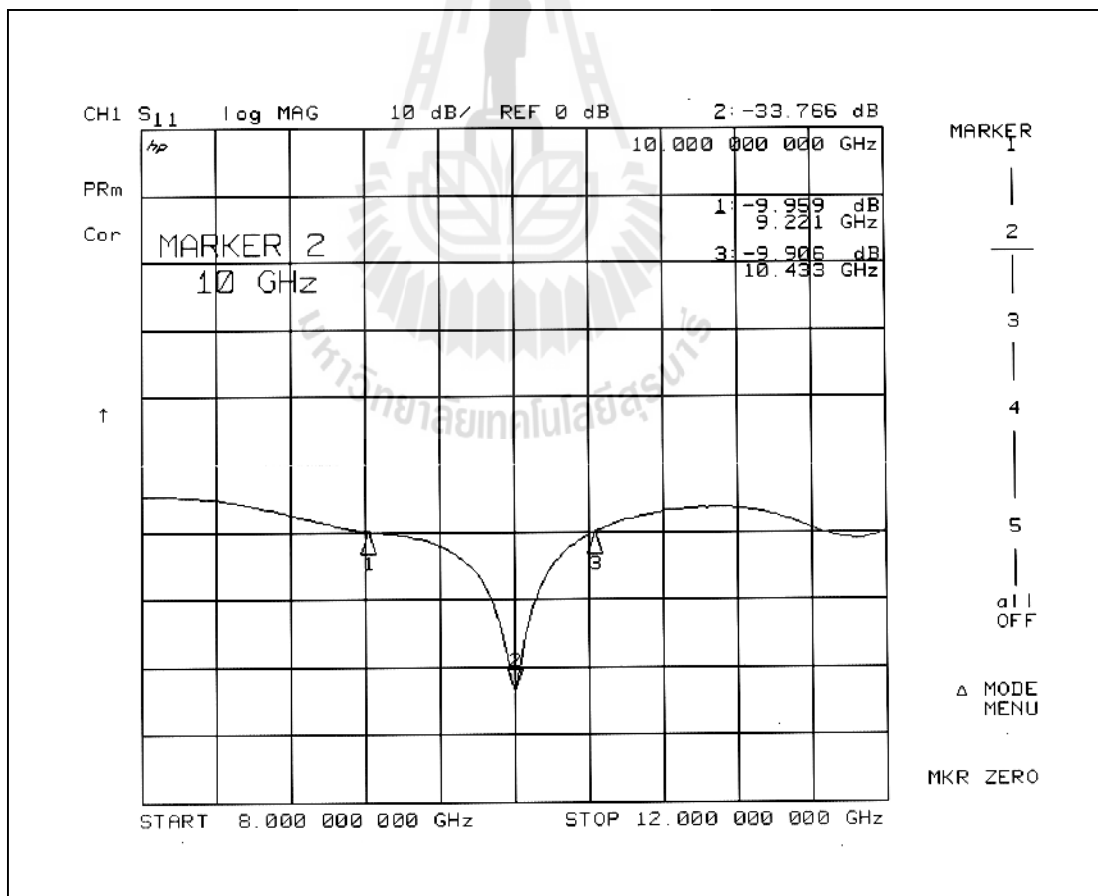
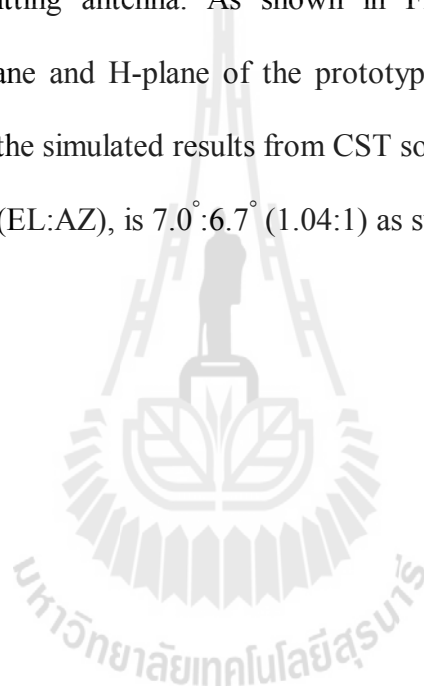


Figure 5.30 Measured bandwidth of the prototype of Type-D circular horn.

5.4.3 Radiation Pattern

Radiation pattern of the prototype of Type-D circular horn is measured in outdoor place and observed in the far field region as shown in Figure 5.31. A conventional rectangular horn antenna is used to be the transmitting antenna, while the prototype of Type-D circular horn antenna is in the receiving mode, which is installed on a turntable with the distance $R > 16.9$ m that was calculated from (5.3), far from the transmitting antenna. As shown in Figure 5.32, the measured far field patterns in E-plane and H-plane of the prototype of Type-D circular horn are plotted together with the simulated results from CST software. The HPBW ratio in the E-plane and H-plane, (EL:AZ), is $7.0^\circ:6.7^\circ$ (1.04:1) as summarized in Table 5.6.



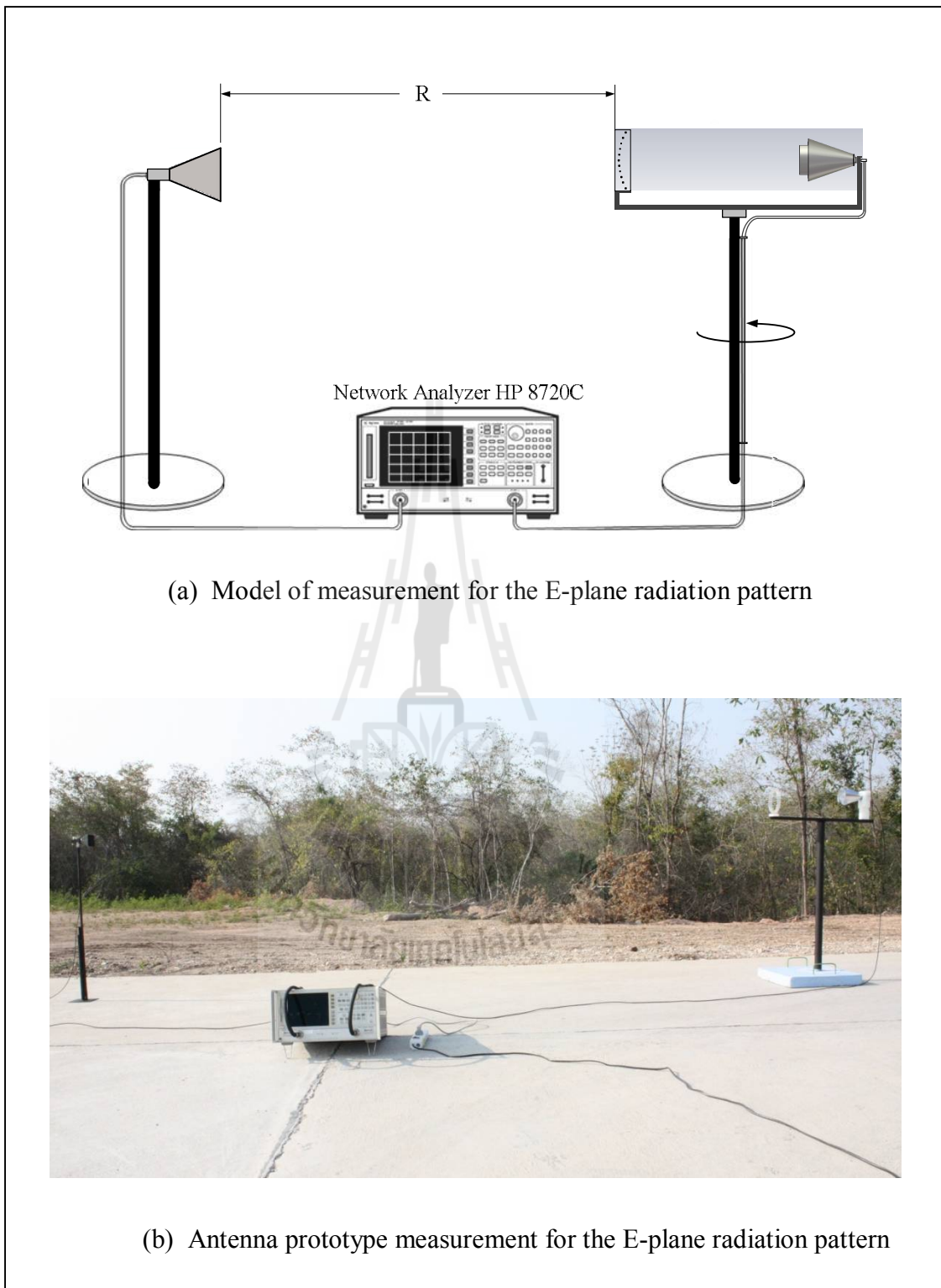


Figure 5.31 Measurement set up for the radiation pattern of the prototype of Type-D circular horn.

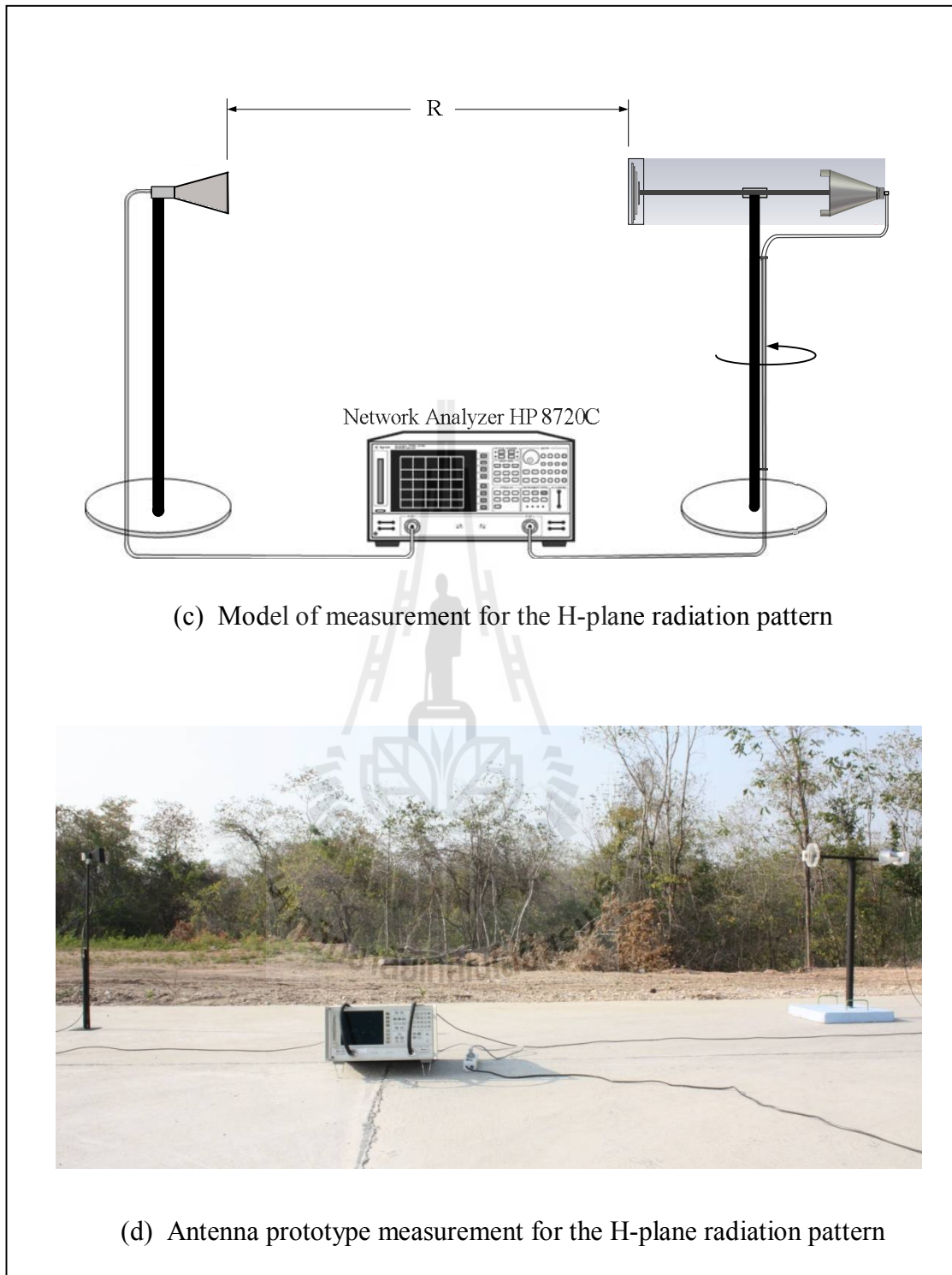


Figure 5.31 Measurement set up for the radiation pattern of the prototype of Type-D circular horn (Continued).

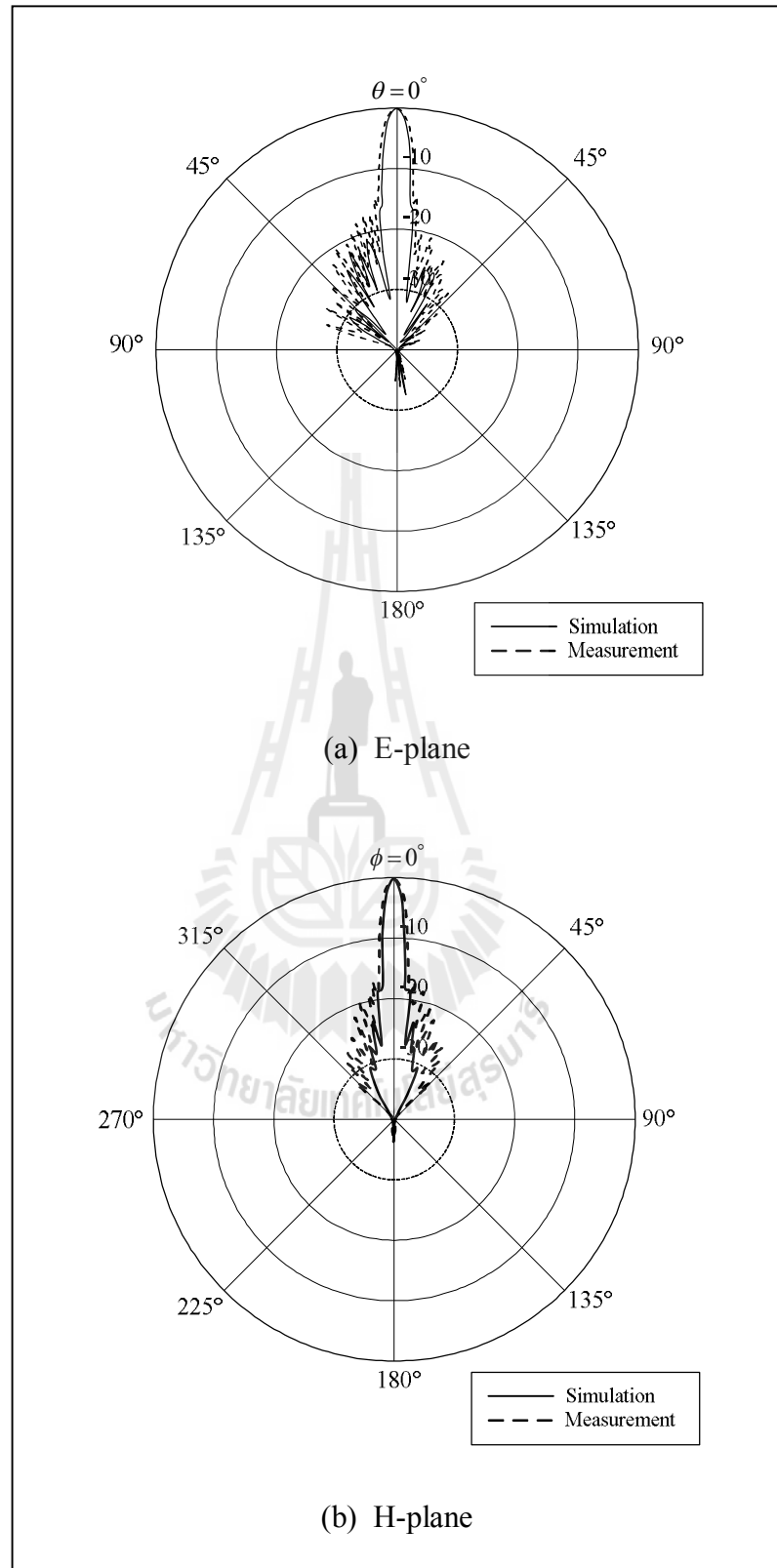
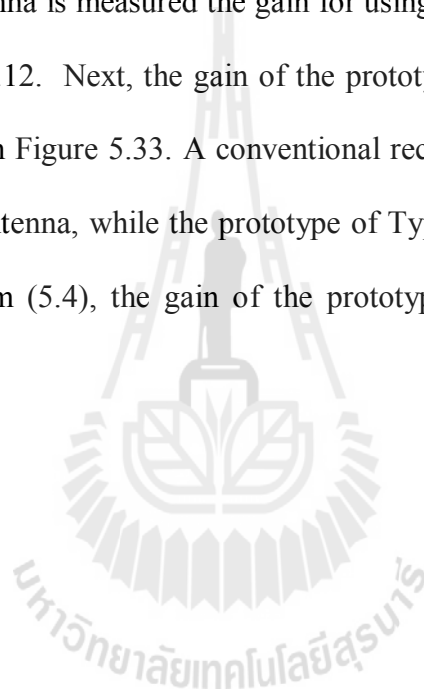


Figure 5.32 The radiation pattern of the prototype of Type-D circular horn.

5.4.4 Gain

In this section, we have described the gain measurement of the prototype of Type-D circular horn. It is based on the Friis transmission formula as expressed in (5.4), which can be applied when two matched polarization antennas aligned for the maximum directional radiation, and separated by a distance R that meets the far field criteria, are used for this gain measurement. Firstly, a conventional rectangular horn antenna is measured the gain for using to be the transmitting antenna as shown in Figure 5.12. Next, the gain of the prototype of Type-D circular horn is measured as shown in Figure 5.33. A conventional rectangular horn antenna is set to be the transmitting antenna, while the prototype of Type-D circular horn is set in the receiving mode. From (5.4), the gain of the prototype of Type-D circular horn is $G_{r,dB} = 25.34$ dB.



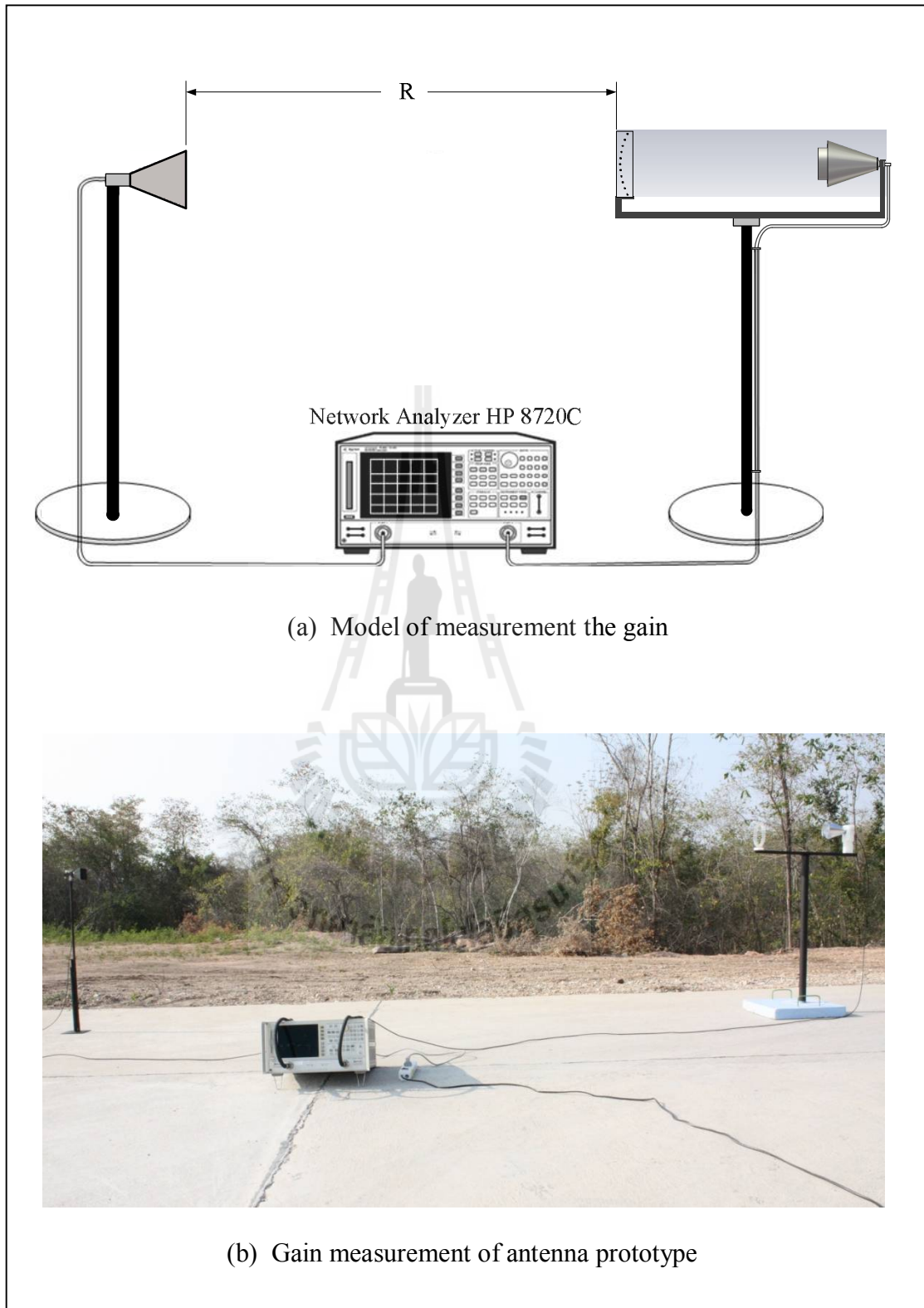


Figure 5.33 Gain measurement of the prototype of Type-D circular horn.

5.5 Simulated and Measured Results Summary

The simulated and measured results of the prototype of Type-D rectangular horn and Type-D circular horn antennas are summarized in Table 5.5.

Table 5.6 Comparison of simulated and measured results for antenna characteristics.

Antenna characteristics	The prototype of Type-D rectangular horn		The prototype of Type-D circular horn	
	Simulated	Measured	Simulated	Measured
The S_{11} (dB)	-26.71	-26.711	-36.11	-33.068
The bandwidth (%)	13.35	10.71	14.40	12.33
The VSWR	1.10	1.0978	1.03	1.0454
The HPBW (EL:AZ)	7.4°:6.6° (1.12:1)	7.6°:6.9° (1.10:1)	6.6°:6.4° (1.03:1)	7.0°:6.7° (1.04:1)
The SLL (dB) (E-plane/H-plane)	-16.3/-16.4	-15.6/-15.8	-15.7/-18.2	-15.1/-17.6
The gain (dB)	25.30	25.01	25.63	25.34

5.6 Chapter Summary

This chapter has presented the design and the construction of the prototype of Type-D rectangular horn and Type-D circular horn antennas. Both antenna measurements are described in order to verify the computed results with measurements to ensure that antenna was correctly modelled in the simulations and correctly assembled. The designed quadratic shaped woodpile EBG structures and the horn antennas with two side-wing slabs were installed on alumina rods for measurement. The measurement field patterns is in the outdoor place. From the measured results, the prototype of Type-D rectangular horn can provide moderately higher gain around 8 dB and the prototype of Type-D circular horn grants a higher gain around 6 dB when compared to the conventional rectangular and circular horn antennas, respectively. Finally, good agreement between simulated and measured results is obtained.

CHAPTER VI

CONCLUSIONS

6.1 Thesis Concluding Remarks

The study of increasing gain of the conventional rectangular and circular horn antennas by using EBG structures has been presented in this thesis. The gain improvement of the horn antennas by modifying the conventional rectangular and circular horns with adding two side-wing slabs on the left and right sides to control the HPBW symmetrically in the E-plane and H-plane and increasing their gain with new technique that is so-called designed quadratic shaped woodpile EBG structures. From the results, they evidently provide not only the symmetrical radiation patterns both in E-plane and H-plane but also the moderately higher gain around 8 dB for a rectangular horn and 6 dB for a circular horn when compared to the conventional horns. For the designed woodpile EBG structures, the various shaped woodpile EBG structures, the distance between a horn antenna and woodpile EBG structures, and the radius of EBG structure are the parameters for this accomplishment especially the shape of woodpile EBG structures is the most important technique, which must be appropriately designed and calculated for both horn antennas. The most proper distance between a horn antenna and woodpile EBG structures of 16.5λ and the radius of quadratic shape of 5.3λ can provide the moderately highest gain at the operating frequency of 10 GHz.

6.2 Remark for Future Studies

From the foundation of knowledge which has been learned and acquired over this research, some recommendations for the future woodpile EBG structures should be presented. This research has used functions of geometries such as planar, triangular, quadratic, circular, gaussian, cosine, and squared cosine structures to investigate the proper shape of woodpile EBG structure. It was found that when we changed woodpile EBG shape, the antenna characteristics are also changed. In the future study, we can change woodpile EBG structures for variety shapes in order to provide the better characteristics of both horn antennas. Because the designed quadratic shaped woodpile EBG is symmetrical shape, therefore, it yields high performance as the additional resonant circuit, exhibit bandgap characteristics at 10 GHz when the radiation patterns of the horn antennas must be also symmetrical. In applying the designed quadratic shaped woodpile EBG structures to increase the gain of horn antennas, it is necessary to control the HPBW symmetrically in the E-plane and H-plane by adding two side-wing slabs on the left and right sides of the aperture. Therefore, in the future, if we can investigate the different geometry of woodpile EBG structure that can be used with the conventional rectangular and circular horn antennas without adding two side-wing slabs, then the utilization of EBG structure will be more easy than the structure in this research.

REFERENCE

- Alam, Md. S., Misran, N., Yatim, B., and Islam, M. T. (2013). **Development of Electromagnetic Band Gap Structures in the Perspective of Microstrip Antenna Design**. Hindawi Publishing Corporation International Journal of Antennas and Propagation. 2013: 1-22.
- Ando, M. (2005). Radiation Pattern Analysis of Reflector Antenna – Discussions and Hybrid Use of Physical Optics and Aperture Field Integration Method. **IEICE Transaction on Communication**. E88-B(5): 1790-1800.
- Bakshi, K.A.; A.V. Bakshi, U.A. Bakshi (2009). **Antennas And Wave Propagation**. Technical Publications.
- Balanis, C. A. (1989). **Advanced Engineering Electromagnetics**. John Wiley & Sons. New York.
- Balanis, C. A. (1997). **Antenna Theory Analysis and Design**. John Wiley & Sons. New York.
- Balanis, C. A. (2005). **Advanced Engineering Electromagnetic (Third edition)**. John Wiley & Sons. New York.
- Bergmann, J. R., Hasselmann, F. J. V., and Branco, M. G. C. (2002). MoM Analysis of a Reflector Antenna Design for Omnidirectional Coverage. **Antennas and Propagation Society International Symposium**. 4: 148-151.

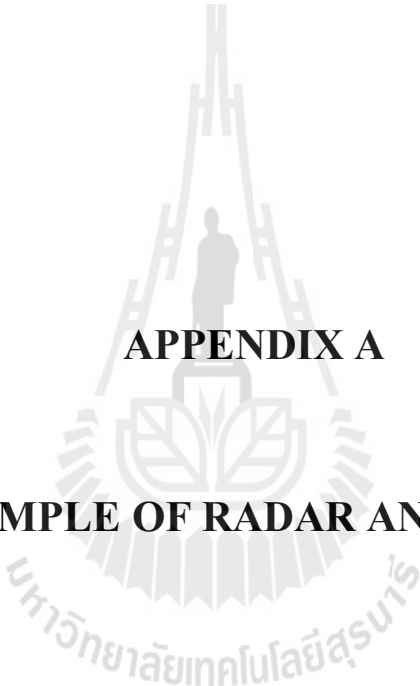
- Bergmann, J. R., Hasselmann, F. J. V., Pereira, L. C. P., and Branco, M. G. C. (1998). **Reflector Antenna Configurations for Radio Base Stations in Cellular Communications. IEEE-APS Conference on Antennas and Propagation for Wireless Communications.** 1-4: 61-64.
- Clenet, M. and Shafai, L. (2000). Investigations on Directivity Improvement of Wide Flare Angle Conical Horns Using Inserted Metallic Discs. **IEE Proceedings on Microwaves Antennas and Propagation.** 147(2): 100-105.
- Davidson, David B. (2010). **Computational Electromagnetics for RF and Microwave Engineering.** Second Edition, Cambridge University Press.
- Frenzel, L. E. (2007). **Principles of Electronic Communication Systems.** Third Edition, McGraw-Hill Science.
- Gonzalo, R., Maagt, P. J. I., and Sorolla, M. (1999). **Enhanced Patch Antenna Performance by Suppressing Surface Waves Using Photonic Band-Gap Structures.** IEEE Transactions on Microwave Theory and Techniques. 47(11): 2131-2138.
- Kampeephat, S., Krachodnok, P., and Wongsan, R. (2012). **A Study of Gain Enhancement of Horn Antenna Using Various Shaped Woodpile EBG.** The 2012 Thailand-Japan MicroWave (TJMW 2012).
- Kampeephat, S., Krachodnok, P., and Wongsan, R. (2014). **Efficiency Improvement for Conventional Rectangular Horn Antenna by Using EBG Technique.** World Academy of Science, Engineering and Technology (WASET), International Journal of Electrical, Robotics, Electronics and Communications Engineering. 8(7): 1009-1014.

- King, A. P. (1950). **The Radiation Characteristics of Conical Horn Antennas**. The Proceedings of the IRE. 38(3): 249 - 251.
- Koerner, M. A. and Rogers, R. L. (2000). Gain Enhancement of a Pyramidal Horn Using E- and H-Plane Metal Baffles. **IEEE Transactions on Antennas and Propagation**. 48(4): 529-538.
- Lee, Y., Lu, X., Hao, Y., Yang, S., Evans, J. R. G., and Parini, C. G. (2009). Low Profile Directive Millimeter-Wave Antennas using Free Formed Three-Dimensional (3D) Electromagnetic Band Gap Structures. **IEEE Transactions on Antennas and Propagation**. 57(10): 2893-2903.
- Levenberg, K. (1944). **A Method for the Solution of Certain Non-linear Problems in Least Squares**. Quarterly of Applied Mathematics. 2(2):164-168.
- Li Yang, M., Fan, F., Chen, J., and She, J. (2005). **A Novel Compact Electromagnetic-Bandgap (EBG) Structure and Its Applications for Microwave Circuits**. IEEE Transaction on Microwave Theory and Techniques. 53(1): 183-190.
- Love, A.W. (1976). **Electromagnetic horn antennas**. IEEE Press, New York.
- Maagt, P., Gonzalo, R., Vardaxoglou, Y. C., and Baracco, J. M. (2003). Electromagnetic bandgap antennas and components for microwave and (sub) millimeter wave applications. **IEEE Transactions on Antennas and Propagation**. 51(10): 2667–2677.
- Marquardt, D.W. (1963). **An Algorithm for the Least-Squares Estimation of Nonlinear Parameters**. SIAM Journal of Applied Mathematics. 11(2):431-441.

- Olver, A. D., Clarricoats, P. J. B., Shafai, L., and Kishk, A. A. (1994). **Microwave horns and feeds**. IEEE Press, New Jersey.
- Rodriguez, V. (2010). A brief history of horns. **In Compliance Magazine**.
- Silver, S. (1949). **Microwave Antenna Theory and Design**. McGraw-Hill.
- Thaivirod, V., Krachodnok, P., and Wongsan, R. (2008). **Radiation Pattern Synthesis from Various Shaped Reflectors Base on PO and PTD Methods for Point-to-Multipoint Applications**. WSEAS Transactions on Communications. 7(6): 531-540.
- Thevenot, M., Cheype, C., Reineix, A., and Jecko, B. (1999). **Directive Photonic Band-Gap Antennas**. IEEE Transactions on Microwave Theory and Techniques. 47(11): 2115-2122.
- Weily, A. R., Horvath, L., Esselle, K. P., Sanders, B. C., and Bird, T. S. (2005). A Planar Resonator Antenna Base on a Woodpile EBG Material. **IEEE Transactions on Antennas and Propagation**. 53(1): 216-223.
- Xu, F. and Hong, W. (2004). **Domain Decomposition FDTD Algorithm for the Analysis of a New Type of E-Plane Sectorial Horn With Aperture Field Distribution Optimization**. IEEE Transactions on Antennas and Propagation. IEEE 52(2): 426-434.
- Yang, F. and Rahmat-Samii, Y. (2003). **Reflection phase characterizations of the EBG ground plane for low profile wire antenna applications**. IEEE Transactions on Antennas and Propagation. 51(10): 2691–2703.

- Yang, F. and Rahmat-Samii, Y. (2005). **A low profile single dipole antenna radiating circularly polarized waves.** IEEE Transactions on Antennas and Propagation. 53(9): 3083–3086.
- Yang, F. and Rahmat-Samii, Y. (2009). **Electromagnetic Band Gap Structures in Antenna Engineering.** Cambridge University Press, Cambridge.





APPENDIX A

EXAMPLE OF RADAR ANTENNAS

A.1 Military Radars

The AN/TPQ-36 firefinder weapon locating radar in use by the army (<http://www.radartutorial.eu/>) is exemplified for military short range radars comparing to the specifications of our prototype horn antennas as shown in Table A.1. We found that, although, our prototype horn antennas provide shorter maximum range but they have the advantages of low profile, light weight, and quite small size when compare to the AN/TPQ-36. Figure A.1 shows the AN/TPQ-36 firefinder weapon locating radar in use by the army and its leaflet.

Table A.1 Comparison of radar antennas.

Antenna Charecteristics	AN/TPQ-36*	The prototype of Type-D rectangular horn	The prototype of Type-D circular horn
Frequency	X-band radar		
Peak transmitted power (kW)	23		
Maximum range (km)	24	20.4	21.1

*<http://www.radartutorial.eu/>



(a) The AN/TPQ-36 firefinder weapon locating system

Figure A.1 The AN/TPQ-36 firefinder weapon locating radar.

AN/TPQ-36 FIREFINDER WEAPON LOCATING SYSTEM

Description:
Medium-Range Surveillance
 ThalesRaytheonSystems' compact, mobile, combat-proven AN/TPQ-36 Firefinder radar accurately, rapidly, and automatically locates medium-range enemy mortars, artillery, and rocket launchers. It can handle simultaneous fire from weapons at multiple locations, tracking and reporting their positions on the first round. No longer must front-line troops and armor be exposed to long periods of enemy mortar, artillery, and rocket attacks. The AN/TPQ-36 directs accurate counterfire to neutralize enemy positions.

The AN/TPQ-36's automatic detection, tracking, and locating process is so fast that an enemy weapon's position can often be pinpointed before its projectile impacts. Locations of enemy weapon positions are automatically corrected for altitude differences, using computer-sourced digital maps, and presented to the operator in map, grid, and altitude coordinates. The system is so automatic and simple to operate that, once set up, the operator need not be present in the operation control shelter to determine a weapon's location.

Rounds from friendly weapons also can be tracked, for more accurate delivery.

Defeats Enemy Firepower, Supports Friendly Weapons
 The AN/TPQ-36's stationary antenna sweeps a rapid sequence of beams along the horizon, forming an electronic radar curtain over a 90° area. Any target, penetrating the curtain triggers an immediate verification beam. On verification, an automatic tracking sequence begins.

While tracking any single target, the radar continues scanning, locating, and tracking others.

The AN/TPQ-36 can detect and report the positions of up to 10 different weapons in seconds, at a maximum range of 24 km. The system also corrects and improves the delivery of friendly fire.

Signal and data processors test each track to filter out birds, aircraft, and other unwanted returns, giving the AN/TPQ-36 an extremely low false-location rate and a very high probability of location. Once the computer establishes a target's validity, it smooths the measured track data, deriving a trajectory that it extrapolates to establish the target's lining position and impact location. These data are displayed on a visual map and printed out in their coordinates.

From the operation control shelter, the power-driven antenna can be tilted or rotated to any azimuth position. The system also offers a 360° sectoring mode, in which it will search one sector for a short period, then automatically rotate in turn to the other sectors.

Highly Mobile
 Compact and highly mobile, the AN/TPQ-36 supports rapid deployment of forces and close combat. It can be positioned and ready for operation in 15 minutes. It can be reloaded for movement in 5 minutes by a five-man crew. Because it can move quickly from one position to another, it is typically located close to the forward battle line in direct support of brigade operations.

The AN/TPQ-36 comprises an antenna-transceiver trailer; a generator; and an operation control shelter that contains processing equipment, the weapon-locating unit, and communications equipment. For the U.S. Army, the 2,500-lb shelter is carried on a HMMWV or a 2.5-ton truck; however, it can also be carried by other tactical vehicles. The manned operation control shelter can be located as far as 50 m away from the unmanned antenna trailer.

Exceptionally Reliable
 With high system reliability and maintainability simplified by computer-controlled, built-in test equipment, ThalesRaytheonSystems' AN/TPQ-36 provides unusually high system availability. On-line fault detection and off-line fault diagnostics alert the operator to system faults, directing repair action to the unit that must be replaced. Ninety percent of all repairs required in the field can be performed by the crew, with a mean-time-to-repair of only 30 minutes.

The AN/TPQ-36's cost effectiveness is enhanced by its 90°-360° sector, small crew, ease of operation, and high availability. The operation control shelter can be used interchangeably with either the AN/TPQ-36 or the longer-range AN/TPQ-37, with only a software change, thereby providing operational flexibility and much greater life-cycle cost effectiveness.

AN/TPQ-36 Firefinder Weapon Locating System	
Capabilities	Specifications
Detects mortars, artillery, and rocket launchers Locates 10 weapons simultaneously Performs high burst, down-pulse, and impact registrations Adjusts friendly fire Interacts with tactical fire Predicts impact of hostile projectiles	Maximum range: 24 km Effective range: 24 km Azimuth: 90° Resolution: 24 m Azimuth sector: 30° Frequency: X-band, 32 frequencies Prime power: 115,000 WAC, 400 Hz, 3-phase, 8 kW Peak transmitted power: 23 kW, min.
Features	
Permissive range for 20 targets Field exercise mode Digital data interface	

ThalesRaytheonSystems

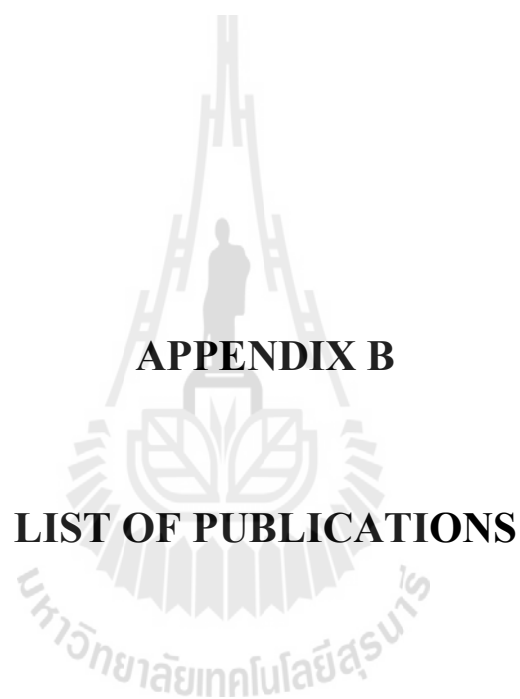
ThalesRaytheonSystems
 1801 Hughes Dr.
 P.O. Box 34035
 Fullerton, California
 92631-3435
 Tel.: +1 714 446 5118
 Fax: +1 714 446 3260

ThalesRaytheonSystems
 1, avenue Camille
 91885 Maissy Corlex France
 Tel.: +33 (0)1 69 75 50 00
 Fax: +33 (0)1 69 75 51 00

www.thalesraytheon.com

(b) The leaflet of AN/TPQ-36

Figure A.1 The AN/TPQ-36 firefinder weapon locating radar (Continued).



APPENDIX B

LIST OF PUBLICATIONS

List of Publications

- Kampeephat, S., Krachodnok, P., and Wongsan, R. (2014). **Efficiency Improvement for Conventional Rectangular Horn Antenna by Using EBG Technique.** World Academy of Science, Engineering and Technology (WASET), International Journal of Electrical, Robotics, Electronics and Communications Engineering. 8(7): 1015-1020. (International Science Index, ISSN: 1307-6892).
- Kampeephat, S., Krachodnok, P., and Wongsan, R. (2012). **High-Gain and Light-Weight Antenna for Radar System Using a Horn Covered with Curved Woodpile EBG.** The 2012 Progress in Electromagnetics Research Symposium (PIERS 2012). 1628-1630.
- Kampeephat, S., Krachodnok, P., and Wongsan, R. (2012). **A Study of Gain Enhancement of Horn Antenna Using EBG.** The 2012 IEEE Asia-Pacific Conference on Antennas and Propagation (APCAP 2012). 195-196.
- Kampeephat, S., Krachodnok, P., and Wongsan, R. (2012). **A Study of Gain Enhancement of Horn Antenna Using Various Shaped Woodpile EBG.** The 2012 Thailand-Japan MicroWave (TJMW 2012).
- Kampeephat, S., Krachodnok, P., and Wongsan, R. (2014). **Gain Improvement for Rectangular Horn Antenna with Additional EBG.** The 2013 Thailand-Japan MicroWave (TJMW 2013).

Kampeephat, S., Krachodnok, P., and Wongsan, R. (2014). **Gain Improvement for Conventional Rectangular Horn Antenna With Additional EBG Structure.** The 2014 International Conference on Electrical Engineering/Electronics, Computer, Telecommunications and Information Technology (ECTI-CON 2014).



Efficiency Improvement for Conventional Rectangular Horn Antenna by Using EBG Technique

S. Kampeephat, P. Krachodnok, R. Wongsan

Abstract—The conventional rectangular horn has been used for microwave antenna a long time. Its gain can be increased by enlarging the construction of horn to flare exponentially. This paper presents a study of the shaped woodpile Electromagnetic Band Gap (EBG) to improve its gain for conventional horn without construction enlargement. The gain enhancement synthesis method for shaped woodpile EBG that has to transfer the electromagnetic fields from aperture of a horn antenna through woodpile EBG is presented by using the variety of shaped woodpile EBGs such as planar, triangular, quadratic, circular, gaussian, cosine, and squared cosine structures. The proposed technique has the advantages of low profile, low cost for fabrication and light weight. The antenna characteristics such as reflection coefficient (S_{11}), radiation patterns and gain are simulated by utilized A Computer Simulation Technology (CST) software. With the proposed concept, an antenna prototype was fabricated and experimented. The S_{11} and radiation patterns obtained from measurements show a good impedance matching and a gain enhancement of the proposed antenna. The gain at dominant frequency of 10 GHz is 25.6 dB, application for X- and Ku-Band Radar, that higher than the gain of the basic rectangular horn antenna around 8 dB with adding only one appropriated EBG structures.

Keywords—Conventional Rectangular Horn Antenna, Electromagnetic Band Gap, Gain Enhancement, X- and Ku-Band Radar.

I. INTRODUCTION

A HORN antenna is widely used as antenna at Ultra-High Frequency (UHF) and microwave frequency, above 300 MHz [1], [2], a type of aperture antenna, which provides the moderately high gain as compared to the other antennas. Consequently, the horn antenna is widely applied for various tasks. A horn antenna has been used in many applications, such as satellite communications, radio astronomy, radar or remote sensing [3], [4]. They are used as feeders for larger antenna structures, as standard calibration antennas to measure the gain of other antennas, and as directive antennas [5], [6]. Their widespread applicability stems from their simplicity in construction, ease of excitation, versatility, large gain, and preferred overall performance [7]. Applications requiring high gain antenna such as the parabolic reflector can be applied with the horn antenna to enhance the higher gain. The insertion of a thin metallic strip into a horn is briefly discussed [8]. The metallic strip is reported to improve the plane directivity of a horn, but it is suggested that mismatch

problems make the technique impractical. Moreover, techniques for improving the performance of a wide-flare pyramidal horn antenna, metallic baffles are placed inside the horn near its throat the antenna's performance is improved significantly [9]. The metal baffles are simple planar structures that reduce phase curvature at the aperture like a lens. However, the disadvantages of metallic are heavy, bulky and not easy to integrate with monolithic microwave integrated circuits (MMICs) components. The smooth walled conical horn (SWCH), by virtue of its desirable qualities such as high gain, construction simplicity and ease of excitation, is used as a standard gain antenna, as a feed for reflectors and in polarization diversity systems [10]. On the other hand, its poor pattern symmetry and high cross-polar radiation level make it unsuitable for high performance applications. Much research has been devoted to high performance conical horns such as corrugated horn, lens corrected horn and multimode horn [11]. These horns, however, in general impose construction difficulties, and are often heavy, bulky and costly.

Wongsan et al. presented an additional Electromagnetic Band Gap (EBG) to improve the gain of a rectangular horn antenna by using woodpile EBG structures, transfer the power from its aperture through EBG structures [12]-[15]. By employing, EBG structures as high-impedance ground planes [16], as planar reflectors [17], or as substrates [18], they are able to eliminate the drawbacks of conducting ground-planes, to prevent the propagation of surface waves, to lower the device profiles, and to improve the performances of antennas, enhancing their directivity and the radiation efficiency. Moreover, they can be formed from dielectric structures that are periodic in one or more dimensions [19]. Therefore, this paper presents a study of the technique to enhance the gain of a conventional rectangular horn antenna by using a variety of shaped woodpile EBG such as planar, triangular, quadratic, circular, gaussian, cosine, and squared cosine structures. They are creating new possibilities for controlling and manipulating the flow of electromagnetic waves. Also, this paper designs to simulate and fabricate a horn antenna with EBG structures based on low loss alumina materials at dominant frequency of 10 GHz, and demonstrate its use in a horn antenna for X- and Ku-Band Radar.

At first, the general approach will be presented which is including the configurations of a rectangular horn antenna, which is improved gain and radiation patterns by adding two side-wing slabs, and the woodpile EBG structures as shown in Sections II and III, respectively. Next, the simulated results of antenna characteristics are calculated by using CST software and discussed in the Section IV.

S. Kampeephat, P. Krachodnok, and R. Wongsan are with the School of Telecommunication Engineering, Institute of Engineering, Suranaree University of Technology, Nakhon Ratchasima, CO 30000 Thailand (phone: +668 1955 2414; fax: +66 4422 4603 e-mail: D5240388@g.sut.ac.th, priam@sut.ac.th, and rangsan@sut.ac.th).

II. HORN ANTENNA CONFIGURATION

A. A Conventional Rectangular Horn Antenna

A horn antenna may be considered as a transformer from the impedance of a transmission line to the impedance of free space, 377Ω . A common microwave transmission line is waveguide, a hollow pipe carrying an electromagnetic wave. The horn antenna consists of a flaring metal waveguide for guiding the radio waves into free space. The design of a conventional rectangular horn antenna (*Type-A* horn) is initiated by determining its aperture dimension as follow [6], with the gain of 17.67 dB, as shown in Fig. 1.

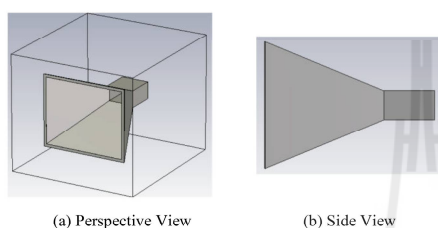


Fig. 1 A conventional rectangular horn antenna (*Type-A* horn)

B. A Horn Antenna with Two Side-Wing Slabs

To improve the radiation pattern and gain characteristics, a conventional rectangular horn antenna will be add two side-wing slabs on the left and right sides (*Type-B* horn) [14] to control the half-power beamwidth (HPBW) symmetrically in the E- and H-Plane as shown in Fig. 2. The design dimension for each side-wing slab is $5\lambda/8$, approximately. The simulated result show that the HPBW, which shown as the ratio of azimuth pattern to elevation pattern (AZ:EL), of a *Type-B* horn is $20.6^\circ:21.7^\circ$ (1:1.05) at the gain of 18.08 dB.

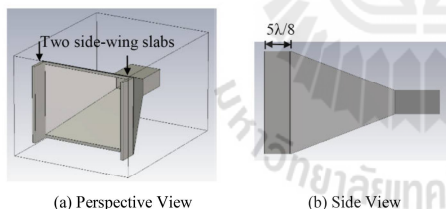


Fig. 2 A conventional rectangular horn antenna with two side-wing slabs (*Type-B* horn)

III. EBG CONFIGURATION

A woodpile is a three-dimension EBG structures made of a stack of square cross-section rod. The unit cell of these structures is shown in Fig. 3. The dimension of woodpile EBG structures is specified by the distance in the horizontal plane (a), the rod width (w), and the rod height (h). To implement the woodpile, this paper has used alumina rods ($\epsilon_r = 8.4$, $\tan\delta = 0.002$) that have a rectangular cross section. The lattice

parameters are given as follow [12] with $a = 0.225\lambda$ and $w = h = 0.064\lambda$.

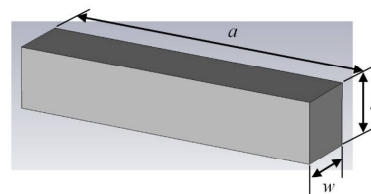


Fig. 3 The unit cell of woodpile EBG rod

To align shaped woodpile EBG structures, this paper has used functions of geometries from [20] as shown in Table I

TABLE I FORMULATIONS OF ELEMENTARY GEOMETRICAL FUNCTION		
Distributed functions	Formulations	Shapes of EBG Structures
Planar	-	
Triangular	$f(x,y) = A \left(1 - \frac{2}{D} \sqrt{x^2 + y^2} \right)$	
Quadratic	$f(x,y) = A \left[1 - \left(\frac{2}{D} \sqrt{x^2 + y^2} \right)^2 \right]$	
Circular	$f(x,y) = A \sqrt{1 - \left(\frac{2}{D} \sqrt{x^2 + y^2} \right)^2}$	
Gaussian	$f(x,y) = A e^{-\left(\frac{2}{D} \sqrt{x^2 + y^2} \right)^2}$	
Cosine	$f(x,y) = A \cos \left(\frac{\pi}{D} \sqrt{x^2 + y^2} \right)$	
Squared Cosine	$f(x,y) = A \cos^2 \left(\frac{\pi}{D} \sqrt{x^2 + y^2} \right)$	

International Science Index Vol:8, No:7, 2014 waset.org/Publication/9998639

BIOGRAPHY

Mr. Saran Kampeephat was born on June 12th, 1984 in Surat Thani Province, Thailand. He graduated with the Bachelor Degree of Engineering in Telecommunication Engineering in 2007 from Suranaree University of Technology, Nakhon Ratchasima Province, Thailand. He then attended Suranaree University of Technology and received a Master's Degree in Telecommunication Engineering in 2009. After that he received scholarship from the National Research Council of Thailand (NRCT) for the Joint Ph.D program in the school of telecommunication engineering, institute of engineering at Suranaree University of Technology. His research interests include the electromagnetic wave applications, antenna engineering, and Electromagnetic Band Gap (EBG).

มหาวิทยาลัยเทคโนโลยีสุรนารี